Trajectory Tracking and Impedance Control of Hybrid Manipulators

A Thesis

Submitted in partial fulfilment of the requirements for the award of degree of

Doctor of Philosophy

in

Mechanical Engineering

Submitted by

Rashmi Arora

Regd. No. 951208007

Under the guidance of

Dr. Tarun Kumar Bera
Associate Professor
Department of Mechanical Engineering
Thapar Institute of Engineering & Technology
(Deemed to be University), Patiala

Department of Mechanical Engineering
Thapar Institute of Engineering & Technology
(Deemed to be University)
Patiala-147004, India

July, 2018

This thesis is dedicated to

My Father, Mother

and

My Son

Arunabh Arora

DECLARATION

I certify that

a. the work contained in this Thesis is original and has been done by me under the guidance of my supervisor.
b. the work has not been submitted to any other Institute for any degree or diploma.
c. I have followed the guidelines provided by the Institute in preparing the Thesis.
d. I have confirmed to the norms and guidelines given in the Ethical Code of Conduct of the Institute.
e. whenever I have used materials (data, theoretical analysis, figures and text) from other sources, I have given due credit to them by citing them in the text of the Thesis and giving their details in the references. Further, I have taken permission from the copyright owners of the sources, whenever necessary.

(Rashmi Arora)

CERTIFICATE

This is to certify that the Thesis entitled '**Trajectory Tracking and Impedance Control of Hybrid Manipulators**', submitted by **Ms. Rashmi Arora** to Thapar Institute of Engineering & Technology (Deemed to be University), Patiala, India, is a record of bona fide research work carried under my supervision and is worthy of consideration for the award of the degree of Doctor of Philosophy of the Institute.

16/7/18

Dr. Tarun Kumar Bera
Associate Professor
Mechanical Engineering Department
Thapar Institute of Engineering & Technology (Deemed to be University),
Patiala, India, 147004
Email: tkbera@thapar.edu

Date: 16-7-18

ACKNOWLEDGEMENT

First of all, I wish to thank Lord for given me an opportunity to carry present research work. I am greatly obliged to the authorities of Thapar Institute of Engineering & Technology (Deemed to be University), Patiala for providing me a chance of being a member of this research project and for providing the facilities for the completion of the work. Words are falling short to express my deepest regards and a sense of gratitude to my supervisor **Dr. Tarun Kumar Bera, Associate Professor, Department of Mechanical Engineering, Thapar Institute of Engineering & Technology (Deemed to be University), Patiala** for his fruitful suggestions, unfailing inspiration, whole-hearted cooperation, thought provoking discussions and painstaking supervision for the entire period of this work and making every tough work interesting. His deep insight into the problem and the ability to provide constructive suggestions have been of immense value in improving the quality of my research work at all stages.

I would be obliged to express my genuine thanks to Director, Thapar Institute of Engineering & Technology (TIET), Patiala, Dean, Research and Sponsored Projects, TIET, Patiala, Head, Mechanical Engineering Department, TIET, Patiala and PhD Coordinator, Mechanical Engineering Department, TIET, Patiala for their encouragement and support during this research work. I am also thankful to the authors whose research has helped me a lot. I also wish to express my deep sense of gratitude and respect to the members of Doctoral Committee, Dr. A.K. Singh (Assistant Professor, Mechanical Engineering Department, TIET, Patiala), Dr. Ashish Singla (Associate Professor, Mechanical Engineering Department, TIET, Patiala) and Dr. Maneek Kumar (Professor, Civil Engineering Department, TIET, Patiala) for their unreserved guidance and productive discussions during the period of research. I also take this opportunity to thank the entire faculty and staff of Mechanical Engineering Department, TIET, Patiala, for their help, inspiration and moral support throughout this period.

I express my sincere thanks to Dr. Santu Maiti (Ex Senior Resident, Department of Obstetrics and Gynaecology, Chittaranjan Seva Sadan, Kolkata), Dr. PC Gupta (Prem

Hospital, Patiala) and Dr. BPS Dhillon (Dhillon Diagnostic Centre, Patiala) for their help and support in completing my research objectives.

In the end, I have the privilege to show regards and express a sincere thanks to my family, especially my mother and my brother, Mr. Vishal Preet Arora and his wife Mrs. Tania, for supporting, motivating and encouraging me at every step of my work and always cooperating with me in every situation. No amount of words is enough to thank my mother, who is always a key behind my every successful work. She single handedly managed all family matters and also took care of my small naughty kid, Arunabh. I had lost all hope and courage to do anything at the beginning of my research. But, it is the power of her as well as my late father's blessings and moral support at every step of my life that I would have been able to complete my research work and dissertation with courage, confidence and zeal for hard work.

I would also like to thank my cousin, Mr. Paramveer Sharma and my peers, Mr. Manarshhjot Singh, Mr. Dharmveer Aggarwal, Mr. Vikram Singh Jamwal, Mr. Jatinder Kataria, Mr. Rajmeet Singh, Mr. Gautam Setia, Mr. Atul Sharma and Ms. Garima Soharu for their help and open discussions. So, I finally thank all the people, who helped me directly or indirectly, in finishing this research work.

(Rashmi Arora)

ABSTRACT

Usually, industrial robots are made up of serial manipulator architecture having large workspace but these suffer from several drawbacks such as low accuracy and heavy structural vibration. Similarly, the parallel architecture robots have better accuracy but small workspace. Therefore, in the last two decades, hybrid manipulators addressed great attention as a combination of serial and parallel chain architectures. In an effort to combine the advantages of serial and parallel chains in these manipulators, a brief introduction of hybrid manipulators is discussed here. These manipulators offer the possibility of having advantages of both architectures and reduce their drawbacks. A comprehensive literature review of kinematic and dynamic analysis of hybrid manipulators is done. Literature review on the overwhelming controller and impedance control is also done. Accordingly, the objectives of work are defined after this. A three dimensional hybrid manipulator with six degrees-of-freedom is proposed in the Thesis and this manipulator is made by placing a three degrees-of-freedom parallel manipulator over the other in series so as to increase its workspace and load carrying capacity. The forward and inverse dynamic models for planar hybrid manipulator as well as for 3D hybrid manipulator are developed. All the models are simulated in bond graph domain. The planar hybrid manipulator is validated for a practical application of lateral bending of human vertebrae and the path followed by the thumb of human hand while picking and placing an object. The 3D hybrid manipulator is also tested for trajectory tracking of the thumb of human hand during drawing an arc on white board with a marker pen. The physical models for planar parallel and hybrid manipulators are also reduced with Eigen value sensitivity method to reduce simulation time and complexity of the system. The response of reduced models is compared with full models to track a circular path. The workspace analysis of planar parallel and hybrid manipulators is done additionally and this illustrates that workspace is increased by connecting two parallel manipulators than a single parallel manipulator. Afterwards, the theory of impedance control with some changes is applied for an operation on a three dimensional L-shaped path having some restrictions imposed on the interactive forces when the manipulator is interacting with an object in its environment along with an approach to eliminate amnesia. Finally, the conclusions of the Thesis are presented in the end with scope for future research work.

Keywords: Hybrid manipulator, trajectory tracking, overwhelming control, model order reduction, work space analysis, impedance control, bond graph.

LIST OF ABBREVIATIONS

ARMA	AutoRegressive Moving Average
AWE	Asymptotic Waveform Evaluation
C	Capacitance
CaHyMan	Cassino Hybrid Manipulator
CTF	Coordinate Transformation
De	Effort Detector
Df	Flow Detector
DOF	Degrees-of-Freedom
EJS	Euler Junction Structure
FDI	Fault Detection and Isolation
FSU	Functional Spine unit
GAWE	Galerkin Asymptotic Waveform Evaluation
HIC	Hybrid Impedance Control
I	Inertance
LTI	Linear Time Invariant
MGAWE	Multi point Galerkin Asymptotic Waveform Evaluation
MIMO	Multi-Input Multi-Output
MPVL	Matrix-Padé via Lanczos
MSe	Modulated Effort Source
MSf	Modulated Flow Source
MTF	Transformer with varying Modulus
PID	Proportional-Integral-Derivative
R	Resistance
RCID	Robotic Controlled Impedance Device
Se, SE	Source of Effort
Sf, SF	Source of Flow

NOMENCLATURE

A	Cross-sectional area of shaft (m^2)
c_a	Overall rotational damping (N m s/rad)
c_c	Damping of coupling (N s/m)
c_n	Nut damping (N m s/rad)
c_r	Overall rotational damping (N m s/rad)
c_{sr}	Rotational damping of shaft (N m s/rad)
C_x, C_y	Current positions in x and y directions, respectively (m)
d	Shaft diameter (m)
E	Modulus of elasticity (N/m^2)
$\mathbf{E}_{IC}$	Effect matrix for independent energy storage elements
$\mathbf{E}_R$	Effect matrix for energy dissipation elements
f_i	Flow in the i^{th} bond
F	Input force (N)
F_x, F_y	Force in respective x and y directions (N)
g	Acceleration due to gravity (m/s^2)
G	Shear modulus (N/m^2)
G_x, G_y	Gain in respective x and y directions
$G(s)$	Transfer function
h	Travel distance during shaft's one revolution (m)
$\mathbf{I}$	Identity matrix
J	Mass moment of inertia (kg m^2)
$\mathbf{J}_{SS}$	Connectivity matrix between the outputs and inputs of the energy storage elements
$\mathbf{J}_{SL}$	Connectivity matrix between the outputs of the dissipation elements and the inputs of the energy storage elements
$\mathbf{J}_{LS}$	Connectivity matrix between the outputs of the energy storage elements and the inputs of the dissipation elements
$\mathbf{J}_{LL}$	Connectivity matrix between the outputs and the inputs of the dissipation elements

k, K	Stiffness (N/m)
k_a	Overall axial stiffness (N/m)
k_b	Axial rigidity of bearing (N/m)
k_c	Torsional rigidity of coupling (N m/rad)
k_n	Rigidity of ball screw nut (N/m)
k_r	Overall rotational stiffness (N m/rad)
k_{sa}	Axial stiffness of shaft (N/m)
k_{sr}	Rotational stiffness of shaft (N m/rad)
l	Length of shaft (m)
l_{eff}	Effective length (m)
$\mathbf{L}$	Matrix of energy dissipation elements
L_i	Length of legs (m) (i = 1….3)
L_i^{min}, L_i^{max}	Length of legs for minimum and maximum radii of concentric circles (m) (i = 1….3)
$\dot{L}_i$	Rate of change of leg length of manipulator (m/s) (i = 1….3)
l_{cg}	Distance between the fixed end and centre of gravity of cylinder
l_p	Distance between the fixed end and centre of gravity of piston
l_{pg}	Distance between the fixed end and centre of gravity of piston-rod assembly (m)
m, M	Mass (kg)
Q_1, Q_2	Difference between target and current positions in respective x and y directions (m)
r, R	Damping coefficient (Ns/m)
s	Complex variable
$\mathbf{S}$	Matrix of energy storage elements
S_1	Length of platform *ag* (AG) of hybrid manipulator (m)
S_2	Length of platform *gb* (GB) of hybrid manipulator (m)
t	Time (s)
V_{ref}	Reference velocity (m/s)
w	Width (m)

x , y , X, Y	Displacement in the x and y direction respectively (m)
x_{a_i}, y_{a_i}	Position components of point A_i in fixed coordinate system attached to manipulator base (i = 1….3) (m)
x_{b_i}, y_{b_i}	Position components of point B_i in mobile coordinate system (i = 1….3) (m)
x_{c_i}, y_{c_i}	Coordinates of centre of circle (i = 1….3) (m)
x_d, y_d	Target positions in respective x and y directions (m)
x_{ref}, y_{ref}	Reference displacement in x and y direction respectively (m)
$\dot{x}$, $\dot{y}$	Velocity in x and y direction (m/s)

Greek characters

α , α_i	Controller gain
θ	Rotation about the z-axis (rad)
θ_{a_i}	Motion of i^{th} leg with respect to base (i = 1….3) (rad)
$\theta_{a_i}^{min}, \theta_{a_i}^{max}$	Motion of i^{th} leg w.r.t. base for minimum & maximum radii of concentric circles (rad)
θ_{ref}	Reference rotation about the z-axis (rad)
$\dot{\theta}$	Angular velocity about z-axis (rad/s)
μ	Transformer modulus
μ_H	High gain for overwhelming controller
μ_i	Transformer modulus (i = 1….n)
μ_L	Low gain for overwhelming controller
ϖ	Angular velocity (rad/s)
λ_i	Eigen values (i = 1….n)
ρ	Density (kg/m^3)
σ_i	Transformer modulii

Subscripts

a, b, c, d, e or	
A, B, C, D, E	Geometric locations on the platform
c, con	Controller
cy	Cylinder
C, C_1, C_2	Controller
f	Friction
F	Forward model
g, G	Centre of gravity
gc	Centre of gravity of cylinder
gp	Centre of gravity of piston
I	Inverse model
j	Joint
m	Motor
n	Nut
p, pad	Pad
pi	Piston
P, P_1, P_2	Plant
s	Shaft
t	Table
x, *y*, *z*	*x*, *y*, *z* directions of three dimensional coordinate frame
vel	Velocity

Superscript

*	An estimate (virtual)

PUBLICATIONS FROM PRESENT WORK

[1] **Arora R** and Bera TK. Trajectory tracking through overwhelming control of human vertebrae as hybrid manipulator, *Simulation, Sage*, 2017; 93 (3): 251–263.

Publisher: SAGE, **Category:** SCI, **Impact Factor:** 0.720

[2] **Arora R** and Bera TK. Physical model reduction of a parallel and hybrid manipulator using eigen value sensisitivity method, *Iranian Journal of Science and Technology*: *Transactions of Mechanical Engineering, Springer*, 2017; 1–11.

Publisher: Springer, **Category:** SCI, **Impact Factor:** 0.595

[3] **Arora R** and Bera TK. Trajectory Tracking of 3D Hybrid Manipulator through Human Hand Motion, *Arabian Journal for Science and Engineering, Springer*, 2018; Published online on May 17, 2018.

Publisher: Springer, **Category:** SCI, **Impact Factor:** 0.865

[4] **Arora R** and Bera TK. A Bond Graph Model for Object Grasping and Fingertip motion, *International Conference on Aeronautical, Robotics and Manufacturing Engineering (ARME'2015*) June 15–16, Bangkok (Thailand), 2015; 87–94.

[5] **Arora R**, Agarwal D and Bera TK. Workspace analysis and trajectory tracking of a planar hybrid manipulator with ball screw feed drive, *Simulation, Sage* (**Under Second Review**).

[6] **Arora R** and Bera TK. Impedance Control of Three-Dimensional Hybrid Manipulator. (**To be communicated to *IEEE Transactions on Robotics***).

[7] **Arora R**, Mehta I, Bimbraw K and Bera TK. Design of an Arduino Based Hybrid Parallel Manipulator. (**To be communicated to *IEEE International Conference on Robotics and Automation, ICRA 2019***).

LIST OF FIGURES

Fig. No.	Figure Captions	Page No.
1.1	Kinematic structures of current hybrid manipulators	3
3.1(a)	Model of planar hybrid manipulator	35
3.1(b)	Location of the centre of gravity with respect to the platform	35
3.2	Forward model (plant) for hybrid manipulator	39
3.3	Manipulator leg as piston-cylinder arrangement	40
3.4	Pictorial representation of concept of overwhelming controller for a third order system	43
3.5	Arrangement of the system in bond graph model displayed in Fig. 3.4 with the controller as the virtual system	44
3.6	Signal flow graph of the system whose arrangement in bond graph modelling is displayed in Fig. 3.5	45
3.7(a)	Performance of overwhelming controller for gain value of 10^6	47
3.7(b)	Performance of overwhelming controller for gain value of 10^4	47
3.8	Comparison between displacement errors for the controller with gain of 10^6 and 10^4	48
3.9	Inverse model (controller) for hybrid manipulator	50
3.10(a)	Model of human vertebrae	53
3.10(b)	A single vertebra with motion in different planes	53
3.11(a)	Schema of hybrid manipulator for human vertebrae	53
3.11(b)	Word bond graph model of hybrid manipulator and controller for human vertebrae	53
3.12(a)	Final position in left bending of spinal cord	55
3.12(b)	Intermediate position in left bending of spinal cord	55
3.12(c)	Straight position of spinal cord (vertebrae)	55
3.13	Different positions of vertebra during left and right bending	55
3.14(a)	Final posture (C_4–T_{11}) in left bending (mirror image) of vertebrae obtained from X-ray	56
3.14(b)	Straight position (C_4–T_{11}) of vertebrae obtained from X-ray	56
3.15(a)	Performance (response) of simulator to track the desired trajectory (command) for vertebral point of L_4	58
3.15(b)	Performance (response) of simulator to track the desired trajectory (command) for vertebral point of T_{10}	58

Fig. No.	Figure Captions	Page No.
3.15(c)	Performance (response) of simulator to track the desired trajectory (command) for vertebral point of T_5	58
3.15(d)	Performance (response) of simulator to track the desired trajectory (command) for vertebral point of C_6	58
3.15(e)	Percentage error in *x* and *y* displacements for vertebral point of T_5	58
3.16(a)	Rate of change of leg length without inertia	59
3.16(b)	Rate of change of leg length with inertia and driving effort required	59
3.16(c)	Rate of change of leg length without inertia for leg 'ac' of the manipulator	59
3.16(d)	Rate of change of leg length with inertia for leg 'ac' of the manipulator	59
3.17	Notations of various joints and their representation in human hand	61
3.18(a)	Final position of fingers	62
3.18(b)	Intermediate position of fingers	62
3.18(c)	Initial position of fingers	62
3.19	A bond graph model for thumb and index finger grasping an object	63
3.20(a)	Final position of fingers obtained from X-ray	63
3.20(b)	Intermediate position of fingers obtained from X-ray	63
3.20(c)	Initial position of fingers obtained from X-ray	63
3.21(a)	Trajectory tracking for thumb in *x*-*y* plane	65
3.21(b)	*y*-displacement of the object	65
3.21(c)	*x*-displacement of the object	65
3.21(d)	Velocity of the object in *y*-direction	65
4.1(a)	A mass-spring-damper system	77
4.1(b)	Its bond graph representation	77
4.2	Reduced bond graph model of mass-spring-damper system	79
4.3	Schema of a planar parallel manipulator	80
4.4	Forward bond graph model of a parallel manipulator	81
4.5	Inverse dynamics arrangement in bond graph of a parallel manipulator	82
4.6	Combined bond graph model of a parallel manipulator	83
4.7	Reduced inverse model for a parallel manipulator	86
4.8	Combined bond graph model for planar hybrid manipulator	86

Fig. No.	Figure Captions	Page No.
4.9(a)	Comparison of response of system with the desired trajectory of full model of parallel manipulator	88
4.9(b)	Comparison of response of system with the desired trajectory of reduced model of parallel manipulator	88
4.10(a)	Absolute error in *x* and *y* displacements for full and reduced model of a parallel manipulator	88
4.10(b)	Percentage error in *x* and *y* displacements for full and reduced model of a parallel manipulator	88
4.11(a)	Comparison of response of system to track the desired command trajectory of full model of hybrid manipulator	90
4.11(b)	Comparison of response of system to track the desired command trajectory of reduced model of hybrid manipulator	90
4.12(a)	Absolute error in *x* and *y* displacements for full and reduced model of a hybrid manipulator	90
4.12(b)	Percentage error in *x* and *y* displacements for full and reduced model of a hybrid manipulator	90
5.1(a)	Schematic model of hybrid manipulator	95
5.1(b)	Word bond graph model of hybrid manipulator	95
5.2	Schematic diagram of ball screw feed drive leg	96
5.3	Mechanical equivalent of ball screw feed drive leg	97
5.4	Forward model of ball screw feed drive	98
5.5	Inverse model of ball screw feed drive	99
5.6	Forward model of the planar hybrid manipulator	101
5.7	Inverse model of the planar hybrid manipulator	102
5.8	Modified forward model of the planar hybrid manipulator	104
5.9	Modified inverse model of planar hybrid manipulator for target reaching	106
5.10(a)	Comparison of plant response with controller command to track the given trajectory for lower manipulator	111
5.10(b)	Comparison of plant response with controller command to track the given trajectory for upper manipulator	111
5.11(a)	Error in absolute values in displacements in *x* and *y* directions for lower manipulator	112

Fig. No.	Figure Captions	Page No.
5.11(b)	Error percentage in displacements in *x* and *y* directions for lower manipulator	112
5.12(a)	Error in absolute values in displacements in *x* and *y* directions for upper manipulator	112
5.12(b)	Error percentage in displacements in *x* and *y* directions for upper manipulator	112
5.13(a)	Displacement of manipulator from initial position to final position	113
5.13(b)	*x*-*y* path of the hybrid manipulator	113
5.14(a)	Workspace of planar hybrid manipulator for lower manipulator	115
5.14(b)	Workspace of planar hybrid manipulator for upper manipulator	115
5.15(a)	Workspace boundaries of lower manipulator	115
5.15(b)	Workspace boundaries of upper manipulator	115
5.16	Workspace of planar hybrid manipulator	116
6.1(a)	A simplified figure of 3D hybrid manipulator	123
6.1(b)	Its word bond graph arrangement	123
6.2	Forward dynamics model with a single leg	126
6.3	Piston-cylinder arrangement	127
6.4	Bond graph model for coordinate transformation	127
6.5	Forward model for 3D hybrid manipulator	130
6.6	Inverse bond graph model of 3D hybrid manipulator	130
6.7	Model of inverse parallel manipulator	132
6.8(a)	Initial position of thumb in *y*-*z* plane	134
6.8(b)	Intermediate position in *y*-*z* plane	134
6.8(c)	Final position in *y*-*z* plane and initial position in *x*-*y* plane	134
6.8(d)	Position in *x*-*y* plane at some extent	134
6.9	X-ray picture showing thumb and index finger holding the marker	135
6.10	Trajectory tracking of thumb for (a) dislocation in *x* path (b) dislocation in *y* path (c) dislocation in *z* path	139
6.11(a)	Percentage error in *x*, *y* and *z* displacements	140
6.11(b)	Percentage error in *y* displacement	140
6.12	Schema of the integrated impedance controller system	142
6.13(a)	Bond graph model for the robot having control of force	143
6.13(b)	Its signal flow graph	143

6.14	Impedance controller with amnesia removal	145
6.15	L-shaped path to be followed by the moving platform	147
6.16(a)	Reference and actual displacement in *x* direction for controlling force without removal of amnesia	149
6.16(b)	Given input and measured output location in *y* direction for controlling force without removal of amnesia	149
6.17(a)	Input *x* position and output *x* position for controlling force with removal of amnesia	150
6.17(b)	Input *y* position and output *y* position for controlling force with removal of amnesia	150
6.18	Forces of interaction along (a) *x*-direction and (b) *y*-direction	151

LIST OF TABLES

Table No.	Table Captions	Page No.
3.1	Routh's stability table	41
3.2	Parameter values for pedagogical example of overwhelming controller	47
3.3	Parameter values for human vertebrae	54
3.4	Initial positions for human vertebrae	57
3.5	Parameter values for human hand motion	62
3.6	Initial positions for human hand motion	64
4.1	Description of connectivity matrices of a system	72
4.2	Multiplication factors used in model reduction	75
4.3	Parameter values for model reduction of a planar parallel manipulator	83
4.4	Initial conditions for parallel manipulator for model reduction	87
4.5	Initial conditions for the hybrid manipulator for model reduction	89
5.1	Values of parameters for trajectory tracking with ball screw feed drive	109
5.2	Initial conditions for the planar hybrid manipulator for trajectory tracking with ball screw feed drive	110
5.3	Parameters and limits on angles of the manipulator	114
6.1	Angular positions of lower and upper manipulators	124
6.2	Linear positions for different joints of lower and upper manipulators	137
6.3	Parameter values for 3D hybrid manipulator	137
6.4	Initial conditions for 3D hybrid manipulator	138
6.5	Parameter values applied for the simulations for impedance control	146
6.6	Initial conditions for the 3D hybrid manipulator for impedance control	146

TABLE OF CONTENTS

Dedication i

Declaration iii

Certificate v

Acknowledgement vii

Abstract ix

List of Abbreviations x

Nomenclature xi

Publications from Present Work xv

List of Figures xvii

List of Tables xxiii

Chapter 1: Introduction 1–12

1.1 Hybrid Manipulators 2

1.1.1 Applications of Hybrid Manipulators 4

1.1.2 Examples of Hybrid Manipulators 4

1.2 Background and Motivation 5

1.3 Contributions of the Thesis 9

1.4 Organisation of the Thesis 10

Chapter 2: Literature Review 13–32

2.1 Introduction 13

2.2 Modelling of Hybrid Manipulators 13

2.3 Simulation and Control of Hybrid Manipulators 17

2.4 Physical Model Reduction 21

2.5 Impedance Control 24

2.6 Bond graph Modelling 27

2.7 Observations from Literature 30

2.8 Objectives of Present Work 31

Chapter 3: Modelling and Control of Hybrid Manipulator 33–66

3.1 Introduction 33

3.2 Modelling of Planar Hybrid Manipulator 34

3.2.1 Kinematic Model 35

3.2.2 Bond Graph Representation of Hybrid Manipulator 37

3.3 Inversion of System through an Overwhelming Controller 39

3.4 Inverse Model for Planar Hybrid Manipulator 48

3.5 Case Study – I : Trajectory Tracking of Human Vertebrae 50

3.5.1 Structure of a Human Vertebrae 51

3.5.2 Simulation Results 53

3.6 Effect of Leg Inertia 59

3.7 Case Study – II : Trajectory Tracking of Thumb and Index Finger for Object Grasping 60

3.7.1 Structure of a Human Hand 60

3.7.2 Simulation Results 61

3.8 Conclusions 66

Chapter 4: Physical Model Reduction of Parallel and Hybrid Manipulator 67–92

4.1 Introduction 67

4.2 Physical Model Reduction Technique 68

4.2.1 Representation of Linear Time Invariant System Using Bond Graph 70

4.2.2 Physical Model Reduction Procedure 74

4.2.3 Model Reduction for Pedagogical Example 77

4.3 Physical Model Reduction of a Planar Parallel Manipulator 80

4.3.1 Forward Model of Planar Parallel Manipulator 80

4.3.2 Inverse Model of Planar Parallel Manipulator 81

4.3.3 Full Bond Graph Model of Planar Parallel Manipulator 83

4.3.4 Reduced Bond Graph Model of Planar Parallel Manipulator 83

4.4 Physical Model Reduction of a Planar Hybrid Manipulator 85
4.5 Simulation Results 87
4.5.1 Results for Planar Parallel Manipulator 87
4.5.2 Results for Planar Hybrid Manipulator 89
4.6 Conclusions 91

Chapter 5: Target Reaching and Workspace Analysis of Hybrid Manipulator 93–118

5.1 Introduction 93
5.2 Modelling of Planar Hybrid Manipulator with Ball Screw Feed Drive 95
5.2.1 Model of Manipulator Leg with Ball Screw Feed Drive 96
5.2.2 Model of Moving Platform with Ball Screw Feed Drive 100
5.3 Target Reaching of Planar Hybrid manipulator 103
5.4 Workspace Analysis 106
5.5 Results of Simulation 108
5.5.1 Trajectory Tracking 110
5.5.2 Target Reaching 112
5.5.3 Workspace Analysis 113
5.6 Conclusions 116

Chapter 6: Impedance Control of Three Dimensional Hybrid Manipulator 119–152

6.1 Introduction 119
6.2 Modelling of 3-D Hybrid Manipulator 122
6.2.1 Kinematic Model 123
6.2.2 Bond Graph Model of 3-D Hybrid Manipulator 125
6.2.3 Inverse Model of 3-D Hybrid Manipulator 130
6.3 Application to Human Hand Motion 132
6.3.1 Structure of a Human Hand 133

6.3.2 Simulation Results of Trajectory Tracking 134
6.4 Impedance Control of 3-D Hybrid Manipulator 141
6.4.1 Impedance Control Technique 142
6.4.2 Amnesia Removal Technique 144
6.4.3 Parameters of System and Initial Positions 145
6.4.4 Interaction Force Control 147
6.5 Conclusions 151
Chapter 7: Conclusions 153–156
References 157–172
Curriculum Vitae 173

Chapter 1

Introduction

Robotics is an exciting, dynamic interdisciplinary field of study. Industrial robots are generally referred as robotic manipulators. Since, the aim of the manipulator is the manipulative task and it is generally identified as the mechanical sub-system due to which a robot has the mechanical capability. Several operations are referred in the term "manipulation", which contains

- Gripping and leaving the objects;
- Interfacing with an object unrelated to robot or with environment;
- Moving and transporting objects and/or robot boundary.

According to the connectivity of kinematics in the structural design of the manipulators, these are classified into two types, namely serial manipulator and parallel manipulator. A serial manipulator is identified as a mechanism which has an end-effector attached to the base through only one serial chain, whereas, a mechanism has a movable platform attached to another platform which is fixed through minimum two kinematic chains. Moreover, there is a familiar distinction between these two manipulators. To be more exact, the kinematics for forward system in a serial manipulator is direct but for inverse system is difficult, whereas, for parallel manipulators, reverse is correct. Most industrial manipulators have a serial kinematic architecture with a cantilever type structure. Fully parallel kinematic architectures had been used for a long time in tyre testing [Gough & Whitehall, 1962], flight simulators [Stewart, 1965–1966] and now also used in case of robots and machine tools.

From the time when manipulators have been introduced, they found applications in numerous fields. In spite of this, none of the identified manipulator designs is appropriate for each and every job. It is noticed significantly that majority of industrial manipulators possess a serial kinematic structure which results in a cantilever type design. This type of structure is mostly suitable for those applications which have a bigger working volume, such as in painting in any automobile industry. Though, the mechanical structure of a

manipulator with a serial kinematic chain requires each segment to support not only the mass of the object, but the mass of all successor segments which also includes the mass of motors, in most cases. This cantilever structure often suffers from a lack of rigidity, introduces positioning inaccuracies and undesired dynamical side effects such as low-frequency oscillations. On the other hand, the load-carrying capacity of most industrial serial robots, when quantified in terms of the ratio of the mass of the load to that of the robot, does not exceed the value of 0.15 [Zanganeh & Kourosh, 1995].

Parallel manipulators have major benefits than serial manipulators related to a large ratio of capacity of manipulator to carry load as compared to weight of the manipulator and ability of positioning due to its rigid architecture. But, this kind of structure has less workspace in comparison of the manipulator's size. Henceforth, both the serial and parallel formations possess individual benefits and drawbacks. So, hybrid manipulator may be used for considering advantages of both the manipulators.

1.1 Hybrid Manipulators

In 1990s, the study of robotics had been specified for the robotic mechanisms having 'hybrid' structure and containing both modules, *i.e.* serial-chain and parallel-chain, which are having either serial or parallel connectivity. A set of planar hybrid manipulators having three parallel elements with single degree-of-freedom (DOF) connected in series was presented [Ricard & Gosselin, 1993].

Hybrid manipulator is termed as a kinematic arrangement combining two groups of kinematic chains, which are named as serial and parallel that produces a design having minimum six degrees-of-freedom. Based on their definitions in the literature, current hybrid manipulators can be categorized into two main groups

- The hybrid *parallel-serial chain* with parallel modules connected in series.
- The hybrid *series-parallel chain* containing parallel modules connected in series by serial sub chains [Zanganeh & Kourosh, 1995].

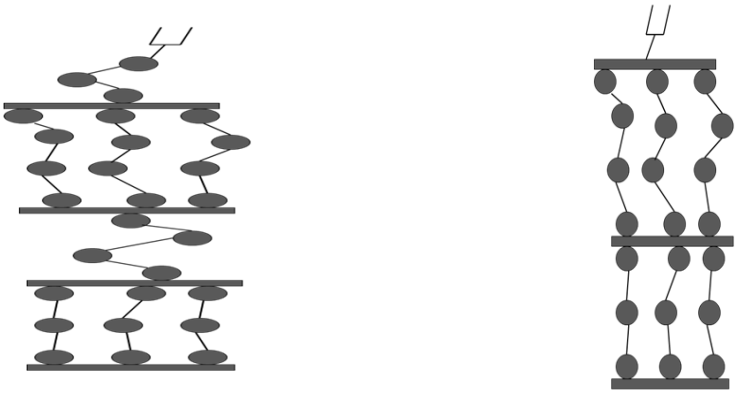

(a) Hybrid series-parallel chains (b) Hybrid parallel-serial chains

Fig. 1.1 Kinematic structures of hybrid manipulators [Zanganeh & Kourosh, 1995]

After observing the opposite benefits coming from both types of manipulators, *i.e.*, serial and parallel, it is obvious that a design including both types in a hybrid arrangement is proposed. Also, it offers new means of designing robotic systems which include multiple-cooperating manipulators, multi fingered grippers and walking machines. One easily finds models of these architectures in humans and animals locomotion system after noticing the high basis of varied designs in nature. The hand of a human being can be considered as an example of a hybrid structure, which in reality is a complicated arrangement of bones, considered as links, muscles and tendons collectively considered as joints and actuators which are controlled in parallel. This pattern in a human hand's structure produces a greatly efficient and superfluous system that is able to move at a very high speed, operate jobs of large accuracy and bear large weights within a noticeable big workspace.

The top attributes of serially connected or parallel connected robotic arrangements are exploited for hybrid manipulators. The robots having parallel connectivity give stiffness in structure with reduction in manipulator's total mass while robots with serial connectivity propose higher workspace. The rigidity and correctness of a hybrid manipulator can be compared with a parallel manipulator and the workspace of a hybrid manipulator can be said equivalent to a serial manipulator.

1.1.1 Applications of Hybrid Manipulators

The major benefits of hybrid manipulators are in the areas which need large precision and handy workspace. These advantages which can be realized through hybrid structures have motivated a number of robotic researchers and manufacturers to develop novel hybrid manipulators. The major applications of hybrid manipulators are as follows:

- Propeller grinding [Lee *et al*., 1999].
- Medical surgery [Ceccarelli *et al*., 2002; Peng *et al*., 2016; Singh *et al*., 2017].
- Pole climbing [Zakerzadeh *et al*., 2004].
- Components manufacturing [Yang *et al*., 2008].
- 3-D manipulation of microscopic objects [Ramadan *et al*., 2009].
- Robotic lion dance [Yan *et al*., 2010].
- Flight simulation [Wang & Chen, 2015a, Wang & Chen, 2015b].
- Robotic devices which include multi fingered grippers, walking machines *etc*. [Zhang & Song, 1992; Boughdiri *et al*., 2012].

1.1.2 Examples of Hybrid Manipulators

Typical industrial examples of hybrid designs can be found in serial manipulators that incorporate parallel actuations such as Cincinnati Milacron [Cincinnati & Milacron, 1980; McCain, 1985], Asea [Heginbotham *et al*., 1979], Cybotech [Ardayfio & David, 1987], *etc*. The examples of hybrid parallel-serial chain are LOGABEX's robot LX [Merlet, 2012] and MultiCraft robot [Kochan, 1996]. Some other significant examples of hybrid manipulators already developed are

- ARTISAN developed in Stanford University (USA) [Waldron *et al*., 1989; Khatib *et al*., 1991].
- HRM developed in Korea Institute of Machinery and Materials (Korea) [Choi *et al*., 1999].
- GEORGEV developed by Institute of Production Engineering and Machine tools (Germany) [Tonchoff *et al*., 1998].

- UPS arm developed at the California University at Davis (USA) [Cheng, 1994].
- CaHyMan (Cassino Hybrid Manipulator) developed at Laboratory of Robotics and Mechatronics in Cassino (Italy) [Carbone, 2001].

1.2 Background and Motivation

The word 'hybrid' basically means mixture or combination of serial and parallel manipulators to exploit top attributes of both of them. A hybrid parallel-serial manipulator is a manipulator having number of parallel manipulators connected serially to each other. In everyday life, popularity of hybrid manipulators is increasing because of their high stiffness, larger workspace, greater accuracy *etc*. as compared to serial and parallel manipulators. It can be used for performing a variety of jobs like trajectory tracking, force control *etc*.

A closed-loop six–DOF parallel manipulator, known as Stewart platform, was formally introduced by Stewart [Stewart, 1965–1966] in 1965 to be used as a flight simulator. Basically, [Gough & Whitehall, 1962] developed it firstly for tyre testing due to its rigidity, high load capacity and precision of position. It was a 6–DOF mechanical device whose upper platform is moving with a fixed base and six prismatic actuators connect them together. A hybrid parallel-serial manipulator is proposed in the thesis which has two three–DOF parallel manipulators connected to each other in series for the planar case. It has a fixed base, a middle platform and an upper movable platform to which the tool would be attached. The base and middle platform are attached to each other by six prismatic actuators through pin joints. These actuators can be actuated hydraulically or electrically.

All the robotic structures should be managed accurately for performing a required job. The motive is generally to chase a particular route at some specific speed. The manipulator's movement is decided within its workspace derived from kinematic analysis. There can be some restrictions on forces of interaction when a manipulator comes in contact with the environment or an object. These control movements require

calculation of forces that the legs (actuators) of a hybrid manipulator apply. The dynamic model of the mechanism, *i.e*. the model for forward dynamics is used to compute the motions resulting from a set of forces acting on the mechanism. In contrast, the model for inverse dynamics of a mechanism is used to compute the forces for required motions. The model for inverse dynamics and inverse kinematics differentiate from each other for the reason that the dynamic model considers the result of the dynamical forces acting on the mechanism.

An overwhelming control approach is a type of indirect approach of doing system inversion and is used in robot control. This scheme is powerful with respect to uncertainties in parameters and measurements. This strategy has already been applied to many serial manipulators and parallel manipulators [Bera *et al*., 2010]. It becomes cumbersome to use it for parallel and hybrid parallel-series manipulators directly because the manipulator links form a closed loop kinematic chain. This thesis involves application of overwhelming control approach for hybrid parallel-series manipulators. To the understanding of this author, no such effort has been reported in the literature.

The performance of the designed controller developed in the thesis for hybrid manipulators is studied through few examples. Firstly, the human vertebrae are considered as hybrid manipulator where each vertebral unit is considered as a parallel manipulator and one vertebra is placed over other in series. The lateral bending of human vertebrae on the frontal plane is checked. Its second application is to track the trajectory by the thumb and index finger considering them as hybrid manipulators while grasping an object. Also, a three-dimensional model of hybrid manipulator is developed in the thesis with its practical application of trajectory tracking of thumb of human hand while drawing an arc. Hence, this hybrid manipulator can be used in multi fingered robotic grippers, pick and place operations, machining operations, moving things *etc*. Further, in another application dealing with L-shaped path to be followed by a tool mounted on the upper moving platform, some compensation are there in order to allow impedance control (force control) by the controller which depends on its interaction with the environment. In case, the interaction forces become more than predetermined limits, these are adjusted by modulating virtual impedances in the controller domain.

The reason for selecting the application of bending of human vertebrae is that the body part of all humanoid robots developed for sports and games is generally rigid. For the application of these robots to execute spine bending sports activities like pole-vault, back vault, high jump *etc*., the body-part must be made of flexible articulated components. To increase the flexibility of these robots, human vertebrae model with flexibility may be implemented. The compression, decompression and the lateral bending of human vertebrae on the frontal plane is mainly controlled by contraction and extension of one of the erector spine muscles. Hence, a biologically inspired flexible robot with articulated vertebrae structure (such as human vertebrae and elephant's trunk) is proposed here and its motion in a plane is considered. The functional spine unit (FSU) along with spine muscle can be treated as the actuators and position sensors are required for online monitoring of humanoid robot body with vertebrae structure. The inverse model of this system along with the high gain-overwhelming controller will control the motion of this artificial human body with vertebrae as per the requirements. This robot may have better dexterity in comparison to existing humanoid robots.

Another application is the movement of different joints for the thumb and index finger of the left hand in *x-y* plane (planar motion) while grasping an object. The fingers gradually come closer to each other and finally, the smaller object is grasped by the finger. The basic idea behind this application is to chase the path followed by a manipulator at the time of object grasping so that it is suitable for use in pick and place operations or moving things *etc*.

Another major area considered in the thesis is to track the trajectory by the different phalangeal joints of thumb of right hand by considering thumb as a three-dimensional hybrid manipulator while drawing an arc of 60° on a white board with the help of a marker pen. The motive behind this is that the hybrid parallel-serial manipulator developed in the thesis can be used for any type of machining operation or performing surgeries in medical field. By using hybrid manipulator in medical field, the efficiency of an operation may be much higher than an operation performed by any human being.

Most of the robotic systems are complex in nature consisting of mechanical, electrical, thermal and fluidic components or sub-systems. The large complex systems are not manageable with respect to design, optimization, storage and computational requirements. An approach to overcome the obstacles of high computation time and cost requirements is there so that a reduced model of the system can be obtained, without compromising on the accuracy. Therefore, a higher order model is reduced to a lower order model (of manageable size) whose response is same as the actual physical system. The model is reduced in such a way that the dynamics of the reduced model remains same as the original system. Henceforth, requirement of less computation time and low cost is the motivation to develop a reduced model for planar hybrid manipulator.

The workspace analysis of planar hybrid manipulator is also illustrated in the thesis to illustrate the increase in workspace area of a hybrid parallel-series manipulator as compared to the parallel manipulator for a specific task. This shows the basic reason for increasing use of hybrid manipulators for different operations in various industries now-a-days.

The overwhelming controller applied for doing inversion of a system is applied for trajectory tracking only. The hybrid manipulator can also perform a variety of jobs like machining and medical surgeries in which interaction force control is essential in addition to the accuracy of position. This force control is known as impedance control which is a difficult assignment. By doing suitable changes, the impedance control can be done with the use of overwhelming controller. The forces of interaction are adjusted at the time of interaction after amending the impedance at the boundary of manipulator with its environment. The case study done in the thesis involves an operation of a L-shaped path in a three-dimensional space with some restrictions applied on the forces of interaction. This study symbolically represents other applications of the hybrid manipulator including impedance control. All the modelling is done using bond graph technique.

Bond graph modelling is a general approach which enables integrated method for the modelling of a physical system in different fields. This skill is most suitable for modelling of large and complicated multibody systems related to a module. Also,

effective algorithms for control can be developed by investigating a structure made in bond graph and hence, model can be suitably changed. The bond graph's causal structure illustrates how computer simulation of the system can be produced by combining element constitutive relations. A model for inverse dynamics can be generated by doing different causal orientation to a bond graph model. This is the reason behind the increasing use of bond graph modelling in design of mechatronic systems. The whole simulation is done in the thesis through bond graph modelling. It is also used to develop a controller model because the hybrid manipulator proposed in the thesis is a simple multibody system involving different areas of energy like mechanical joints, hydraulically actuated legs and electronics/electrical controller in force control.

1.3 Contribution of the Thesis

The major contributions of work presented in dissertation are as follows:

- The detailed bond graph models illustrating forward and inverse dynamics for a three degrees-of-freedom planar hybrid manipulator (including actuated legs) have been developed and validated through two applications of lateral bending of human vertebrae and trajectory tracking of thumb of a human hand at the time of object grasping.
- An effective and correct model showing inverse dynamics of planar hybrid manipulator has been developed for its application in real life. It was demonstrated that an inverse controller representing all kinematic constraints whereas neglecting few dynamic factors, was adequately correct due to the large gains of feedback used for overwhelming control scheme.
- A reduced bond graph model for planar parallel manipulator and planar hybrid manipulator has been developed and tested for trajectory tracking so that dynamics of the system remains same and accuracy is not affected.
- Another bond graph model for planar hybrid manipulator which has actuators as ball screw feed drive mechanisms has been developed for forward and inverse dynamic arrangements. This also contains forward and inverse sub-models of ball

screw feed drive mechanisms. The result was validated for trajectory tracking of a double semi-circular path.

- The workspace analysis for planar parallel and planar hybrid manipulators has been done with the workspace area also being computed for a particular path along a double semi-circle.
- A detailed bond graph model for a three-dimensional six degrees-of-freedom hybrid manipulator has been designed and this includes bond graph sub models of 3D actuators, coordinate transformations and Euler-junction structures. The three-dimensional model is tested for a real-time application of trajectory tracking of thumb of a human hand while drawing an arc of 60°on the board.
- Different control approaches for hybrid manipulator have been examined like overwhelming control and impedance/force control scheme. A complementary approach has been suggested for impedance control including the method for removing amnesia.
- The approach for impedance control has been validated by considering operation on a L-shaped path when some restrictions are imposed on the interactive force of the tool and object. Accuracy in position becomes less at the time of force control in a hybrid manipulator. This error in position, known as amnesia, has been eliminated when there is no interaction with the help of an amnesia removal technique.

1.4 Organization of the Thesis

The dissertation includes seven chapters in total including this chapter followed by list of references referred in the work. An outline of the role of other six chapters is discussed as follows:

Chapter 2 presents an extensive review of the literature related to the kinematic and dynamic analysis of hybrid manipulators and bond graph modelling of parallel manipulators. Literature on the force/impedance control and overwhelming controller is also explained in this chapter. Then, objectives of the present work are identified from observations illustrated in the literature.

The modelling of planar hybrid manipulator is described in Chapter 3. A control strategy of bond graph implementation of an overwhelming controller understanding inverse model for planar hybrid manipulator is discussed after developing the basic concepts of overwhelming control. The demonstration of forward dynamic model which includes leg inertia is also done in the chapter. Furthermore, it is illustrated that an estimated model for inverse dynamics, which is totally effective, produces rationally correct presentation of trajectory tracking. This inverse model is used to build a combined model for trajectory tracking. The full bond graph model is validated with two real-time applications. First application includes lateral bending of human vertebrae model on the frontal plane and this can increase the flexibility of the humanoid robots for sports and games. Second application discusses trajectory tracking of the various phalangeal joints in thumb of a human hand while grasping an object so that it is suitable for use in multi-fingered robotic grippers *etc*.

Chapter 4 highlights the importance of model reduction methods used to reduce a bond graph model by removing unnecessary elements from the model. The procedure of model reduction by Eigen value sensitivity method is discussed and applied for doing physical model reduction of planar parallel and hybrid manipulator. The model is reduced in such a way that the dynamics of the system remain same but its performance is not affected. The performance of full model with reduced model is compared for chasing a circular path.

The bond graph models for forward and inverse dynamics of a ball screw feed drive mechanism are developed in Chapter 5. Then, this mechanism is used to actuate the prismatic legs of planar hybrid manipulators. Further, these actuator models are used to construct the forward and inverse dynamic models of hybrid manipulator. These models are tested for trajectory tracking of a double semi-circular path. A target reaching model is presented afterwards to show that the manipulator reaches the given target in a suitable time. Additionally, the workspace analysis is also done for planar parallel and planar hybrid manipulators. The workspace area is also calculated from this analysis.

Chapter 6 describes forward and inverse dynamics bond graph modelling of three-dimensional hybrid manipulator. The bond graph models for 3D actuators are also developed. The coordinate transformations and Euler-junction structure are represented in a bond graph arrangement. Finally, this three-dimensional model is simulated for an application of trajectory tracking by different phalangeal joints of thumb in a human hand to draw an arc on a board with the help of a marker pen. The theory of force of interaction and impedance control is discussed in addition to it. Later, a modified theory of impedance control with an approach to eliminate amnesia is illustrated. Finally, this theory is applied for an operation on a L-shaped path which have some restrictions imposed on the interactive forces and its simulation results are detailed here.

Chapter 7 concentrates the conclusions derived from the research work carried out in the thesis. The scope for future research work is also presented in this chapter.

Afterwards, a list of references pertinent to whole thesis is presented in the end. These references have already been cited in all chapters of the thesis.

Chapter 2

Literature Review

2.1 Introduction

In this chapter, a survey of literature on modelling, simulation and control of hybrid manipulators are presented. Afterwards, the literature on physical model reduction is reviewed. In the control of hybrid manipulators, a special focus is thrown on overwhelming control strategy and impedance control as these strategies are applied in the thesis for hybrid robotic manipulators. Later on, a detailed literature review on bond graph modelling is done and this shows how bond graph has been used for modelling of various systems in different fields. In the last, the objectives of the present research work are summarised based on the observations made from the literature.

2.2 Modelling of Hybrid Manipulators

Hybrid manipulators play a major role in automation and robotics applications. The major applications like flight simulators [Wang & Chen, 2015a, Wang & Chen, 2015b] and medical surgeries [Ceccarelli *et al*., 2002; Peng *et al*., 2016; Singh *et al*., 2017] require a large workspace as well as greater accuracy which can't be achieved by serial or parallel manipulators alone. The hybrid manipulators have a bigger workspace and high stiffness with high efficiency. Therefore, these can also be used in various robotic devices like multi fingered grippers [Zhang & Song, 1992] and walking machines [Boughdiri *et al*., 2012].

A closed-loop six DOF parallel manipulator, known as Stewart platform, was formally introduced by Stewart [Stewart, 1965–1966] in 1965 to be used as a flight simulator. Basically, Gough & Whitehall [1962] developed it firstly for tyre testing due to its rigidity, high load capacity and precision of position. The hybrid manipulators came into existence in 1980–1990. A development on hybrid manipulators was carried out by presenting a set of planar hybrid manipulators having three parallel elements with single

degree-of-freedom connected in series [Ricard & Gosselin, 1993]. The position and velocity kinematics [Huang *et al.*, 1993; Huang & Ling, 1994] was studied for a class of 6 DOF hybrid robot mechanisms which have a 3 DOF actuated module in series attached with the movable plate of one more 3 DOF actuated manipulator in parallel. Most common approaches to solve the problems for forward and inversed dynamics have been launched for elements connected in both serial and parallel chains. Firstly, the conditions for constraint compatibility required for getting proper results is found and afterwards, the formulation result for a joint rate for the joint hybrid system is illustrated along with its authenticity demonstrated. One more type of hybrid parallel-serial manipulator named as CaHyMan (Cassino Hybrid Manipulator) was examined in characteristics of terms of stiffness [Carbone & Ceccarelli, 2004]. The conduct of stiffness has been explored with use of proper approaches so that solutions in closed form are obtained. The stiffness matrices for serial and parallel manipulator are calculated separately and then stiffness of the hybrid manipulator is found. It is confirmed that the manipulator operates very efficiently in static or quasi-static applications like surgeries. The design of a planar free-flying manipulator was proposed with a new methodology [DasGupta, 2007]. A planar manipulator having two links attached on a satellite base is used to simplify the non-holonomic motion planning problem for its application in space robots.

A hydraulic actuation system is generally used to actuate the legs of a hybrid parallel-series manipulator that includes servo mechanism, servo cylinder, controller, loads, and hydraulic power supply. The force and position control of a hybrid manipulator is also done with hydraulic actuators with greater accuracy [Sirouspour & Salcudean, 2001]. The dynamics of the actuators should be taken into account for predicting the performance in tracking a position. A dynamic system can be improved using passive or active compensation, or both combined [Connoly & Longoria, 2009]. An explicit way is presented for formulating topologies of the system so that passive and active elements can be employed for achieving the desired target.

Flexible joints can be used for a six link serial manipulator [Sarkhel *et al.*, 2013] to have higher performance efficiency as compared to a manipulator with rigid joints. The joints of a hybrid manipulator in present work are mainly translational or prismatic joints.

A prismatic joint generally represents a pure linear motion along its axis. This motion is only a single degree-of-freedom motion in one direction along the axis of joint which describes the direction of relative translation between two links connecting that joint. The various links of robot mechanisms, axially moving beams and spacecraft members are also connected using prismatic joints [Yuh *et al.*, 1989]. The effect of inertia of the slider should be considered for motion at high speeds whereas it can be ignored for small speeds [Stoenescu & Marghitu, 2004].

Some multibody systems having parallel structure with closed loops like Stewart platform were kinematically formulated recursively which provides dynamic equations of motion to be represented in minimum order for requirement in control and simulation of large systems [Saha & Schiehlen, 2001]. Like parallel manipulators, inverse dynamics must be calculated for controlling hybrid manipulators. Very few research articles are available in literature for studying inverse dynamics of hybrid manipulators for real-time control applications. The major objective of present research is to build a fairly accurate and computationally efficient model to represent inverse dynamics of hybrid manipulators in such a way that the control system can be implemented in a real-time and the system can satisfactorily track the position. An algorithm for the solution of inverse problems by boundary element method is illustrated by Mitra & Das [1992]. In this algorithm, the areas of flaws in material are identified even if shape and location of a part of boundary is unknown to us. But, to solve the straight forward problem of inverse dynamics, bi-causal bond graphs have been used [Gawthrop, 2000] which provides accurate answer for explicit inverse dynamics system [Ngwompo *et al.*, 2001]. In contrast, a loop for feedback having a higher value of gain is employed in indirect inverse system for providing answers to inverse dynamics [Samantaray & Ould Bouamama, 2008]. A strategy of overwhelming control is to be used as a strong inversion approach for greater accuracy in trajectory tracking and impedance control with suitable changes [Hogan *et al.*, 1985]. The non-linear dynamic response to discuss the effects of stress softening on hyper elastic strings having ballooning motion rising from the constant speed circular motion with one end fixed were presented to illustrate stability analysis [Bhattacharyya *et al.*, 2015].

The dynamic equations for mechanical systems are generally represented by Lagrange-Euler equations or Newton-Euler equations. This practice is very organized but it needs high logical aptitude. Because of this reason, a well-organized approach was developed [Karnopp & Margolis, 1979] to model planar mechanisms with the help of bond graphs. The dynamic modelling of a commonized Stewart platform was represented by bond graph technique [Yildiz *et al.*, 2007] involving whole dynamics with gravitational effects, dynamics of linear motor along with the viscous friction at the joints. Here, the linear DC motors are considered as method of actuation. Any rigid body in space has minimum six-degrees-of-freedom. The motion of such type of rigid body can be controlled by Newton-Euler equations in a multibody system. These equations are represented in a body-fixed frame which is in line along with the principal axes of the rigid body. A solid technique for representing these Newton-Euler equations is provided by bond graph modelling through a star-shaped junction or constraint structure called Euler Junction Structure (EJS) [Karnopp *et al.*, 2000; Mukherjee *et al.*, 2006]. Newton-Euler equations and Lagrange-Euler equations of motion are derived for dynamics of serial multibody systems like Stanford arm through decoupled natural orthogonal complement matrices [Saha, 1999]. A six degrees-of-freedom hybrid manipulator is proposed in the thesis. It is represented in a bond graph arrangement developed with sub-model of actuators as piston-cylinder models and Euler Junction Structure (EJS) is included for considering gyroscopic terms [Karnopp *et al.*, 2000; Mukherjee *et al.*, 2006]. The actuators of planar hybrid manipulator are also modelled as ball screw feed drive mechanisms to reach a particular target given to the manipulator and to perform its workspace analysis. The linear motion in high speed machine tools are generally given by ball screw feed drives. The dynamics of ball screw feed drives are arranged in a flexible model [Frey *et al.*, 2012] so that rotational motion is transformed into linear motion easily.

The bond graph modelling has been implemented for modelling of general multibody dynamics [Cho, 1998] in terms of kinematic influence coefficients so that computer simulation can be done easily. The potential of powerful bond graph approach is utilized to model and simulate systems which are multidisciplinary [Borutzky, 2009] *i.e.* the

systems consisting of mechanical, electrical, hydraulic or pneumatic components along with the communication of physical effects from different domains of energy. The planar mechanisms which are composed of rigid bodies joined together by a set of joints are represented by modular bond graph modelling [Bera & Samantaray, 2011]. The bond graph modelling is also done for revolute joints with clearance and/or flexibility and mass distribution in prismatic joints so that proper dynamic loads are calculated. The bond graph modelling of planar slider component is done and validated on Rapson slide [Bera *et al*., 2012a]. This technique is used for calculating the dynamic loads in a planar slider component to develop models for V-twin engine and a 3D model of a prismatic joint.

The two rigid bodies connected to each other have some kinematic constraints between them which are implemented by coordinate transformations in such a way that their motions in individual coordinate frames which are fixed to the body are converted into an inertial frame. Consecutively, these coordinate transformations need calculation of Euler angles. The approach of bond graph modelling provides a handy way for performing all these transformations with the help of transformer junction structures. It is noted here that the kinematic transformations are done through the transformer junction structures and the forces can also be transformed with the same junction structure. Therefore, the velocity and force are transformed at the same time in a bond graph model resulting in a well organized representation of the model.

2.3 Simulation and Control of Hybrid Manipulators

The planar mechanisms can be incorporated into models for dynamic systems with usage of bond graphs by utilizing stiff coupling springs at the joints of mechanism [Karnopp & Margolis, 1979]. The inversion of a system is basically a method to find the correct data of input from the given system response with a number of restrictions satisfied. A good approach for inversion of a system is needed for developing control algorithms for mechanisms with great performance. The inversion of a system confirms the restrictions in terms of ranges of the actuators, their slew rates and output levels [Ngwompo & Gawthrop, 1999]. The position and orientation of a planar hybrid manipulator can be identified by three parameters. The torques of the couples which are active in nature are

computed easily if one knows the platform's motion after calculating each joint's rate of change of position and velocity with time and consecutively calculating the linear and rotational forces that acts on a single body in multibody dynamics system. There are three methods to model the inverse dynamics of a system and these are the Newton-Euler classical procedure, the equations developed by Lagrange and multipliers formalism and virtual work principle.

The structure made with the bond graph junctions has conservative nature and hence, it can be utilized to solve the problem of inverse dynamics of a system. In spite of this, the model of an inverse system cannot be suitably illustrated by utilizing usual causality from bond graph glossary. Bi-causal bond graph were built up exclusively with this aim [Gawthrop, 2000; Gawthrop & Bevan, 2007]. This notation of bi-causality divides the assignment of causality into two power factors, named as effort and flow. Two-way information is imposed at one end of a bond by separating the causal strokes. The steps for input can be calculated in terms of parameters of the system, the given response and its derivatives with respect to time up to a definite order if a model made with bond graph is appropriately bi-causalled. This approach is officially termed as an *explicit system inversion* as it is providing an accurate answer for the difficulty in inverse dynamics [Ngwompo *et al.*, 1996; Ngwompo *et al.*, 2001a; Ngwompo *et al.*, 2001b]. If the values of the parameters of system are fully known and the given response is smooth and fully known, it is possible to obtain a neat input sequence. Due to this, bi-causalled bond graphs are a great tool for offline design, such as open-loop control law design and actuator sizing [Ngwompo & Gawthrop, 1999]. However, assigning bi-causality to a complicated system with no linearity and also multi-input multi-output (MIMO) system models in such a way that the resulting model structure is solvable. Furthermore, the given response in virtual applicable system is developed from a simulation model or a prototype of the real system and the values of the parameters are unknown and noisy signals are present. Therefore, a bi-causalled bond graph model-based inversion or any other explicit means of inversion of such systems is unsuitable for real-time applications.

Conversely, methods of *implicit system inversion* utilize a feedback loop with high gain to provide approximate inverse solutions [Samantaray & Ould Bouamama, 2008].

By selecting the parameters of gain suitably, the criterion for convergence is convinced in the limit. The implicit system inversion based on the bond graph model produces differential causalities which are removed through stiff spring-damper combinations in parallel. These stiff spring-damper combinations act as low-pass filters (called propersing filters [Samantaray & Ould Bouamama, 2008]). Hence, it is very easy for handling noisy data in the implicit system inversion scheme. The approach of developing a prototype for a system and simulating control strategies in a software before validating with hardware like developing two different control strategies for sinusoidal and square wave are applied on brushless DC motor [Chaudhari *et al.*, 2016] which has been used in the thesis for present work.

Inverse dynamics of a hybrid manipulator includes many difficulties because of uncertainties in modelling [Tsai, 2000]. Even if the inertia of actuators play a part for approximately 20% in the actuators force; the force due to gravity and actuators inertia are usually removed from the inverse dynamic model so that computational efficiency can be improved [Zhang *et al.*, 2003]. Furthermore, the weight placed on the manipulator is required to be variable. Therefore, the controller must overwhelm these uncertainties while taking these as disturbances which are not known, *i.e.* the controller should be robust against parametric uncertainties.

Overwhelming control approach is a kind of inversion approach of implicit system which is successful regarding uncertainties in parameters and fairly efficient regarding uncertainties in measurements [Ghosh *et al.*, 1991; Pathak *et al.*, 2005; Pathak *et al.*, 2006a; Pathak *et al.*, 2006b; Pathak *et al.*, 2008]. Furthermore, one can apply extra restrictions along with the given trajectory on the performance of a system like force or impedance control with addition of passive degrees-of-freedom to the system model in the controller domain [Hogan *et al.*, 1985; Ghosh *et al.*, 1991; Youcef-Toumi & Gutz, 1994; Pathak *et al.*, 2005; Pathak *et al.*, 2006a; Pathak *et al.*, 2006b; Pathak *et al.*, 2008; Zhu & Barth, 2008]. The approach of overwhelming control has already been utilized by different researchers for getting accuracy in trajectory tracking and controlling force or impedance [Hogan *et al.*, 1985; Youcef-Toumi & Gutz, 1994; Zhu & Barth, 2008]. Therefore the same overwhelming control scheme has been selected to develop an

inverse dynamics system and for controlling force/impedance in a hybrid manipulator in the present research. A proportional-integral-derivative (PID) controller is used for control of a six DOF serial manipulator [Sarkhel *et al*., 2013]. The non-linear dynamic response to discuss the effects of stress softening on hyper elastic strings having ballooning motion rising from the constant speed circular motion with one end fixed were presented to illustrate stability analysis [Bhattacharyya *et al*., 2015]. The outcome of softening of stress on the weight dynamics which is held up by the rubber strings is illustrated graphically [Sarangi *et al*., 2008].

In some applications where environmental conditions are hostile to presence of human beings, for example active military zones and extraterrestrial surfaces, robust mobile systems are used. Hence, a new strategy is proposed [LeSage & Longoria, 2014] to do bi-variate characterization of the process of a mission so that assessment for mission feasibility is improved especially for the missions operating near failure. A novel methodology for parallelization of continuous and hybrid techniques was developed for discrete event system specification [Bergero *et al*., 2012]. For avoiding the global synchronization cost, the time required for simulation for each sub-model is synchronized locally and this new strategy is named as scaled real-time synchronization. Same kind of approach can be used for modelling of a complex system where each sub-model is modelled and then they are connected together. The simulation of a hydrostatic drive system with two motors is done after its modelling with bond graph [Dasgupta *et al*., 2013] and its dynamic performance is analysed. A multi energy complex system built up with bond graph for hoisting mechanism attached to the vehicle having planar oscillation has been analysed with various approaches used for fault isolation, robustness in fault diagnosis, estimation of parameters and prognostics [Ghoshal & Samanta, 2011]. A diagnostic hybrid bond graph model including parameter uncertainties in a system has been used to derive global analytical redundancy relations to address the problem of robust fault detection and isolation [Ghoshal *et al*., 2012].

2.4 Physical Model Reduction

The multi energy domain dynamic systems consisting of mechanical, electrical, thermal and fluidic components or sub-systems are of great importance in today's life. The dynamic systems are very complex in nature as the time required for simulation is large and their computations become difficult. Therefore, the model reduction is done such that the dynamics of the systems are preserved as well as accuracy is same. With this, the simulation time and number of calculations are reduced to a great extent. This reduced model can be used further in design and analysis of a system as it can be more quickly solved than the bigger complex system. The model reduction techniques have been studied by many researchers for the last two decades.

Model order reduction can be done in two ways: First is to solve the full model and then, apply mathematical techniques for obtaining the results in reduced form. Second is to reduce the system and then, find its solution. There are many techniques for model reduction [Orbak *et al.*, 2004]. One such approach is singular value decomposition method [Zhou *et al.*, 1996; Singh, 2015] based on the coordinate transformations. Here, a transformation matrix containing the dynamic characteristics of the system is split into three singular values. The system is first rotated into an intermediate space. Then, it is scaled and rotated into the desired space. Another method based on coordinate transformations is the balancing approach studied by [Moore, 1981]. Here, the system is converted to a particular stable structure to obtain the reduced model. It targets at the worst case scenarios and hence, reduces the order of the transfer matrix between command and response. The shortcomings of the previous method [Moore, 1981] are improved by [Safonov & Chiang, 1989]. They have proposed a Schur method to do stable truncation model reduction. Here, two specific methods are developed to compute random bases for the left and right Eigen value spaces linked with the high Eigen value of the product of the observability and controllability gramians and then projections are defined in terms of these arbitrary bases. A similar type of algorithm to decompose an unstable continuous/discrete time system into fully balanced and unbalanced subsystems with use of actual Schur transformation approach was developed by [Nagar & Singh, 2004]. This algorithm was applied on unstable linear time invariant (LTI) plant. A major

drawback of these methods is that these don't have any information regarding the system's internal structure. Hence, these methods cannot be directly used for the modelling and reducing the systems in physical domain.

There are many methods which provide good approximations and these are generally known as time and frequency domain methods. One of the commonly used time domain methods is moment matching method proposed by [Davidson & Walters, 1988]. It employs singular value decomposition approximation and eliminates some time moments with its help. Another similar method is derived by [Lalonde *et al*., 1992], named as least squares model reduction method. A lesser order equation to predict autoregressive moving average (ARMA) is computed from an ARMA equation having bigger order for this method and power of curve fitting is used to reduce the model. There are many methods related to the frequency domain that exist in the literature. One of such methods is component cost analysis to reduce a model used by [Skelton & Yousuff, 1983]. Component cost analysis determines the contribution of each system element in the overall dynamic performance of the system. The technique for separate treatment of low-frequency and mid frequency ranges is proposed by Xiheng [1987] in Pade approximation method. In this method, the matrix continued fraction is generated by expanding the matrix transfer function and by using the matrix for Routh algorithm with the inversion process and continued fraction expansion.

All the above methods are purely numerical in nature. In addition to these methods, another approach of model reduction in physical domain [Ye & Youcef-Toumi, 2000] is presented to show that the energy exchange pattern of dynamic elements in a system is utilized to identify their importance and lesser important elements can be easily removed from the complex system to make it smaller. This approach can be used for both linear and non-linear systems. Another technique of model reduction [Orbak *et al*., 2003] is used to obtain the reduced model of a system by removing some physical components from the actual model. It is seen that all the components of a system do not significantly contribute to the dynamic behaviour of a system. So, these components which have less power flow are removed from the original model [Louca *et al*., 1997]. Another physical based model reduction method is the singular perturbation method developed by Sueur &

Dauphin-Tanguy [1991]. This technique reduces the system's dimension by estimating the fast and slow dynamics of bond graph models after calculating causal loop gains using reciprocal systems. Some other approaches like Eigen value separation method and Eigen value sensitivity method are also discussed [Orbak, 2010] and these show the relative contribution of components of the system on the system's Eigenvalues with the help of decomposition of physical systems.

A comparison of some model order reduction techniques used for circuit analysis is done by [Slone *et al*., 2002]. These techniques are asymptotic waveform evaluation (AWE), Galerkin asymptotic waveform evaluation (GAWE), multi point Galerkin asymptotic waveform evaluation (MGAWE) and matrix-Padé via Lanczos (MPVL). These techniques are compared using several illustrative numerical examples which analyze how the methods can change depending on the consideration of a radiation or a scattering problem. It is also shown that the efficiency of a method is dependent on the number of outputs required from the FEM mesh. Finally, the MGAWE method is found to be most computationally efficient method, followed by GAWE and then by AWE. A brief introduction to model order reduction is given by Schilders [2008]. The model order reduction is needed for complex problems to save the simulation time and to reduce the storage capacity without any effect on the accuracy of the system. Various examples were considered and analyzed for this work. There is much needed demand for model reduction in the electronics industry containing many inputs and outputs.

Full and reduced order models made in bond graph domain for a Stewart platform which includes the outcomes of dynamics and gravity was studied [Yildiz & Ömürlü, 2011]. The full non linear model included dynamics of a motor with linear motion and viscous friction in all joints whereas reduced order model does not include linear motor dynamics. The state space equations with non-linearity are printed by seeing each model in bond graph and Eigen values for each matrix of system are found for 14 boundary locations of the workspace. Four trajectories are applied to both structures and findings from simulation are matched to verify the performance. A stability analysis of both systems is launched utilizing the state matrix of dynamic structures. This shows that dynamics of a system are not affected much if dynamics of motor are not considered and

the count of state variables are also reduced. The same approach has been used in the present work to develop a model in bond graph with lesser order for planar hybrid manipulator that includes all effects related to dynamics and gravity. Then its performance is compared with full dynamic model for trajectory tracking of a circular path.

2.5 Impedance Control

The forces developed during the safe interaction of the manipulator in company of environment or any object need to be controlled in such a way that the force provided by the manipulator must be less than the secure weight limits of the object with which interaction of manipulator takes place. Hence, it becomes a cumbersome task. This force control is also essential in trajectory tracking because the object or the manipulator can be damaged unexpectedly by any type of discrepancy. In the case of a machine tool attached to the hybrid manipulator coming in contact with the object, chattering phenomenon takes places very commonly. This phenomenon may be abolished by controlling interaction force.

There are two kinds of approaches used to control forces in manipulators. These are direct and indirect approaches [DeSchutter *et al.*, 1997; Siciliano & Villani, 2000]. Force measurement is not needed in indirect scheme. Mass at the point of contact and either stiffness or damping can be controlled in this scheme. The accurate representation of the thing of the environment must be recognized fully whereas it is not necessary in direct force control scheme. The fault between the required force and calculated force is needed in direct scheme. The direct scheme can also be called as hybrid position force control scheme [Assuncao & Schumacher, 2003] while taking in consideration the approach of switching a mode to control force for regulating the impact velocity and for dissipating the kinetic energy before force control. Takaiwa & Noritsugu [2003] have built up an instrument to display force with the use of hybrid manipulator to observe the compliance characteristics on the human skin. In this, force control is done with method of compliance control or indirect force control without the use of force/moment sensor and observing the disturbance. The force at point of contact is identified with estimation of

force/moment and the target compliance is illustrated according to compliance control scheme. The force control can also be done by method of generalized damping control for the manipulator having parallel links with hydraulic actuators having control of velocity [Kosuge *et al.*, 1996]. The indirect disturbance compensation control of planar parallel manipulator is addressed having uncertainties in parameters and external disturbances [Vinoth *et al.*, 2014].

The approach of impedance control has started in late eighties. An algorithm for robot control with non-linearity was presented on a task of contact that involves free motion, constrained motion and the changeover between these two motions [Hogan, 1987]. Then, it was implemented for impedance control without computing inverse kinematics. Both force control and motion control is essential when a manipulator has some contact with the environment. So, force and impedance control was implemented for models having both linearity and non-linearity [Goldenberg, 1988]. The outcomes of dynamics of a manipulator on the performance of position-based and torque-based impedance control approaches were illustrated [Lawrence, 1988] which offers to select the best approach for a specific manipulator. For jobs like grinding and deburring involving disturbances with high frequency which must be rejected by a robot while a steady force is applied, the control approaches must be classy. Hence, a general strategy for impedance control termed as hybrid impedance control (HIC) was launched [Anderson & Spong, 1988] and this suitably tells that which type of control can be used in a particular environment. This strategy has been further expanded as an adaptive control strategy for the condition in which unknown dynamic parameters of the robot are there [Hosseinzadeh *et al.*, 2010] to adjust the uncertainties and achieving system stability. When the impedance control is specified in terms of a required trajectory of motion and a required relationship of dynamics between position errors and forces of interaction, there is generally a mismatch of parameters between the model and the manipulator. The sensitivity of design arises out of this which is reduced by implementing two adaptive controllers to control impedance in a model having no linearity [Kelly *et al.*, 1989]. An approach for impedance control in robot manipulator was introduced by Chan *et al.* [1991]. The impedance is specified as a function of the

required trajectory for motion and for forces of interaction as well as a function of the required second-order impedance function between errors of motion and forces of interaction.

Impedance control can also be achieved without the use of force sensors for a manipulator which can be directly driven [Tachi *et al*., 1991] just by calculating the torque required for each joint so that it can be applied for achieving the required impedance. A continual problem for impedance control is established for manipulators [Cheah & Wang, 1998] in which a target impedance to be followed by a system is given as the actions are repeated. It is fully solved with application on a SCARA robot. In case of an industrial manipulator coming in contact with a planar surface in an environment that is a rigid object with known geometry but position and orientation varying with time, al algorithm was proposed which detects the pose of object based on the forces and moments arising due to environmental interaction and camera's visual data. This strategy is termed as position based visual impedance control [Lippielo *et al*., 2007]. Another approach for impedance control, known as robotic controlled impedance device (RCID) has been introduced [Lopes & Almeida, 2007] and this is basically an acceleration based impedance controller for a six DOF parallel manipulator. This facilitates force limited impedance control as well as position limited force control.

In a flexible robot manipulator, the general strategy of altering the manipulator dynamics into required dynamics of impedance with feedback control having non-linearity cannot be used due to the reason that the number of dynamic equations is more than that of control inputs. Henceforth, an impedance control scheme that utilizes method of trajectory tracking can be used for this case [Jiang, 2008]. The strategy of impedance control is designed for flexible robot arms in which conversion of impedance control into trajectory tracking takes place. This allows impedance control approach to govern motion of a system when some external force acts on an end-effector having some uncertainties in parameters. This also makes the system stable. In the recent times, another robust adaptive impedance control structure is presented [Luo *et al*., 2011]. Here, the robot's arm moves fast towards the target while slowing down its speed to eliminate steady state error before it comes in contact with object so that stability of system is maintained. The

impedance control scheme has already been applied for a parallel manipulator consisting of a fixed and a moving platform attached to each other by three linear actuators which have a prismatic joint, top spherical joint and a revolute joint at the base [Arabshahi & Novinzaeh, 2014]. The inverse dynamics control [IDC] forms the basis for impedance control scheme that utilizes a control term to get rid of non-linearity in the system. A somewhat similar type of scheme for impedance control is used in the present work for hybrid manipulator.

Only a limited number of research papers are accessible in the literatures which handle both the force and trajectory control of hybrid manipulators. It is noted that both force and trajectory cannot be controlled simultaneously; their control is done in steps. The force control becomes active only in the case if forces of interaction are more than the already set limits and the trajectory control becomes active in remaining time. Force control is shown with machining on a spherical surface so that performance of the developed controller can be illustrated [Bera *et al*., 2012b]. Force can be controlled with controlling impedance at the point of contact between the serial space robot and the environment with use of a virtual foundation [Pathak *et al*., 2005] in the controller. This impedance relies on the compensation gain. In the duration of interaction period, force control can be done by modulating the compensation gain. In consequence of this, the response trajectory deviates from the command that is known as amnesia. In simple language, amnesia is the position error accumulated at the time of force control and it can be eradicated when there is no interaction.

2.6 Bond Graph Modelling

Modelling and simulation of physical systems have significant contribution to understand the fundamental principle of their physical phenomena. The essential steps required in modelling are firstly to write the equations for each elementary physical system, second to sort these equations and in last to implement them in a solver. But this strategy turns out to be a lingering process if the system becomes complicated and multi-disciplinary in nature. Hence, a common tool is required which enables to unify the physical modelling of different disciplines. This tool or approach is known as bond graph modelling which

was proposed by Paynter [1961]. The use of bond graph modelling in different fields of engineering has increased to a great extent since its inception. [Breedveld, 1984; Gawthrop & Smith, 1996; Karnopp *et al.*, 2000; Thoma & Ould Bouamama, 2000; Dauphin-Tanguy, 2000; Borutzky, 2004; Mukherjee *et al.*, 2006; Brown, 2007; Samantaray & Ould Bouamama, 2008]. The bond graph is a modelling technique which is preferred than other techniques for educating students in modelling continuous time physical systems [Cellier, 1995].

In the present work, bond graph modelling is used to represent forward and inverse dynamics of the various sub-models that form a hybrid manipulator. A bond graph model is a brief pictographic illustration of dynamics of a system. It is specifically helpful to do analysis of multi-body systems which are made up of sub-systems existing in various energy domains. Therefore, bond graph is a graphic representation of system dynamics which reveal the interaction of energy between the various elements of a system having different energy domains. It is a very powerful tool in modelling complex systems consisting of sensors, actuators and control systems [Gawthrop, 1995; Dauphin-Tanguy *et al.*, 1999; Margolis & Shim, 2001]. It is better than other representations of a system like block diagram and signal flow graph as it represents the bidirectional flow of energy for a system whereas block diagram and signal flow graph represent unidirectional flow. The various softwares which are used for performing the modelling and simulation of physical systems are ENPORT, SYMBOLS Shakti, CAMP-G, Dymola, 20-Sim *etc*. The software used in present research work is Symbols Shakti for bond graph modelling and simulation.

The approach of bond graph modelling is very much adaptable to model a system and formulate its equations. The modelling of the systems having different domains of energy can be easily done in an integrated way depending on the flow of energy and information [Samantaray & Ould Bouamama, 2008]. It is also noted that bond graph is not a tool to solve a problem numerically; it is just an illustration of the structure of a system. Hence, it provides equations of motion having static and dynamic restrictions, but it does not provide numerical solution straight forwardly. For performing the calculative work, one must exploit the general numerical methods. The structure of a

model is exposed by the illustration of lumped parameters and constraints in a bond graph model. The interactions of energy between the elements of a model can be interpreted by seeing the physical connections from the model structure. Simultaneously, the structure of the resulting equations of motion can be observed from which one can predict the problems required for calculation and hence essential modifications can be done to the model which is basically a theoretical sample of model. For this reason, a bond graph model remains in the middle of a portrayal of a physical system and its portrayal mathematically in the form of differential algebraic equations.

In a convoluted energetic system or a mechatronic system, the different energetic models are integrated with multi-disciplinary modelling with bond graph. The strategy of bond graph is also applicable to do modular modelling of big physical systems [Borutzky, 1999]. Complicated systems with multi bodies can be represented in a compact way with multi bond graph modelling [Bos, 1986] or vector bond graph approach [Cho, 1998]. An object oriented modelling language providing a modular approach for modelling of big systems inter-connected to each other is there and named as Dymola [Otter *et al.*, 1996]. A bond graph library was developed through graphical Dymola support [Cellier & Nebot, 2005] and its application shown for different energy domains. Furthermore, effective algorithms for control of a system can be developed easily by doing bond graph structural analysis [Gawthrop, 1995; Dauphin-Tunguy *et al.*, 1999; Ngwompo & Gawthrop, 1999; Pathak *et al.*, 2008]. It is because of all these reasons that applications of bond graph modelling have been increasing day-by-day in designing mechatronic systems [Gawthrop, 1991; Karnopp *et al.*, 2000; Granda, 2002].

The bond graph environment simplifies a dynamic model of a multi-body system [Cho, 1998]. The modelling for dynamics of rigid bodies, mechatronic systems and robotic manipulators has been done widely by bond graphs [Granda, 2002]. The characteristics related to the causal structure of a model representation in bond graph can be utilized to simulate dynamics of a multi-energy system as already done for calculating the dynamic loads in a planar slider component to develop models for V-twin engine and a 3D model of a prismatic joint [Bera *et al.*, 2012a]. These characteristics have also been used to design algorithms for detection and isolation of faults *i.e.* FDI algorithms as well

to monitor chemical reactors [Ould Bouamama *et al*., 2012] and for investigating fault detection and isolation (FDI) characteristics related to the structure of mechatronic systems [Ould Bouamama *et al*., 2000]. The bond graph modelling can also be integrated with external models for FDI of smart actuators [Ould Bouamama *et al*., 2005]. The multi energy models represented in a bond graph arrangements have been utilized to do actuator fault diagnosis [Ould Bouamama *et al*., 2001]. The bond graph modelling can also be used in thermal fields like supervision of an industrial device for generating steam that consists of complicated industrial components [Ould Bouamama *et al*., 2006; Medjaher *et al*., 2006] and simulation of a U-tube steam condenser with vertical arrangement along with a device used for exchanging heat [Medjaher *et al*., 2009]. The bond graphs are also able to do modelling and simulation in case of electrical fields like switched power junction, a three-phase inverter, a series DC motor, rotary electric machines, AC motor *etc*. [Junco *et al*., 2007, Junco & Donaire, 2011]. The planar mechanisms can be very easily modelled with the bond graph approach [Khadabadi & Pilli, 2005]. The area of magnetic levitation has also been explored using the bond graph modelling offering the control of magnetic force in a levitating ball by electromagnet [Mishra *et al*., 2013]. The bond graph tool can also be combined with functional analysis for intelligent and autonomous systems [Chatti N. *et al*., 2013]. Hence, it is observed that the bond graph approach is well suited to model a big complicated system by developing sub-models and connecting them together afterwards to develop a final model.

2.7 Observations from Literature

After doing detailed study of literature on hybrid manipulators, their modelling and simulation, model reduction, impedance control and bond graph modelling, the observations from the literature are as follows:

- It is noted that there are different hybrid manipulators available in literature and kinematic analysis has been done. Forward and inverse kinematic analysis of various hybrid manipulators have already been done but not much work has been done with regard to *dynamic analysis***.**

- Spinal cord and human hand may be considered as hybrid manipulator. The motion of these parts may be analyzed using bond graph technique for *trajectory tracking, target reaching and work space analysis*.
- Parallel manipulators may be converted into hybrid manipulator combining one with the other in series. So, the model of hybrid manipulator must be *reduced in order to simulate faster*.
- The *interaction force* of hybrid manipulator with the environment must be controlled for its safe operation.

2.8 Objectives of the Present Work

According to the literature review, it is found that bond graph is a unified method of modelling physical systems. Bond graph is very powerful in modelling complex systems with interaction of several energy domains [Mukherjee *et al*., 2012]. There is lack of literature in the analysis of hybrid parallel-series manipulator. The objectives of present work are formulated and summary of these objectives are given below:

1. To increase the workspace, maintain trajectory and load carrying capacity of a manipulator by making a hybrid manipulator (parallel-series type) and develop its bond graph model.
2. To perform forward and inverse dynamic analysis for the hybrid manipulator.
3. To perform workspace analysis for the hybrid manipulator.
4. To perform forward and inverse dynamic analysis (trajectory tracking) for the 3-D hybrid manipulator.
5. To perform impedance control of the hybrid manipulator with the help of bond graph.

Chapter 3

Modelling and Control of Hybrid Manipulator

3.1 Introduction

The main characteristic of a hybrid manipulator is its closed loop kinematic architecture just like a parallel manipulator in which all actuators are dependent on each other. The rigidity of a hybrid manipulator is given by the closed loop kinematic architecture that also provides better trajectory tracking accuracy being its key feature. Generally, the control of a serial manipulator is comparatively easier than parallel manipulator because it has actuators that can function independently [Kumar & Mukherjee, 1989; Kumar, 1994]. This chapter deals with the model based control of a hybrid manipulator through overwhelming control strategy.

For real-time implementation of a hybrid manipulator, its model based control needs a geometrically effective and precise model of the system. Furthermore, a detailed model of the system is required for the design of hybrid platform, its components and the control system that accurately represents the dynamic loads. Hence, the size of actuators can be decided suitably and the optimization of the response time of the system and controllers can be done. Therefore, the leg inertias, actuator electro-hydraulics, dynamics of components *etc*. must be taken into account. In addition, any task allotted to the controller like trajectory tracking and impedance control must be performed with this even if some parameters are unreliable and noisy measurements are there. The bond graph modelling is utilized for developing system and controller model and the scheme of overwhelming control is chosen for this. This has already been explained in detail in the literature review presented in Chapter 2.

The organization of this chapter is as follows: Firstly, a planar six degrees-of-freedom hybrid manipulator is modelled with its actuators considered as hydraulic piston-cylinder arrangement. Then, the scheme of overwhelming control for that manipulator is

developed. The pad arrangements (flexibility) are embodied in the inverse dynamic model with bond graph arrangement of the planar hybrid manipulator to eliminate the causal loops. Henceforth, a pedagogical example is shown to prove that trajectory tracking is done accurately and efficiently by an overwhelming controller based simple inverse model. Then, this philosophy is used to form the scheme of overwhelming control for a six degrees-of-freedom (DOF) planar hybrid manipulator. The actuator dynamics or the leg inertia is included in the forward model of planar hybrid manipulator while these are not considered in the inverse system. Hence, the geometrical efficiency of the real-time control system is improved. Then two case studies are shown to illustrate the practical application of planar hybrid manipulator.

3.2 Modelling of Planar Hybrid Manipulator

The schematic model of planar hybrid manipulator is shown in Fig. 3.1(a) where one parallel manipulator is supported on other manipulator in series. The base 'cde' is fixed to the ground and it is attached to the moving platform 'ab' through three legs which are considered as prismatic pairs *i.e.* 'ac', 'ad' and 'be'. The moving platform 'ab' of the lower manipulator becomes base 'c_1e_1' for the upper manipulator. Leg 1 is attached to the base through point 'c' and it is attached to the platform through point 'a'. Leg 2 is attached to the base through point 'd' and it is attached to the platform through the same point with which leg 1 is attached, *i.e.* point 'a'. Similarly, leg 3 is attached to the base through point 'e' and it is attached to the platform through point 'b'. Generally, spherical or universal joints are used to join the legs with the base and the platform in a three-dimensional manipulator. However, here in the planar hybrid manipulator considered here, all the joints are considered as pin joints. The entire pin joints in Fig. 3.1are passive joints because these are not directly controlled. Moreover, the positions of the joints can be changed by the user if required. All the actuators acting as prismatic joints are active joints as these control the movement of moving platform providing effort to the platform. The points 'a', 'g' and 'b' of lower manipulator become points 'c_1', 'd_1' and 'e_1' of base of upper manipulator shown in Fig. 3.1(a). The three leg lengths can be measured and the forces in these legs can be controlled. The leg lengths are calculated by integrating the rate of change of leg lengths that are calibrated using flow sensors in the bond graph

representation. The position and orientation of the platform are calculated by the values of these leg lengths. The base is parallel to the *x*-axis of a fixed coordinate frame '*xyz*' as shown in Fig. 3.1(a). The point 'g' that is centre of gravity is assumed to be in the centre of platform, *i*.e. line 'ab' that is inclined at an angle θ_G with the horizontal axis. The lengths of segments of platform 'ag' and 'bg' are taken as S_1 and S_2, respectively. The location of centre of gravity (g) of the combined system is shown in Fig. 3.1(b). The trajectory and reference velocities of point 'g' will be shown for different applications considered in this thesis work.

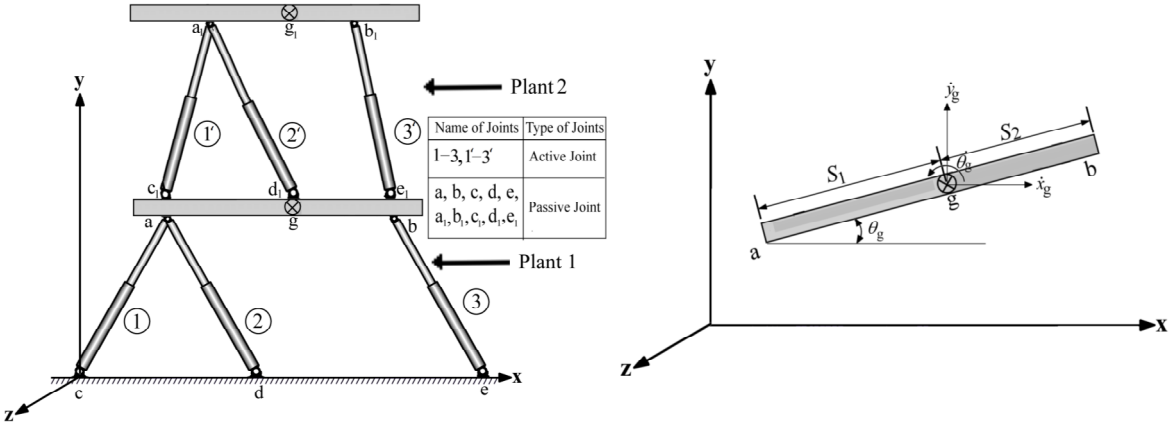

Fig. 3.1(a) Model of planar hybrid manipulator and (b) location of the centre of gravity with respect to the platform

The trajectory and the velocities of point 'g' will be established from an external source in the inverse model and an overwhelming controller is used to calculate the corresponding control forces in all legs. The trajectory specified by the external source can be either a simulation model or measurements from the real system.

3.2.1 Kinematic Model

The points 'a' and 'b' that support the platform have linear velocities denoted by $(\dot{x}_a, \dot{y}_a)$ and $(\dot{x}_b, \dot{y}_b)$, respectively. Similarly, the points 'c', 'd' and 'e' have linear velocities $(\dot{x}_c, \dot{y}_c)$, $(\dot{x}_d, \dot{y}_d)$ and $(\dot{x}_e, \dot{y}_e)$, respectively. In an inertial frame, the platform's points 'a' and 'b' have linear velocities which can be expressed in the form of linear

velocity of the point 'g' in *x*-*y* plane $\left(\dot{x}_g, \dot{y}_g\right)$ and centre of gravity's angular velocity when it rotates about *z*-axis $\left(\dot{\theta}_g\right)$ as

$$\dot{x}_a = \dot{x}_g + \dot{\theta}_g S_1 \sin\theta_g \tag{3.1}$$

$$\dot{y}_a = \dot{y}_g - \dot{\theta}_g S_1 \cos\theta_g \tag{3.2}$$

$$\dot{x}_b = \dot{x}_g - \dot{\theta}_g S_2 \sin\theta_g \tag{3.3}$$

$$\dot{y}_b = \dot{y}_g + \dot{\theta}_g S_2 \cos\theta_g \tag{3.4}$$

The contemporary length $\left(L_1\right)$ of the leg 1 may be expressed as

$$L_1^{\,2} = (x_a - x_c)^2 + (y_a - y_c)^2 \tag{3.5}$$

Differentiating Eq. (3.5) with respect to time, one obtains

$$\dot{L}_1 = \left(\frac{x_a - x_c}{L_1}\right)\dot{x}_a + \left(\frac{y_a - y_c}{L_1}\right)\dot{y}_a \tag{3.6}$$

Similarly, the rates of change of lengths L_2 and L_3 for legs 2 and 3, respectively are obtained as

$$\dot{L}_2 = \left(\frac{x_a - x_d}{L_2}\right)\dot{x}_a + \left(\frac{y_a - y_d}{L_2}\right)\dot{y}_a \tag{3.7}$$

$$\dot{L}_3 = \left(\frac{x_b - x_e}{L_3}\right)\dot{x}_b + \left(\frac{y_b - y_e}{L_3}\right)\dot{y}_b \tag{3.8}$$

The acceleration analysis is not essentially required if linear velocities are written in an inertial frame for representing in bond graph. The considered system can be represented by bond graph and its model can be constructed using Eqs. (3.1–3.4, 3.6–3.8). It is also further noted that the accurate representation of the dynamical constraints is given by the bond graph model that is built from the system because the bond graph

structure is power conservative. Hence, all the force and the moment balance equations are formed automatically.

3.2.2 Bond Graph Representation of Hybrid Manipulator

The forward dynamics for the hybrid manipulator can be represented as the arrangement of a bond graph model as displayed in Fig. 3.2. It is named as 'plant' model. In forward model, the linear velocities $\dot{x}_g, \dot{y}_g$ are represented by the junctions $1_{\dot{x}_g}$ and $1_{\dot{y}_g}$, respectively and rotational velocity $\dot{\theta}_g$ is represented by the junction $1_{\dot{\theta}_g}$. Similarly, points 'a' and 'b' on the moving platform have linear velocities which are represented by the junction pairs $(1_{\dot{x}_a}, 1_{\dot{y}_a})$ and $(1_{\dot{x}_b}, 1_{\dot{y}_b})$, respectively. The lines that have half arrows at their end in this model represent power bonds and the lines having full arrows at their end show exchange of information among the bonds. This forward model is a sub-model that can be connected to the inverse model for trajectory tracking.

The system considered has an assumption that the forces in all actuators are controlled independently. The force in each actuator is assumed to be acting along the direction specified by its orientation. These forces in actuators are modelled by three modulated sources of effort or MSe-elements as shown in Fig. 3.2. The control signals u_1, u_2 and u_3 modulate these MSe-elements and α_1, α_2 and α_3 are the gain parameters linked with the overwhelming control strategy. To measure the rate of deformation of three actuators, three flow sensors *i.e.* Df-elements are attached to the junctions $1_{\dot{L}_1}$, $1_{\dot{L}_2}$ and $1_{\dot{L}_3}$ in the bond graph model. Using Eqs. (3.1–3.4), the junction structure is constructed for transforming the velocities, both linear and angular, of the centre of gravity 'g' to the velocities of points 'a', 'b' and 'c'. In an inertial frame, the centre of gravity has the velocities represented by the 1-junctions that are connected with three I-elements to show the platform's mass (M_P) and the mass moment of inertia (J_P). The source of effort attached to $1_{\dot{y}_g}$ junction that represents the centre of gravity's velocity in the vertical direction models the moving platform's weight. The joints that connect the

actuators 1 and 2 are considered joints having no friction. Likewise, the joint connecting the actuator 3 is also frictionless. The flow detectors (flow sensors) are added to the velocity points for modulating the transformer elements in the model.

The lengths of the three legs 'ac', 'ad' and 'ae' are taken as L_1, L_2 and L_3, respectively. Rate of change of leg lengths are represented by the junctions $1_{\dot{L}_1}$, $1_{\dot{L}_2}$ and $1_{\dot{L}_3}$, respectively and these are given by

$$\dot{L}_1 = \mu_{X1}\left(\dot{x}_a - \dot{x}_c\right) + \mu_{Y1}\left(\dot{y}_a - \dot{y}_c\right) \tag{3.9}$$

$$\dot{L}_2 = \mu_{X2}\left(\dot{x}_a - \dot{x}_d\right) + \mu_{Y2}\left(\dot{y}_a - \dot{y}_d\right) \tag{3.10}$$

$$\dot{L}_3 = \mu_{X3}\left(\dot{x}_b - \dot{x}_e\right) + \mu_{Y3}\left(\dot{y}_b - \dot{y}_e\right) \tag{3.11}$$

where $\mu_{X1} = \frac{(x_a - x_c)}{L_1}$, $\mu_{Y1} = \frac{(y_a - y_c)}{L_1}$, $\mu_{X2} = \frac{(x_a - x_d)}{L_2}$, $\mu_{Y2} = \frac{(y_a - y_d)}{L_2}$, $\mu_{X3} = \frac{(x_b - x_e)}{L_3}$ and $\mu_{Y3} = \frac{(y_b - y_e)}{L_3}$

In this system, the effect of leg inertia is considered only for the plant model. However, the leg inertia is not considered in the inverse model, the controller overwhelms it. The bond graph model of this actuator is given in [Bera *et al.*, 2010]. The support point 'a' connects legs 1 and 2 with frictionless pin joints and point 'b' connects leg 3 in a similar way. The forward model given in Fig. 3.2 can be modified to include the leg model. The dotted portion (plane impedance model) may be replaced by three actuators for considering leg inertia. In Fig. 3.2, the leg joints with the platform may be modelled by a capacitor element having stiffness represented by K_j and a damping element having damping coefficient represented by R_j connected mechanically parallel to each other. Here, the joints cannot be shown (in Fig. 3.2) due to space constraints. The joints should be free to have a free motion of the platform. Joint clearance effects may be modelled [Zeid & Overholt, 1995].

In the actual system, the flow detectors (Df) which are connected to the linear and angular velocities in the inertial frame are not present. Therefore, this inertial sensor is

not implemented in the actual system. The flow detectors are considered in bond graph model to modulate the modulated transformer elements in the part of the junction structure developed using Eqs. (3.1–3.4) and these are used to plot the results.

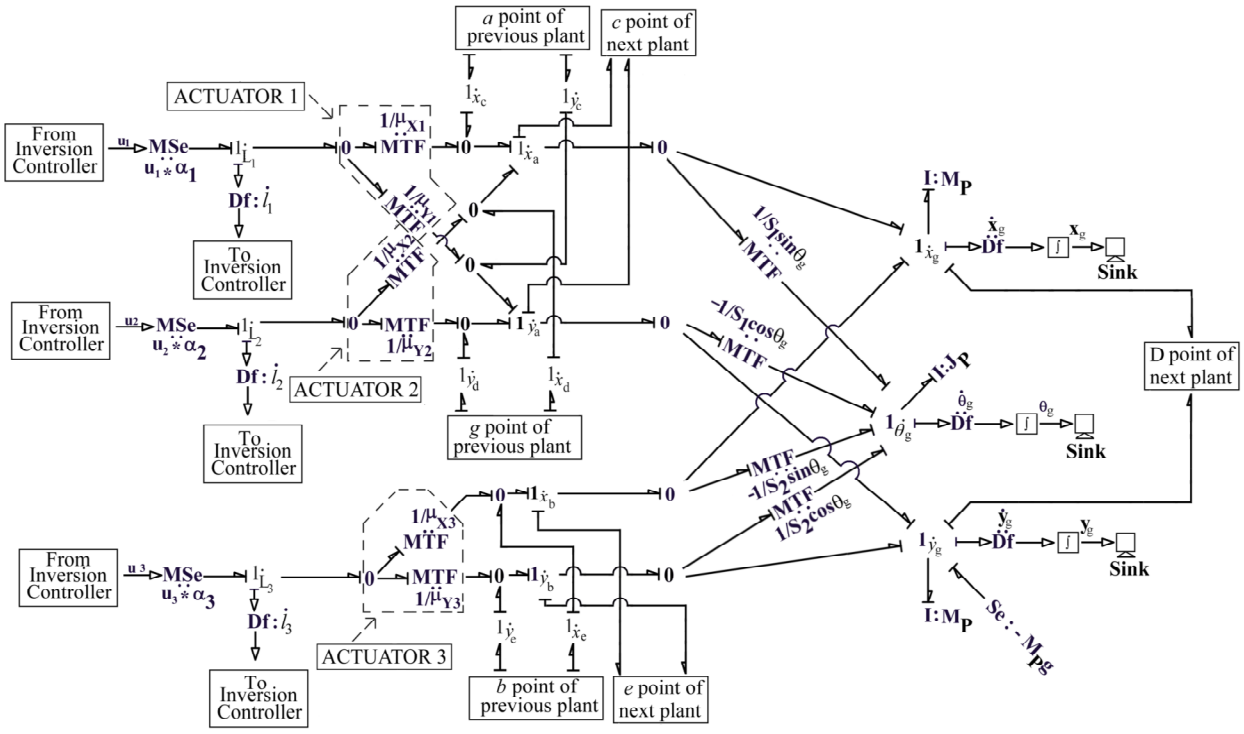

Fig. 3.2 Forward model (plant) for hybrid manipulator

Each actuator of this planar hybrid manipulator is considered a piston-cylinder link as shown in Fig. 3.3 where two ends of actuator are attached to platform and base. In Fig. 3.3 shown here, point 1 is attached to fixed base end and point 2 is attached to end of moving platform. The piston's centre of gravity along with rod is taken as 'gp' that is l_{gp} distant from the rod end. Similarly, the cylinder's centre of gravity is taken as 'gc' and its distance from the fixed end is taken as l_{gc}.

3.3 Inversion of System through an Overwhelming Controller

The plant dynamics are overwhelmed by the controller and this controller is referred as overwhelming controller. It dictates the plant to follow the unaccounted dynamics. A

similar type of example can be taken from real life where a baby (plant here) walks the path dictated by an adult (controller here) who is holding one hand of the baby. Even though the path walked by the baby or the dynamics of the plant is deviated in some directions from the desired path required by an adult or a controller, the overall performance for trajectory tracking is acceptable. In the past, the notion of overwhelming controller has already been used for developing controllers for serial manipulators [Hogan, 1985; Pathak *et al.*, 2005; Pathak *et al.*, 2006a; Pathak *et al.*, 2006b; Pathak *et al.*, 2008] and parallel manipulators and other applications [Youcef-Toumi & Gutz, 1994; Krishnaswamy & Li, 2006; Zhu & Barth, 2008].

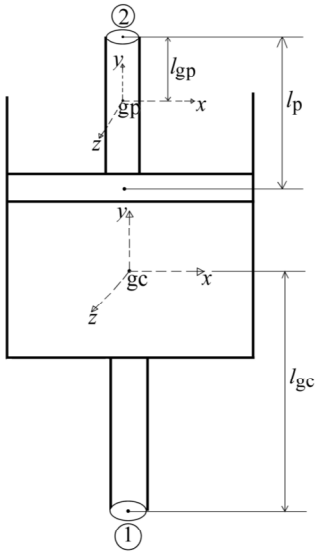

Fig. 3.3 Manipulator leg as piston-cylinder arrangement

For a single degree-of-freedom system with overwhelming controller, the transfer function between the response of the system to the command velocity given to the controller can be written as

$$G(s)=\frac{\mu M_c\left(k_p+r_p s\right)}{M_P M_c s^2+M_P\left(k_p+r_p s\right)+\mu M_c\left(k_p+r_p s\right)} \tag{3.12}$$

All notations are already given in the nomenclature. The characteristic equation for the system is given by

$$M_P M_c s^2 + M_P\left(k_p + r_p s\right) + \mu M_c\left(k_p + r_p s\right) = 0 \tag{3.13}$$

For the stability of the system, Routh's Hurwitz criterion may be used. The tabular presentation of Routh's stability criterion is given by

Table 3.1 Routh's stability table

	s^2	s^1	s^0
s^2	$M_P M_c$	$M_P k_p + \mu M_c k_p$	0
s^1	$M_P r_p + \mu M_c r_p$	0	0
s^0	$M_P k_p + \mu M_c k_p$	0	0

From Routh's Table 3.1, it can be seen that the system will be stable if the following conditions are satisfied:

(1) $M_P M_c > 0$

(2) $M_P r_p + \mu M_c r_p > 0$ or $\mu > -\dfrac{M_P}{M_c}$ if $r_p \neq 0$

(3) $M_P k_p + \mu M_c k_p > 0$ or $\mu > -\dfrac{M_P}{M_c}$ if $k_p \neq 0$

As only positive gains are considered here, the above conditions are trivially satisfied.

The gain of the overwhelming controller needs to be very large for trajectory tracking as per theoretical formulations. But, if the gain value in the actual system is chosen to be too large, the presence of measurement noise and high gain feedback can lead to system instability. In this work, the measurement noise has been neglected. Another disadvantage of high-gain is that it causes the simulations to be stiff and hence, the computations to be performed in the overwhelming controller domain can give feedback delay and that can cause system instability.

The high-gain implicit system inversion concept is demonstrated in [Samantaray & Ould Bouamama, 2008]. If the trajectory to be followed is sharp, high-gain can give unwanted transients. Therefore, a low-pass filter is also used in the feedback loop. The overwhelming controller is similar to that where the functionality of the low-pass filter is implemented by the spring and damper in the overwhelming controller.

A system is passive if it cannot produce energy on its own and can only dissipate the energy that is stored in it initially. More generally, an input/output map is passive if, on average, increasing the output requires increasing the input. Most physical systems are passive. The Passivity Theorem holds that the negative-feedback interconnection of two strictly passive systems is passive and stable. As a result, it is desirable to enforce passivity of the controller for a passive system. In practice, passivity can easily be destroyed by the phase lags introduced by sensors, actuators and communication delays. These problems have led to extension of the Passivity Theorem that considers excesses or shortages of passivity, frequency-dependent measures of passivity and a mix of passivity and small-gain properties.

In this work, the phase lags introduced by sensors, actuators and communication delays are not considered. Thus, the passivity can be demonstrated by Nyquist plot of the system and the controller. A system is passive if the Nyquist plot lies entirely in the right half of the complex plane. For all positive values of system parameters M_p, k_p, r_p and controller parameters M_c, k_c and r_c, it can be shown that the system as well as the controller are passive. As a consequence, stability at any positive gain is guaranteed.

A plain theoretical example is considered here to help in explaining the fundamental theory of robust overwhelming control. The schematic model of a plant and a virtual system in the controller with third order is demonstrated in Fig. 3.4 as an example. The plant is represented on the right side and the controller part is represented on the left side. In Fig. 3.4, the mass, stiffness and damping parameters are represented by M, K and R, respectively and subscripts P and C refer to the real physical domain and controller

domain, respectively. This method is referred as *physical model-based* control where the system's mirror image can be utilized for the controller domain for deriving laws of the controller [Sharon *et al.*, 1991; Gawthrop, 1995].

The velocity pick up picks or senses the velocity of the plant (right side of Fig. 3.4) and then this sensed velocity is compared with the signal of velocity of reference V_{ref}. The difference of these velocities or the error is utilized for the considered system in computational domain (left side of Fig. 3.4), *i.e.* the controller model or the virtual system. The velocity actuator shown in Fig. 3.4 is not a real actuator. A conceptual actuator applies this error in the velocity to the controller system. Then the system in computational domain develops the reactive force as an output. The virtual force sensor senses this force and it is amplified with gain α. Then a real force actuator applies this amplified force to the real system. Hence, a real sensor and a real actuator are used in this system shown in Fig. 3.4. The block's velocity in the actual system is a measured variable and the force applied at that mass is an actuated variable. The controller on the left side of the model controls this force applied at the mass in real system such that the mass in the physical domain moves in a particular way according to the controller. Though a replica of the real system is being used here in the controller side, still it is supposed that the values of the parameters of the real system are not known completely. Due to this reason, the values of the parameters used in real system might be distinct from the equivalent values used in the controller side.

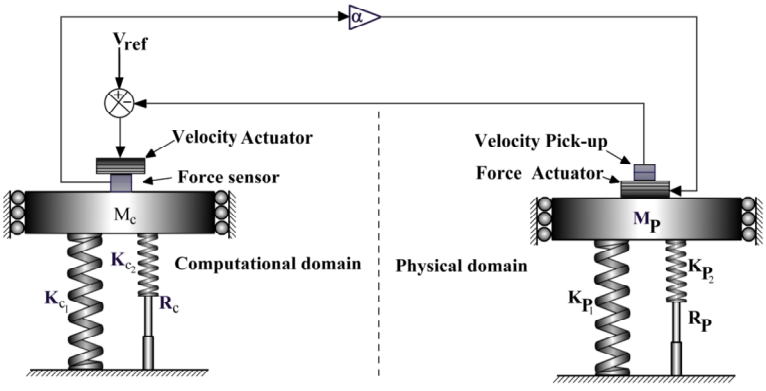

Fig. 3.4 Pictorial representation of concept of overwhelming controller for a third order system

The integrated system in bond graph arrangement with full causalities is displayed in Fig. 3.5(b). This near to actual behaviour of the sensors and actuators used in the model is denoted by superscript *. To overcome various external disturbances and parameters like weight which are not modelled, the body's weight is not included for the controller domain purposely so that the controller's ability to overwhelm external forces or disturbances which are un-modelled.

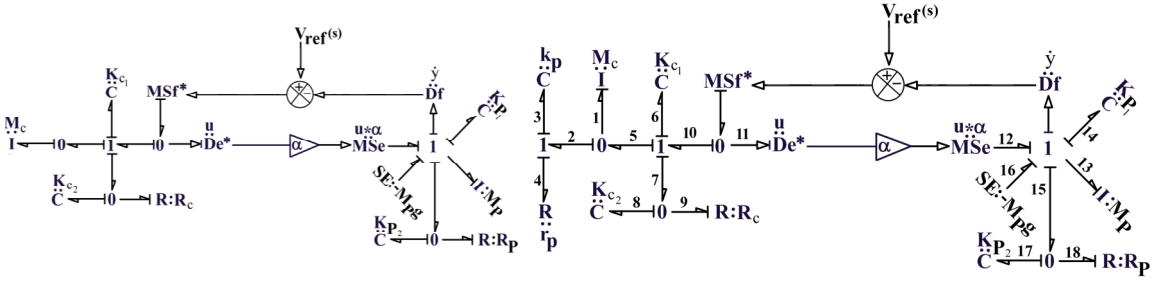

Fig. 3.5 Arrangement of the system in bond graph model displayed in Fig. 3.4 with the controller as the virtual system (a) in differential causality and (b) in integral causality by adding flexibility

After developing bond graph of the system, it is observed that an inertial element representing the mass of the controller has differential causality as shown in Fig. 3.5(a). Due to this, some terms representing the differentiation of measured variables in the real system are introduced. This inertial element is of a dependent port and it cannot be transferred to any independent port here. To avoid this differential causality, a coupling capacitor [Samantaray & Ould-Bouamama, 2008] or flexibility [Ghosh *et al.*, 1991; Pathak *et al.*, 2005; Mukherjee *et al.*, 2006; Pathak *et al.*, 2006a; Pathak *et al.*, 2006b; Pathak *et al.*, 2008] is provided in the system at particular locations, as shown in Fig. 3.5(b). This coupling capacitor or pad is attached at the place at which the mass of controller is modelled in the form of (1-C-R) structure. It can also be connected with the 0-junction at the place where virtual actuator (MSf*) element is attached [Ghosh *et al.*, 1991; Pathak *et al.*, 2005; Pathak *et al.*, 2006a; Pathak *et al.*, 2006b; Pathak et al., 2008].

The solution stiffness confronted at the time of simulation is reduced by introducing the R-element in the pad. The dynamic effects of the pad are reduced by giving some higher values to C and R elements. It is also noted that there are two opposing conditions

here that need to be satisfied, *i.e.* correctness of the solution and the simulation time taken by the system. These are satisfied by means of making the stiffness parameter of the pad with a very high value and the damping parameter is adjusted with trial and error. Furthermore, it is observed that actual feeling is more significant than accuracy of position in virtual reality simulators while accuracy of position is more significant in machining operations.

The signal flow graph [Samantaray & Ould-Bouamama, 2008] corresponding to the bond graph of third order system shown in Fig. 3.5(b) is shown in Fig. 3.6.

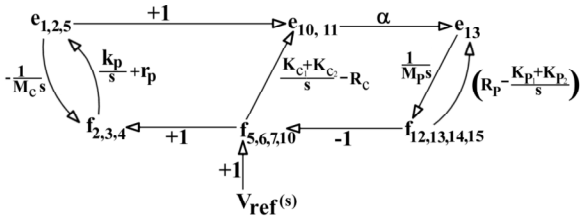

Fig. 3.6 Signal flow graph of the system whose arrangement in bond graph modelling is displayed in Fig. 3.5(b)

After Mason's gain rule is applied directly, the transfer function between the forward model velocity and the reference velocity is obtained as

$$G(s)=\frac{f_{13}(s)}{V_{\text{ref}}(s)}=\frac{\alpha H_2(s)}{H_1(s)+\alpha H_2(s)} \tag{3.14}$$

where

$$H_1(s)=M_C M_P s^4+R_P M_C s^3+\left(K_{P_1}+K_{P_2}\right)M_C s^2+k_p M_P s^2+M_P r_p s^3+r_p R_P s^2+R_P k_p s+\left(K_{P_1}+K_{P_2}\right)r_p s+k_p\left(K_{P_1}+K_{P_2}\right)$$

$$H_2(s)=M_C R_C s^3+\left(K_{C_1}+K_{C_2}\right)M_C s^2+k_p M_C s^2+M_C r_p s^3+r_p R_C s^2+R_C k_p s+\left(K_{C_1}+K_{C_2}\right)r_p s+k_p\left(K_{C_1}+K_{C_2}\right)$$

Divide Eq. (3.14) by α

$$G(s)=\frac{H_2(s)}{\frac{H_1(s)}{\alpha}+H_2(s)} \tag{3.15}$$

Hence $$\lim_{\alpha\to\infty} G(s)\cong\frac{H_2(s)}{H_2(s)}=1 \tag{3.16}$$

Therefore, the command is followed by the plant when the amplifier gain is very large. Hence, one can apply overwhelming controller for studying inverse dynamics of the hybrid manipulator. This was the aim of inversion scheme of implied system [Samantaray & Ould-Bouamama, 2008]. It is also further noted that the parameters of plant ($m_{\mathrm{P}}, K_{\mathrm{P}_1}, K_{\mathrm{P}_2}$ and R_{P}), come only in the term $H_1(s)$ and controller used here overwhelms all these terms. Hence, these parameters of the plant do not come in the term $H_2(s)$. Therefore, it can be said that this controller may be utilized to study inverse dynamics of the hybrid manipulator. Furthermore, it is also observed that in Eq. (3.14), the value of the numerator is lesser than the value of the denominator. The controller's causal form deteriorates into a non-causal form (Eq. (3.16)) as the gain parameter approaches infinity.

However, practically, gain parameter is not advisable with very high value as this high value will give rise to sensitivity of noise and it increases the simulation time [Pathak *et al.*, 2008]. In addition, the response may overshoot with increase in value of gain parameter and hence, the response may surpass the capacity of actuator.

It is noted that stiffness of pad (k_{p}) and damping (r_{p}) have very high values. This is because of the reason that only low frequency response is important in many simulator applications. This also shows that if stiffness of controllers (K_{C_1} and K_{C_2}) are high, G(s) approaches unity even for lesser gain values in low frequency range. Hence, it is concluded from this approach that a low value of gain is required for high values of K_{C_1} and K_{C_2}. Similarly, higher values of gain are needed if K_{C_1} and K_{C_2} have smaller values.

The value of the gain must be chosen along with the values of parameters of the controller [Sharon *et al.*, 1991]. The aim of a proper design should be such that the values of controller parameters must be chosen in such a way that they absorb the measurement noise in a particular frequency range [Samantaray & Ould-Bouamama, 2008] and also do the trajectory tracking in satisfactory limitations. There must be a compromise between large gain value and noise frequency range [Pathak *et al.*, 2008] so that the system's sensitiveness to the noise and its stiffness during the simulation is reduced.

The values of various parameters chosen for judging the performance of overwhelming controller for the application considered in example are shown in Table 3.2. In Table 3.2, the parameter values of the plant (real system) and inverse system may be considered anything arbitrarily as the overwhelming controller can overwhelm un-modelled parameters as well as external disturbances, as already discussed.

Table 3.2 Parameter values

Sub system	Parameter values			
Plant	$M_{\mathrm{P}} = 10$ kg	$K_{\mathrm{P_1}} = 10^6$ N/m	$K_{\mathrm{P_2}} = 10^4$ N/m	$R_{\mathrm{P}} = 10$ Ns/m
Inverse system	$M_{\mathrm{C}} = 1$ kg	$K_{\mathrm{C_1}} = 10^3$ N/m	$K_{\mathrm{C_2}} = 10^3$ N/m	$R_{\mathrm{C}} = 1$ Ns/m
	$k_{\mathrm{p}} = 10^8$ N/m	$r_{\mathrm{p}} = 50$ Ns/m	$g = 9.81$ m/s^2	

As seen from Table 3.2, the values of the controller parameters have different values than the similar plant parameters and this is done intentionally. As per Eq. (3.15), the gain (α) must have very high value (mathematically infinite) for the minimal error between the command and the response of the plant. The plant mass is displaced by 3.99 m. The given command for displacement is a symmetric sine curve with velocity amplitude 10 m/s and frequency of 5 rad/s. The dynamics of actuator have no restrictions during this period.

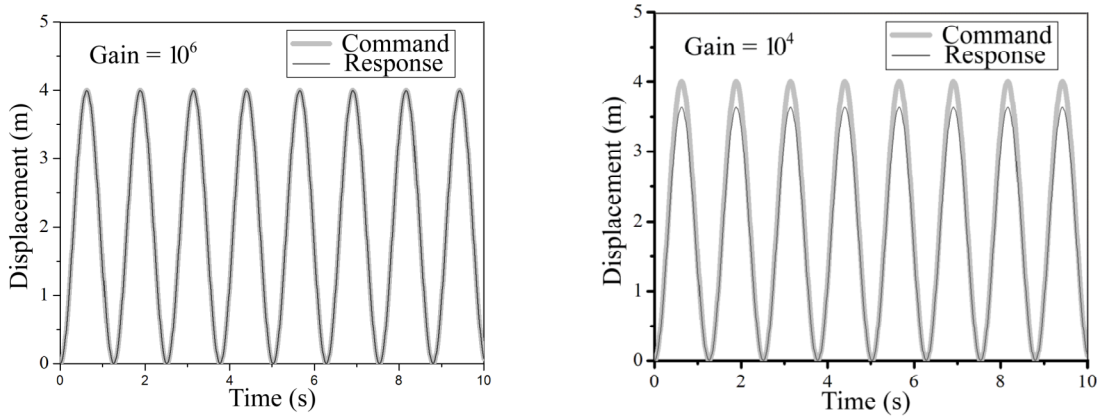

(a) **(b)**

Fig. 3.7 Performance of overwhelming controller for gain value of (a) 10^6 and (b) 10^4

In Fig. 3.7(a), the response of the plant is shown for a higher value of gain ($\alpha = 10^6$) and it is compared with smaller gain value ($\alpha = 10^4$) in Fig. 3.7(b). In Fig. 3.8, the

comparison between displacement errors with gain values 10^6 and 10^4 for overwhelming controller is shown. It is observed from Fig. 3.8 that displacement error between command and the response decreases if the gain for the overwhelming controller is increased from10^4 to 10^6.

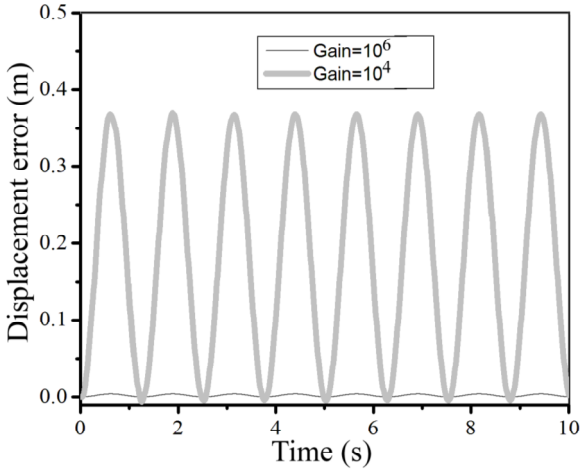

Fig. 3.8 Comparison between displacement errors for the controller with gain of 10^6 and 10^4

Therefore, it is concluded that the command is tracked by response even if the controller and plant parameters are entirely different from each other and the controller does not include self-weight of the system. Hence, the controller's power is validated for modelling the dynamics of system and uncertainties in parameters.

3.4 Inverse Model for Planar Hybrid Manipulator

The simplification of the forward dynamics model of actuator needs to be done for developing the fast mathematical inverse model for the system. The different actuators of the planar hybrid manipulator can be modelled as per Eqs. (3.6–3.8) so that computational efficiency of the inverse system can be improved. The overwhelming controller is assumed satisfactorily strong here so that it treats un-modelled inertial forces as disruptions and works properly.

The inverse dynamics or the controller model for the hybrid manipulator is shown in Fig. 3.9. This model is a mirror image of the forward model as shown in Fig. 3.2 with

few modifications done [Yildiz *et al.*, 2009]. The plant model in Fig. 3.2 is inverted as the input given here is *x*, *y* and θ positions of the centre of gravity '*g*' and output coming is force applied in three legs of the manipulator. Here representation of various joints with previous or next controller is explained as follows: Encircled numbers 1–6 and 7–10 indicate the corresponding joints with previous controllers and next controller, respectively. Encircled numbers 11–13 indicate the reference velocity ports in *x*, *y* and θ directions. The controller produces the driving efforts u_1, u_2 and u_3 which are then employed in the actual hybrid platform. The centres of gravity's velocities are modelled by the 1-junctions which have plant inertias attached with them. The superscript * here shows the approximate parameters, *i.e.* the values of these parameters are estimated. The inertias of the plant are approximated firstly, which are not required in the inverse model.

The literature study of serial manipulators [Ghosh *et al.*, 1991; Pathak *et al.*, 2005; Pathak *et al.*, 2006a; Pathak *et al.*, 2006b; Pathak *et al.*, 2008] show that overwhelming controller based inverse dynamics bond graph models do not have any causal loops in the model. These causal loops appear only in parallel manipulators or parallel-series hybrid manipulators and in parallel mechanisms [Bidard, 1991].

In the present thesis work, the closed loop architecture of the system is broken to solve the problem of causal loops. The points of linear velocities have two pairs of velocities for point A of platform which are represented by junctions $1_{\dot{x}_a}$ and $1_{\dot{y}_a}$ and the motion of centre of gravity has two triplets of junctions ($1_{\dot{x}_g}$, $1_{\dot{y}_g}$ and $1_{\dot{\theta}_g}$ junctions). These duplicate junctions correspond to a specific kind of motion for a specific point and these have a constraint that they will be representing a common velocity. This constraint is applied in the model by including the coupling capacitors having stiffness represented by k_p and damping represented by r_p or stiff spring-damper combinations in the model to represent the two pairs' common velocity and two triplets of junctions' common velocity separately. The bond graph model now has no causal loops. The final bond graph model is very easily computed as shown in Fig. 3.9. A pedagogical example has been considered (Fig. 3.5) to show the effectiveness of overwhelming controller. In Fig. 3.5,

K_{P_2} and R_P are in series in the plant model; so, K_{C_2} and R_C (mirror image of K_{P_2} and R_P) are in series in the controller (computational zone) side. So, K_{C_2} (mirror image of K_{P_2}) and R_C (mirror image of R_P) are included in Fig. 3.9.

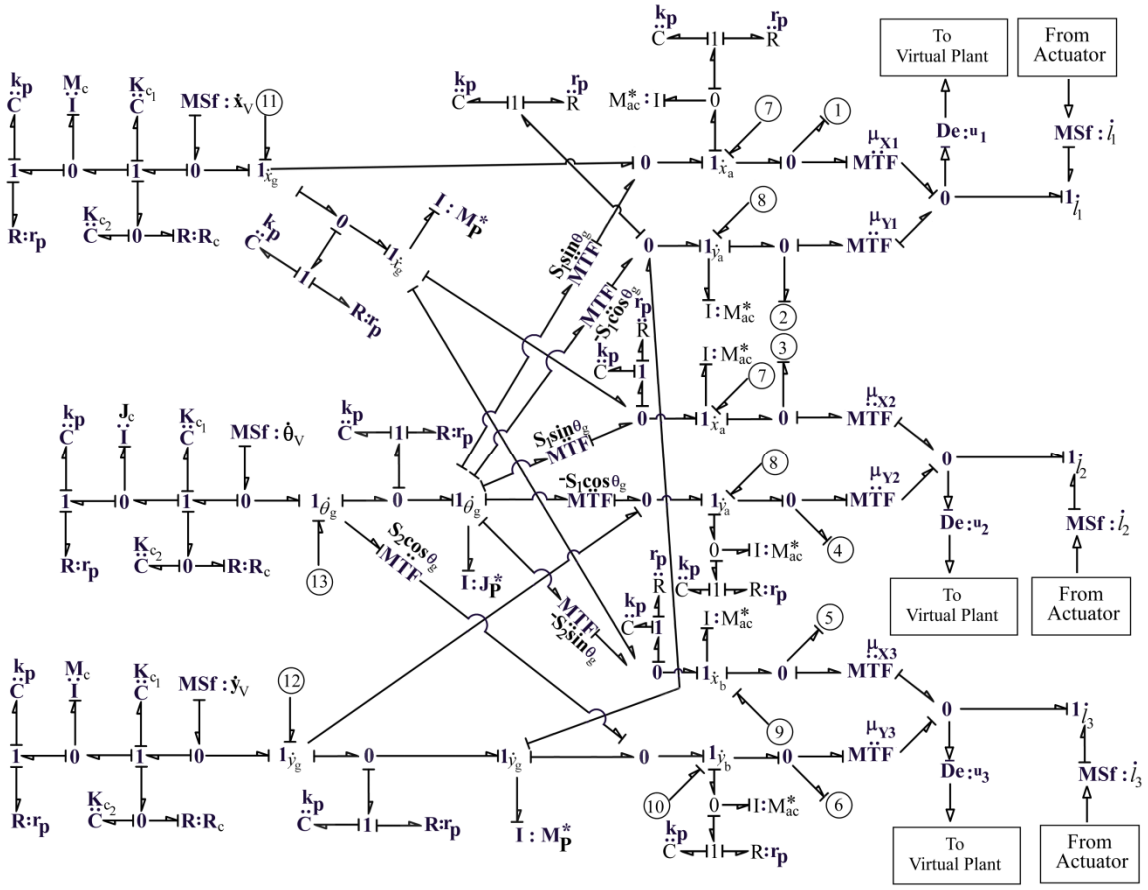

Fig. 3.9 Inverse model (controller) for hybrid manipulator

3.5 Case Study–I: Trajectory Tracking of Human Vertebrae

Different types of humanoid robots have been developed for industrial applications and sports. However, the main drawback for these types of robots is that the body part is generally rigid. For the application of these robots to execute spine bending sports activities like pole-vault, back vault, high jump *etc*., the body-part must be made of flexible articulated components. To increase the flexibility of these robots, human vertebrae model with flexibility may be implemented. The compression, decompression

and the lateral bending of human vertebrae on the frontal plane is mainly controlled by contraction and extension of one of the erector spine muscles. Hence, a biologically inspired flexible robot with articulated vertebrae structure (such as human vertebrae and elephant's trunk) is proposed here and its motion in a plane is considered. The human vertebrae are considered as hybrid manipulator where each vertebral unit is considered as a parallel manipulator and one vertebra is placed over other in series. The functional spine unit (FSU) along with spine muscle can be treated as the actuators and position sensors are required for online monitoring of humanoid robot body with vertebrae structure. The inverse model of this system along with the high gain-overwhelming controller (which remains in the *computational domain*) will control the motion of this artificial human body with vertebrae as per the requirements. This robot may have better dexterity in comparison to existing humanoid robots. The model presented in this thesis is a hybrid parallel-series manipulator where one parallel manipulator with three–DOF is supported on other parallel manipulator in series. The parallel manipulator has three prismatic legs that connect the upper and lower platforms.

3.5.1 Structure of a Human Vertebrae

The spine has some discrete elements known as vertebrae [Banton, 2012] that are connected by passive ligamentous restraints whereas intervertebral discs and articulating joints separate them and muscular activation controls it in dynamic sense. The spinal cord is classified broadly into five regions: the cervical spine, the thoracic spine, the lumbar spine, the sacrum and the coccyx, out of which only first three regions are considered here as shown in Fig. 3.10(a). The cervical spine (C-spine) is consisting of 7 vertebrae (C_1-C_7) in all mammals, the thoracic spine (T-spine) consists of 12 vertebrae (T_1-T_{12}) and the lumbar spine (L-spine) is consisting of 5 vertebrae (L_1-L_5) in humans. This full arrangement as a spine can experience axial, lateral, and sagittal rotations and axial, lateral, and anteroposterior translations. Hence, the spine can move in six directions [Banton, 2012]. A functional spinal unit (FSU) contains an upper vertebra, middle or intervertebral disc and lower vertebra osteoligamentous unit. Henceforth, a FSU can also have 6–DOF as the spine and it is considered as the fundamental part while studying spine movement. Each vertebra has a relative movement with other vertebra; therefore,

the movement of FSU is explained in this Section. This FSU along with inter vertebral soft part and the body muscle are the three linear actuators represented in Fig. 3.1(a). Each vertebral unit can be considered as a parallel manipulator and because one vertebra is placed over other in series, so the human vertebrae is considered as a hybrid manipulator.

A single vertebra with translations and rotations in various planes is shown in Fig. 3.10(b). The movements of the vertebra around an axis are known as *rotational movement* [Lowrance & Latimer, 1967]. There is a change in the orientation of the vertebra due to all rotations. The movements of the whole vertebra by the same amount in a given direction are referred as *translational movement*, which cause no change in the orientation of the vertebra. The horizontal plane is called transverse plane and the vertical plane parallel to human face is called frontal plane. The plane perpendicular to both frontal and transverse planes is known as sagittal plane. The translations in *x*-direction are known as right and left lateral shear in right and left directions respectively. The rotation about the *x*-axis in clockwise direction is referred as extension and in anti-clockwise direction is referred as flexion and is denoted by $\dot{\theta}_x$. Similarly, the translations in *y*-direction are known as compression and decompression in upward and downward directions, respectively. The rotation about the *y*-axis in clockwise direction is referred as right axial rotation and in anti-clockwise direction is referred as left axial rotation and is denoted by $\dot{\theta}_y$. Posterior shear and anterior shear are referred as the translations in *z*-direction in inner and outer directions respectively. The rotation about the *z*-axis is denoted by $\dot{\theta}_z$ and is referred as left lateral bending in clockwise direction and right lateral bending in anti-clockwise direction.

The motion considered is translation (compression and decompression) on frontal plane with right and left lateral bending about z-axis as the planar hybrid manipulator with 3-DOF is the main consideration of this chapter. Other DOFs shown in Fig. 3.1(b) are not considered in this case study. The schematic model of planar hybrid manipulator for this case is displayed in Fig. 3.11(a).

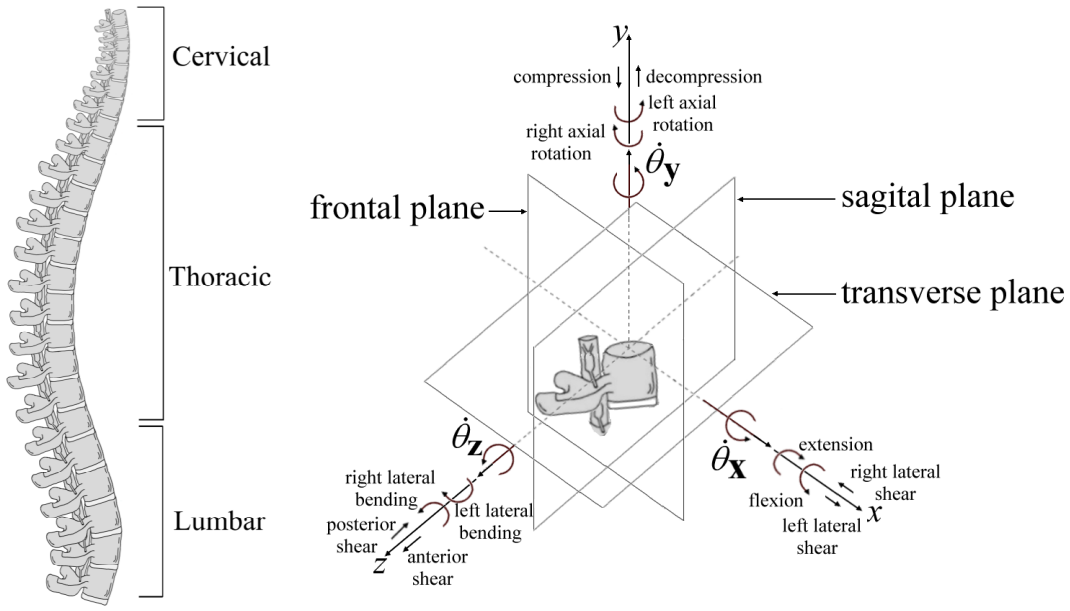

(a) (b)

Fig. 3.10(a) Model of human vertebrae and (b) a single vertebra with motion in different planes

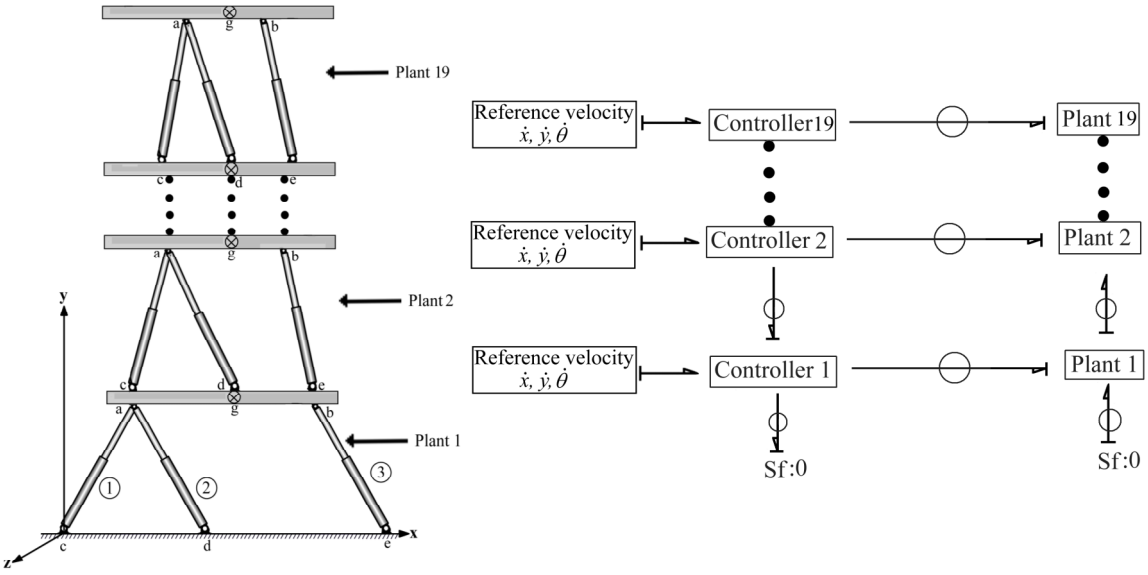

(a) (b)

Fig. 3.11 (a) Schema of hybrid manipulator for human vertebrae and (b) word bond graph model of hybrid manipulator and controller for human vertebrae

3.5.2 Simulation Results

Only the side bending of human body and lateral compression and decompression are considered in this simulation. Average weight per unit vertebra in the cervical segment is

6.3 gm, in the thoracic is 8.7 gm and in the lumbar is 17.9 gm. Other parameters used in simulation are chosen suitably and are given in Table 3.3.

Table 3.3 Parameter values for human vertebrae

Sub systems	Parameter values			
Platform	$M_{\mathrm{P}} = 6.3\,\mathrm{g}, 8.7\,\mathrm{g}, 17.9\,\mathrm{g}$	$J_{\mathrm{P}} = 0.01\,\mathrm{kg\,m^2}$	$K_{\mathrm{j}} = 10^8\,\mathrm{N/m}$	$R_{\mathrm{j}} = 50\,\mathrm{Ns/m}$
Actuator (with inertia condition)	$l_{\mathrm{cg}} = 0.5\,\mathrm{cm}$	$l_{\mathrm{p}} = 0.5\,\mathrm{cm}$	$l_{\mathrm{pg}} = 0.4\,\mathrm{cm}$	$w_{\mathrm{pi}} = 0.03\,\mathrm{cm}$
	$M_{\mathrm{cy}} = 1\,\mathrm{g}$	$M_{\mathrm{pi}} = 1\,\mathrm{g}$	$J_{\mathrm{cy}} = 0.01\,\mathrm{kg\,m^2}$	$J_{\mathrm{pi}} = 0.01\,\mathrm{kg\,m^2}$
	$k_{\mathrm{b}} = 10^6\ \mathrm{N/m}$	$k_{\mathrm{p_1}} = 10^8\ \mathrm{N/m}$	$r_{\mathrm{p}} = 50\,\mathrm{Ns/m}$	$R_{\mathrm{f}} = 0.0\,\mathrm{Ns/m}$
Inverse system	$M^*_{\mathrm{p}} = 0.025\,\mathrm{kg}$	$J^*_{\mathrm{p}} = 0.025\,\mathrm{kg\,m^2}$	$M_{\mathrm{c}} = 3\,\mathrm{kg}$	$J_{\mathrm{c}} = 0.1\,\mathrm{kg\,m^2}$
	$K_{\mathrm{c_1}} = K_{c_2} = 10^4\ \mathrm{N/m}$	$R_{\mathrm{c}} = 1\,\mathrm{Ns/m}$	$\alpha = 500$	

- **Trajectory Tracking**

Various points of vertebrae from C_1-L_5 were marked by fluorescent stickers on a human being by an orthopaedician for the command points (for the vertebral motion) as shown in Fig. 3.12(a). The snap shots (camera- Sony-α 77, Japan) of seven different positions (only three positions are shown in Fig. 3.12) on the frontal plane at different angles were taken to spinal cord in left direction for time duration of 1.2 s. The intermediate posture of spinal cord during left bending is shown in Fig. 3.12(b) and the final posture is shown in Fig. 3.12(c). The positions of all seven positions during left and right bending are shown in Fig. 3.13. In this way, positions of centre of gravity for various points from C_1-L_5 were noted down at different angles assuming the point L_5 as a fixed point. Hence, the command trajectory for various points from C_1-L_5 is obtained in this way. The X-ray photography was taken only for the straight and final posture. As more than four x-rays at a time are not clinically allowed by the orthopaedician, photographs were taken for the vertebral motion in left bending. The simulation of the system was performed for time duration of 1.2 s. The reference trajectories are the displacements of centroid of a

vertebra in three directions i.e. x, y and θ for various points. These reference positions of human vertebrae were fed to the inverse model. Not all the points are considered in simulation due to the complexity of the model. Hence, only selected points *i.e.* C_6, T_5, T_{10}, L_4 and L_5 (considered as fixed vertebra) are considered here in simulation. Then these motions obtained from command points are compared with the corresponding motions obtained from response points for different positions of spinal cord obtained from simulation results. Afterwards, the simulation results are matched with the response positions obtained from X-ray photographs so that results are validated fully.

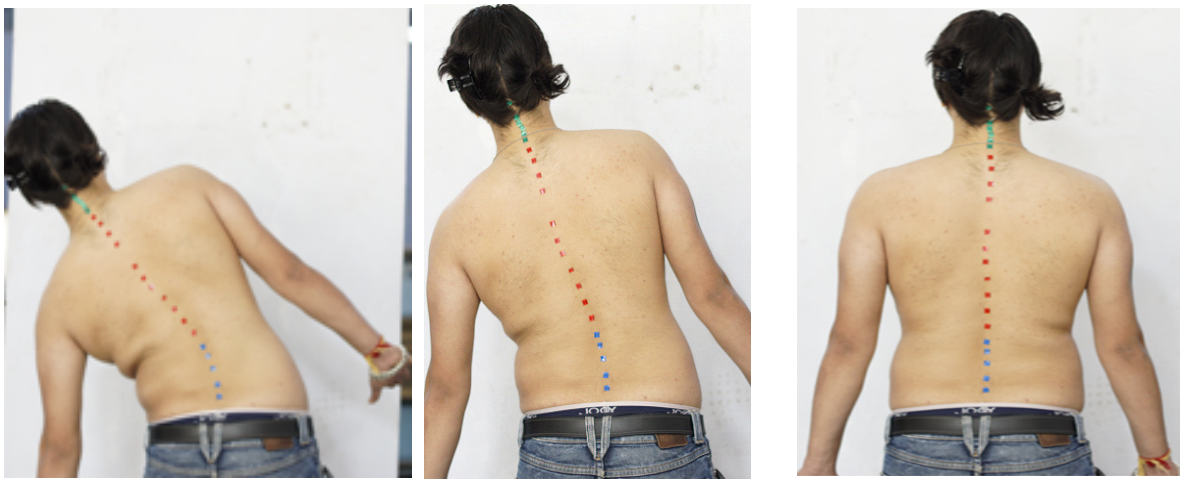

(a) (b) (c)

Fig. 3.12(a) Final position in left bending, (b) intermediate position in left bending and (c) straight position of spinal cord (vertebrae)

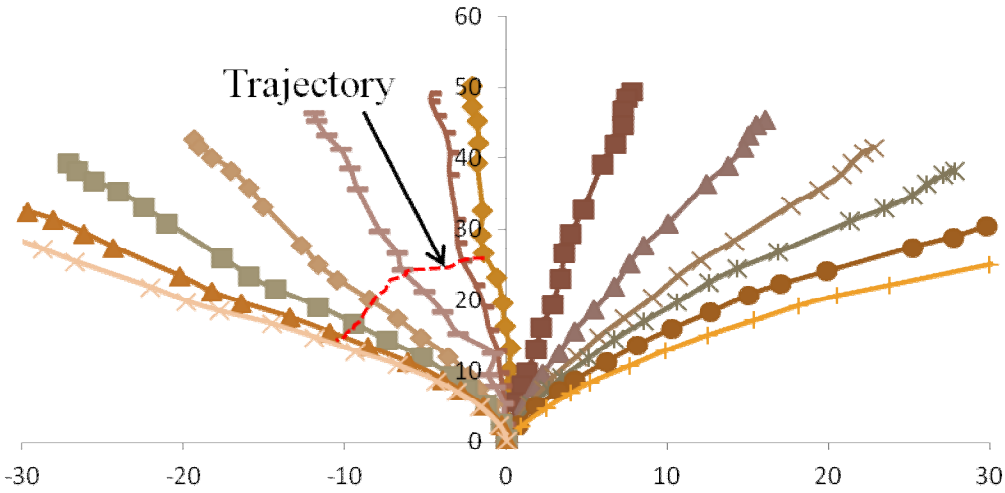

Fig. 3.13 Different positions of vertebra during left and right bending

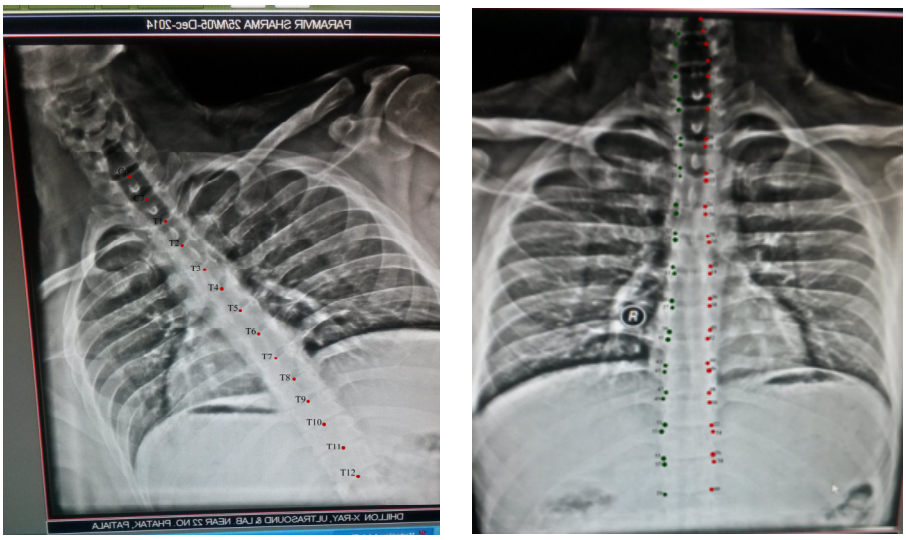

(a) (b)

Fig. 3.14(a) Final posture (C_4-T_{11}) in left bending (mirror image) and (b) straight position (C_4-T_{11}) of vertebrae obtained from X-ray

A mirror image of the actual X-ray for the left most position is shown in Fig. 3.14(a) and Fig. 3.14(b) shows the straight position. As seen in Fig. 3.14(b), not all the points appear in single X-ray plate and only points from C_4–T_{11} appear in X-ray. Therefore, simulation is done starting from point C_6 as points C_4 and C_5 are not clear in X-ray. Hence, the points from C_1–C_5 are not considered and 19 points from C_6–L_5 are included in simulation. The lumbar spine is not shown in Fig. 3.14 as these points don't appear in a single X-ray plate. The structure from L_1–L_5 is very rigid and their dimensions are more than the cervical and thoracic vertebrae. The lumbar vertebrae have the capacity to withstand the load of cervical and thoracic vertebrae. Hence, the final structure with 19 plants will not be unstable.

The initial conditions for different points of vertebrae considered here are given in Table 3.4. The initial conditions are taken from the straight position of the vertebrae from X-ray (Fig. 3.14(b)). The c point of the L_5 vertebra is considered as the origin of the coordinate axes. Only the initial positions of the vertebrae L_5, L_4, T_5, T_{10} and C_6 are given in Table 3.4.

Table 3.4 Initial positions

Vertebrae	Points	*x* (m)	*y* (m)	Vertebrae	Points	*x* (m)	*y* (m)
L_5	A	0.001	0.003	L_4	A	0.004	0.007
	G	0.016	0.003		G	0.015	0.007
	B	0.030	0.003		B	0.026	0.007
	C	0	0		C	0.001	0.003
	D	0.013	0		D	0.016	0.003
	E	0.027	0		E	0.030	0.003
T_{10}	A	-0.0001	0.059	T_5	A	0.009	0.179
	G	0.018	0.059		G	0.021	0.179
	B	0.036	0.059		B	0.034	0.179
	C	0.002	0.035		C	0.008	0.154
	D	0.019	0.035		D	0.021	0.154
	E	0.037	0.035		E	0.034	0.154
C_6	A	0.011	0.329				
	G	0.021	0.329				
	B	0.033	0.329				
	C	0.012	0.304				
	D	0.022	0.304				
	E	0.032	0.304				

The final results of trajectory tracking by the vertebrae for the points L_4, T_{10}, T_5 and C_6 are displayed in Fig. 3.15(a), (b), (c) and (d), respectively. It can be observed that the *x*-displacement for point L_4 varies from -2.2 cm to 1.534 cm and *y*-displacement ranges from -0.695 cm to 0.676 cm. For the vertebral point T_{10} the range of displacement in *x*-direction is from -10.44 cm to 1.833 cm and range of displacement in *y*-direction is from 1.28 cm to 5.958 cm. The displacement in *x*-direction for the point T_5 ranges from 23.518 cm to 3.571 cm and *y*-displacement varies from 6.334 cm to 18.108 cm. The range of *x*-displacement for vertebral point C_6 is from -34.901 cm to 6.13 cm and the range of *y*-displacement is from 10.163 cm to 33.44 cm. Hence, it is observed that the simulator tracks the desired trajectory for vertebral point L_4 and C_6 with minimal error whereas for other points T_{10} and T_5 the trajectory is tracked with some error, out of which percentage error with respect to time for the point T_5 is shown in Fig. 3.15(e). The maximum error in *x*-displacement is 20% and in *y*-displacement is 0.25% that is minimal. The forward

model follows the commands fed to the inverse controllers for the controller gain of 500. If the controller gain is further increased, the error can be minimized.

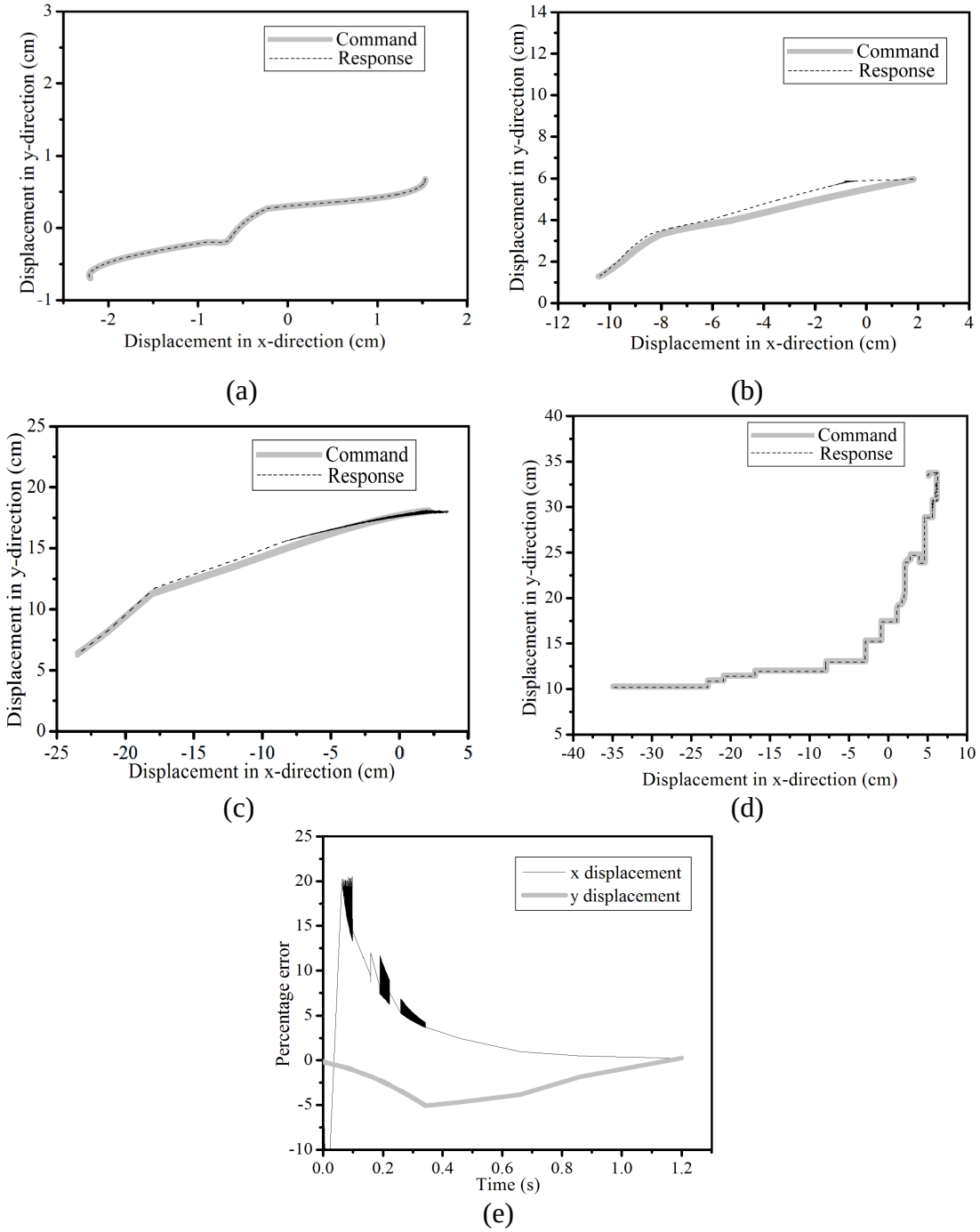

Fig. 3.15 Performance (response) of simulator to track the desired trajectory (command) for vertebral points of (a) L_4, (b) T_{10}, (c) T_5, (d) C_6 and (e) percentage error in *x* and *y* displacements for vertebral point T_5

3.6 Effect of Leg Inertia

The leg inertias are considered for the forward model but these are not considered in the controller model because the controller is robust to overcome the inertias of the legs that are not modelled. The initial length of actuator 1 is taken as 0.35 cm, actuator 2 is 1.266 cm and actuator 3 is 0.502 cm. The rate of change of length for the actuator 1 without inertia and with inertia is shown in Fig. 3.16(a) and (b). The change in length and driving effort required for actuator 1 is considered only for 0.04 s because the rate of change of leg length (as shown in Fig. 3.16(a) and Fig. 3.16(b)) decreases and gradually becomes zero and driving effort becomes steady after that time as shown in Fig. 3.16(c). It is observed that the leg length for actuator 1 increases if leg inertia is taken into account.

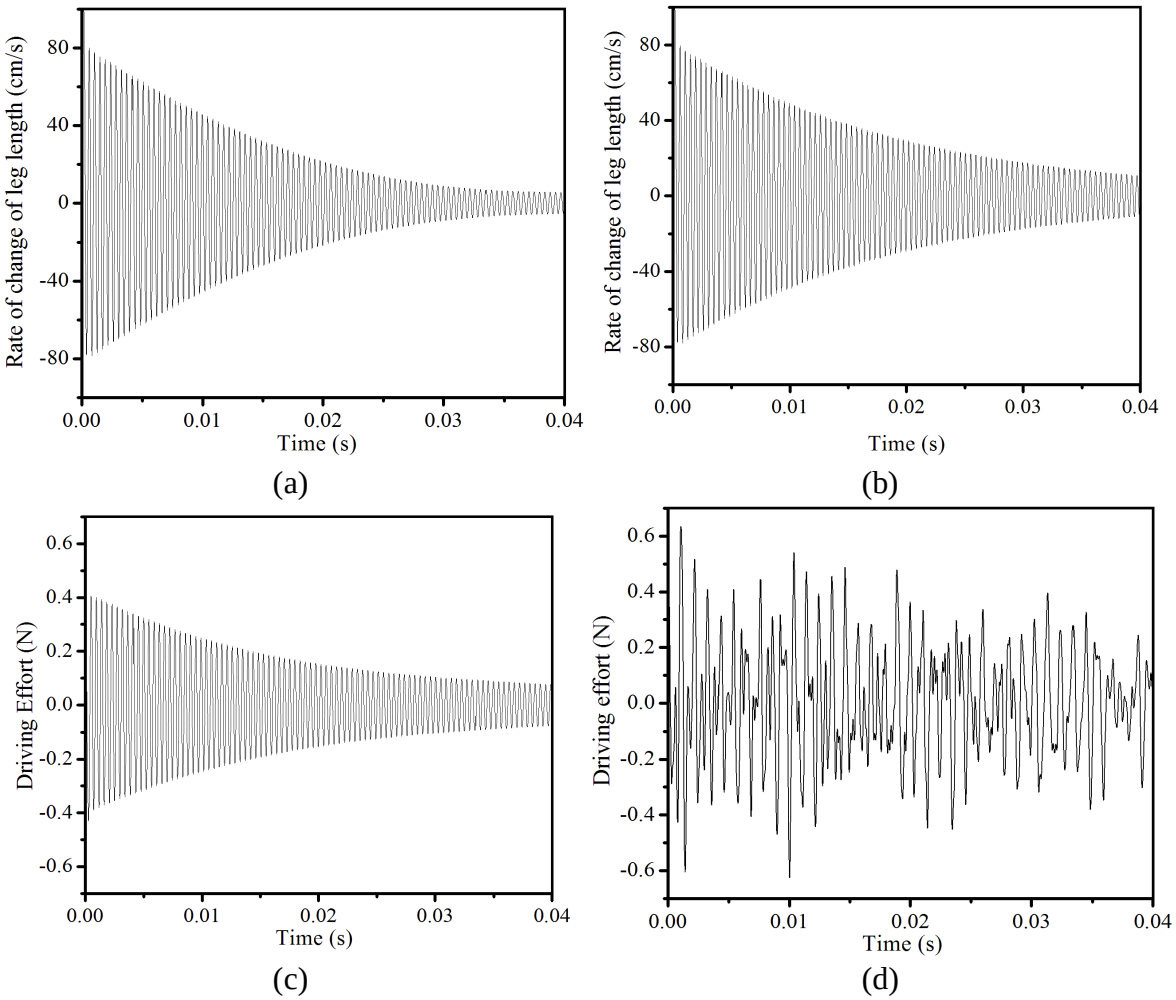

Fig. 3.16 Rate of change of leg length (a) without inertia and (b) with inertia and driving effort required (c) without inertia and (d) with inertia for leg 'ac' of the manipulator

The driving effort required in actuator 1 without inertia and with inertia is shown in Fig. 3.16(c) and (d). If we assume all the legs to be massless, then range of driving effort is -0.4301 N to 0.40623 N to track the given trajectory. The actuator 1 needs the driving effort ranging from -0.62552 N to 0.63417 N to track the same trajectory when leg inertia is taken into account. After seeing these results of simulation, it is observed that a 6 per cent disparity is there in the leg force calculated if we neglect the leg inertia. In addition, the driving effort required is less if legs are considered without mass and it increases substantially with the leg inertia.

Thus, it is concluded from this case study that human vertebrae can be taken as a hybrid manipulator and this human vertebrae model may be implemented to increase the flexibility of body part of humanoid robot.

3.7 Case Study–II: Trajectory Tracking of Thumb and Index Finger for Object Grasping

The objective of this case study is to track the trajectory by the thumb and index finger considering them as hybrid manipulators while grasping an object. Hence, this hybrid manipulator can be used in multi fingered robotic grippers, pick and place operations and moving things *etc*.

3.7.1 Structure of a Human Hand

The structure of a human hand is such that the position of the thumb is on one side of hand such that it is parallel to the arm. The palm of each hand contains five bones which are called metacarpal bones. Human hands include fourteen digital bones, which are known as phalanges or phalanx bones, out of which two bones are there in the thumb namely the distal phalanx and the proximal phalanx. The thumb has no intermediate or middle phalanx. Each of the remaining four fingers contains three bones. These are the distal phalanx, which carries the nail, the middle phalanx, and the proximal phalanx. Hence, twelve bones of fingers and two bones of thumb which means total bones contained in a human hand are fourteen. Each finger in a human hand can be considered

as a hybrid manipulator where each phalanx is considered as a parallel manipulator and one phalanx is placed over other in series.

The various joints between these phalanges are shown in Fig. 3.17. The movement of these joints for the thumb and index finger of the left hand in *x-y* plane is considered in this thesis while grasping an object. The fingers gradually come closer to each other and finally, the smaller object is grasped by the finger.

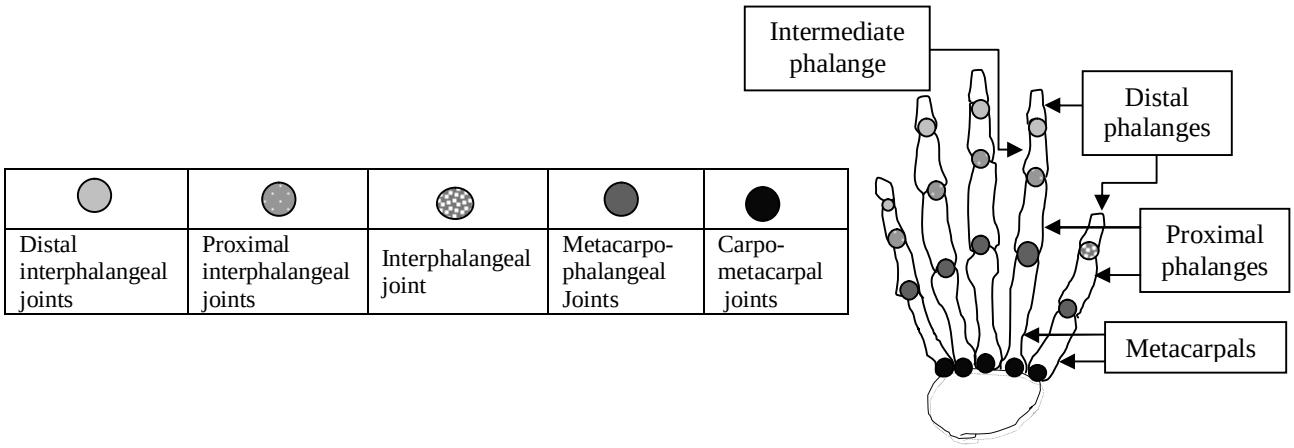

Fig. 3.17 Notations of various joints and their representation in human hand

3.7.2 Simulation Results

Average weight of a joint in a finger is taken as 0.0125 kg. Other parameters used in simulation are chosen suitably and are given in Table 3.5. The snap shots (camera- Sony-α 77, Japan) of eight different positions (only three positions are shown in Fig. 3.18) for holding different chalk lengths (from 1 cm to 8 cm) in *x-y* plane were taken for the left hand for a time duration of 1.4 s. Different joints for the thumb and index finger were marked to note their positions. The picture of thumb and index finger holding smallest chalk length of 1 cm is shown in Fig. 3.18(a). The picture of thumb and index finger holding intermediate chalk length of 5 cm is shown in Fig. 3.18(b). The picture of thumb and index finger holding biggest chalk length (initial position) of 8 cm is shown in Fig. 3.18(c).

Table 3.5 Parameter values for human hand motion

Sub systems	Parameter values			
Platform	$M_P = 0.0125\,\text{kg}$	$J_P = 0.001\,\text{kg m}^2$	$K_j = 10^8\,\text{N/m}$	$R_j = 50\,\text{Ns/m}$
Actuator	$k_p = 10^8\,\text{N/m}$	$r_p = 50\,\text{Ns/m}$		
Inverse system	$M^*_P = 0.025\,\text{kg}$	$J^*_P = 0.025\,\text{kg m}^2$	$M_c = 3\,\text{kg}$	$J_c = 0.1\,\text{kg m}^2$
	$K_c = 10^4\,\text{N/m}$	$R_c = 1\,\text{Ns/m}$	$\alpha = 100$	

In this way, positions of centre of gravity for various joints for the thumb and index finger were noted down at different positions assuming the joint 1 as a fixed point. The *x* and *y* directions are shown in Fig. 3.18(a). Parallel spring damper combinations are attached with the tip of thumb and finger for grasping object effectively as shown in Fig. 3.18(a).

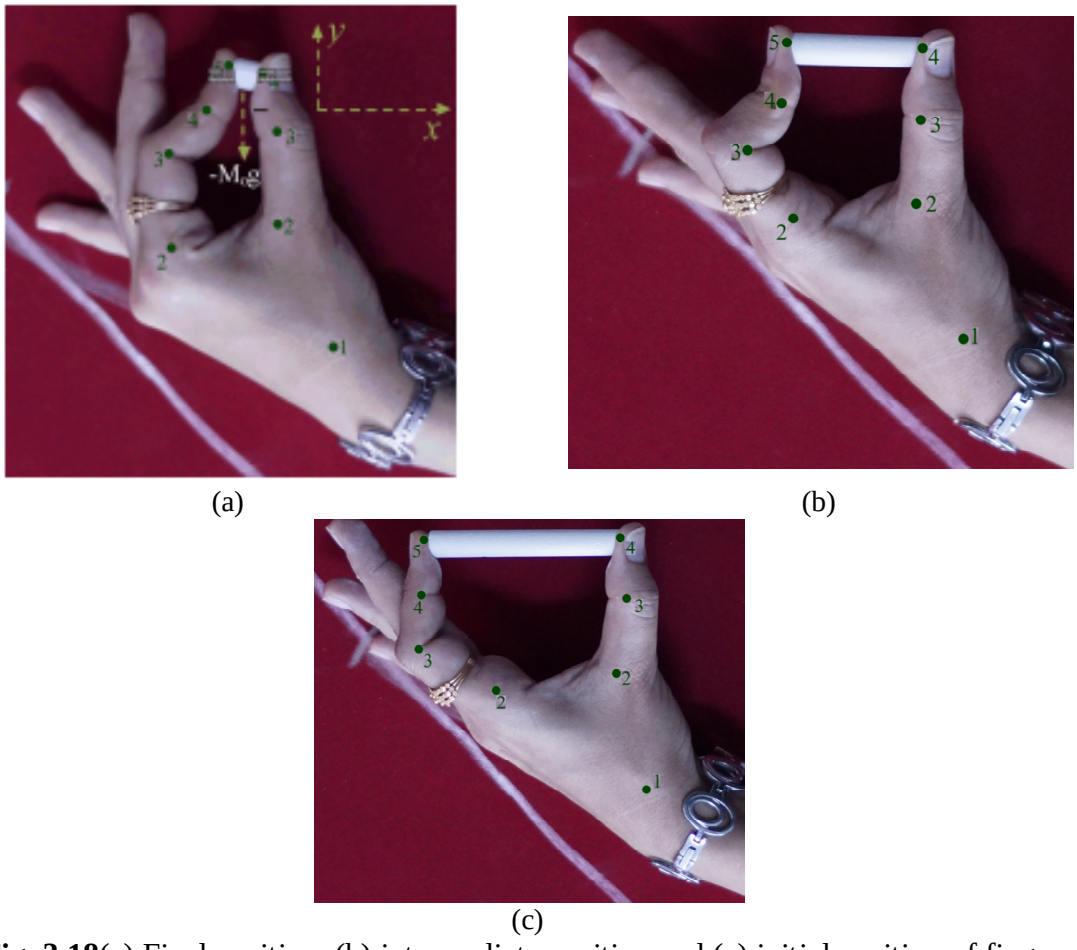

(a) (b)

(c)

Fig. 3.18(a) Final position, (b) intermediate position and (c) initial position of fingers

The weight of the object i.*e*. chalk in this case acts in the downward direction and taken as 10 g for the present case. The arrangement of thumb and finger having bond graph modelling is displayed in Fig. 3.19 where weight of the object is taken into consideration in *y*-direction.

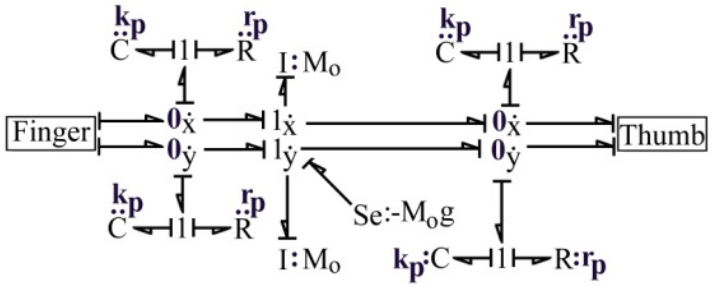

Fig. 3.19 A bond graph model for thumb and index finger grasping an object

The X-ray photography was taken only for the chalk length of 1 cm, 5 cm and 8 cm as shown in Fig. 3.20. The simulation of the system was performed for time duration of 1.4 seconds. The reference trajectories are the displacements of centroid of a joint in two directions *i.e. x* and *y* positions for various points. The inverse model was given these reference positions of joints. The motions from command points are matched with the equivalent motions obtained from response points for different positions of thumb and index finger obtained from simulation results.

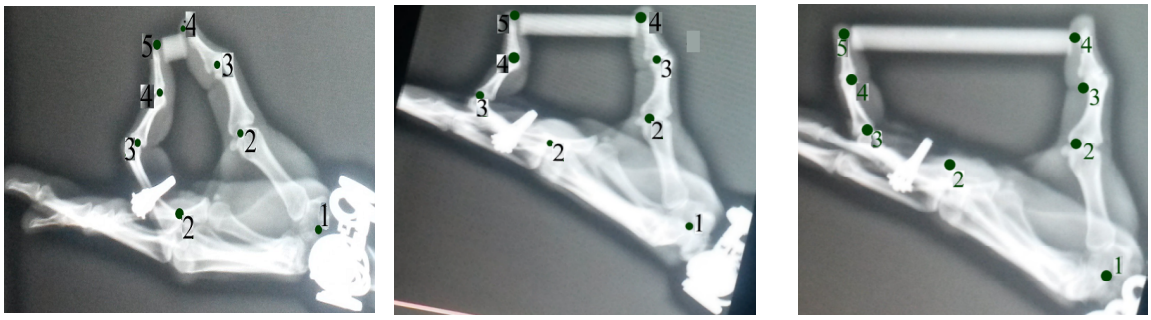

(a) (b) (c)

Fig. 3.20 (a) Final position, (b) intermediate position and (c) initial position of fingers obtained from X-ray

The initial conditions for different points of thumb and finger considered here are given in Table 3.6. The initial conditions are taken from the position with the biggest

chalk length *i.e.* 8 cm from X-ray (Fig. 3.20(c)). The 1 point is considered as the origin of the coordinate axes.

Table 3.6 Initial positions

Thumb	Points	*x* (m)	*y* (m)	Thumb	Points	*x* (m)	*y* (m)
Metacarpal	A	0.002	0.049	Proximal phalange	A	0.006	0.069
	G	0.008	0.049		G	0.011	0.069
	B	0.014	0.049		B	0.015	0.069
	C	0	0		C	0.002	0.049
	D	0.004	0		D	0.008	0.049
	E	0.016	0		E	0.014	0.049
Distal phalange	A	0.003	0.088				
	G	0.007	0.088				
	B	0.012	0.088				
	C	0.006	0.069				
	D	0.011	0.069				
	E	0.015	0.069				
Finger	Points	*x* (m)	*y* (m)	Finger	Points	*x* (m)	*y* (m)
Metacarpal	A	-0.011	0.0409	Proximal phalange	A	-0.040	0.054
	G	-0.006	0.0409		G	-0.037	0.054
	B	0.002	0.0409		B	-0.033	0.054
	C	-0.013	0		C	-0.011	0.041
	D	-0.009	0		D	-0.006	0.041
	E	0	0		E	0.002	0.041
Intermediate phalange	A	-0.046	0.072	Distal phalange	A	-0.047	0.089
	G	-0.043	0.072		G	-0.045	0.089
	B	-0.040	0.072		B	-0.044	0.089
	C	-0.040	0.054		C	-0.046	0.072
	D	-0.037	0.054		D	-0.043	0.072
	E	-0.033	0.054		E	-0.040	0.072

The result for trajectory tracking by the thumb is displayed in Fig. 3.21(a). Fig. 3.21(b) and (c) show the displacements of the object (chalk) in *y* and *x* direction respectively. The velocity of the object in y-direction is shown in Fig. 3.21(d). It can be easily seen that that the *x*-displacement for the tip of the thumb varies from 7.52 mm to -9.09 mm and *y*-displacement ranges from 87.94 mm to 94.69 mm. The displacement and velocity of the object is noted for 2 s. A small portion of the graph for 0.008 s is shown in Fig. 3.21(c) and (d) to have a clear picture. Therefore, it is noted that the desired trajectory is tracked by the simulator for the thumb tip with minimal error. The

commands fed to the inverse controllers are followed by the forward model for the controller gain of 100. If the controller gain is further increased, the error can be minimized.

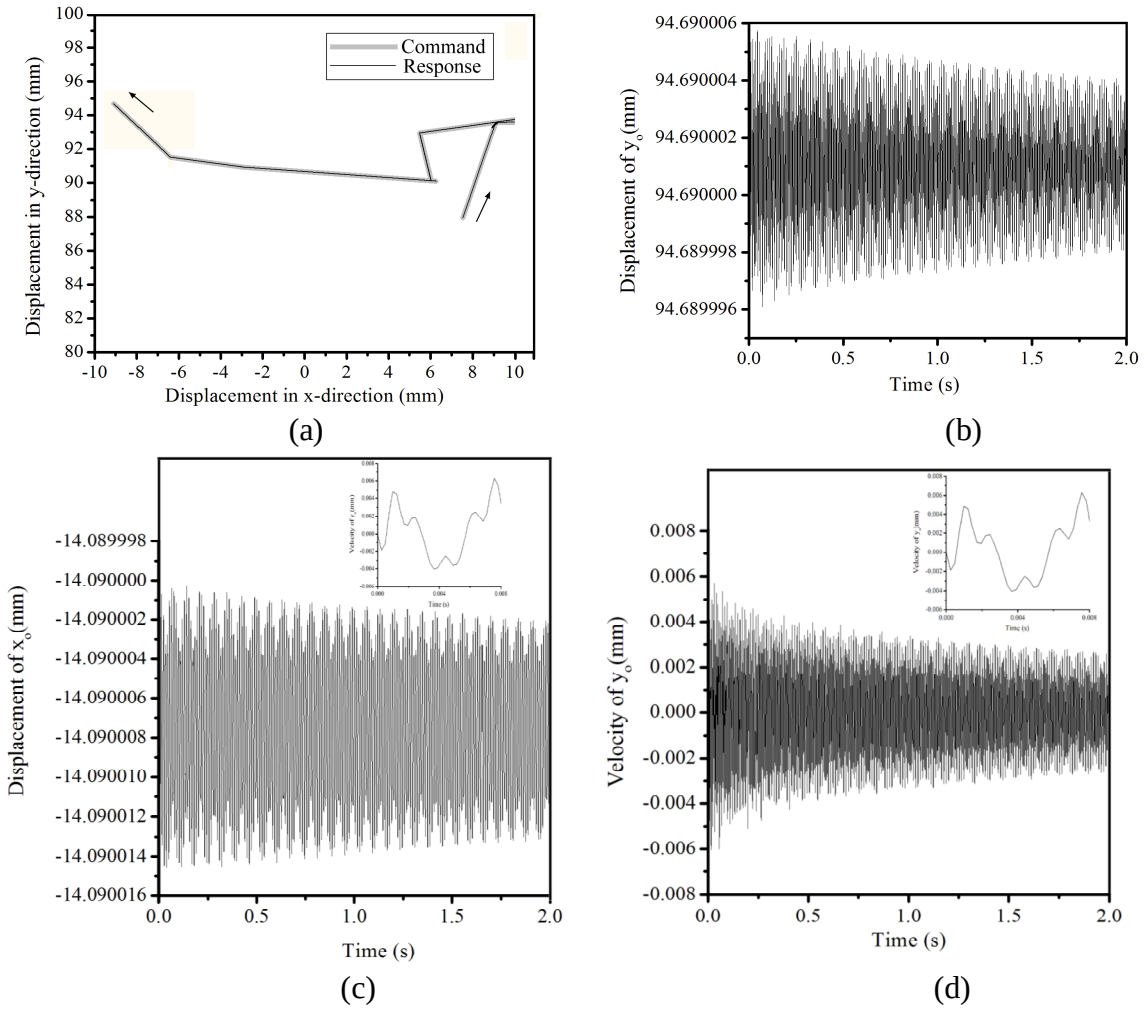

Fig. 3.21 (a) Trajectory tracking for thumb in *x*-*y* plane, (b) *y*-displacement of the object (chalk), (c) *x*-displacement of the object (chalk) and (d) velocity of the object (chalk) in *y*-direction

Hence, it is concluded from this case study that the thumb and finger in human hand can be taken as an example of a hybrid manipulator for which trajectory tracking was done for different phalangeal joints. Within the acceptable range, the command given to the controllers is followed by the response of the plants. If the gain of the overwhelming controller is further increased, the error limit can be decreased but the time taken by simulation is very large in that case.

3.8 Conclusions

Initially, a planar hybrid manipulator was developed and then an overwhelming controller was built for this manipulator in this chapter. The forward dynamics model was then made and same kinematic constraints were used to develop a simple and computationally efficient inverse model but some dynamic constraints were not considered in it. Furthermore, an overwhelming controller was used in the inverse model and this controller is stable against disturbances and uncertainties of some parameters so that a precise controller could be developed for implementing it in real time. This controller was well examined with two example applications, one concerning trajectory tracking of human vertebrae and the other, trajectory tracking of thumb and index finger grasping an object.

The power of the controller parameters was analyzed using simulations, especially pad parameters and controller gains. The power of leg inertias of the actuator was explored and it was observed that the inertias of the actuator have a significant effect on the force at the actuators. In addition, the strength of the controller was assessed with regard to uncertainties of parameters and noise measurement under various conditions.

At last, an overwhelming controller for a planar hybrid Manipulator was implemented with the bond graph approach. The model and controller was developed using the knowledge obtained from analysis of the planar hybrid manipulator. A simplified inverse model was developed neglecting the inertia of the actuators and other dynamics. Model reduction of these forward and inverse models would be done in Chapter 4 later. Then this planar hybrid manipulator would be used to do its workspace analysis later in Chapter 5. A three dimensional forward model with 3-D actuator models would also be developed in the thesis, which is used later in Chapter 6. The trajectory tracking of thumb and index finger while drawing an arc was done and impedance control for a L-shaped path was done using these forward and inverse models for a 3-D planar hybrid manipulator in Chapter 6.

Chapter 4

Physical Model Reduction of Parallel and Hybrid Manipulator

4.1 Introduction

The multi energy domain dynamic systems consisting of mechanical, electrical, thermal and fluidic components or sub-systems are of great importance in today's life. The synthesis, analysis and simulation for these types of complex systems depend on accurate and compact models which require systematic modelling procedures. An important aspect in the designing of a system is its simulation before the actual production. Simulation of various systems before their actual production is a very important part of the design process. However, now due to the application of various new forms of control techniques and algorithms, the need of simulation does not end with the design process. Today many complex systems are controlled by powerful algorithms which continuously monitor the system surroundings and simulate the system on the go. This simulation allows the algorithms to predict and hence, control the system in a better manner, with more accuracy. Most of the software packages are based on mathematical equations which cannot be solved analytically but can only be solved numerically. So, with the increase in complexity of the system, the simulation time and computational complexity increase and it is difficult to handle bigger systems. Hence, the large complex systems are not manageable with respect to design, optimization, storage and computational requirements. An approach to overcome the obstacles of high computation time and cost requirements is there so that a reduced model of the system can be obtained, without compromising on the accuracy. Hence, such a mathematical model can be solved quickly and the response characteristics for the reduced model have minimum error compared to the full model. So, model reduction methods have been studied since long time. Therefore, a higher order model is reduced to a lower order model (of manageable size) whose response is same as the actual physical system. The model is reduced in such a way that the dynamics of the reduced model remains same as the original system. This reduced model can be used further in design and analysis of a system as it can be more quickly solved than the bigger complex system.

In this thesis, the bond graph modelling approach [Dauphin-Tanguy *et al.*, 1999; Granda, 2002; Samantaray & Ould-Bouamama, 2008] is used for representing the information exchange within the sensors, actuators and control systems in a system. When a system has different energy domains, the energy interaction between elements is graphically represented by bond graph [Borutzky, 2004]. This chapter discusses the Eigen value sensitivity method for model reduction in detail in which a linear time invariant (LTI) system is represented using bond graph. The detailed procedure of this method is then discussed and implemented on a pedagogical example of a mass spring damper system to illustrate the application of model reduction method. Then physical model reduction of a planar parallel and hybrid manipulator is done using Eigen value sensitivity method. The bond graph models for forward and inverse dynamics of parallel and hybrid manipulators are also shown in which full bond graph model is presented at first and then its reduced bond graph dynamic model is presented. Same is done for hybrid manipulator as well. An attempt has been made to achieve to the reduced dynamic model for planar parallel and hybrid manipulator by mathematically finding the redundant elements, which do not add to the dynamics of the system but increase the calculation time by increasing the complexity of the system. The redundant elements could be neglected from the system and hence, reducing the complexity without compromising on the accuracy. The Eigen values are calculated from the system matrix and effect matrices are formed. The row and column based on Eigen values can be reduced to form a reduced model. The trajectory tracking for a circular path is done for planar parallel and hybrid manipulators by both full model and reduced model. Henceforth, simulation results for trajectory tracking of both the manipulators for full model and reduced model are presented.

4.2 Physical Model Reduction Technique

Model reduction is related mainly to the open loop aspects. The model reduction techniques have been studied by many researchers for the last two decades. Model order reduction can be done in two ways: First is to solve the full model and then, apply mathematical techniques for obtaining the results in reduced form. Second is to reduce the system and then, find its solution. There are many techniques for model reduction

[Orbak *et al*., 2004]. A major drawback of these methods is that these don't have any information regarding the system's internal structure, so these cannot be directly used for the modelling and reducing the systems in physical domain. All the methods are purely numerical in nature. An approach known as model reduction in physical domain [Orbak *et al*., 2003] is used to obtain the reduced model of a system by removing some physical components from the actual model. It is seen that all the components of a system do not significantly contribute to the dynamic behaviour of a system. So, these components which have less power flow are removed from the original model [Louca *et al*., 1997]. Another physical based model reduction method is the singular perturbation method developed by [Sueur & Dauphin-Tanguy, 1991]. This technique reduces the system's dimension by estimating the fast and slow dynamics of bond graph models after calculating causal loop gains using reciprocal systems. Some other approaches like Eigen value separation method and Eigen value sensitivity method are also discussed [Orbak, 2010] and these show the relative contribution of components of the system on the system's Eigen values with the help of decomposition of physical systems.

The model order reduction is needed for complex problems to save the simulation time and to reduce the storage capacity without any effect on the accuracy of the system. Various examples were considered and analyzed for this work. There is much needed demand for model reduction in the electronics industry containing many inputs and outputs.

The main advantages for using the reduced order models are:

- The physical dynamics of the original system becomes simple to understand by using lower order model as these focus on the most important component of the system
- The time required for simulation of reduced system is lesser than that of actual system
- The controller is more efficient in numerical terms
- The computational complexity is reduced and it is more accurate than the actual system

- As the control laws become simpler, the hardware and software requirements for the controller are reduced. Therefore, the controller becomes cost effective with the reduced model
- It reduces the problem to a smaller manageable size. Hence, the model has less storage and computational requirements

The Eigen value sensitivity method is based on the general analysis of physical state variables involved in the system's behaviour and their relation to residues and Eigen values. Very simple results are obtained with the use of system matrices. According to Eigen value sensitivity method, firstly the Eigen values are found out using Eigen vectors and after that, the sensitivities of Eigen values for all elements storing energy and energy dissipating elements are computed with the help of Eigen values. This shows the relationship of each energy storage element and energy-dissipating element with state variables for any given Eigen value. Further these relationships are analyzed. The relative importance of physical parameters on a selected Eigen value is indicated by the two effect matrices (one each for energy storage and dissipating elements) in this analysis. These effect matrices identify the irrelevant components and give a relative measure of their contribution to the Eigen values. Hence, the physical parameters not affecting an Eigen value of interest can be removed.

The inertial (I) elements, compliance (C) elements and dissipative (R) elements should be represented in different groups because they have separate magnitude scales. The most important advantage of Eigen value sensitivity method as compared to the Eigen value separation method is that this method can manage the process in an improved way due to the exact location of Eigen values known to us. Moreover, a huge part of this process can be automated in different ways.

4.2.1 Representation of Linear Time Invariant System using Bond Graph

A linear physical system is characterized by several matrices that define the system's structure and parameters [Ye & Youcef-Toumi, 2000; Rosenberg, 1971]. There are two

effect matrices namely $\mathbf{E}_{IC}$ and $\mathbf{E}_{R}$ that represent the parameters of the components of energy storage and energy dissipating elements. The energy storage elements and the dissipation elements are represented by matrices **S** and **L**, respectively. The matrix **S** is defined as [Orbak 2010]

$$\mathbf{Z}_i = \mathbf{S}x_i \tag{4.1}$$

where

- x_i is generalized momentum/displacement vector associated with the i^{th} independent energy storage element
- Z_i is the causal output as flow/effort of that element
- **S** is a square matrix with diagonal elements as [s_1, s_2…….s_n] and all other elements being zero.

where $s_i = \frac{1}{C_i}$, if i^{th} energy storage element is a capacitive element.

or $s_i = \frac{1}{I_i}$, if i^{th} energy storage element is an inertial element.

The matrix containing the parameters for the dissipation elements is represented by **L** and is defined as

$$d_{\text{out}\,j} = \mathbf{L}d_{\text{in}\,j} \tag{4.2}$$

where $d_{\text{in}\,j}$ and $d_{\text{out}\,j}$ are causal input and causal output of the j^{th} dissipation element, respectively.

If *n* is the number of independent single port energy storage elements in LTI system and if *m* is the number of single port dissipation elements,

S is a diagonal matrix of the form [s_1, s_2…….s_n], where s_i's are the variables of the energy storing elements.

L is a diagonal matrix of the form [l_1, l_2…….l_m], where l_i's are the variables of the energy dissipation elements.

Moreover, $s_i = \frac{1}{C_i}$, if the i^{th} independent energy storage element is a capacitance. $s_i = \frac{1}{I_i}$ if the i^{th} independent energy storage element is an inertance. $l_j = R_j$, if the j^{th}

dissipation element has the causal input as a flow or an effort. $l_j = \frac{1}{R_j}$ if the j^{th} dissipation element has the causal output as an effort or a flow.

The entries in matrix **S** considered in this thesis are not constant and depend on the configuration of the system. So, the proposed approach can be implemented for systems with rotational generalized coordinates also. The matrices that describe the structure of the system are shown in Table 4.1 as follows:

Table 4.1 Description of connectivity matrices of a system

Matrix Name	Description
$\mathbf{J_{SS}}$	Connectivity between the outputs and inputs of the energy storage elements.
$\mathbf{J_{SL}}$	Connectivity between the outputs of the dissipation elements and the inputs of the energy storage elements.
$\mathbf{J_{LS}}$	Connectivity between the outputs of the energy storage elements and the inputs of the dissipation elements.
$\mathbf{J_{LL}}$	Connectivity between the outputs and the inputs of the dissipation elements.
$\mathbf{J_{SU}}$	Connectivity among the inputs from the sources **U** and the inputs of the energy storage elements.
$\mathbf{J_{LU}}$	Connectivity among the inputs from the sources **U** and the inputs of the dissipation elements.

All these connectivity matrices can be calculated from the system's signal flow graph drawn from the bond graph arrangement of the system. However, it is cumbersome to understand a huge signal flow graph as the system becomes more and more complex. Hence, a procedure is devised to calculate the connectivity matrices straight forwardly from the system's bond graph arrangement [Singh, 2015]. This method of obtaining connectivity matrices straight forwardly from the system's bond graph arrangement resembles the procedure of obtaining connectivity matrices by drawing system's signal flow graph. The basic rule in this direct method is that only those elements can be taken into account as connected to each other that are linked to each other by a causal path.

The other rules in this procedure to calculate the connectivity matrices straight forwardly from the system's bond graph arrangement are described below:

1. $\mathbf{J_{ss}}$ is a square matrix whose transpose equals its negative i.e. $\mathbf{J}_{SS}^{T} = -\mathbf{J}_{SS}$. As $\mathbf{J_{ss}}$ is a skew symmetric matrix; hence, only the upper triangular elements or the lower triangular elements are calculated.
2. Also, $\mathbf{J}_{SL} = -\mathbf{J}_{LS}^{T}$. Therefore, only one of these two matrices is calculated.
3. Then check if the output from an element to the system is flow or effort, check the conduct of all intermediate points on the causal path.

The procedure to calculate the connectivity matrices straight forwardly from the system's bond graph arrangement is described below:

1. Connectivity is considered as 1-junction. The junctions impose some factors that are multiplied with connectivity.
2. For a 1-junction:

(a) If flow output is there, factor is 1.

(b) If effort output is there, check if the bonds representing exchange of information have same power orientation. If both the entry and exit of information have direction going inside, then the factor is -1. If both the entry and exit of information have direction going outside, then the factor is 1.

3. For a 0-junction:

(a) If effort output is there, factor is 1.

(b) If flow output is there, check if the bonds representing exchange of information have same power orientation. If both the entry and exit of information have direction going inside, then the factor is -1. If both the entry and exit of information have direction going outside, then the factor is 1.

4. For a transformer element:

   If same power direction is there for two bonds attached to the transformer, then the factor is μ and if power direction is opposite for two bonds attached to the transformer, then the factor is $1/\mu$. (where μ is the modulus of the transformer)

5. For a gyrator element:

(a) Factor is η where η is the modulus of gyrator.

(b) For the remaining path, sense of output is changed from effort to flow and vice-versa.

6. Activated bonds can only be followed if the activation is same as the sense of path followed and the power direction is similar to the direction of path followed.

Hence, the overall equations are (Rosenberg, 1971)

$$\dot{x} = \mathbf{J_{SS}} z + \mathbf{J_{SL}} d_{\text{out}} + \mathbf{J_{SU}} u \tag{4.3}$$

$$d_{\text{in}} = \mathbf{J_{LS}} z + \mathbf{J_{LL}} d_{\text{out}} + \mathbf{J_{LU}} u \tag{4.4}$$

where the matrices $\mathbf{J}_{SS}$, $\mathbf{J}_{SL}$, $\mathbf{J}_{SU}$, $\mathbf{J}_{LS}$, $\mathbf{J}_{LL}$ and $\mathbf{J}_{LU}$ are described as in Table 4.1.

Therefore, the equation representing the system's state space is

$$\dot{x} = \mathbf{A}x + \mathbf{B}u \tag{4.5}$$

where

$$\mathbf{A} = [\mathbf{J_{SS}} + \mathbf{J_{SL}}\mathbf{L}(\mathbf{I} - \mathbf{J_{LL}}\mathbf{L})^{-1}\mathbf{J_{LS}}]\mathbf{S} \equiv \mathbf{JS} \tag{4.6}$$

$$\mathbf{J} = \mathbf{J_{SS}} + \mathbf{J_{SL}}\mathbf{L}(\mathbf{I} - \mathbf{J_{LL}}\mathbf{L})^{-1}\mathbf{J_{LS}} \tag{4.7}$$

$$\mathbf{B} = \mathbf{J_{SU}} + \mathbf{J_{SL}}\mathbf{L}(\mathbf{I} - \mathbf{J_{LL}}\mathbf{L})^{-1}\mathbf{J_{LU}} \tag{4.8}$$

where the matrices $\mathbf{J}_{SS}$, $\mathbf{J}_{SL}$, $\mathbf{J}_{SU}$, $\mathbf{J}_{LS}$, $\mathbf{J}_{LL}$ and $\mathbf{J}_{LU}$ are described as in Table 4.1. **S** represents a matrix containing energy storage elements. **L** represents a matrix containing energy dissipating elements. For any LTI continuous time system

$$\dot{x} = \mathbf{A}x \tag{4.9}$$

where matrix **A** is same as described in Eq. (4.6).

4.2.2 Physical Model Reduction Procedure

Physical model reduction procedure gives an appropriate reduced order model with the physical relevance to the full order model retaining the almost same dynamic behaviour. The procedure for calculating the effect matrices describing storage & dissipating elements and identifying the irrelevant components is as follows:

1. The system matrices **S**, $\mathbf{J}_{SS}$, **L**, $\mathbf{J}_{SL}$, $\mathbf{J}_{LS}$, and $\mathbf{J}_{LL}$ described above are calculated from the bond graph of the system.

2. The state matrix of the system $\mathbf{A} = \mathbf{JS}$ is formed where **J** is given by Eq. (4.7).

3. The Eigen values of state matrix **A** are calculated.

4. Then the left and right Eigenvector matrices of the state matrix **A**, i.e. **V** and **U** matrices respectively, are calculated.

5. For each Eigen value, the physical parameter sensitivities are calculated as follows:

$$\frac{\partial y_i}{\partial s_j} = v_i^T (\mathbf{J}\, t_j e_j e_j^T) u_i \tag{4.10}$$

$$\frac{\partial y_i}{\partial s_j} = v_i^T (\mathbf{J}_{\mathrm{SL}} \frac{\partial \mathbf{L}}{\partial l_j} (I - \mathbf{J}_{\mathrm{LL}}\mathbf{L})^{-1} \mathbf{J}_{\mathrm{SL}}\mathbf{S} + \mathbf{J}_{\mathrm{SL}}\mathbf{L}(I - \mathbf{J}_{\mathrm{LL}}\mathbf{L})^{-2} \mathbf{J}_{\mathrm{LL}}\mathbf{J}_{\mathrm{LS}}\mathbf{S}) u_i \tag{4.11}$$

where all the matrices are already described above. If $J_{\mathrm{LL}} = 0$

$$\frac{\partial y_i}{\partial s_j} = v_i^T (\mathbf{J}_{\mathrm{SL}}\ z_j e_j e_j^T \mathbf{J}_{\mathrm{LS}}\mathbf{S}) u_i \tag{4.12}$$

where t_j and z_j are multiplication factors given in Table 4.2.

6. Then the absolute values of $\frac{\partial \lambda_j}{\partial s_j}$ and $\frac{\partial \lambda_j}{\partial l_j}$ which are known as sensitivity values are calculated.

Table 4.2 Multiplication factors

Domain	R-element	$z = \frac{\partial R}{\partial l}$	I-element	$t_j = \frac{\partial I}{\partial s}$	C-element	$t_j = \frac{\partial C}{\partial s}$
Mechanical translation	B	1	$\frac{1}{m}$	$-\frac{1}{m^2}$	K	1
Mechanical rotation	C	1	$\frac{1}{J}$	$-\frac{1}{J^2}$	K	1
Hydraulic	R	1	$\frac{1}{I}$	$-\frac{1}{I^2}$	$\frac{1}{C}$	$-\frac{1}{C^2}$
Electrical	R	1	$\frac{1}{L}$	$-\frac{1}{L^2}$	$\frac{1}{C}$	$-\frac{1}{C^2}$

7. Using the sensitivity values, the matrices $\mathbf{E_{IC}}$ and $\mathbf{E_R}$ are formed such that each row shows one Eigen value and each column represents one energy storage or energy dissipation element, respectively, *i.e.*

$$\mathbf{E_{IC}} = \begin{bmatrix} \left|\frac{\partial \lambda_1}{\partial s_1}\right| & \left|\frac{\partial \lambda_1}{\partial s_2}\right| & \cdots\cdots\cdots & \left|\frac{\partial \lambda_1}{\partial s_r}\right| \\ \left|\frac{\partial \lambda_2}{\partial s_1}\right| & \left|\frac{\partial \lambda_2}{\partial s_2}\right| & \cdots\cdots\cdots & \left|\frac{\partial \lambda_2}{\partial s_r}\right| \\ \vdots & \vdots & \vdots & \vdots \\ \left|\frac{\partial \lambda_n}{\partial s_1}\right| & \left|\frac{\partial \lambda_n}{\partial s_2}\right| & \cdots\cdots\cdots & \left|\frac{\partial \lambda_n}{\partial s_r}\right| \end{bmatrix} \tag{4.13}$$

$$\mathbf{E_R} = \begin{bmatrix} \left|\frac{\partial \lambda_1}{\partial l_1}\right| & \left|\frac{\partial \lambda_1}{\partial l_2}\right| & \cdots\cdots\cdots & \left|\frac{\partial \lambda_1}{\partial l_m}\right| \\ \left|\frac{\partial \lambda_2}{\partial l_1}\right| & \left|\frac{\partial \lambda_2}{\partial l_2}\right| & \cdots\cdots\cdots & \left|\frac{\partial \lambda_2}{\partial l_m}\right| \\ \vdots & \vdots & \vdots & \vdots \\ \left|\frac{\partial \lambda_n}{\partial l_1}\right| & \left|\frac{\partial \lambda_n}{\partial l_2}\right| & \cdots\cdots\cdots & \left|\frac{\partial \lambda_n}{\partial l_m}\right| \end{bmatrix} \tag{4.14}$$

The effect matrix $\mathbf{E_{IC}}$ is the effect matrix for energy storage elements *i.e.* inertia elements and capacitive elements. Similarly, the effect matrix $\mathbf{E_R}$ is an effect matrix for energy dissipating elements *i.e.* resistive elements. The elements of the effect matrices are the measure of sensitivity of Eigen value to an element. The relative importance of the elements for some specific Eigen value can be obtained by performing some suitable operations on the matrices. Hence, the elements in every row of sensitivity matrices are divided by the biggest element in that row to have a comparison among one type of elements, which indicates relative importance of each element for any particular Eigen value. The Eigen values which are very small are neglected. The rows of the effect matrices, corresponding to the Eigen values that can be neglected, are dropped completely. The columns that have very low magnitude as compared to the other columns in the effect matrices are found and neglected. Then, the element corresponding to that column is removed from the system. Finally, a reduced system is obtained which is modelled with the help of bond graph. The results are compared between the full system and reduced system.

The major constraint of this Eigen value sensitivity method followed in the thesis is that it can be applied only to linear time invariant (LTI) systems. The model reduction of non-linear systems can be done by Eigen value sensitivity method only after the non-linear models are linearized. Another major constraint is that some elements that are observed minimal active from the calculations cannot be removed straight forwardly from the system's bond graph arrangement because the system may become unstable after the removal of these elements. Hence, these elements must be added in the system manually at a later stage.

4.2.3 Model Reduction for Pedagogical Example

The Eigen value sensitivity method is applied to a mass-spring-damper system as shown in Fig. 4.1(a). The bond graph representation of this system is shown in Fig. 4.1(b). The parameters are taken arbitrarily as:

$m_1 = m_2 = m_3 = 1$ kg, $k_1 = 4$ N/m, $k_2 = k_3 = 1$ N/m, $k_4 = 2.5$ N/m, $k_5 = 5$ N/m, $R_1 = 1.5$ Ns/m, $R_2 = 0.5$ Ns/m, $R_3 = 1$ Ns/m, $R_4 = 0.4$ Ns/m, $R_5 = 0.2$ Ns/m.

The various system matrices for this example are:

S is 8×8 square matrix with diagonal elements [$1/m_1$, $1/m_2$, $1/m_3$, k_1, k_2, k_3, k_4, k_5] and all other elements are zero. Similarly, **L** is 5×5 square matrix with diagonal elements [R_1, R_2, R_3, R_4, R_5] and all other elements are zero. **I** is 5×5 identity matrix and $\mathbf{J_{LL}}$ is 5×5 zero matrix.

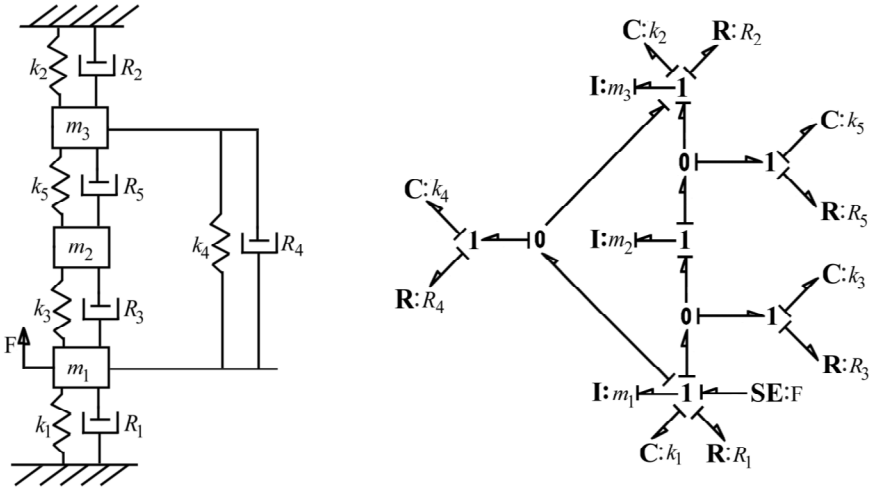

(a) (b)

Fig. 4.1 (a) A mass-spring-damper system and (b) its bond graph representation

Other system matrices **Jss**, $\mathbf{J_{SL}}$ and $\mathbf{J_{LS}}$ formed from the bond graph model are as follows:

$$\mathbf{J_{SS}} = \begin{bmatrix} 0 & 0 & 0 & -1 & 0 & -1 & -1 & 0 \\ 0 & 0 & 0 & 0 & 0 & -1 & 0 & -1 \\ 0 & 0 & 0 & 0 & -1 & 0 & 1 & -1 \\ 1 & 0 & 0 & 0 & 0 & 0 & 0 & 0 \\ 0 & 0 & 1 & 0 & 0 & 0 & 0 & 0 \\ 1 & 1 & 0 & 0 & 0 & 0 & 0 & 0 \\ 1 & 0 & -1 & 0 & 0 & 0 & 0 & 0 \\ 0 & 1 & 1 & 0 & 0 & 0 & 0 & 0 \end{bmatrix} \tag{4.15}$$

$$\mathbf{J_{SL}} = \begin{bmatrix} 1 & 0 & 1 & 1 & 0 \\ 0 & 0 & 1 & 0 & 1 \\ 0 & -1 & 0 & 1 & 1 \\ 0 & 0 & 0 & 0 & 0 \\ 0 & 0 & 0 & 0 & 0 \\ 0 & 0 & 0 & 0 & 0 \\ 0 & 0 & 0 & 0 & 0 \\ 0 & 0 & 0 & 0 & 0 \end{bmatrix} \tag{4.16}$$

$$\mathbf{J_{LS}} = \begin{bmatrix} 1 & 0 & 1 & 0 & 0 & 0 & 0 & 0 \\ 0 & 0 & 0 & 0 & 0 & 0 & 0 & 0 \\ 1 & 1 & 0 & 0 & 0 & 0 & 0 & 0 \\ 1 & 0 & 1 & 0 & 0 & 0 & 0 & 0 \\ 0 & 1 & 1 & 0 & 0 & 0 & 0 & 0 \end{bmatrix} \tag{4.17}$$

Then system matrix **A** is calculated as defined by Eq. (4.6). The Eigen values of matrix **A** are calculated as:

$$\left.\begin{aligned} \lambda_{1,2} &= 0.1125 \pm 3.5644i \\ \lambda_{3,4} &= 1.7150 \pm 2.1439i \\ \lambda_{5,6} &= 0.5225 \pm 1.0102i \\ \lambda_{7} &= -4.0540 \times 10^{-17} \\ \lambda_{8} &= 8.6752 \times 10^{-17} \end{aligned}\right\} \tag{4.18}$$

Now, with the calculation of Eigenvectors, the effect matrices are formed as:

$$\mathbf{E_{IC}} = \begin{bmatrix} 0.269648 & 0.261526 & 0.800221 & 0.021202 & 0.062921 & 0.004944 & 0.159553 & 0.154058 \\ 0.269648 & 0.261526 & 0.800221 & 0.021202 & 0.062921 & 0.004944 & 0.159553 & 0.154058 \\ 0.758134 & 0.22819 & 0.048327 & 0.100581 & 0.006412 & 0.217556 & 0.049428 & 0.053166 \\ 0.758134 & 0.22819 & 0.048327 & 0.100581 & 0.006412 & 0.217556 & 0.049428 & 0.053166 \\ 0.070918 & 0.233583 & 0.169468 & 0.054825 & 0.131012 & 0.056045 & 0.028415 & 0.005511 \\ 0.070918 & 0.233583 & 0.169468 & 0.054825 & 0.131012 & 0.056045 & 0.028415 & 0.005511 \\ 1.24\times10^{-34} & 4.47\times10^{-33} & 6.96\times10^{-33} & 1.64\times10^{-18} & 3.31\times10^{-17} & 6.25\times10^{-18} & 2.25\times10^{-17} & 2.09\times10^{-18} \\ 1.24\times10^{-34} & 4.47\times10^{-33} & 6.96\times10^{-33} & 1.64\times10^{-18} & 3.31\times10^{-17} & 6.25\times10^{-18} & 2.25\times10^{-17} & 2.09\times10^{-18} \end{bmatrix} \quad (4.19)$$

$$\mathbf{E_R} = \begin{bmatrix} 0.029103 & 0 & 0.017631 & 0.04088 & 0.549403 \\ 0.029103 & 0 & 0.017631 & 0.04088 & 0.549403 \\ 0.30715 & 0 & 0.59729 & 0.454143 & 0.145966 \\ 0.30715 & 0 & 0.59729 & 0.454143 & 0.145966 \\ 0.144103 & 0 & 0.063742 & 0.392297 & 0.006267 \\ 0.144103 & 0 & 0.063742 & 0.392297 & 0.006267 \\ 1.01\times10^{-33} & 0 & 7.90\times10^{-34} & 4.09\times10^{-33} & 2.64\times10^{-33} \\ 5.79\times10^{-33} & 0 & 1.51\times10^{-33} & 2.31\times10^{-32} & 4.43\times10^{-33} \end{bmatrix} \quad (4.20)$$

It is seen that Eigen values $\lambda_{7,8}$ have no imaginary components with very high real values. So, their effects will diminish soon and hence, they are neglected *i.e.* the rows 7 and 8 are deleted from both the effect matrices $\mathbf{E_{IC}}$ and $\mathbf{E_R}$. It is also seen that column 2 in $\mathbf{E_R}$ matrix has zero value. So, the element R_2 corresponding to that column is also eliminated from the system's bond graph arrangement. After all these eliminations, a reduced bond graph of the system is obtained as shown in Fig. 4.2. This reduced bond graph model does not have R_2 element.

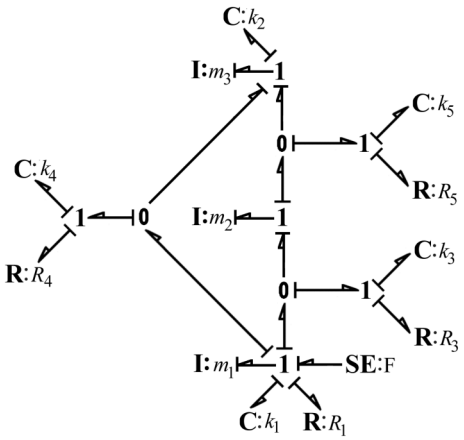

Fig. 4.2 Reduced bond graph model of mass-spring-damper system

Here due to the simple system, only 1 element is eliminated from the bond graph model of the system. But, as the complexity of the system increases, its bond graph model becomes large and hence more number of bonds will be removed from the

system's bond graph arrangement as explained for a planar parallel manipulator and planar hybrid manipulator in Sections 4.3 and 4.4 later in this chapter.

4.3 Physical Model Reduction of a Planar Parallel Manipulator

A planar hybrid manipulator was proposed in Fig. 3.1(a) of Chapter 3 in which two parallel manipulators, each having six degree of freedom, are supported serially upon each other. In this section, the model reduction for this single parallel manipulator is being done. This parallel manipulator was developed by [Bera *et al*., 2010]. The same model is displayed in Fig. 4.3. Its arrangement is same as the hybrid manipulator shown in Fig. 3.1(a) in Chapter 3. The base CDE is fixed and this is considered as the ground link. It is connected to the moving platform AGB by three legs AC, AD and BE whose lengths are L_1, L_2 and L_3, respectively. Point G is the centre of gravity of the moving platform and lengths of AG and BG are considered a and b, respectively. All the legs are prismatic pairs and joints are considered as pin joints. Point G is considered to be in the mid of line AB which makes an angle θ_G with the horizontal axis. The kinematic Eqs. (3.1 – 3.11) used in Chapter 3, are used here also for framing the bond graph model to represent forward and inverse dynamics of this planar parallel manipulator.

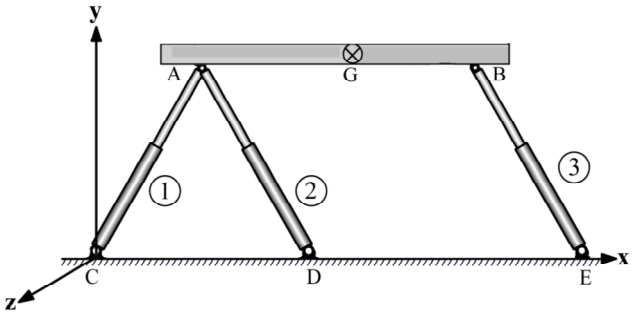

Fig. 4.3 Schema of a planar parallel manipulator [Bera *et al*., 2010]

4.3.1 Forward Model of Planar Parallel Manipulator

The forward dynamics of this manipulator are represented in a bond graph arrangement and that arrangement is displayed in Fig. 4.4. For this forward dynamics arrangement, the junctions $1_{\dot{x}G}$ and $1_{\dot{y}G}$ represent the linear velocities of point G in x and y directions,

respectively. The representation of all other junctions has already been explained in Section 3.2.2 in Chapter 3. All the inertial, capacitor and damping elements *i.e.* I, C and R elements in the forward bond graph model as well as in the inverse bond graph model are numbered as 1, 2, 3…. *etc.* so that recognition of these elements in effect matrices becomes easy. Only kinematic equations are required to frame a bond graph model. The dynamic equations can be generated directly from the model. This is one of the major advantages of bond graph modelling technique. Hence, the final forward model for a planar parallel manipulator is displayed in Fig. 4.4.

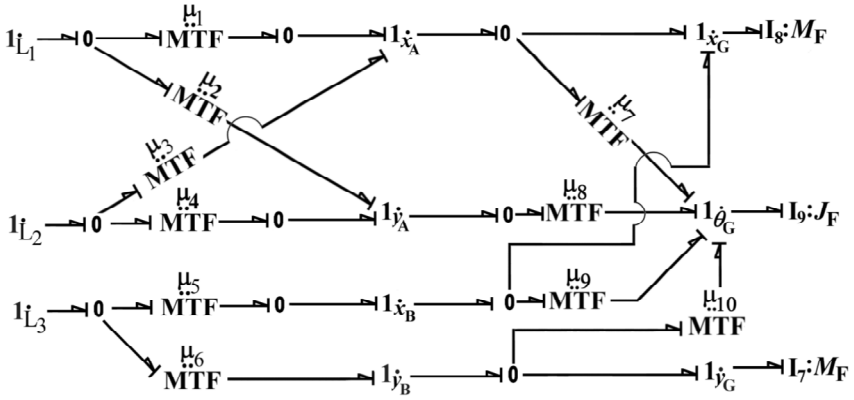

Fig. 4.4 Forward bond graph model of a parallel manipulator

The commands given to this forward model are the efforts applied in three legs (actuators) of the manipulator. The linear and angular positions of centre of gravity of the platform 'AB' are taken as outputs here which will be further matched with the command positions given to the inverse model for doing trajectory tracking of the manipulator, which will be shown later in Section 4.5 of this chapter.

4.3.2 Inverse Model for Planar Parallel Manipulator

The inverse dynamic model constructed for the planar parallel manipulator is the mirror image of the forward model shown above in Fig. 4.4. Only the numbers of velocity ports are increased to avoid differential causality. This has already been explained in Chapter 3. The mass (*M*) and the moment of inertia (*J*) of the platform are shown by the three I-elements connected to 1-junctions. Pads (coupling capacitors) are added to avoid

differential causality at necessary points. The elements with subscript "con" are known as ghost controller elements are added at the three inputs of the inverse model for the implementation of overwhelming controller which is used here to study the trajectory tracking. The use of pads for removing differential causality and controller along with the use of overwhelming control strategy for inverse model has already been explained in detail in Section 3.3 of Chapter 3. Therefore, the final bond graph model representing the inverse dynamics of planar parallel manipulator is displayed in Fig. 4.5. The inputs given to the inverse model are the reference positions in linear *x* and *y* directions and angular path in θ direction. The outputs come in the form of efforts applied in three legs (actuators) of the manipulator.

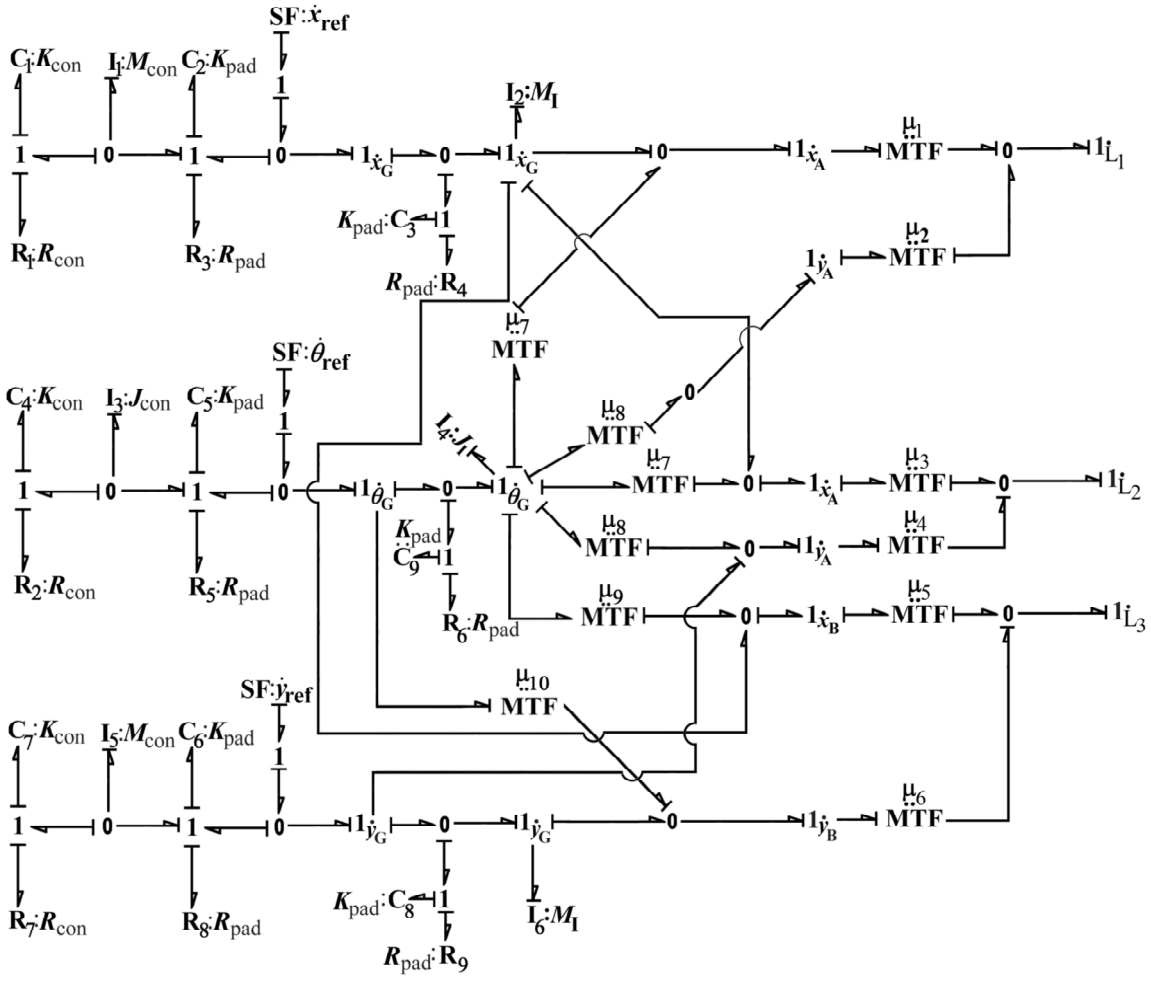

Fig. 4.5 Inverse dynamics arrangement in bond graph of a parallel manipulator

4.3.3 Full Bond Graph Model of Planar Parallel Manipulator

The inverse and forward dynamic models of this manipulator are combined for trajectory tracking through a circular path, the results of which will be shown later in this chapter. This combined model for trajectory tracking is shown in Fig. 4.6. The command positions in *x* and *y* directions are given to the inverse model as inputs and outputs coming from the inverse model in the form of efforts for three legs are given as inputs to the forward model. Finally the output positions coming from the forward model are matched with the input positions given (command values).

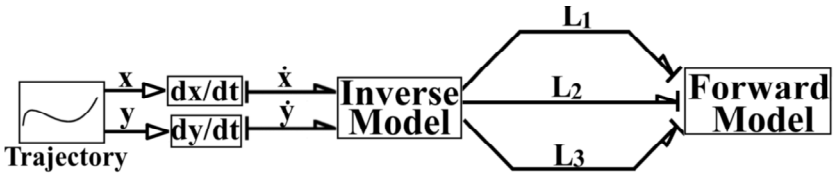

Fig. 4.6 Combined bond graph model of a parallel manipulator

4.3.4 Reduced Bond Graph Model of Planar Parallel Manipulator

The parameters used in reducing the model are chosen suitably and are given in Table 4.3.

Table 4.3 Parameter values

Sub systems	Parameter values			
Platform	$M_{\mathrm{F}} = 11\ \mathrm{kg}$	$J_{\mathrm{F}} = 0.1\ \mathrm{kg\ m^2}$	$K_{\mathrm{pad}} = 10^8\ \mathrm{N/m}$	$R_{\mathrm{pad}} = 50\ \mathrm{Ns/m}$
Actuator	$K_{\mathrm{pad}} = 10^8\ \mathrm{N/m}$	$R_{\mathrm{pad}} = 50\ \mathrm{Ns/m}$		
Inverse system	$M_{\mathrm{I}} = 0.25\ \mathrm{kg}$	$J_{\mathrm{I}} = 0.25\ \mathrm{kg\ m^2}$	$M_{\mathrm{con}} = 30\ \mathrm{kg}$	$J_{\mathrm{con}} = 1\ \mathrm{kg\ m^2}$
	$K_{\mathrm{con}} = 10^4\ \mathrm{N/m}$	$R_{\mathrm{con}} = 1\ \mathrm{Ns/m}$	$\mu_{\mathrm{H}} = 10000$	$\mu_{\mathrm{L}} = 1$
Circular path	$\omega = 1\ \mathrm{rad/s^2}$	$r = 0.1\ \mathrm{m}$		

Using the Eigen value sensitivity method, the various system matrices are developed from the bond graph model. Then Eigen values are calculated from the system matrices. From these Eigen values, effect matrices are generated and finally, these are simplified for the reduction of the model.

The various system matrices formed for planar parallel manipulator are as follows:
S is 18×18 square matrix with diagonal elements [$1/I_1$, $1/I_2$, $1/I_3$, $1/I_4$, $1/I_5$, $1/I_6$, $1/I_7$, $1/I_8$, $1/I_9$, C_1, C_2, C_3, C_4, C_5, C_6, C_7, C_8, C_9] and all other elements being zero.
Similarly, **L** is a square matrix of 9×9 order with diagonal elements [R_1, R_2, R_3, R_4, R_5, R_6, R_7, R_8, R_9] and all other elements are zero. *I* is 18×9 identity matrix. Also $\mathbf{J_{LL}}$ is 9×9 zero matrix.

Other system matrices **Jss**, $\mathbf{J_{SL}}$ and $\mathbf{J_{LS}}$ are calculated similar to as they were calculated in Section 4.3.2 above. The system matrix **A** is calculated and based on it, left and right Eigen vector matrices are calculated as described earlier in Section 4.3.2. The final Eigen values will be 18 in number for the system and these are:

$\lambda_1 = 5\times10^{9}$
$\lambda_{2,3} = 1.1715\times10^{2} \pm 8.6865\times10^{4}i$
$\lambda_4 = 3.9403\times10^{4}$
$\lambda_5 = -3.9565\times10^{4}$
$\lambda_{6,7} = 3.4042\times10^{2} \pm 1.4259\times10^{4}i$
$\lambda_{8,9} = 4.1273\times10^{2} \pm 8.5878\times10^{3}i$
$\lambda_{10,11} = 8.7975\times10^{1} \pm 1.3833\times10^{3}i$
$\lambda_{12,13} = 6.1637\times10^{-1} \pm 1.0165\times10^{2}i$
$\lambda_{14,15} = 3.2030 \pm 60.9747i$
$\lambda_{16} = 0.6171$
$\lambda_{17,18} = 0.0165 \pm 18.65i$

The final effect matrices $\mathbf{E_{IC}}$ and $\mathbf{E_R}$ can also be formed using these Eigen values similar to Section 4.3.2. The matrix $\mathbf{E_{IC}}$ is a matrix of 18×18 order and another matrix $\mathbf{E_R}$ is a 18×9 matrix. Now, from the Eigen values calculated above, it is seen that λ_1 has no imaginary component with a higher real component; so its effect will diminish soon and hence, it is neglected. Also, $\lambda_{14,15}$ and $\lambda_{17,18}$ have very high imaginary component with lower real component. So, these Eigen values do not contribute much to the system and hence, are neglected. Moreover, real component of $\lambda_{12,13}$ is near to zero therefore, it is also neglected. Therefore, the rows 1, 12, 13, 14, 15, 17 and 18 from the effect matrices

corresponding to these values are deleted. Then after doing comparison, it is seen that columns 1, 3, 5, 10, 11, 12, 13, 14, 15, 16, 17 and 18 in $\mathbf{E_{IC}}$ matrix have very low magnitude. These columns are also neglected and system elements corresponding to these columns I_1, I_3, I_5, C_1, C_2, C_3, C_4, C_5, C_6, C_7, C_8 and C_9 can be neglected and a reduced bond graph of the system is obtained. The reduced inverse model formed after all these eliminations is shown in Fig. 4.7 and the forward model remains the same as shown in Fig. 4.4. So, the combined full model and reduced model are compared for trajectory tracking of the circular path for a parallel manipulator.

4.4 Physical Model Reduction of a Planar Hybrid Manipulator

The hybrid manipulator is considered by placing a parallel manipulator of Fig. 4.3 over the other in series so that it becomes a parallel-series hybrid manipulator as already been shown in Fig. 3.1(a) of Chapter 3. The points A, G and B of the moving platform of the lower manipulator become points C, D and E, respectively of the upper manipulator. The forward and inverse bond graph models for this planar hybrid manipulator are same as shown in Fig. 3.2 and Fig. 3.9, respectively in Chapter 3. Here, in this model, plant 1 and plant 2 are vectorially connected to the controller 1 and controller 2, respectively as shown in Fig. 4.8. There is a provision for giving command to each controller separately according to the needs. Three overwhelming controllers are implemented between each set of inverse controller and the forward model. The input signals for the overwhelming controllers are u_1, u_2 and u_3, respectively and these are denoted by MSe elements (modulated source of effort) with controller gains of α_1 α_2 and α_3, respectively. The parameters for the hybrid manipulator remain same as given in Table 4.3 above. The model reduction for hybrid manipulator is done in a similar way as it was explained in Section 4.3.4 above. The elements which were removed from inverse model of planar parallel manipulator are also eliminated from the inverse bond graph model of the hybrid manipulator.

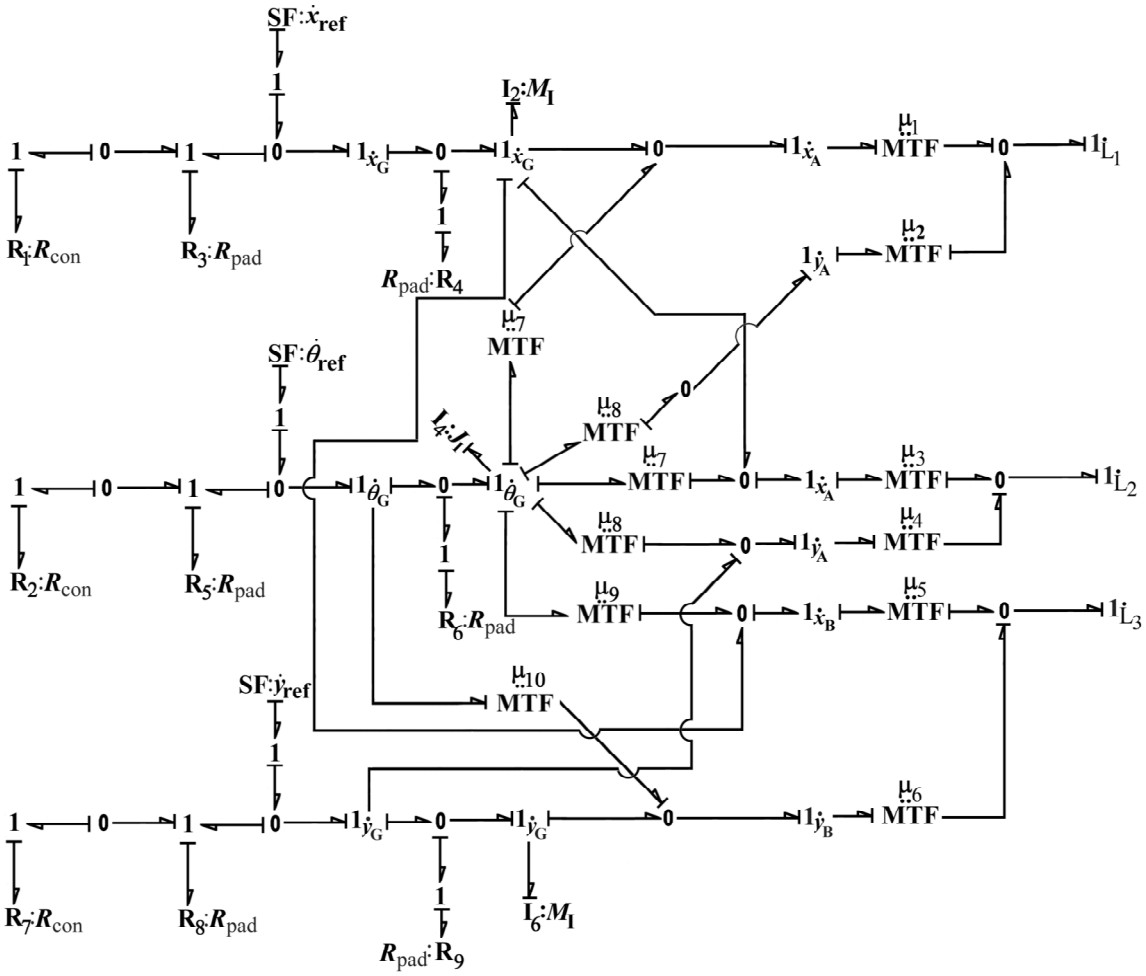

Fig. 4.7 Reduced inverse model for a parallel manipulator

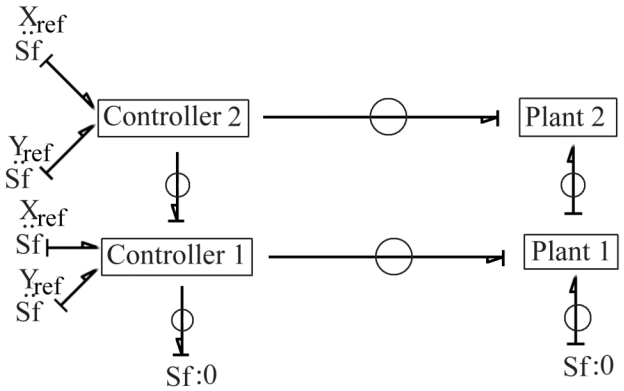

Fig. 4.8 Combined bond graph model for planar hybrid manipulator

4.5 Simulation Results

The simulation was performed for the time duration of 6.28 s. The parameter values for both planar parallel and hybrid manipulator are already given in Table 4.3. The desired trajectory in this case is considered as a circle with radius of 0.1 m and centre as (1.5, 1).

4.5.1 Results for Planar Parallel Manipulator

For a planar parallel manipulator, the inverse model was given reference positions corresponding to the displacements of centre of gravity of the moving platform in *x* and *y* directions. Then the command is compared with the response of the manipulator. The initial conditions of different points of manipulator are given in Table 4.4 below considering moving platform as horizontal initially.

Table 4.4 Initial conditions for parallel manipulator

Points	A	G	B	C	D	E
x (m)	0.5	1.5	2.5	0	1	2
y (m)	1	1	1	0	0	0

The full model shown in Fig. 4.5 and the reduced model shown in Fig. 4.7 are simulated separately. But, command is same for both the cases. The results of trajectory tracking for a circular path by the parallel manipulator obtained from full model and reduced model are shown in Fig. 4.9(a) and (b), respectively. This is the motion of the centroid (*G*) of the moving platform. The command is the input given to the inverse controller and the response is the position of the forward model in which the velocities of the centroid is sensed by velocity sensors.

It is observed that the range of *x*-displacement for full model is from 1.3 m to 1.5 m and for reduced model is also from 1.3 m to 1.5 m. The *y*-displacement ranges from 0.9 m to 1.1 m for both the models. Both the models fully follow the circular path with a slight variation in command and response which can be neglected. The absolute and

percentage error in x and y displacements for full and reduced models of a planar parallel manipulator are displayed in Fig. 4.10(a) and (b), respectively.

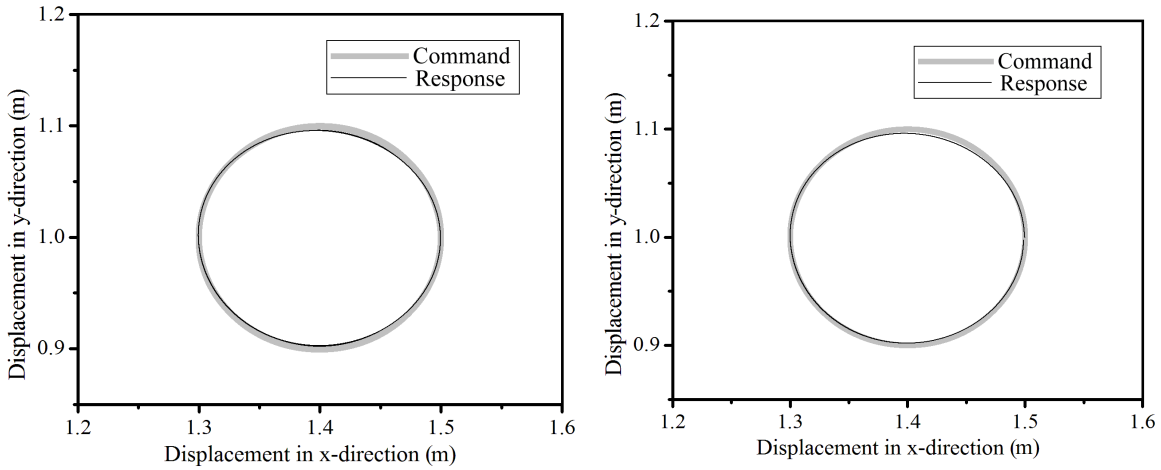

Fig. 4.9 Comparison of response of system with the desired trajectory of (a) full model and (b) reduced model of parallel manipulator

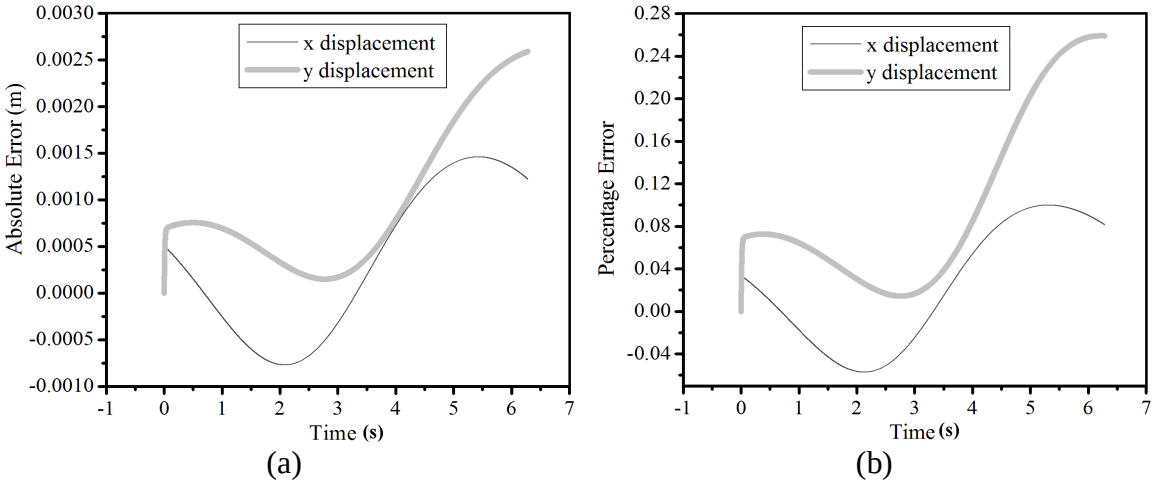

Fig. 4.10 (a) Absolute error and (b) percentage error in *x* and *y* displacements for full and reduced model of a parallel manipulator

The range of absolute error for *x*-displacement is from -0.000771 m to 0.001460 m while for *y*-displacement, the absolute error varies from 0 to 0.002591 m, as observed from Fig. 4.10(a). The percentage error, as seen from Fig. 4.10(b) varies from 0.057114% to 0.099937% for *x*-displacement and from 0 to 0.259207% for *y*-displacement.

4.5.2 Results for Planar Hybrid Manipulator

In this hybrid manipulator model, commands for trajectory tracking are given to both the inverse controllers. The plant 1 and plant 2 behave as per the commands given to the controller 1 and controller 2, respectively. Here, the results are shown only for plant 2 and controller 2. The initial conditions considered for planar hybrid manipulator are given in Table 4.5.

Table 4.5 Initial conditions for the hybrid manipulator

	Points	*x* (m)	*y* (m)		Points	*x* (m)	*y* (m)
Lower Manipulator	A	0.5	1.0	Upper Manipulator	A	1.0	2.0
	G	1.5	1.0		G	2.0	2.0
	B	2.5	1.0		B	3.0	2.0
	C	0	0		C	0.5	1.0
	D	1.0	0		D	1.5	1.0
	E	2.0	0		E	2.5	1.0

The final trajectory tracking results for a circular path by the planar hybrid manipulator, *i.e.* motion of centroid of plant 2 obtained from full model and reduced model are shown in Fig. 4.11(a) and (b), respectively. The command and response remain same as for parallel manipulator, explained above.

The range of *x*-displacement, as seen from Fig. 4.11(a) and (b), is from 1.8 m to 2 m for full model and from 1.79 m to 2.00 m for reduced model. Also, the range of *y*-displacement for full model is from 1.9 m to 2.1 m and for reduced model is from 1.9 m to 2.096 m. Fig. 4.12(a) and (b), respectively show the absolute error and percentage error in *x* and *y*-displacements for full and reduced models for the planar hybrid manipulator, respectively.

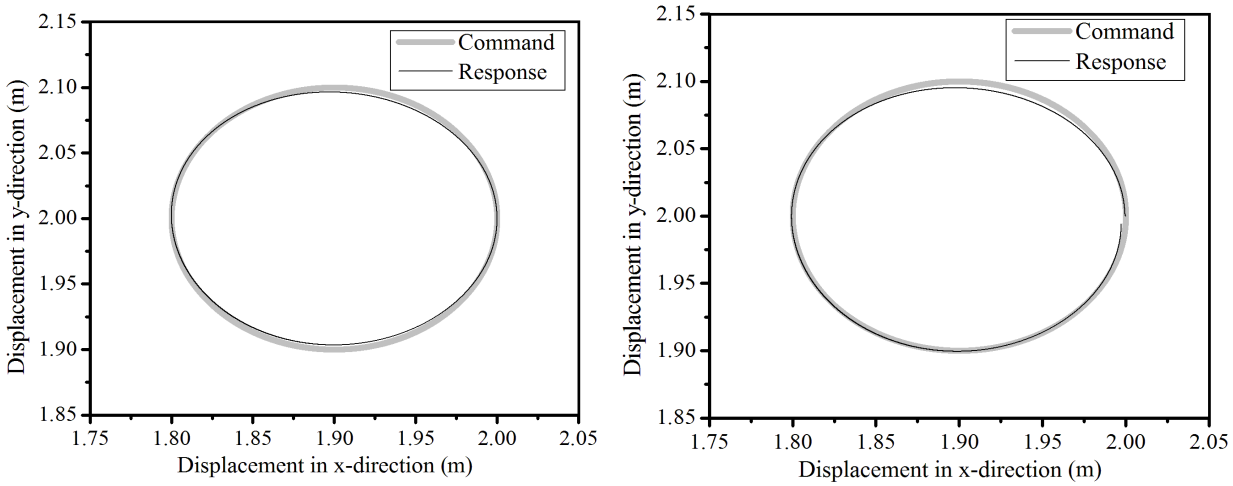

(a) (b)

Fig. 4.11 Comparison of response of system to track the desired command trajectory of (a) full model and (b) reduced model of hybrid manipulator (centroid motion of plant 2)

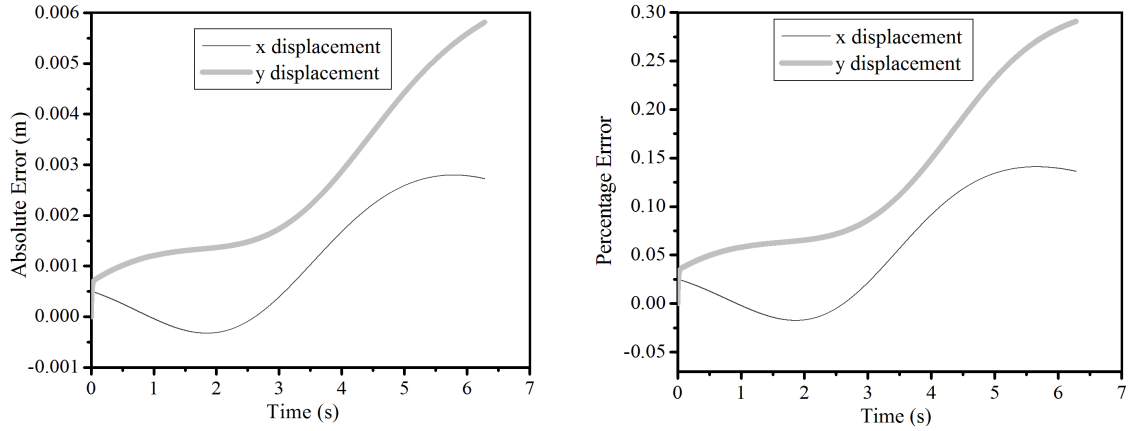

(a) (b)

Fig. 4.12(a) Absolute error and (b) percentage error in *x* and *y* displacements for full and reduced model of a hybrid manipulator (centroid motion of plant 2)

It is observed that the absolute error for *x*-displacement varies from -3.3×10^{-4} m to 2.797×10^{-3} m and for *y*-displacement; the absolute error varies from 0 m to 5.818×10^{-3} m. Moreover, the percentage error in *x*-displacement ranges from -1.746×10^{-2} % to 1.409×10^{-2} % and in *y*-displacement, the range is from 0% to 0.291% which is very small and hence, can be neglected.

4.6 Conclusions

In this chapter, the Eigen value sensitivity method for reducing the number of elements of the bond graph model in physical domain is presented and applied on a planar parallel and hybrid manipulator. The most relevant energy storage elements are identified from two effect matrices that are formed from the Eigen values. The Eigen value sensitivity matrix provides a reduced model for any time scale, the selection of which can be done by selecting the Eigen values. The discussed methodology is applicable not only for LTI systems, algorithms can be developed to reduce non-linear models using these techniques. The trajectory tracking was done for circular path for both the models and results were found to be quite close to each other. The error for circular path tracking is less than one percent. The error can be further decreased by increasing the gain of overwhelming controller. The reduced model and full model represent same dynamics of the system but the simulation time and the amount of calculations are reduced with the reduced model.

Chapter 5

Target Reaching and Workspace Analysis of Hybrid Manipulator

5.1 Introduction

In everyday life, use of control systems is increasing day by day for use in industries as well as for personal use. Also, popularity of hybrid manipulators is also increasing because of their high stiffness, larger workspace and greater accuracy *etc*. as compared to serial and parallel manipulators. Henceforth, hybrid manipulators have control systems equipped in them now-a-days. These control systems are able to solve complex algorithms and calculations. They are also able to handle different tasks with greater efficiency and accuracy. Therefore, opportunities for their research in various fields like machining, welding, heavy applications for industrial usage, medical usage like walking machines and multi fingered grippers, space usage like flight simulators, pick and place operations, trajectory tracking, target reaching *etc*. are vastly increasing. Along with the trajectory tracking, the workspace analysis for hybrid manipulators has also become a challenging task. But workspace analysis is not a generalized technique. The literature review for workspace analysis of different serial and parallel manipulators was already discussed in Chapter 2. Basically, determination of workspace for planar hybrid manipulators depends on the structure and kinematics of hybrid manipulator.

As already discussed, the serial manipulators have kinematic structures with open loop structure where one link is fixed to the ground and the last link is connected to the end effectors. The parallel manipulators have kinematic structures with closed loop structure where all links are connected to the base and end effectors simultaneously [Kumar & Mukherjee, 1989; Kumar, 1994]. But the hybrid manipulators have kinematic structures with both open loop and closed loop properties. The actuators of planar hybrid manipulator proposed in Chapter 3 were considered to be linear actuators which can be used in industries that require linear motions. These types of actuators can be of pneumatic, hydraulic, mechanical or electro-mechanical type. The actuators used in present planar hybrid manipulator are mechanical actuators which convert rotational

velocity into linear velocity and operate on basic mechanisms like screw mechanism, cam mechanism, wheel and axle mechanism *etc*.

The forward dynamics and inverse dynamics of six degrees-of-freedom planar hybrid manipulator were already represented with bond graph arrangement in Chapter 3. But the models shown in Chapter 3 had inputs coming from the inverse model directly applied to the forward model after using overwhelming controller strategy. In Chapter 3, the legs are modelled as plane impedance model. But in this chapter, the ball screw feed drives are used as prismatic legs for all actuators of planar hybrid manipulator. The ball screw mechanism, the lead screw mechanism, screw jack mechanism and roller screw mechanism are some of the examples working on screw mechanism that uses mechanical linear actuators. Ball screw feed drives [Frey *et al*., 2012] find wide acceptance and applications in industry due to their positional accuracy and mechanical efficiency. These are used as prismatic joints in the manipulator legs by virtue of their ability to convert rotational motion into linear motion. For the workspace analysis, this ball screw technique is applied in the planar hybrid manipulator which was already proposed in Chapter 3. The model of manipulator leg with ball screw feed drive for forward and inverse dynamics will be shown later in this chapter.

Basically, a ball screw is a mechanical linear actuator having rolling contact which has balls made of steel are housed in a nut which generates motion by rolling over the surface. Therefore, the ball screw has low wear and tear because of this rolling friction which further leads to low cost maintenance, reduced lubrication and greater mechanical efficiency.

This chapter is organized as follows: Firstly, the planar hybrid manipulator proposed in Chapter 3 is shown along with its bond graph model where forward and inverse dynamic models with ball screw feed drives used as prismatic actuators are presented and ball screw feed drive is discussed with its forward and inverse models. In this section, models of manipulator leg and moving platform with their bond graph representation are shown. Further, the bond graph model to reach a particular destination by the manipulator i.e. target reaching model by planar hybrid manipulator is presented in next section. The

method of workspace analysis of hybrid manipulator done with ball screw feed drive is discussed further. The trajectory tracking for planar hybrid manipulator having ball screw feed drive is also done in this chapter for a semi-circular path. The results of simulation for trajectory tracking for this semi-circular path along with the results to reach the given target by planar hybrid manipulator and its workspace analysis are presented at the end of this chapter.

5.2 Modelling of Planar Hybrid Manipulator with Ball Screw Feed Drive

A planar hybrid manipulator has already been proposed in Chapter 3. It was a parallel-series hybrid manipulator in which two parallel manipulators are connected in series. Three legs 'AC', 'AD' and 'BE' modelled as plane impedance model in Chapter 3 are considered as linear actuators in terms of ball screw mechanism in present chapter. Ball screw feed drive is used to impart motion to the manipulator. These actuators connect the base which is fixed or the ground 'CDE' to the upper mobile platform 'AB'.

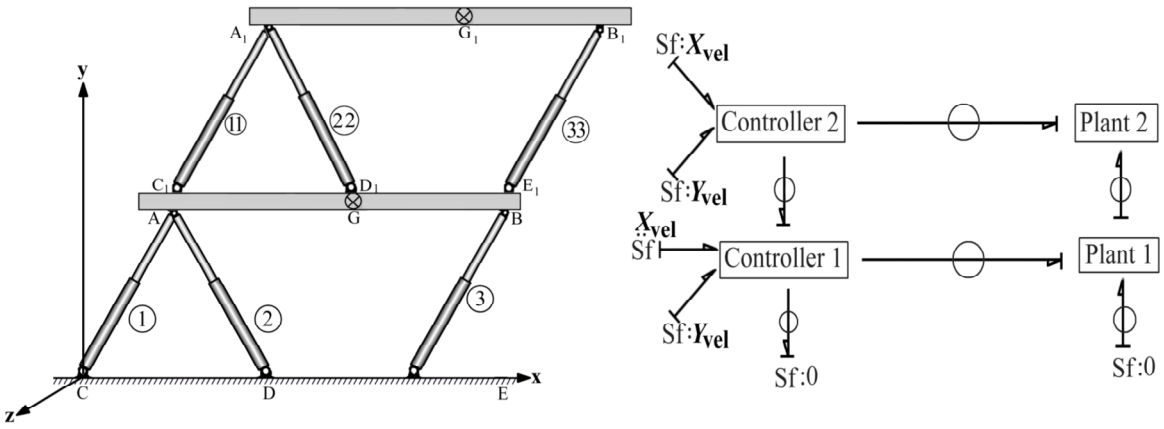

(a) **(b)**

Fig. 5.1 (a) Schematic model of hybrid manipulator and (b) word bond graph model of hybrid manipulator

The point 'G' is taken to be the mid-point of platform 'AB' and centre of gravity of planar parallel manipulator. The two parts of Fig. 5.1 shows the schematic model of this planar hybrid manipulator and corresponding word bond graph model. This bond graph

model shown in Fig. 5.1(b) is used for trajectory tracking later in the chapter. The bond graph model used to reach the target by the planar hybrid manipulator will be shown later in the chapter.

5.2.1 Model of Manipulator Leg with Ball Screw Feed Drive

As already discussed, ball screw feed drives are greatly used in industries for many applications now-a-days because these drives have higher mechanical efficiency and greater accuracy in position than other drives. Therefore, these ball screw feed drives have been used as prismatic actuators for six degrees-of-freedom planar hybrid manipulator in the present chapter so that their capability for transforming rotational motion into linear motion is properly utilized to do workspace analysis. The schematic diagram of a typical ball screw used as a prismatic leg is presented in Fig. 5.2.

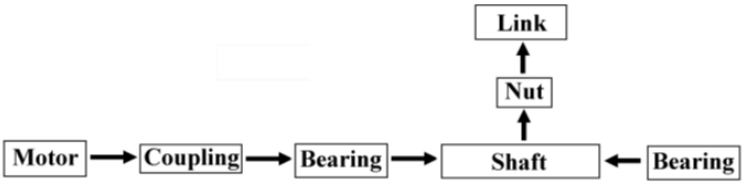

Fig. 5.2 Schematic diagram of ball screw feed drive leg

It consists of a motor connected through a coupling to a threaded shaft which is supported by bearings which are fixed to base of manipulator. As torque is applied to the motor, the rotation of the shaft produces linear motion as a result of threads and screw action on the link and supported by nut. The mechanical equivalent of this ball screw feed drive prismatic leg assembly is depicted in Fig. 5.3. In this, the various components are represented as masses, springs and dampers [Frey *et al.*, 2012]. For simplicity, the shaft parameters are segregated into two branches *i.e.* linear and rotational.

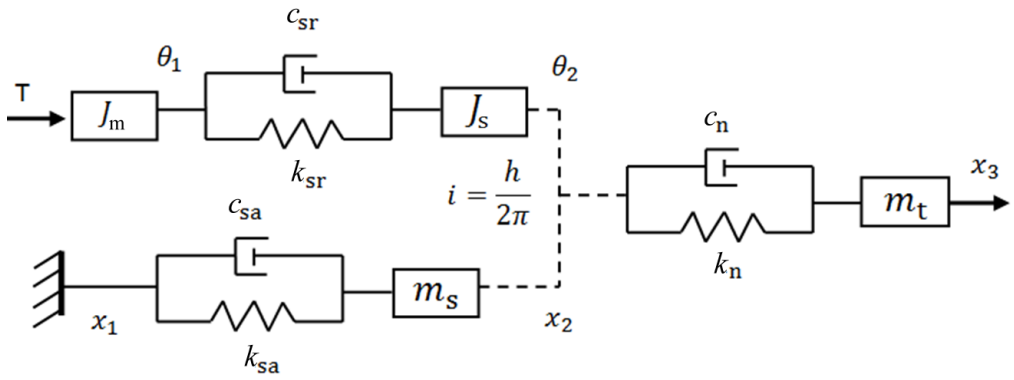

Fig. 5.3 Mechanical equivalent of ball screw feed drive leg

The parameters taken in the model displays their physical values. These are shown like mass of the link as m_t, ball screw shaft mass as m_s, rotary inertia of shaft as J_s and rotary inertia of motor as J_m. The other parameters being shown as linear springs are axial rigidity of the fixed bearing k_b, the rigidity of the ball screw nut k_n and the torsional rigidity of the coupling k_c. The transmission ratio i couple both the motions corresponding to the real mechanical system. The characteristics of the shaft have two different components, axial characteristic k_{sa} and rotational characteristic k_{sr}. The overall axial k_a and rotational value k_r are represented by the following equations which consider all the values of shaft k_{sa} and k_{sr}, coupling k_c and bearing k_b. The transmission ratio i is expressed as the travel distance h during shaft's one revolution.

$$i = \frac{h}{2\pi} \tag{5.1}$$

$$k_r = \left(\frac{1}{k_{sr}} + \frac{1}{k_c} \right)^{-1} \tag{5.2}$$

$$k_a = \left(\frac{1}{k_{sa}} + \frac{1}{k_b} \right)^{-1} \tag{5.3}$$

where $k_{sa} = \frac{EA}{l_{eff}} = \frac{\pi^2 d^2 E}{4 l_{eff}}$, $k_{sr} = J_s (2\pi f_s)^2 = \frac{\pi}{32} d^4 l \rho (2\pi f_s)^2$, $f_s = \frac{1}{4l}\sqrt{\frac{G}{\rho}}$.

The symbols d, l and l_{eff} represent the equivalent diameter, length and effective length, respectively.

Figures 5.4 and 5.5 show the forward bond graph model and inverse bond graph model of the ball screw mechanism, respectively. These models have been developed as per the mechanical equivalent of the ball screw feed drive discussed above. The torque is given to the servo motor as effort input and position of the table is considered as flow output in the forward model. Junctions $1_{\dot{\theta}_1}$ and $1_{\dot{\theta}_2}$ represent the angular velocities of motor and shaft, respectively. I and R-elements connected to these two junctions represent corresponding values of moment of inertia ($J_{\mathrm{m}}, J_{\mathrm{s}}$) and damping coefficients (R_{m}). The stiffness and damping of the rotational component of the system are represented by stiffness element having parameter k_{r} and damping element having parameter c_{r} and these are parallel connected to each other. Similarly, the stiffness and damping of the translational component of the system are represented by the stiffness element having parameter k_{a} and damping element having parameter c_{a}. The angular velocity of the shaft is transformed into linear velocity by transformer element and added with the translational velocity which is represented by $1_{\dot{x}_4}$-junction. The C and R-elements with stiffness and damping parameters k_{n} and c_{n} are used to model the nut so as to generate the motion of the link represented by $1_{\dot{x}_3}$ junction to which an I-element with parameter m_{t} is connected. The torque applied to the motor is the system's input whereas the response of the system is the mobile platform's movement.

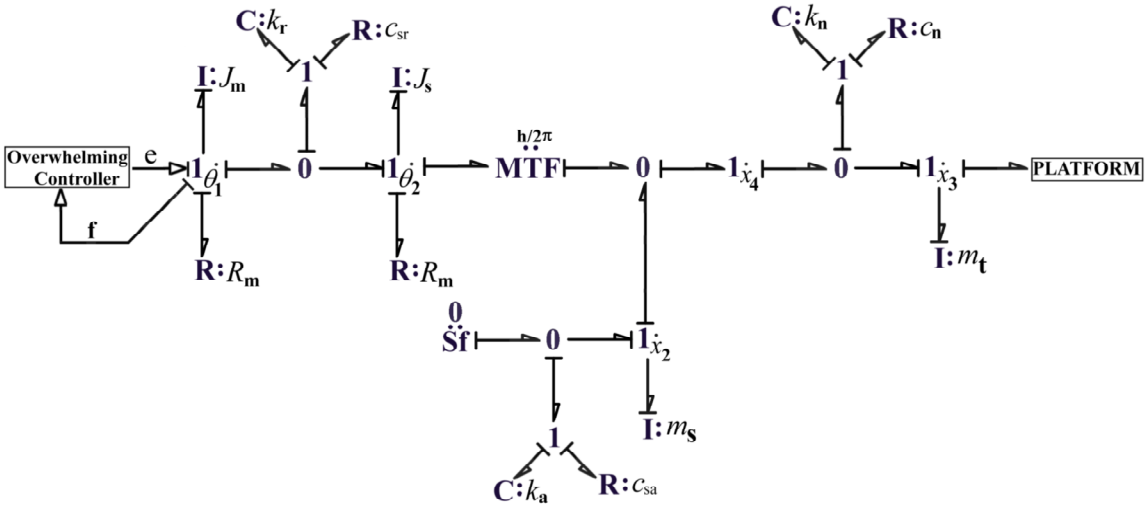

Fig. 5.4 Forward model of ball screw feed drive

The bond graph model for inverse dynamics of the ball screw feed drive is shown in Fig. 5.5. In the inverse model, all the physical parameters, relations and connections between the different elements are same as in the forward model but the power directions of the bonds have been reversed and the model is redrawn. The input to the inverse model is the effort at the link whereas output of the system is angular velocity of the motor.

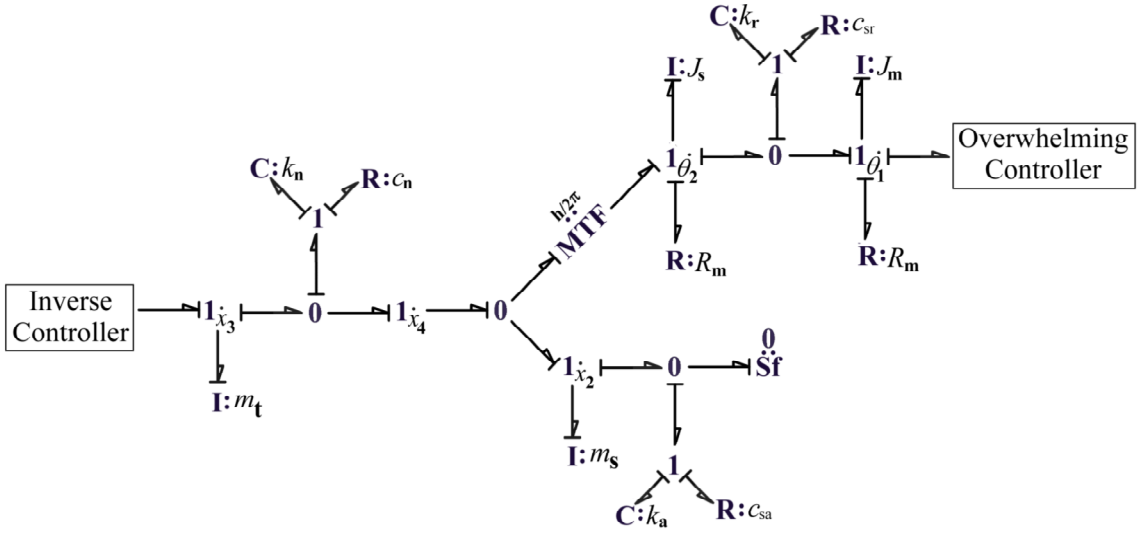

Fig. 5.5 Inverse model of ball screw feed drive

The greatest challenge while developing an inverse controller of a plant is to estimate various characteristic such as un-modelled inertia, friction, backlash, *etc*. which continuously change with time. The strategy to deal with this challenge is to develop such robust controllers which are least sensitive to the concerned parameters. Overwhelming control is one such method to deal with the parameter uncertainties. In an overwhelming control, the controller mass M_{P}^{*} is rigidly attached to the plant mass in physical domain and it drags the plant mass together with itself. The plant dynamics are completely overwhelmed by the controller dynamics by the application of a high gain, $\mu_{\mathrm{H}} >> 1$ at the same maintaining the similarity of motion with the plant by the application of a low gain, $\mu_{\mathrm{L}} = 1$. Consequently, the dynamics of plant mass become a small perturbation on controller dynamics. In an overwhelming control, the controller parameters are focused upon to generate the desired plant performance. Therefore, overwhelming controller is used here to develop the inverse bond graph model of planar hybrid manipulator so that

the unmodelled parameters don't affect the trajectory tracking performance of the manipulator and results are achieved with higher accuracy.

5.2.2 Model of Moving Platform with Ball Screw Feed Drive

Based on the construction and working of planar hybrid manipulator discussed in Chapter 3, this chapter has ball screw feed drives included in the actuators of planar hybrid manipulator. Based on the working of ball screw feed drives, the forward and inverse bond graph models of the planar hybrid manipulator with ball screw mechanism are developed to do trajectory tracking, target reaching and for workspace analysis. Equations (3.1–3.8) used in Chapter 3 to calculate the linear and rotational velocities of all points in terms of velocities of centre of gravity are used here also in this chapter. The same structure of pad elements, doublet junctions and ghost controller elements used in Chapter 3 is used here also to develop the forward model of planar hybrid manipulator for observing trajectory tracking. The leg lengths are also taken as same and lengths of platforms 'AG'and 'BG' are also considered similar to Chapter 3. Based on all these things, the forward bond graph model of planar hybrid manipulator including forward ball screw model is shown in Fig. 5.6 where BS denotes sub model of ball screw, which is the model shown in Fig. 5.4 as already discussed in the chapter. The efforts in three actuators, coming from the inverse model, are amplified with overwhelming controller and then fed as inputs to the forward model through ball screw feed drives to get the x and y velocities.

The inverse model of planar hybrid manipulator is shown in Fig. 5.7 which is the mirror image of the forward model of the hybrid manipulator as developed for a parallel manipulator [Bera & Samantaray, 2011] earlier in Chapter 3. The inverse model shown in Fig. 5.7 includes the sub model of inverse ball screw denoted by INV-BS, which is the model shown in Fig. 5.5 as already discussed in the chapter. The forward model is named as plant model and inverse model is named as controller model.

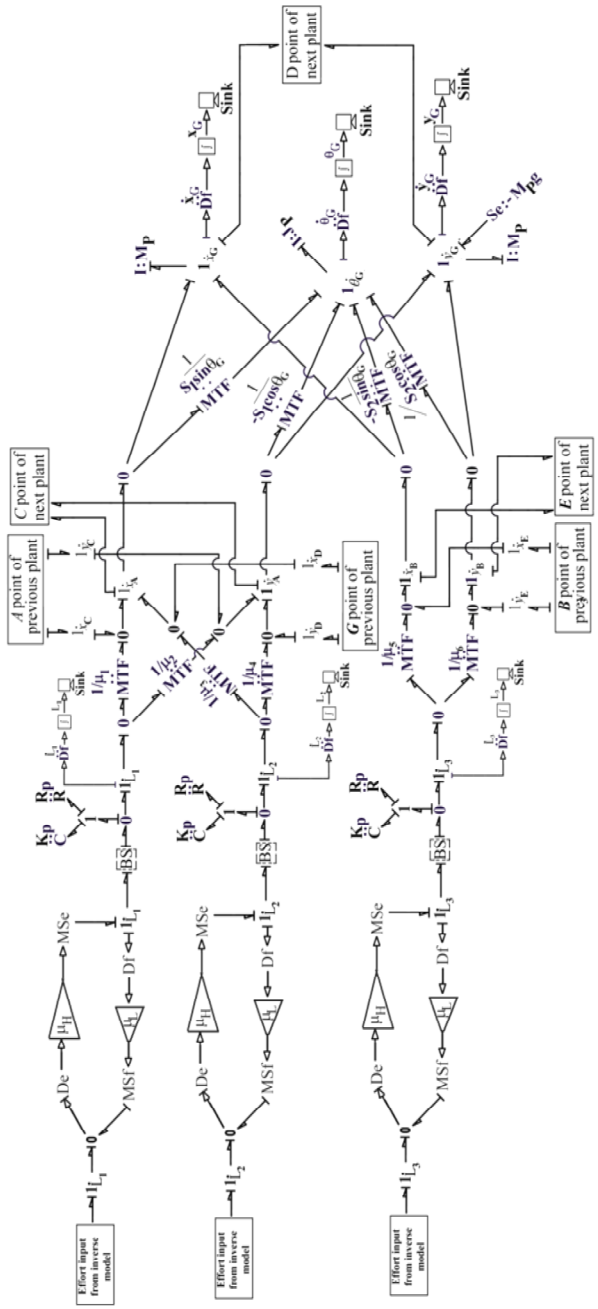

Fig. 5.6 Forward model of the planar hybrid manipulator

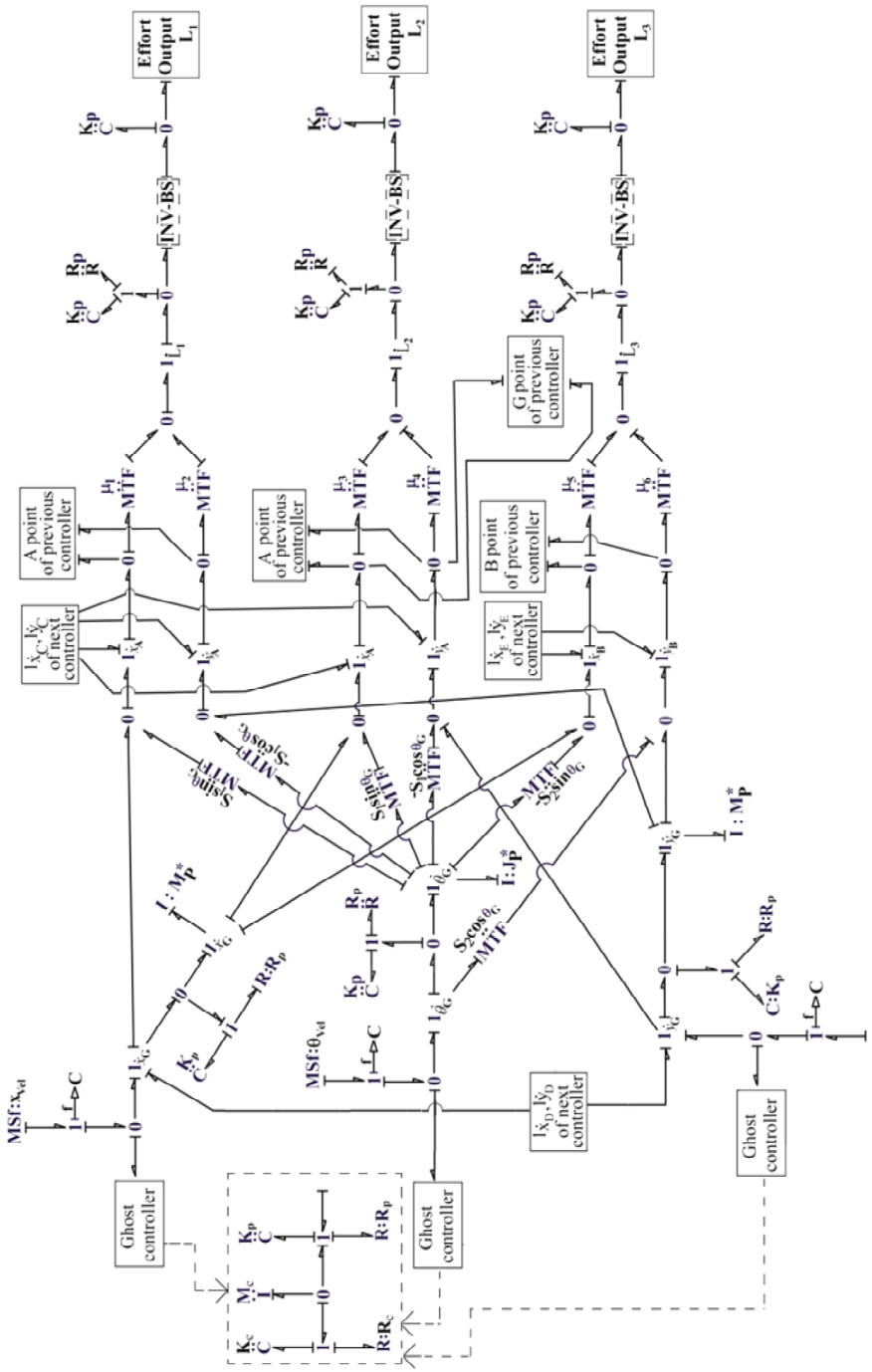

Fig. 5.7 Inverse model of the planar hybrid manipulator

Further, these are joined by overwhelming controller for trajectory tracking as it overwhelms the plant dynamics [Bera *et al*., 2010] and amplifies the effort received from inverse model. To measure the deformation rate of the legs, flow detectors are added at some points. The *x* and *y* velocities for a particular trajectory are given to the inverse model and effort in three legs are taken as outputs. These efforts are then amplified with

overwhelming controller and then fed as inputs to the forward model to get the *x* and *y* velocities. Then, final response is matched with the input for trajectory tracking and this will be discussed in Section 5.5.1 later in the chapter. Fig. 5.6 and Fig. 5.7 are the forward model and inverse model of hybrid manipulator, respectively. The effort output L_1, L_2 and L_3 ports of inverse model are directly connected with the effort input ports L_1, L_2 and L_3 ports of forward model, respectively. Three incoming ports A, B and G of any plant are connected to the previous forward plant model. Similarly, three outgoing ports C, D and E of any plant are connected to the next forward plant model. Three incoming ports C (4 bonds), D (2 bonds) and E (2 bonds) of any inverse model are connected to the next inverse model. Similarly, four outgoing ports A (2 bonds), A (2 bonds), B (2 bonds) and G (2 bonds) of any inverse model are connected to the previous inverse model. In inverse model, two sets of centroidal velocities ports are considered to avoid problems in causalities. A ghost controller is also added during input velocities at the centroidal velocity ports. The output from the inverse model is the torque required for the prismatic leg.

5.3 Target Reaching of Planar Hybrid Manipulator

The incident of the end effector of the manipulator arriving or reaching at a particular destination given to it is known as target reaching of the planar hybrid manipulator. This destination or target is usually fed in terms of its coordinates and the manipulator is required to reach the given target irrespective of the path travelled to reach it. The basic characteristic of a target reaching system is reaching at the given target with negligible errors. In this section, the forward and inverse bond graph models to reach a particular target given to the planar hybrid manipulator will be developed. The manipulator's position is discussed here moving from initial point (x_g, y_g) to the final point (x_d, y_d) in *x*-*y* plane.

The forward model is essentially the same model as already displayed in Fig. 5.6. It is basically the platform model together with actuators which are actuated by ball screw feed drives which get input from the inverse model. The proportional controller is used in target reaching model to calculate the forces whereas overwhelming controller is used in trajectory tracking model. The overwhelming controller is not used in the forward model

here and effort input is directly applied to the forward ball screw model because the main aim of manipulator is to reach the target irrespective of the path followed. This modified forward model is displayed in Fig. 5.8 where the forward ball screw model modelled in the previous section, is displayed as BS in the present forward model. The flow detectors are added to the x_G, y_G and θ_G junctions of centre of gravity in the forward model to detect the current positions, which will be subtracted from the target positions later.

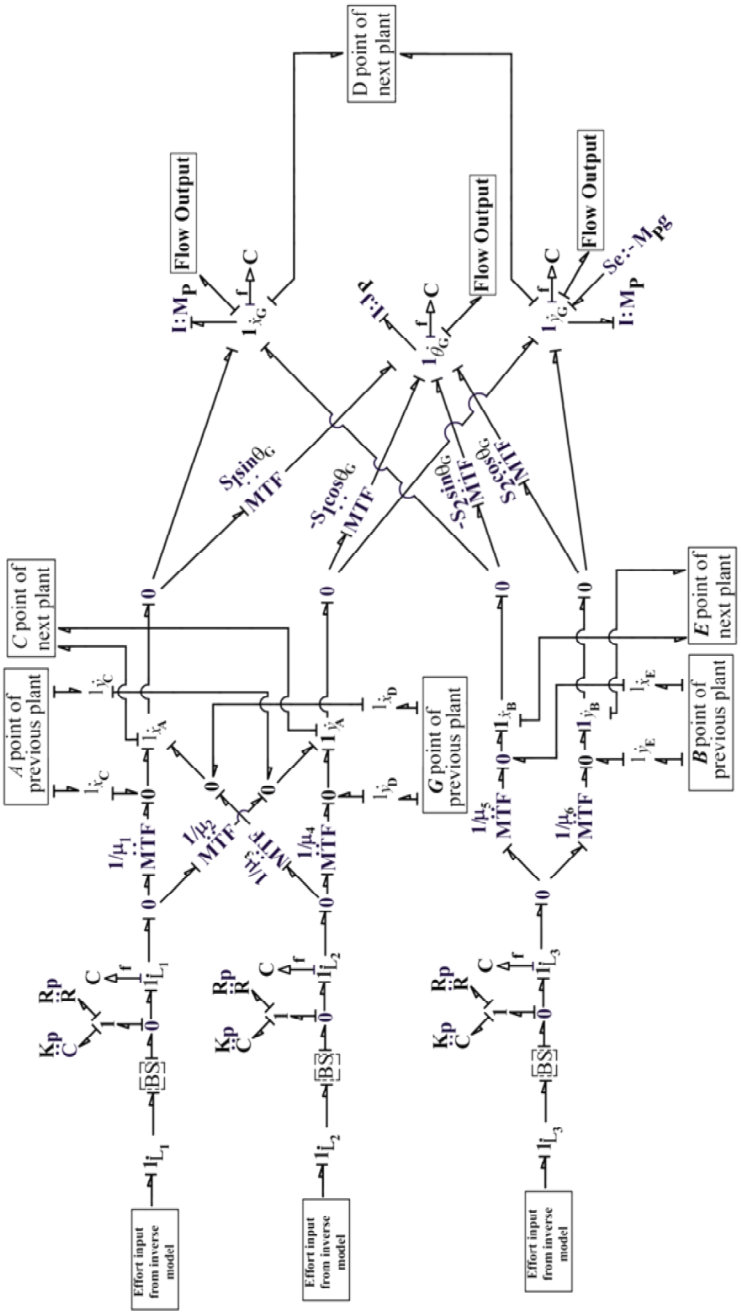

Fig. 5.8 Modified forward model of the planar hybrid manipulator

The inverse model, developed as a mirror image of the above model shown in Fig. 5.8, is displayed in Fig. 5.9. Instead of flow inputs in two directions, the efforts in two directions F_x and F_y are directly applied to the inverse model as displayed in Fig. 5.9 without considering ghost controller and these forces are given by

$$F_x = G_x F \cos\theta \tag{5.4}$$

$$F_y = G_y F \sin\theta \tag{5.5}$$

where G_x and G_y are the corresponding proportional gains, the values of which can be taken arbitrarily, F is the input force and θ is the angle with the horizontal.

Forces acting at the centre of gravity of the moving platform in *x* and *y* directions are given as inputs to the inverse model through two sources of effort so that the manipulator reach the given target. Also, overwhelming controller is not used in the forward model (Fig. 5.8) here and effort input is directly applied (Fig. 5.8) to the forward ball screw model. The doublet junctions for x_G, y_G and θ_G and stiff pads and ghost controller used above in Fig. 5.7 are not used in the inverse model here for target reaching because there is no differential causality due to input as force and not velocity. The inverse model of ball screw feed drive modelled in Section 5.2.1 earlier is shown as 'INV-BS' in Fig. 5.9. C-elements added after 'INV-BS' sub model return efforts which are given to the forward model. Hence, effort inputs are directly applied in $1_{\dot{x}_G}$, $1_{\dot{y}_G}$ and $1_{\dot{\theta}_G}$ junctions.

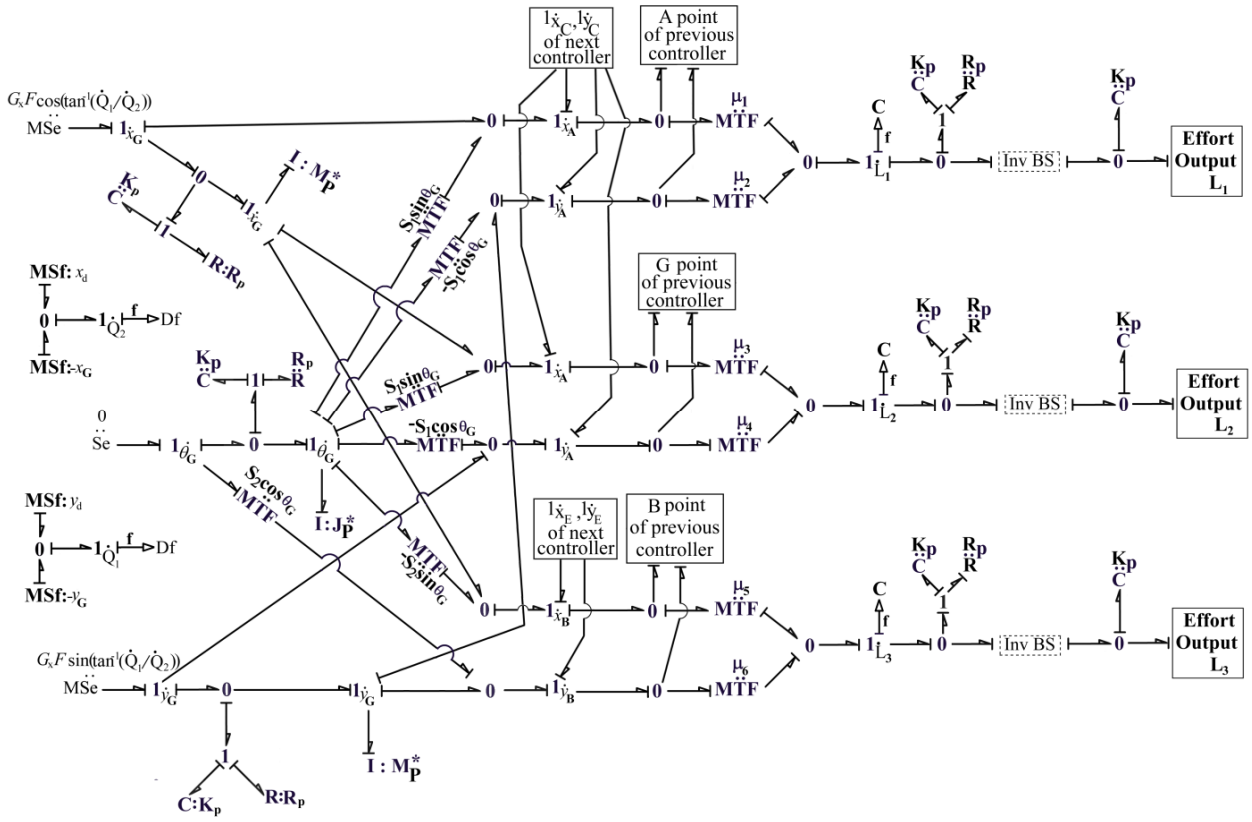

Fig. 5.9 Modified inverse model of planar hybrid manipulator for target reaching

The point-to-point model of the manipulator to reach the target position is shown in Fig. 5.9 where the present position at any point of time is calculated by subtracting it from the target position. Here, x_d, y_d denotes the target position and x_G, y_G denotes the current position in *x*-*y* plane extracted from plant model of upper manipulator. The current positions and target positions are fed by respective source of flows. These are subtracted by the 0-junctions and the differences are obtained by flow detectors added to the 0-junctions. The tangent of angle θ is calculated finally by dividing the difference in *y* coordinates of target and current positions to the difference in *x* coordinates of target and current positions.

5.4 Workspace Analysis

A three dimensional space to show the manipulator's workspace area can be represented by three Cartesian coordinates (x, y, Θ_G) [Gosselin & Angeles, 1988] where Θ_G is the

orientation of the platform. When platform is horizontal i.e. one of the coordinates is fixed, then two-dimensional representations can be shown by the parts of this volume [Gosselin & Jean, 1996]. There are two coordinate frames: an inertial Cartesian frame O_{xy} is attached to the point 'C' of the manipulator base with *x*-axis of the frame parallel to the horizontal base of the manipulator. Another non-inertial coordinate frame $O_{x'y'}$ is attached at the point 'G' i.e. centre of gravity of the manipulator with *x*-axis of this frame parallel to the moving platform and making an angle ø with the horizontal. The coordinates of fixed revolute joints expressed in inertial frame O_{xy} are x_{a_i}, y_{a_i} and the coordinates of moving revolute joints expressed in non-inertial frame are x_{b_i}, y_{b_i}. The coordinates of centre of gravity are *x*, *y* and ø expressed in an inertial frame.

Henceforth, if the unactuated joints have no constraints and orientation of the platform is known, then the workspace can be shown as the intersection of three regions where each region is covered by two concentric circles with centres of the circle at $\left(x_{c_i}, y_{c_i}\right)$ (i=1, 2, 3) for three legs of the manipulator. The three leg lengths (L_i where i = 1, 2, 3) are now defined as [Chablat *et al.*, 1998]:

$$L_i^2 = \left(x - x_{c_i}\right)^2 + \left(y - y_{c_i}\right)^2 \tag{5.6}$$

where $x_{c_i} = x_{a_i} - x_{b_i}\cos\theta_G + y_{b_i}\sin\theta_G$ and $y_{c_i} = y_{a_i} - x_{b_i}\sin\theta_G - y_{b_i}\cos\theta_G$

(x_{a_i}, y_{a_i}) denotes the point A_i position in a fixed coordinate system attached to the manipulator base and (x_{b_i}, y_{b_i}) denotes the point B_i position in a moving system attached to the platform of the manipulator.

The minimum and maximum radii of i^{th} pair of concentric circles are defined by the respective lengths of the i^{th} leg denoted by L_i^{min} and L_i^{max}. The above equations show that the intersection of three regions is the workspace of the manipulator with no joint limits.

If there is a limit on the range of motions then i^{th} leg motion relative to the base is shown as angle θ_{a_i} and it is described as

$$\theta_{a_i}^{\min} \le \theta_{a_i} \le \theta_{a_i}^{\max} \qquad i=1, 2, 3 \qquad (5.7)$$

Where $\theta_{a_i}^{\min}$ and $\theta_{a_i}^{\max}$ are the lowest and highest values of motion of the i^{th} leg, respectively.

The application of the constraints of each unactuated joint generates sectors on its corresponding annular region which is closed by a boundary of concentric circles. Therefore, the workspace of the planar parallel manipulator with angular limits of the regions is shown as the intersection or common area of three zones which are parts of three sectored annular regions. This workspace analysis of planar hybrid manipulator will be shown later in Section 5.5.3. Then workspace area is calculated by doing integration of its boundary from limits obtained by the calculation of intersection points of the intersecting curves. This whole process of workspace analysis and calculation of area of workspace of planar hybrid manipulator is done by doing simulation on MATLAB, which will be discussed in detail in next section.

5.5 Results of Simulation

This section of the chapter shows different results obtained from the simulations carried out for six degrees-of-freedom planar hybrid manipulator for trajectory tracking, target reaching and workspace analysis. The results for trajectory tracking and target reaching have been found by running the bond graph models of planar hybrid manipulator on bond graph simulator and workspace analysis has been done along with the calculation of workspace area has been calculated by MATLAB program.

The various parameter values used in the simulation are shown in Table 5.1. The parameter values for forward and inverse model are different. The overwhelming controller which is used for trajectory tracking can overwhelm the unknown system parameters, noises from the environment and unknown controller parameters. Different

parameter values for the system and controller are considered intentionally to check whether the overwhelming controller is able to overcome those changes.The values of parameters for plant, pad and controller in the inverse system and moving platform have been chosen suitably according to the application. The gain 'α' of overwhelming controller is intentionally taken as 1000 here because a high value of gain implies overwhelming control strategy in a better way and there is minimum error in trajectory tracking. Some parameters of ball screw feed drive have been taken from [Frey *et al.*, 2012] and some others have been chosen suitably.

Table 5.1 Values of parameters

Sub systems	Values of parameters			
Platform	$M_P = 11$ kg	$J_P = 0.1\,\text{kg m}^2$	$K_P = 10^8$ N/m	$R_P = 50$ Ns/m
Ball screw feed drive	$h = 0.02$ m	$J_m = 6.4\times10^{-3}\,\text{kg m}^2$	$J_s = 6.5\times10^{-4}\,\text{kg m}^2$	$l = 2$ m
	$k_c = 141\times10^3$ Nm/m rad	$d = 0.038$ m	$C_c = 0.01$ Ns/m	$C_{sr} = 0.01$ Ns/m
	$k_b = 250\times10^6$ N/m	$k_n = 500\times10^6$ N/m	$R_m = 0.01$ Ns/m	$C_n = 0.01$ Ns/m
	$k_r = 50$ Ns/m	$k_a = 50$ Ns/m	$m_s = 0.1$ kg	$m_t = 11$ kg
Inverse system	$E = 210\times10^9$ N/m^2	$G = 81\times10^9$ N/m^2	ρ = 7800 kg/m^3	
	$M_p^* = 0.25$ kg	$J_p^* = 0.25\,\text{kg m}^2$	$M_c = 30$ kg	$J_c = 1$ kg
	$K_c = 10^8$ N/m	$R_c = 1$ Ns/m	$J_c = 1\,\text{kg m}^2$	$\alpha = 1000$

The initial conditions of the hybrid manipulator are shown in Table 5.2. The point 'C' of the base of lower manipulator is taken as origin (hence its coordinates are (0, 0)) and other positions of all points have been taken suitably. The points 'A','G' and 'B' of lower manipulator becomes 'C','D' and 'E' of upper manipulator. Hence, these have same coordinates. The lengths of base and platform of the manipulator have been taken as 2 m each. The point 'D' is taken as the mid-point of base and point 'G' is taken as the mid-point of platform. Accordingly, their *x* and *y* coordinates have been chosen.

Table 5.2 Initial conditions for the planar hybrid manipulator

	Points	x (m)	y (m)		Points	x (m)	y (m)
Lower Manipulator	A	0.5	1	Upper Manipulator	A	1	2
	G	1.5	1		G	2	2
	B	2.5	1		B	3	2
	C	0	0		C	0.5	1
	D	1	0		D	1.5	1
	E	2	0		E	2.5	1

5.5.1 Trajectory Tracking

The input trajectory consists of two semi-circles. The trajectory given to lower manipulator consists of a semi-circle and it works only for initial time of 3.14 s. From 3.14 s to 6.28 s, the trajectory is given to upper manipulator consisting of second semi-circle. The angular velocity 'ω' is taken as 1 rad/s so that value of π/ω becomes 3.14. The velocities in x and y directions given to lower manipulator are described by Eqs. (5.8) and (5.9). These equations clearly show that x and y velocities are zero after time 3.14 seconds for lower manipulator. Similarly, x and y velocities given to upper manipulator are described by Eqs. (5.10) and (5.11). These equations depict that for time less than 3.14 seconds, the velocities in x and y directions are taken as zero for upper manipulator.

$$\dot{x} = -\omega r \sin(\omega t) \quad \text{if } (t <= \frac{\pi}{\omega}) \quad \text{else } \dot{x} = 0 \tag{5.8}$$

$$\dot{y} = \omega r \cos(\omega t) \quad \text{if } (t <= \frac{\pi}{\omega}) \quad \text{else } \dot{y} = 0 \tag{5.9}$$

$$\dot{x} = 0 \quad \text{if } (t <= \frac{\pi}{\omega}) \quad \text{else } \dot{x} = -\omega r \sin\left[\omega\left(t - \frac{\pi}{\omega}\right)\right] \tag{5.10}$$

$$\dot{y} = 0 \quad \text{if } (t <= \frac{\pi}{\omega}) \quad \text{else } \dot{y} = \omega r \cos\left[\omega\left(t - \frac{\pi}{\omega}\right)\right] \tag{5.11}$$

In the end i.e. after time 6.28 s, the final displacement of plant model is compared with the input displacement of the controller model. The final trajectory tracking results

for the motion of centre of gravity of both the manipulators obtained after applying the above equations and giving velocities to both the manipulators, show that the given trajectory is exactly followed with minor error for lower and upper manipulators as shown in Fig. 5.10(a) and (b). The total simulation time is 6.28 seconds with angular velocity ω=1 rad/sec and radius of semi circle r=0.1 m. The final position of lower manipulator achieved is (1.5, 1) and for upper manipulator is (2, 2) as depicted in Fig. 5.10.

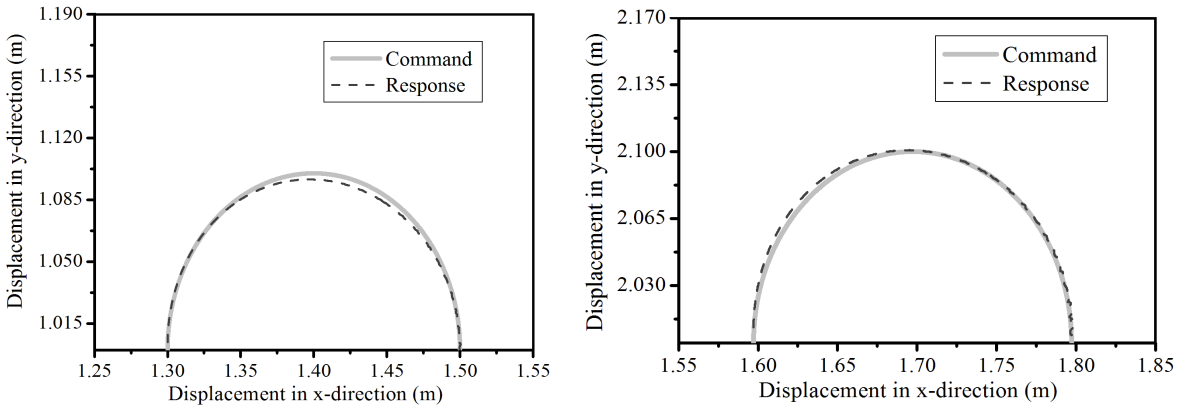

Fig. 5.10 Comparison of plant response with controller command to track the given trajectory (a) for lower manipulator and (b) for upper manipulator

Figures 5.11(a) and (b), respectively show the error in absolute value and error percentage value in displacements along x and y directions for the lower manipulator, respectively. Fig. 5.12(a) and (b), respectively show the error in absolute value and error percentage value in displacements along x and y directions for upper manipulator. The observation here is largest absolute error in displacements in both x and y directions for lower manipulator are 4.5×10^{-4} m and 10.05×10^{-4} m, respectively which is very less and hence can be neglected. The maximum error percentage in displacements in both x and y directions for lower manipulator are 2.9×10^{-2} % and 9.9×10^{-2} %, respectively. Similarly, the maximum error in absolute values in displacements in both x and y directions for upper manipulator are -1.23×10^{-8} m and -4.18×10^{-3} m, respectively which can be neglected being very small. The maximum error percentage in displacements in both x and y directions for upper manipulator are -6.82×10^{-7} % and -0.209 %, respectively.

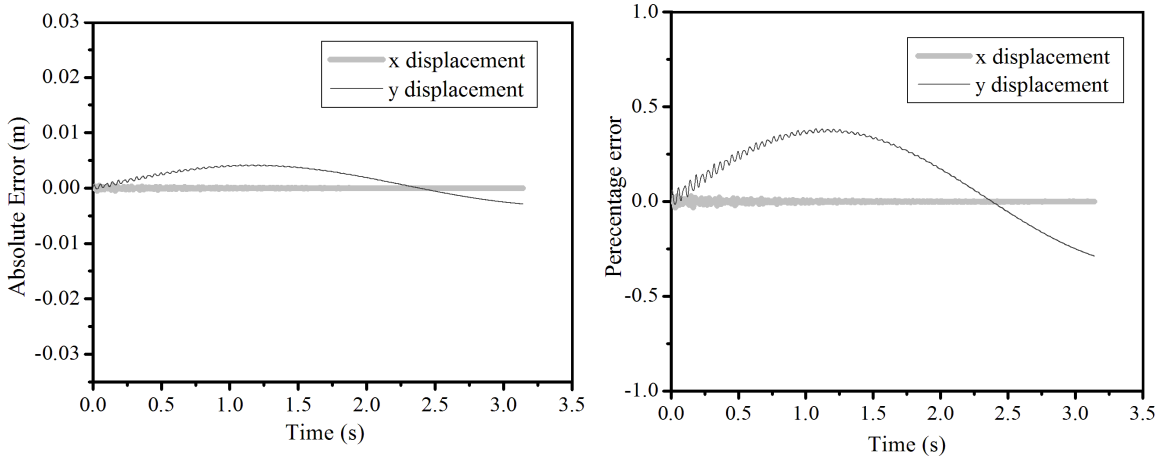

Fig. 5.11 (a) Error in absolute values and (b) error percentage in displacements in *x* and *y* directions for lower manipulator

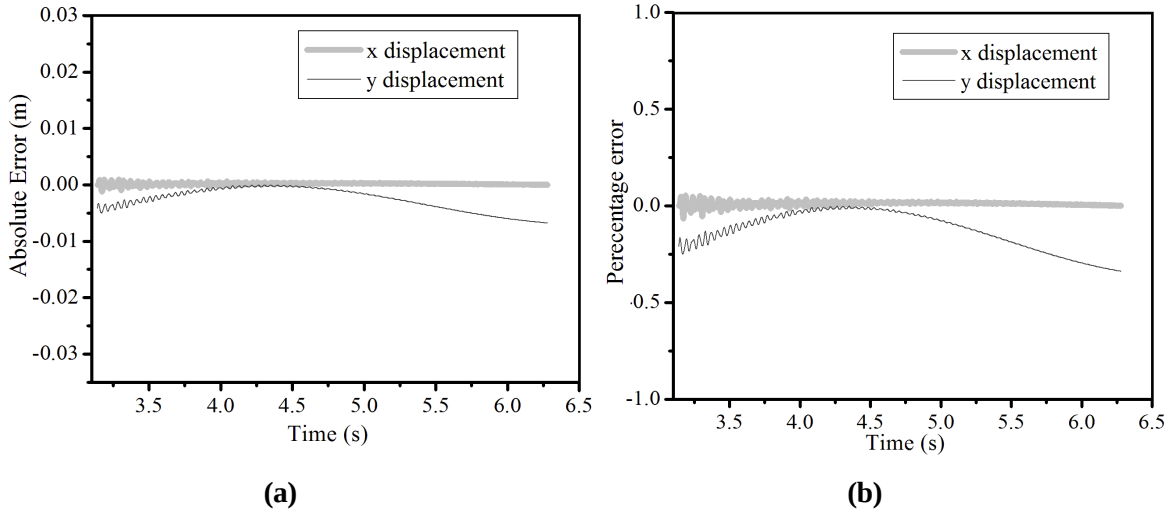

Fig. 5.12 (a) Error in absolute values and (b) error percentage in displacements in *x* and *y* directions for upper manipulator

5.5.2 Target Reaching

As already displayed in Table 5.2, the initial position of centre of gravity for upper manipulator is (2, 2). The target given to the manipulator is (2.3, 2.3) which is fed continuously through two source of flows attached to the controller model in Fig. 5.1(b). Gains in both directions G_x and G_y are taken as 10 each using hit and trial method with

input force applied at centre of gravity also equal to 10 N. The controlling action is done in such a way that the slope of the trajectory becomes unity after few seconds of travel. At each step of time, the movement of manipulator is noted down and it shows that it is chasing the target properly. Finally, after 26.28 seconds it finally reaches the target position given as (2.3, 2.3). Hence, the time taken by planar hybrid manipulator to reach the target is 26.28 seconds. Here displacement of centre of gravity of planar hybrid manipulator is shown in Fig. 5.13(a) moving from initial position (2, 2) to final position (2.3, 2.3) in 26.28 seconds. Fig. 5.13(b) shows *y* displacement versus *x* displacement of the planar hybrid manipulator which clearly shows the path followed by planar hybrid manipulator to reach the target.

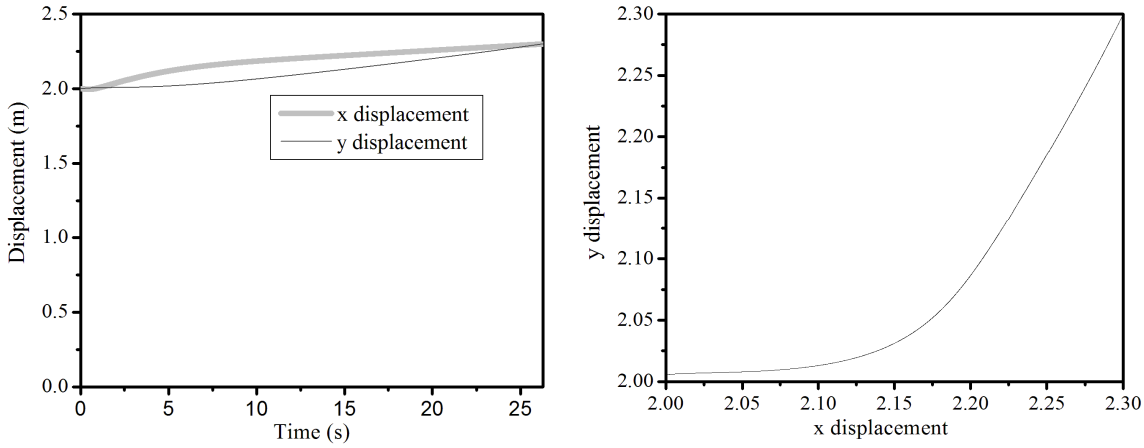

(a) **(b)**

Fig. 5.13 (a) Displacement of manipulator from initial position to final position and (b) *x*-*y* path of the hybrid manipulator

5.5.3 Workspace Analysis

The workspace connected with the trajectory tracked by the planar hybrid manipulator of a semi-circle has already been discussed and analyzed in Section 5.5.1. From this simulation of trajectory tracking, the kinematic parameters were obtained along with the joint limits for each joint. After all these parameters were considered, the workspace analysis is done as already discussed in detail in Section 5.4. The parameters and limits

on angles of the lower and upper manipulator taken for the simulation of workspace analysis are shown in Table 5.3.

Table 5.3 Parameters and limits on angles of the manipulator

	Lower manipulator			Upper manipulator		
I	1	2	3	1	2	3
x_{a_i}	0	1	2	0.3	1.3	2.3
y_{a_i}	0	0	0	1	1	1
x_{b_i}	-1	-1	1	-1	-1	1
y_{b_i}	0	0	0	0	0	0
$L_i^{\min}$	1.044 m	1.118 m	1.049 m	1.044 m	1.118 m	1.049 m
$L_i^{\max}$	1.177 m	1.266 m	1.169 m	1.177 m	1.266 m	1.169 m
$\theta_{a_i}^{\min}$	1.107 rad	2.023 rad	1.107 rad	1.110 rad	2.026 rad	1.110 rad
$\theta_{a_i}^{\max}$	1.283 rad	2.179 rad	1.284 rad	1.286 rad	2.182 rad	1.287 rad

The orientation of the platform is considered to be zero. Then, the simulation program for determining the workspace associated with it is run on MATLAB. Figures 5.14(a) and 5.14(b) show the workspace of the lower and upper parallel manipulators, respectively with no orientation of the platform where concentric circles are shown and workspace region is the intersection of three regions. Actuators 1 and 3 are parallel to each other and have same lengths so their minimum and maximum lengths are also same. In Fig. 5.14 (a), the red coloured concentric circles show the minimum and maximum lengths of actuators 1 and 3 of lower manipulator and green coloured concentric circles show the minimum and maximum lengths of actuator 2 of lower manipulator. The radius of the circle is same as the instantaneous length of the actuator. The same thing of upper manipulator is represented in Fig. 5.14 (b). The intersection points of different circles are shown by black colour. The workspace boundary is shown by thick green colour. The

same colour coding is used for Fig. 5.15 and Fig. 5.16. The coloured portion inside the common area of intersection of circles is the calculated workspace. A clearer picture of the separate workspace boundaries of the centre of gravity of lower and upper manipulators are displayed in Figs. 5.15(a) and (b), respectively. The semi-circle trajectories tracked by the lower and upper manipulators separately are also shown in the workspace area where the initial position of centre of gravity of lower manipulator is shown as (1.5, 1) and for the upper manipulator is (2, 2) in Figs. 5.15(a) and (b).

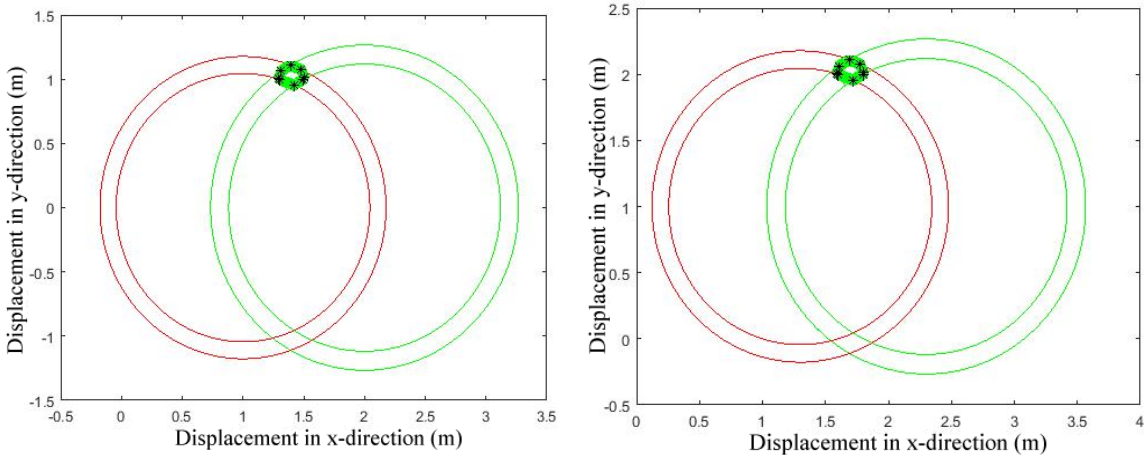

(a) **(b)**

Fig. 5.14 Workspace of planar hybrid manipulator for (a) lower manipulator and (b) upper manipulator

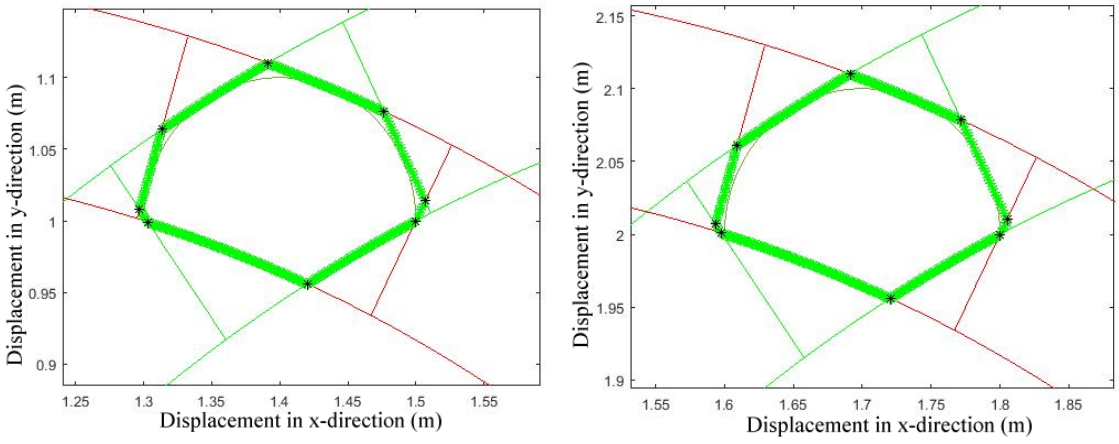

(a) **(b)**

Fig. 5.15 Workspace boundaries of (a) lower manipulator and (b) upper manipulator

Full workspace boundary for full trajectory of double semi-circle of the planar hybrid manipulator is shown in Fig. 5.16. This displays the required workspace determined from the common region obtained from the intersection of green coloured arcs which represents the joint limits.

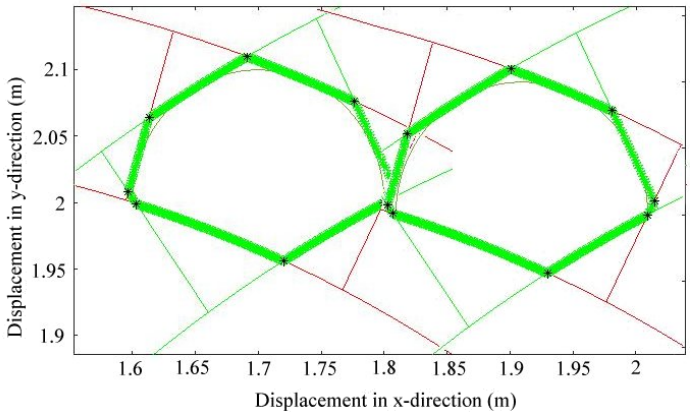

Fig. 5.16 Workspace of planar hybrid manipulator

The semi-circle arcs inside the workspace area displayed show the trajectory with starting point as (2, 2) and final position as (1.6, 2). This satisfactorily fits inside the workspace area which validates the accuracy of the workspace analysis done by us. Now the area of the workspace is calculated by integrating the boundary of workspace region displayed between appropriate limits. Therefore, area of the workspace of the lower manipulator is calculated to be 2.09×10^{-2} m^2 and for upper manipulator is 2.087×10^{-2} m^2. Henceforth, the area of the workspace of the hybrid manipulator by adding these two areas is 4.177×10^{-2} m^2.

5.6 Conclusions

This chapter used ball screw feed drive mechanism instead of piston-cylinder model for the planar hybrid manipulator earlier developed. The bond graph models for forward and inverse dynamics of ball screw mechanism are shown in the chapter. The planar hybrid manipulator with ball screw feed drives used as its actuators are modelled for forward and inverse dynamics in the chapter. The ball screw feed drive mechanism has been used due to its ability to convert rotary motion into linear motion with great ease and better

accuracy. Furthermore, an overwhelming controller was used for trajectory tracking in which a double semi-circle is tracked by the planar hybrid manipulator with minimum errors which can further be reduced if gain of overwhelming controller is increased.

Also, proportional controller is used to develop the target reaching bond graph model. The manipulator is moved from a pre defined position to the target position after which simulation results are described. These clearly show that the planar hybrid manipulator developed in the chapter reaches the target given to it successfully.

Workspace analysis for the same trajectory earlier tracked by planar hybrid manipulator is done and presented in chapter with the calculation of the workspace area. The shape of the workspace along with its minimum area is determined in which the trajectory should be clean and free from the disturbance of any foreign object to avoid collision.

In next chapter, this planar hybrid manipulator will be extended for a three dimensional model with 3-D actuator models. The trajectory tracking of thumb and index finger while drawing an arc would be done and impedance control for a L-shaped path would also be done using these forward and inverse models for a 3-D planar hybrid manipulator in Chapter 6.

Chapter 6

Impedance Control of Three Dimensional Hybrid Manipulator

6.1 Introduction

The forces which are developed when the manipulator interacts safely in company of environment or any object are known as contact forces. These forces need to be controlled in such a way that the force provided by the manipulator must be less than the secure weight limits of the object with which interaction of manipulator takes place. This force control is also essential in trajectory tracking because the object or the manipulator can be damaged unexpectedly by any type of discrepancy. There are two kinds of approaches used to control forces in manipulators. These are direct and indirect approaches used for force control [DeSchutter *et al*., 1997; Siciliano & Villani, 2000]. Force measurement is not needed in indirect scheme. Mass at the point of contact and either stiffness or damping can be controlled in this scheme. The accurate representation of the thing of the environment must be recognized fully whereas it is not necessary in direct force control scheme. The fault between the required force and calculated force is needed in direct scheme.

The control of impedance at the point where the end-effector is in contact with the object is main trustworthy approach [Raibert & Craig, 1981; Anderson & Spong, 1988; Assuncao & Schumacher, 2003] for direct force control scheme. The direct scheme can also be called as hybrid position force control scheme [Takaiwa & Noritsugu, 2003; Kosuge *et al*., 1996] for which a virtual foundation is combined with an overwhelming controller to apply the impedance control [Chiaverini & Sciavicco, 1993]. A compensation gain is used to adjust the impedance at the interface of manipulator and environment. The response has some trajectory tracking error from command during the interaction period. This error is known as amnesia and is removed when the manipulator and object are not interacting. One more loop of compensation is added in the controller for this.

Impedance control is a technique by which we can control the dynamics when a robot interacts with environment. Control of this kind is appropriate to communicate with the environment and to manipulate an object. The basic idea of this approach is that the environment behaves opposite of impedance whereas the robot behaves like impedance. This suggests the statement "no controller can make the manipulator appear to the environment as anything other than a physical system." The regulation described by Hogan could also be expressed as: "in the most common case in which the environment is an admittance (*e.g.* a mass, possibly kinematically constrained) that relation should be an impedance, a function, possibly nonlinear, dynamic, or even discontinuous, specifying the force produced in response to a motion imposed by the environment" [Hogan, 1984]. The position or force is not regulated by impedance control. But the relation of force with acceleration, velocity and position is regulated. The relationship hence is known as impedance, which needs input in the form of position (velocity or acceleration) and output comes in the form of resultant force. Admittance is the inverse of impedance which enforces position. Hence, a relation of dynamics is maintained which expresses force in terms of acceleration, velocity and position as: $F = Kx + Cv + Ma$ + friction and modelling of a spring-mass-damper system is done. The elements that store energy are Mass and spring (stiffness) but the element that dissipates energy is a damper. Therefore, exchange of energy at the time of interaction (the work done) can be controlled by controlling impedance. Hence, impedance control is basically interaction control [Buchli, 2011]. Henceforth, impedance control is applied in fields like robotics as a common approach for sending instructions to a robotic manipulator which considers non-linear dynamics of the object that is to be manipulated.

The controller for a hybrid manipulator must control the interaction forces for various applications. During the interaction period of manipulator with environment, the environmental forces are adjusted by adjusting the impedance at manipulator interface. This chapter has proposed a scheme for controlling force in a hybrid parallel-series manipulator with the help of overwhelming control scheme. To control force or impedance by modulating the impedance in the controller domain, an overwhelming

controller can be used [Hogan, 1985; Sharon *et al.*, 1991]. This approach has been followed in this chapter for impedance control of a three dimensional hybrid manipulator.

The six degrees-of-freedom planar hybrid manipulator was proposed in Chapter 3. It has already been used for trajectory tracking of human vertebrae and object grasping by thumb and index finger. Then this planar hybrid manipulator was implemented with ball screw feed drives used as its actuators in Chapter 5. The model with ball screw feed drives has been implemented for trajectory tracking for a semi-circular path and to reach the target given to planar hybrid manipulator in a suitable time. Now, the final objective of thesis is to make the planar hybrid manipulator a three dimensional hybrid manipulator and then do its impedance control. Then it becomes a 3-D hybrid parallel-series manipulator which demonstrates the approach of thesis. It is already found from the preceding chapters that for a good representation of dynamics of planar hybrid manipulator, two models are essential. One model is required to represent the suitable forward dynamics and second model required to display the proper inverse dynamics of manipulator so that efficiency is maintained. Now, in the present chapter, a three dimensional actuator model will be constructed first which shows each actuator as piston-cylinder arrangement as already described in Chapter 3. Then this 3-D actuator model will be used to develop the full forward dynamics model of 3-D hybrid manipulator. Afterwards, the inverse dynamics model with overwhelming controller will be developed from the forward model. Modelling of the whole system is done with the help of bond graph. The trajectory followed by the manipulator is a simple inverted mirror L-shaped path considered here as an illustration. The results of simulation with bond graph have been illustrated to prove the efficiency of the force controller for a three dimensional hybrid manipulator.

This chapter is structured as follows: Firstly, a kinematic model of 3D hybrid manipulator will be presented and then its bond graph model is also shown in which the full dynamics model for forward and inverse dynamics is discussed. The actuators are considered as piston-cylinder arrangements. The inverse model is developed with overwhelming control scheme. Henceforth, its practical application is shown with trajectory tracking of thumb and index finger of human hand while drawing an arc on the

white board. Then the impedance controller design is presented in which the concept of the virtual foundation is introduced. A control scheme built up for removal of amnesia, which is the accumulated position error during force control, is developed. Ultimately, this impedance control scheme developed is implemented to another application of an inverted mirror L-shaped path on the surface of a submissive object.

6.2 Modelling of 3-D Hybrid Manipulator

The planar hybrid manipulator with its schematic representation and bond graph model has already been presented in Chapter 3. The main objective here is to develop the planar hybrid manipulator into a three dimensional hybrid manipulator. The schematic diagram of 3D hybrid manipulator is shown in Fig. 6.1(a) where two 3D parallel manipulators are connected serially with each other. The base is fixed to the ground and it is attached to the moving platform through six legs at points numbered from 1 to 6 in Fig. 6.1(a). These six actuators are considered as prismatic pairs, the arrangement of which will be discussed later. The moving platform of the lower manipulator becomes base for the upper manipulator. This is a six DOF manipulator in which all the joints are taken as pin joints, as already taken in planar hybrid manipulator proposed in Chapter 3. The centre of gravity G is considered to be in the centre of top moving platform with bottom base fixed. The upper and middle platforms are attached to each other with six legs (actuators) which are considered as prismatic pairs. Similar attachment of middle and lower platforms is required. The lengths of all six legs can be measured and the forces in these legs can be controlled. The leg lengths are calculated by integrating the rate of change of leg lengths that are calibrated using flow sensors in the bond graph representation. The location and direction of the platform are calculated by the values of these leg lengths. *xyz* coordinate system is connected at the base, middle platform and upper platform as shown in Fig. 6.1(a). The directions of *x*, *y* and *z* are taken as same for all coordinate systems. *x* direction is taken as parallel to base and *y*-direction is taken as perpendicular to the plane of base, as displayed in Fig. 6.1(a). The actuator makes three angles with three axis, *i.e.* angles θ_x, θ_y and θ_z with the *x*, *y* and *z* axis, respectively. The trajectory and reference velocities of point 'G' will be shown for the application considered in this chapter. The trajectory and the velocities of point 'G' can be detected from an external

source in the inverse model and afterwards an overwhelming controller is utilized for computing the corresponding control forces in all legs. The trajectory specified by the external source can be either a simulation model or measurements from the real system.

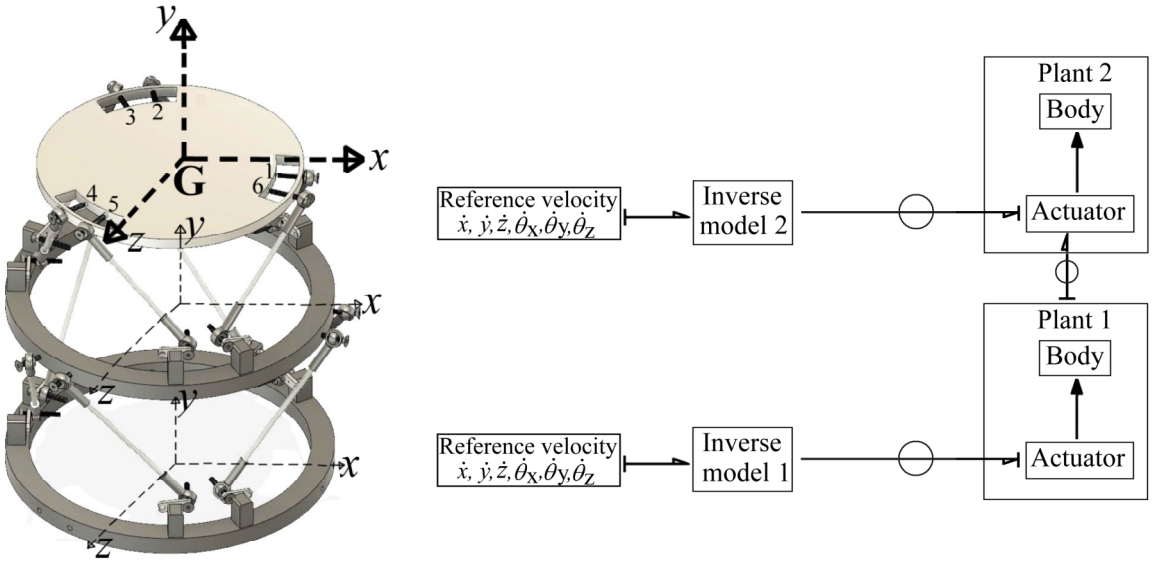

(a) (b)

Fig. 6.1(a) A simplified diagram of 3D hybrid manipulator and (b) its word bond graph arrangement

6.2.1 Kinematic Model

The points '1' to '6' that support the upper platform have linear velocities denoted by $(\dot{x}_1, \dot{y}_1, \dot{z}_1), (\dot{x}_2, \dot{y}_2, \dot{z}_2), (\dot{x}_3, \dot{y}_3, \dot{z}_3), (\dot{x}_4, \dot{y}_4, \dot{z}_4), (\dot{x}_5, \dot{y}_5, \dot{z}_5)$ and $(\dot{x}_6, \dot{y}_6, \dot{z}_6)$, respectively. In an inertial frame, the platform's points '1' to '6' have linear velocities which can be expressed in the form of linear velocity of the point 'G' $(\dot{x}_G, \dot{y}_G, \dot{z}_G)$ in three dimensions and centre of gravity's angular velocities when it rotates about *x*, *y* and *z*-axis $(\dot{\theta}_x, \dot{\theta}_y, \dot{\theta}_z)$, respectively as

$$\dot{x}_1 = \dot{x}_G + z_1\dot{\theta}_y - y_1\dot{\theta}_z \tag{6.1}$$

$$\dot{y}_1 = \dot{y}_G + x_1\dot{\theta}_z - z_1\dot{\theta}_x \tag{6.2}$$

$$\dot{z}_1 = \dot{z}_G + y_1\dot{\theta}_x - x_1\dot{\theta}_y \tag{6.3}$$

$$\dot{x}_2 = \dot{x}_G + z_2\dot{\theta}_y - y_2\dot{\theta}_z \tag{6.4}$$

$$\dot{y}_2 = \dot{y}_G + x_2\dot{\theta}_z - z_2\dot{\theta}_x \tag{6.5}$$

$$\dot{z}_2 = \dot{z}_G + y_2\dot{\theta}_x - x_2\dot{\theta}_y \tag{6.6}$$

$$\dot{x}_3 = \dot{x}_G + z_3\dot{\theta}_y - y_3\dot{\theta}_z \tag{6.7}$$

$$\dot{y}_3 = \dot{y}_G + x_3\dot{\theta}_z - z_3\dot{\theta}_x \tag{6.8}$$

$$\dot{z}_3 = \dot{z}_G + y_3\dot{\theta}_x - x_3\dot{\theta}_y \tag{6.9}$$

$$\dot{x}_4 = \dot{x}_G + z_4\dot{\theta}_y - y_4\dot{\theta}_z \tag{6.10}$$

$$\dot{y}_4 = \dot{y}_G + x_4\dot{\theta}_z - z_4\dot{\theta}_x \tag{6.11}$$

$$\dot{z}_4 = \dot{z}_G + y_4\dot{\theta}_x - x_4\dot{\theta}_y \tag{6.12}$$

$$\dot{x}_5 = \dot{x}_G + z_5\dot{\theta}_y - y_5\dot{\theta}_z \tag{6.13}$$

$$\dot{y}_5 = \dot{y}_G + x_5\dot{\theta}_z - z_5\dot{\theta}_x \tag{6.14}$$

$$\dot{z}_5 = \dot{z}_G + y_5\dot{\theta}_x - x_5\dot{\theta}_y \tag{6.15}$$

$$\dot{x}_6 = \dot{x}_G + z_6\dot{\theta}_y - y_6\dot{\theta}_z \tag{6.16}$$

$$\dot{y}_6 = \dot{y}_G + x_6\dot{\theta}_z - z_6\dot{\theta}_x \tag{6.17}$$

$$\dot{z}_6 = \dot{z}_G + y_6\dot{\theta}_x - x_6\dot{\theta}_y \tag{6.18}$$

The following Table 6.1 depicts the angular coordinates of platform and base of lower and upper manipulators taken from [Szufnarowski, 2012]:

Table 6.1 Angular positions of lower and upper manipulators

	Actuators →	1	2	3	4	5	6
Lower manipulator	Base	37.5°	142.5°	157.5°	262.5°	277.5°	22.5°
	Upper platform	77°	103°	197°	223°	317°	343°
Upper manipulator	Base	37.5°	142.5°	157.5°	262.5°	277.5°	22.5°
	Upper platform	77°	103°	197°	223°	317°	343°

The word bond graph model for trajectory tracking of 3D hybrid manipulator is shown in Fig. 6.1(b). In this figure, three linear reference input velocities in *x*, *y* and *z* directions and three rotational velocities in three directions of *x*, *y* and *z* are given to inverse system. The efforts from the inverse model are given to the actuators. Then effort outputs coming from forward model (Plant) in the form of leg lengths rate of change for six legs (actuators) of moving platform of lower and upper manipulators are given to the manipulator bodies. Separate velocities are given to the lower and upper manipulators but same inverse model is used for both.

6.2.2 Bond Graph Model of 3D Hybrid Manipulator

The forward dynamics bond graph model for hybrid manipulator is shown in Fig. 6.2 in which an effort input coming from inverse model is attached to $1_{\dot{L}}$ junction for each leg (actuator). This contemporary length (L) of each actuator can be represented in the form of equation as follows:

$$L = \sqrt{(x_2 - x_1)^2 + (y_2 - y_1)^2 + (z_2 - z_1)^2} \tag{6.19}$$

where 1 and 2 represent two end points of an actuator. Differentiating Eq. (6.19) with respect to time, one obtains

$$\dot{L} = \frac{(x_1 - x_2)}{L}(\dot{x}_1 - \dot{x}_2) + \frac{(y_1 - y_2)}{L}(\dot{y}_1 - \dot{y}_2) + \frac{(z_1 - z_2)}{L}(z_1 - z_2) \tag{6.20}$$

Each actuator is considered to be a piston-cylinder link as shown in Fig. 6.3 where two ends of actuator are attached to piston end and cylinder end. The modelling of piston and the cylinder are done by considering them as stiff masses with six degrees-of-freedom each comparable to the movable platform. The inertial velocities of the point 1 that is fixed and point 2 attached to the piston rod end are calculated similar to the method to calculate the inertial velocities of the points '1' to '6' of the movable platform. In Fig. 6.3 shown here, point 1 is attached to fixed cylinder end and point 2 is attached to moving piston end. The piston's centre of gravity is taken as *gp* which is placed at l_{gp} distance from the end of rod. Similarly, the cylinder's centre of gravity is taken as *gc* and

its distance from the fixed end is taken as l_{gc}. The *xyz* coordinate systems are attached at centre of gravity of piston as well as centre of gravity of cylinder. The velocities in inertial frame are given to base platform for three directions of *x*, *y* and *z* and then transferred to the top platform in respective directions as shown in Fig. 6.2.

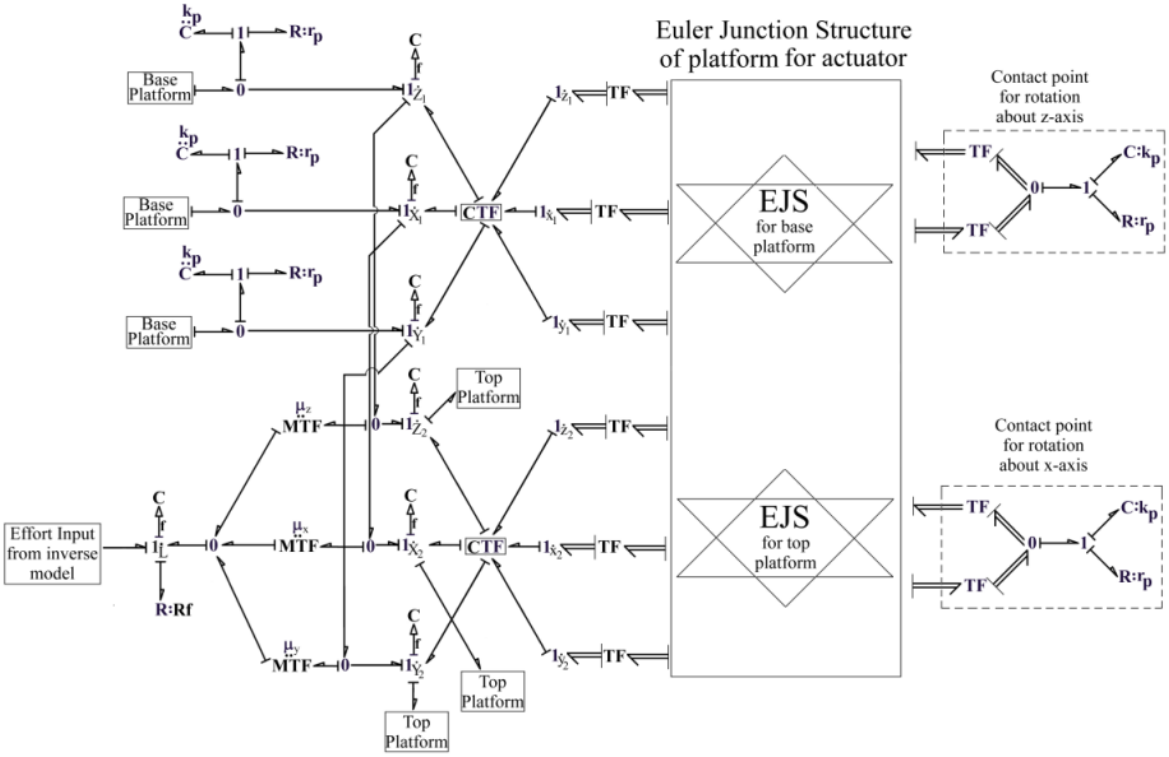

Fig. 6.2 Forward dynamics model with a single leg

The inertial velocities of piston end and cylinder end are converted to body fixed velocities by coordinate transformation model represented as CTF in Fig. 6.2. Equations (6.1–6.6) are used to calculate these body fixed velocities. The detailed bond graph representation for coordinate transformation is shown in Fig. 6.4 where transformer moduli vary according to its use in forward and inverse models. Coordinate transformation (CTF) is done to convert the forces acting at all joints given by six actuators from inertial frame to body fixed frame of moving platform. Rate of change of leg lengths are represented by the junctions $1_{\dot{L}_1}, 1_{\dot{L}_2}, 1_{\dot{L}_3}, 1_{\dot{L}_4}, 1_{\dot{L}_5}$ and $1_{\dot{L}_6}$ respectively for six legs. All other representation is same as done in Section 3.2.2 of Chapter 3. The weight of the platform operates in non-inertial frame converted from inertial frame through coordinate transformation (CTF).

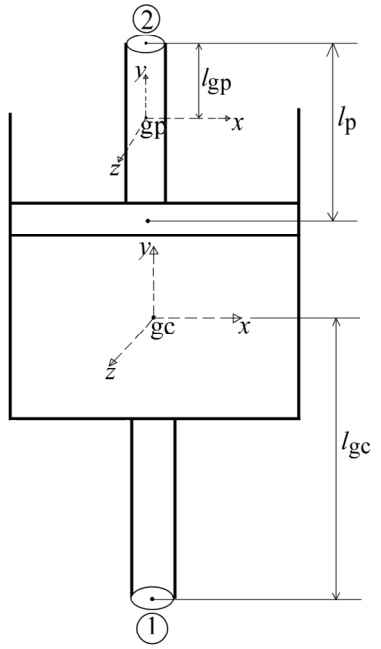

Fig. 6.3 Piston-cylinder arrangement

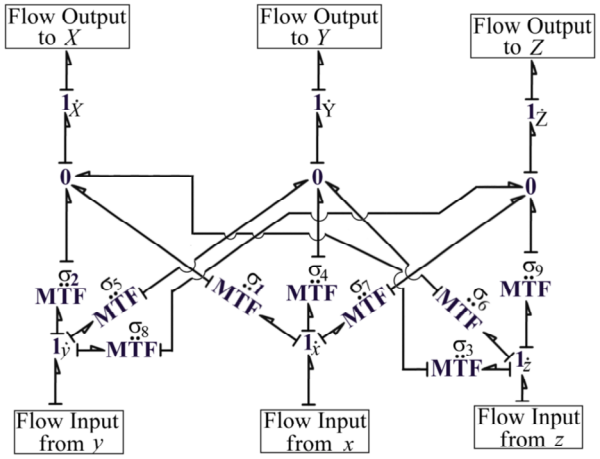

Fig. 6.4 Bond graph model for coordinate transformation

The values of different transformer moduli of CTF model for actuator model are

$$\left.\begin{aligned}
&\sigma_1 = \cos\alpha\cos\gamma, \sigma_2 = \cos\gamma\sin\alpha\sin\beta - \sin\gamma\cos\beta, \sigma_3 = \cos\gamma\sin\alpha\sin\beta + \sin\gamma\cos\beta,\\
&\sigma_4 = \sin\gamma\cos\alpha, \sigma_5 = \sin\alpha\sin\gamma\sin\beta + \cos\alpha\cos\beta, \sigma_6 = \sin\alpha\sin\gamma\cos\beta - \cos\alpha\sin\beta,\\
&\sigma_7 = -\sin\alpha, \sigma_8 = \cos\alpha\sin\beta, \sigma_9 = \cos\alpha\cos\beta
\end{aligned}\right\} \quad (6.21)$$

where α, β and γ are rotational velocities in *x*, *y* and *z* directions, respectively.

i.e. $\alpha = \dot{\theta}_x, \beta = \dot{\theta}_y, \gamma = \dot{\theta}_z$

Then these velocities are attached to Euler junction structures represented as EJS in Fig. 6.2, the detailed model of which are taken from [Bera *et al*., 2011] through which normal body fixed velocities of cylinder end V_{CY_1}, V_{CY_2} and piston end V_{PI_1}, V_{PI_2} at the contact points 1 and 2, respectively, are calculated as per following equations:

$$V_{\mathrm{CY}_1} = \left\{ \dot{x}_{\mathrm{gc}} + \dot{\theta}_{z_C} \left(l - l_p - l_{\mathrm{gc}} - \frac{d}{2} \right) \right\} \left(\sin\theta_y \sin\theta_x \sin\theta_z + \cos\theta_y \cos\theta_z \right) \quad (6.22)$$

$$V_{\mathrm{PI}_1} = \left\{ \dot{x}_{\mathrm{gp}} + \dot{\theta}_{z_P} \left(-l + l_{\mathrm{gp}} - \frac{d}{2} \right) \right\} \left(\sin\theta_y \sin\theta_x \sin\theta_z + \cos\theta_y \cos\theta_z \right) \quad (6.23)$$

where *d* is the width of the piston and cylinder end. Similarly, the body fixed velocities V_{CY_2} and V_{PI_2} for contact point 2 can be calculated. 1 is the contact point for rotation in *xy* horizontal plane where rotation is carried out about *z* axis and 2 is the contact point for rotation in *yz* vertical plane where rotation is carried out about *x* axis. Here 3 flow outputs are there in actuator model for *x*, *y* and *z* directions which will be further attached to pad elements. The complete forward model for a three dimensional hybrid manipulator is shown in Fig. 6.5 in which 6 effort inputs coming from inverse model are attached to 6 actuator models for six actuators. Then each actuator is attached to 3 pad elements for 3 different directions. The model of this pad element is shown at bottom of Fig. 6.5 at right side to have a clear picture of the model. This model converts flow input supplied by each actuator into the effort output. These effort outputs coming from pad elements are given as input to *x*, *y* and *z* points for each actuator. The coordinate transformation is further done to convert these forces from inertial frame to body fixed frame using the bond graph arrangement of Fig. 6.4. Here, all power directions will be opposite in CTF model to the model shown in Fig. 6.4. Instead of flow inputs and flow outputs, effort inputs are there in top and effort outputs are there at the bottom for *x*, *y* and *z* directions.

The values of different transformer moduli used in CTF model here are

$$\left.\begin{aligned} &\sigma_1 = \cos\beta\cos\gamma, \sigma_2 = \cos\gamma\sin\alpha\sin\beta - \sin\gamma\cos\alpha, \sigma_3 = \cos\gamma\cos\alpha\sin\beta + \sin\gamma\sin\alpha, \\ &\sigma_4 = \sin\gamma\cos\beta, \sigma_5 = \sin\alpha\sin\gamma\sin\beta + \cos\alpha\cos\gamma, \sigma_6 = \sin\beta\sin\gamma\cos\alpha - \cos\gamma\sin\alpha, \\ &\sigma_7 = -\sin\beta, \sigma_8 = \cos\beta\sin\alpha, \sigma_9 = \cos\alpha\cos\beta \end{aligned}\right\} \quad (6.24)$$

The *x*, *y* and *z* points are attached to various transformer elements shown as vector bond graph in Fig. 6.5 which calculate body fixed frame velocities of six leg attachment points according to Eqs. (6.1–6.18). An Euler Junction structure [Karnopp *et al.*, 2000; Mukherjee *et al.*, 2006] is attached further in which a pair of gyrator rings, one for linear and the other for angular velocities couples the inertias (masses and moment of inertias in three directions of *x*, *y* and *z* axis) M_x, M_y, M_z, I_{xx}, I_{yy} and I_{zz}. The following equations are used to calculate forces in all six directions:

$$\sum F_x = M_x \ddot{x}_g + M_x(\dot{z}_g\dot{\theta}_y - \dot{y}_g\dot{\theta}_z) \tag{6.25}$$

$$\sum F_y = M_y \ddot{y}_g + M_y(\dot{x}_g\dot{\theta}_z - \dot{z}_g\dot{\theta}_x) \tag{6.26}$$

$$\sum F_z = M_z \ddot{z}_g + M_z(\dot{y}_g\dot{\theta}_x - \dot{x}_g\dot{\theta}_y) \tag{6.27}$$

$$\sum M_x = I_{xx}\ddot{\theta}_x + \dot{\theta}_z\dot{\theta}_y\left(I_{zz} - I_{yy}\right) \tag{6.28}$$

$$\sum M_y = I_{yy}\ddot{\theta}_y + \dot{\theta}_x\dot{\theta}_z\left(I_{xx} - I_{zz}\right) \tag{6.28}$$

$$\sum M_z = I_{zz}\ddot{\theta}_z + \dot{\theta}_y\dot{\theta}_x\left(I_{yy} - I_{xx}\right) \tag{6.29}$$

These are equations described by Newton-Euler for the moving platform [Drozdz & Pacejka, 1991] with axes connected to the body and aligned with the principal axes of inertia. Finally, six flow outputs coming from centre of gravity in six directions of *x*, *y*, *z*, θ_x, θ_y and θ_z are there which will be compared with flow inputs given to the inverse model for trajectory tracking performance.

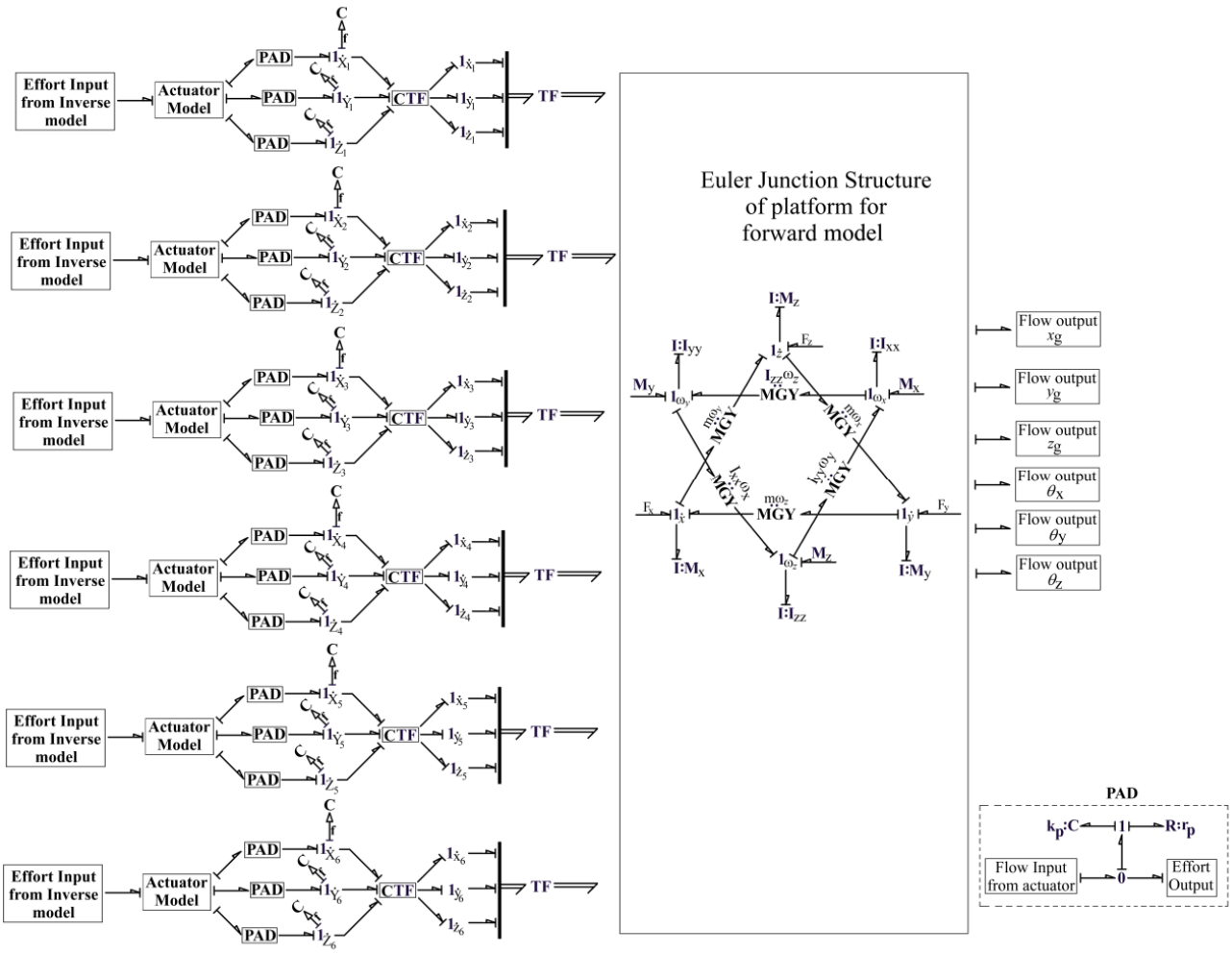

Fig. 6.5 Forward model for 3D hybrid manipulator

6.2.3 Inverse Model of 3D Hybrid Manipulator

The inverse dynamics for a three dimensional hybrid manipulator is represented by bond graph arrangement and is displayed in Fig. 6.6. Here, six flow inputs are given to centre of gravity in six paths of *x*, *y*, *z*, θ_x, θ_y and θ_z. Leg inertia is not taken into account here. Addition of pad elements to avoid differential causality has already been explained in Section 3.4 of Chapter 3. The combinations of stiff spring damper with stiffness k_p and damping r_p are attached for removal of causal loops in a similar way as for the inverse model developed for planar hybrid manipulator in Chapter 3. A sub-model named as 'ISP' model is shown in Fig. 6.6. This ISP model is shown in detail in Fig. 6.7. Six flow inputs are attached to the Euler Junction structure of platform for inverse model. Then

various transformer elements are attached to various points to represent the linear velocities as in Eqs. (6.1–6.18). These body fixed velocities are converted to the velocities in inertial frame by coordinate transformation model as shown in Fig. 6.4. Here, the values of different transformer moduli used for CTF model are shown in Eq. (6.30).

$$\left.\begin{aligned}\sigma_1 &= \cos\beta\cos\alpha, \sigma_2 = \cos\gamma\sin\alpha\sin\beta - \sin\gamma\cos\alpha, \sigma_3 = \cos\gamma\cos\alpha\sin\beta + \sin\gamma\sin\alpha,\\ \sigma_4 &= \sin\gamma\cos\beta, \sigma_5 = \sin\alpha\sin\gamma\sin\beta + \cos\alpha\cos\gamma, \sigma_6 = \sin\beta\sin\gamma\cos\alpha - \cos\gamma\sin\alpha,\\ \sigma_7 &= -\sin\beta, \sigma_8 = \cos\beta\sin\alpha, \sigma_9 = \cos\alpha\cos\beta\end{aligned}\right\} \tag{6.30}$$

Then CTF is attached to transformer elements and further to $1_{\dot{L}}$ junctions to represent rate of change of leg length as shown in Eq. (6.20) so that it becomes a mirror image of the forward model shown in Fig. 6.5. Six effort outputs coming from six actuators will be overwhelmed by the overwhelming controller to overwhelm different external disturbances and vibrations as shown in Fig. 6.6. The concept to use overwhelming controller for constructing the inverse model of a hybrid manipulator has already been explained in Section 3.3 of Chapter 3. Finally, six effort outputs of the inverse model will be given as commands to the forward model for six actuators to do trajectory tracking of 3D hybrid manipulator.

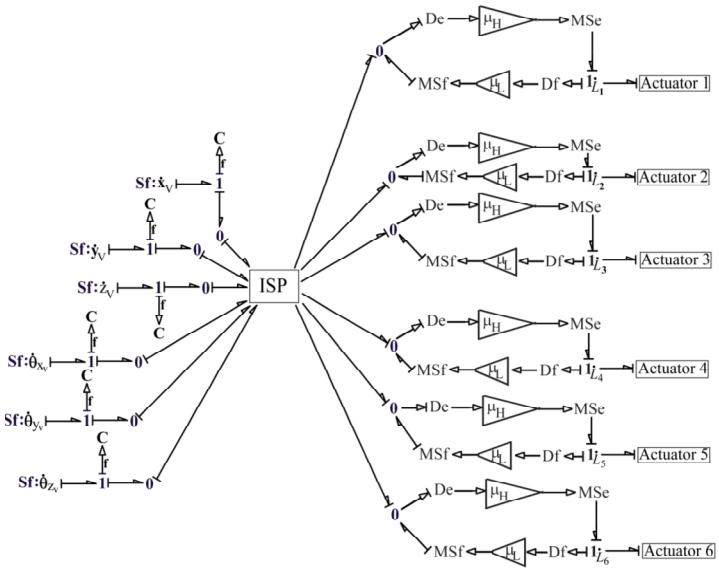

Fig. 6.6 Inverse bond graph model of 3D hybrid manipulator

6.3 Application to Human Hand Motion

The objective of this section is to track the trajectory by the different phalangeal joints of thumb of right hand by considering thumb as a three dimensional hybrid manipulator while drawing an arc of 60° on a white board with the help of a marker pen. Hence, this three dimensional hybrid manipulator is suitable for use in multi fingered robotic grippers, pick and place operations, machining operations and moving things *etc*.

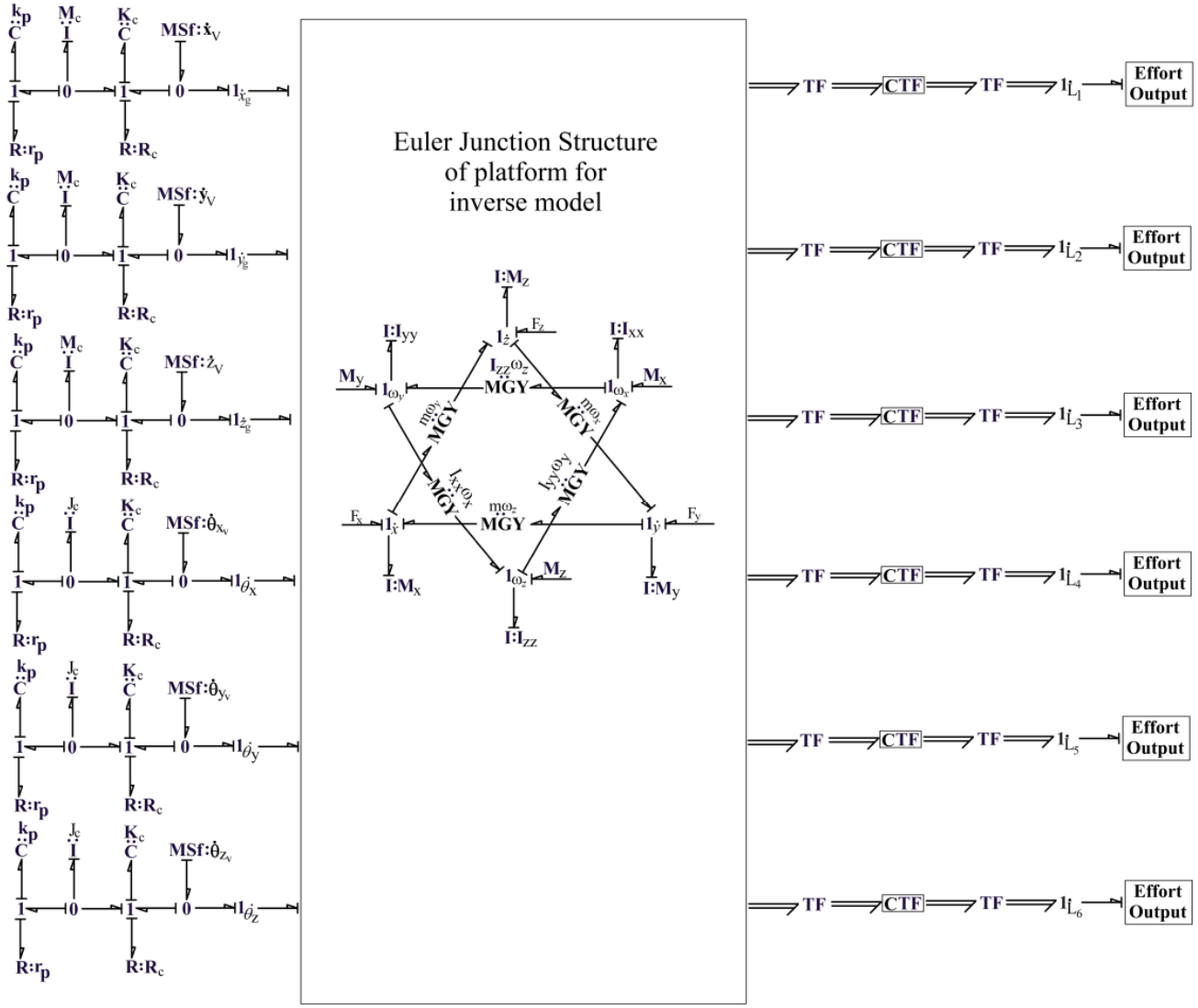

Fig. 6.7 Model of inverse parallel manipulator

6.3.1 Structure of a Human Hand

The basic structure of a human hand has already been explained in Section 3.7.1 of Chapter 3. Each normal human has two hands and one thumb located to the side of fingers on each hand. The five joints where thumb and all fingers are attached to the palm have metacarpal bones. Other than this, thumb has proximal and distal phalanges. All other fingers have proximal, intermediate and distal phalanges. The bones and joints of thumb and index finger are shown in Fig. 3.16 of Chapter 3. In this thesis, thumb and index finger are considered as a three dimensional hybrid manipulator each where one phalanx can be considered as 3D parallel manipulator and one parallel manipulator or phalanx is placed over other in series.

The metacarpal bone of thumb is taken as lower manipulator whereas proximal and distal bones are together considered as upper manipulator. Similarly, in index finger, intermediate and distal phalanges are taken as one parallel manipulator placed in series over the other parallel manipulator which is considered to be made of metacarpal and proximal phalanges. The three dimensional trajectory tracking of these joints for thumb is considered in this thesis while drawing an arc of 60° in *x*-*y* plane on a white board with the help of a marker pen. The *z* direction is taken as perpendicular to *x* and *y* axis. The end position is taken at 10° arc because of complexity of simulation program. The snap shots (camera-professional mode-Motorola G4 Plus) of four different positions in *xyz* coordinate system in different planes were taken of thumb and index finger of right hand for a time duration of 10 seconds. These positions are shown in Fig. 6.8. The directions of *x*, *y* and *z* axis are also shown in this figure for each position. The starting position of thumb is considered in *y*-*z* plane with marker pen placed at some distance from the white board as shown in Fig. 6.8(a). The intermediate position of thumb in *y*-*z* plane is shown in Fig. 6.8(b) with marker moving near to the white board for drawing an arc. The final position of thumb in *y*-*z* plane is shown in Fig. 6.8(c) with marker placed on the white board at 0° arc so that drawing is just started. The final position in *y*-*z* plane is same as the initial position in *x*-*y* plane when we begin to draw arc at 0°. The final position of thumb in *x*-*y* plane shown in Fig. 6.8(d) is considered with placement of marker pen at an arc of 10°. The arc of 90° is shown here in Fig. 6.8 with divisions marked at 10° each to

have a better understanding that this three dimensional hybrid manipulator can be used for large drawings too.

The X-ray photography for initial position in *y-z* plane was also taken as shown in Fig. 6.9 in which point 'O' is marked at starting of metacarpal joint of thumb and taken as fixed joint. Point 'A' is marked at end of metacarpal joint and beginning of proximal joint. Point 'B' is marked at tip of thumb i.e. at the end of distal joint. All the phalanges are also marked in Fig. 6.9. So, lower manipulator is considered from 'O' to 'A' and upper manipulator is considered from 'A' to 'B'. The trajectory tracking of points 'A' and 'B' are done here with point 'O' assumed as fixed joint. Similarly, for index finger, point 'O' is marked at beginning of metacarpal phalanx and 'A' is marked at end of proximal phalanx which shows that lower manipulator is considered from 'O' to 'A'. The upper manipulator is from 'A' to 'B' i.e. intermediate and distal phalanges are considered in it.

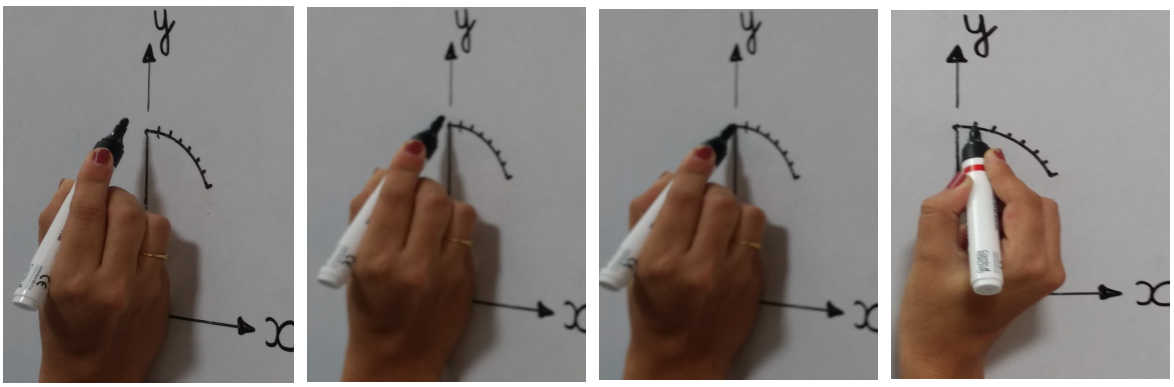

(a) (b) (c) (d)

Fig. 6.8 (a) Initial position of thumb in *y-z* plane, (b) intermediate position in *y-z* plane, (c) final position in *y-z* plane and initial position in *x-y* plane and (d) position in *x-y* plane at some extent

6.3.2 Simulation Results of Trajectory Tracking

The trajectory tracking of thumb is considered here while drawing an arc of 60° on a board with the help of a marker pen. The simulation is done in *y-z* plane for 5 s and in *x-y* plane for another 5 s. The reference trajectories will be linear velocities in *x*, *y* and *z* directions as no rotational velocities are considered here. The lengths of both

manipulators are measured from x-ray position and are taken as 48.67 mm for lower manipulator and 39.27 mm for upper manipulator in *y*-direction. The diameter of base of lower manipulator is measured to be 15.92 mm and of upper platform is 11.92 mm. Similarly, the diameter of base of upper manipulator is measured as 11.92 mm and of upper platform is 8.68 mm. The linear coordinates of all points of lower and upper manipulator are calculated based on their angular positions already shown in Table 6.1 as explained below:

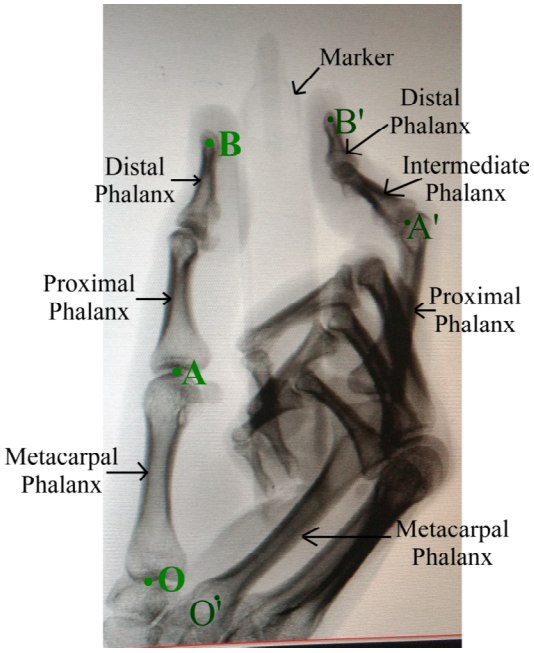

Fig. 6.9 X-ray picture showing thumb and index finger holding the marker

For base of lower manipulator, linear coordinates of *y* are taken as 0 mm for all six actuators as it lies on *y*-axis of *xyz* coordinate system. The values of *x* and *z* coordinates for six actuators for base of lower manipulator are calculated based on the following equations:

$$x = r\cos\theta \tag{6.31}$$

$$z = -r\sin\theta \tag{6.32}$$

where r is radius of base circle and taken as 7.96 mm and θ angles are taken from Table 6.1.

Similarly, value of *y* for upper platform of lower manipulator is taken as 48.67 mm for all six actuators. The values of *x* and *z* coordinates for six actuators for upper platform

of lower manipulator are calculated based on the Eqs. (6.31 and 6.32). Radius (r) of upper platform of lower manipulator is taken as 5.96 mm. As base of upper manipulator and upper platform of lower manipulator is same hence forth value of y for base of upper manipulator is also taken as 48.67 mm for all six actuators. The values of x and z coordinates for six actuators for base of upper manipulator are calculated based on the Eqs. (6.31 and 6.32). Radius (r) of base of upper manipulator is also taken as 5.96 mm. The value of y for upper platform of upper manipulator is taken as 87.94 mm for all six actuators. The values of x and z coordinates for six actuators for upper platform of upper manipulator are calculated based on the Eqs. (6.31 and 6.32). Radius (r) of upper platform of upper manipulator is taken as 4.34 mm. The values of all θ angles for all actuators have been taken from Table 6.1. Table 6.2 shows all these coordinates based on sine and cosine components.

Based on the x, y and z positions, actuator lengths of all six actuators are calculated from Eq. (6.19) for lower manipulator as 48.93 mm and for upper manipulator as 39.45 mm. Other parameters used in simulation are taken accordingly as shown in Table 6.3.

The initial conditions calculated for different actuators used in simulation are shown in Table 6.4. Simulation is done for 10 seconds. For initial 5 seconds, movement of thumb is done from bringing the marker pen at some distance from the board to place it on the board at arc of 0° for drawing further arc, i.e. movement of thumb is done as shown in Fig. 6.8(a) to Fig. 6.8(c). Since this movement is done in yz plane, command velocity given in x direction is null. The angular distance travelled by thumb for this particular movement is assumed to be 15°. So, the command velocities given to the inverse model for initial 5 seconds of trajectory tracking are as follows:

$$\left.\begin{array}{ll} \dot{x} = 0 & \\ y = r\cos\theta & \dot{y} = -r\sin\theta \times \dot{\theta} \\ z = -r\sin\theta & \dot{z} = -r\cos\theta \times \dot{\theta} \end{array}\right] \qquad (6.33)$$

where r is taken as 48.67 mm for lower manipulator and 87.94 mm for upper manipulator as already explained.

Table 6.2 Linear positions for different joints of lower and upper manipulators

		Actuators →	1	2	3	4	5	6
Metacarpal (Lower manipulator)	Base	x (mm)	6.315	-6.315	-7.38	-1.039	1.039	7.38
		y (mm)	0	0	0	0	0	0
		z (mm)	-4.845	-4.845	-2.98	7.892	7.892	-2.9818
	Upper platform	x (mm)	1.34	-1.34	-5.699	-4.358	4.358	5.699
		y (mm)	48.67	48.67	48.67	48.67	48.67	48.67
		z (mm)	-5.807	-5.807	1.742	4.064	4.064	1.742
Proximal + Distal (Upper manipulator)	Base	x (mm)	4.728	-4.728	-5.526	-0.778	0.778	5.526
		y (mm)	48.67	48.67	48.67	48.67	48.67	48.67
		z (mm)	-3.628	-3.628	-2.232	5.909	5.909	-2.232
	Upper platform	x (mm)	0.976	-0.976	-4.15	-3.174	3.174	4.15
		y (mm)	87.94	87.94	87.94	87.94	87.94	87.94
		z (mm)	-4.228	-4.228	1.268	2.959	2.959	1.268

Table 6.3 Parameter values

Sub systems	Parameter values			
Platform	$M_x, M_y, M_z = 2\,\text{kg}$	$I_{xx}, I_{yy}, I_{zz} = 1\,\text{kg m}^2$		
Actuator	$l_{gc} = 0.01\,\text{m}$ (lower manipulator), 0.012 m (upper manipulator)	$l_p = 0.016\,\text{m}$ (lower manipulator),0.024 m (upper manipulator)	$l_{gp} = 0.013\,\text{m}$ (lower manipulator), 0.012 m (upper manipulator)	$d = 0.04\,\text{m}$
	$M_x, M_y, M_z = 0.5\,\text{kg}$	$I_{xx}, I_{yy}, I_{zz} = 0.5\,\text{kg m}^2$	$R_f = 0.0\,\text{Ns/m}$	$k_p = 1e7\,\text{N/m}$ $r_p = 100\text{Ns/m}$
Inverse system	$M_x, M_y, M_z = 1\text{kg}$	$I_{xx}, I_{yy}, I_{zz} = 1\,\text{kg m}^2$	$\mu_L = 1$	$\mu_H = 100000$
Pad	$k_p = 1e8\,\text{N/m}$	$r_p = 100\text{Ns/m}$		
Controller	$K_c = 1e8\,\text{N/m}$	$R_c = 100\,\text{Ns/m}$	$M_c = 2\,\text{kg}$	$J_c = 1\text{kg/m}^2$
	$g = 9.8\,\text{m/s}^2$			

Table 6.4 Initial conditions

	Actuators →	1	2	3	4	5	6
Metacarpal (Lower manipulator)	θ_x (radians)	1.672	1.468	1.536	1.638	1.505	1.605
	θ_y (radians)	0.103	0.103	0.103	0.103	0.103	0.103
	θ_z (radians)	1.59	1.59	1.474	1.649	1.649	1.474
	x_c (mm)	5.059	-5.094	-6.967	-1.85	1.8	6.96
	y_c (mm)	11.936	11.936	11.936	11.936	11.936	11.936
	z_c (mm)	-5.079	-5.079	-1.822	6.95	6.95	-1.823
	x_p (mm)	2.56	-2.559	-6.11	-3.54	3.4	6.11
	y_p (mm)	36.733	36.733	36.733	36.733	36.733	36.733
	z_p (mm)	-5.566	-5.566	0.583	-5	5	0.584
Proximal + Distal (Upper manipulator)	θ_x (radians)	1.666	1.475	1.536	1.631	1.51	1.605
	θ_y (radians)	0.095	0.095	0.095	0.095	0.095	0.095
	θ_z (radians)	1.723	1.723	1.482	1.645	1.645	1.482
	x_c (mm)	3.58	-3.58	-5.1074	-1.5	1.507	5.109
	y_c (mm)	60.61	60.61	60.61	60.61	60.61	60.61
	z_c (mm)	-5.4	-5.4	-11.67	5.013	5.013	-11.67
	x_p (mm)	2.11	-2.1	-4.56	-2.44	2.44	4.572
	y_p (mm)	75.9	75.9	75.9	75.9	75.9	75.9
	z_p (mm)	-7.8	-7.8	-0.203	3.86	3.86	0.203

where x_c, y_c and z_c are the x, y and z coordinates of cylinder end and x_p, y_p and z_p are x, y and z values of piston end. The angular velocity for this movement is calculated as

$$\dot{\theta} \text{ or } \varpi = \frac{15^\circ}{5\,\text{sec}} = 0.05236\,\text{rad/s}$$
$$\theta = \varpi\ t$$

Similarly, thumb is moved in x-y plane in next 5 seconds for drawing an arc from 0° to 10°, *i.e.* movement of thumb is done as displayed in Fig. 6.8(c) to Fig. 6.8(d). The command velocities given for 5–10 s of this movement are as

$$\left.\begin{aligned} x &= r\sin\theta & \dot{x} &= r\cos\theta \text{ x } \dot{\theta} \\ y &= r\cos\theta & \dot{y} &= -r\sin\theta \text{ x } \dot{\theta} \\ \dot{z} &= 0 \end{aligned}\right] \qquad (6.34)$$

where r is taken as 1.069 mm for lower manipulator and 3.069 mm for upper manipulator.

The linear velocity in *z* direction is given to be zero as the movement is in *x*-*y* plane. The angular velocity given for 5–10 seconds of time is calculated as:

$$\dot{\theta} \text{ or } \varpi = \frac{10^\circ}{5\,\text{sec}} = 0.0349\,\text{rad/s}$$
$$\theta = \varpi\, t$$

Therefore, the reference trajectories are the displacements of centroid of a joint in three directions i.e. *x*, *y* and *z* positions for various points. The inverse model was given these reference positions of joints. The motions from command points are matched with the equivalent motions obtained from response points for different positions of thumb obtained from simulation results. The final results of trajectory tracking for dislocations in *x*, *y* and *z* paths are displayed in Fig. 6.10(a), (b) and (c), respectively.

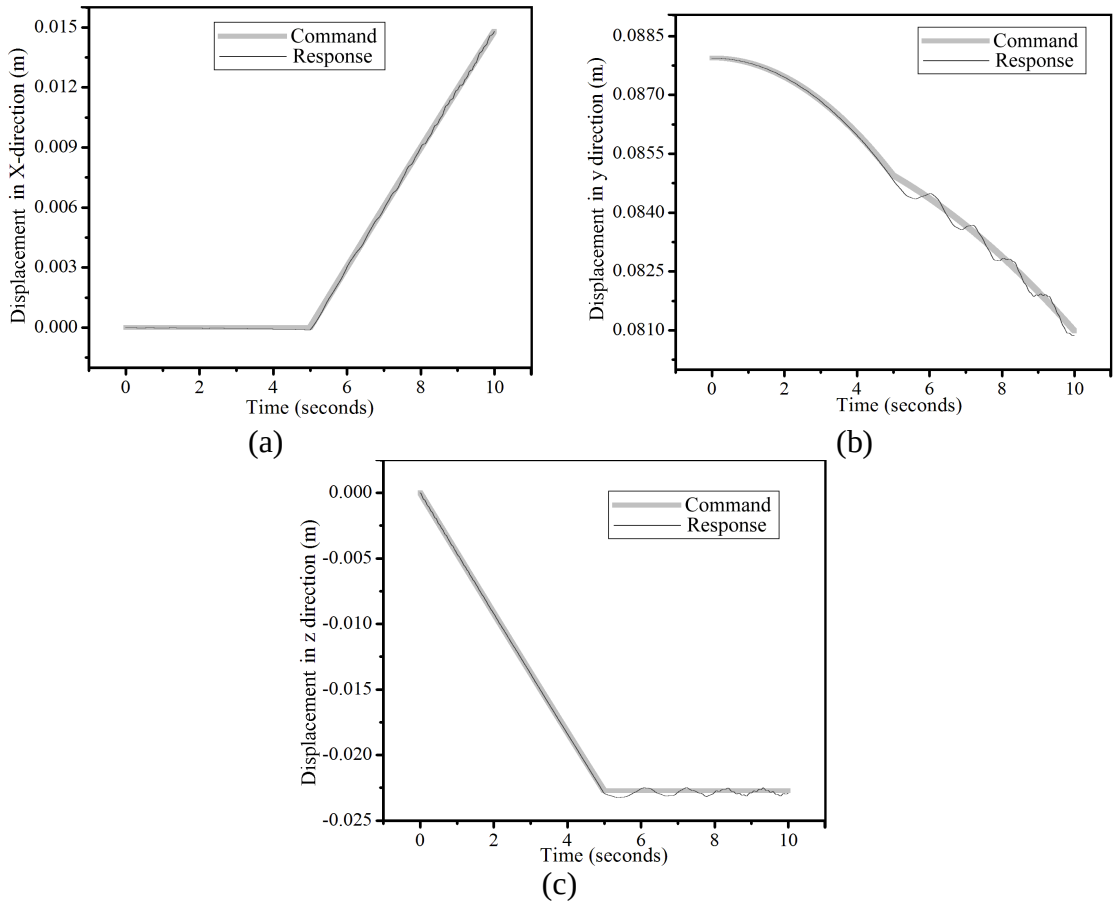

Fig. 6.10 Trajectory tracking of thumb for (a) dislocation in *x* path (b) dislocation in *y* path and (c) dislocation in *z* path

Therefore, it is noted that the desired trajectory is tracked by the simulator for the thumb tip exactly in *x*-direction for full simulation of 0–10 s of time. The displacements in *y* and *z* directions are fully followed by the manipulator for initial 5 s and with minimal error for 5–10 s. The percentage error in *x*, *y* and *z* displacements are shown in Fig. 6.11(a). The percentage error in *y* displacement is shown in detail in Fig. 6.11(b) to have a clear understanding of result.

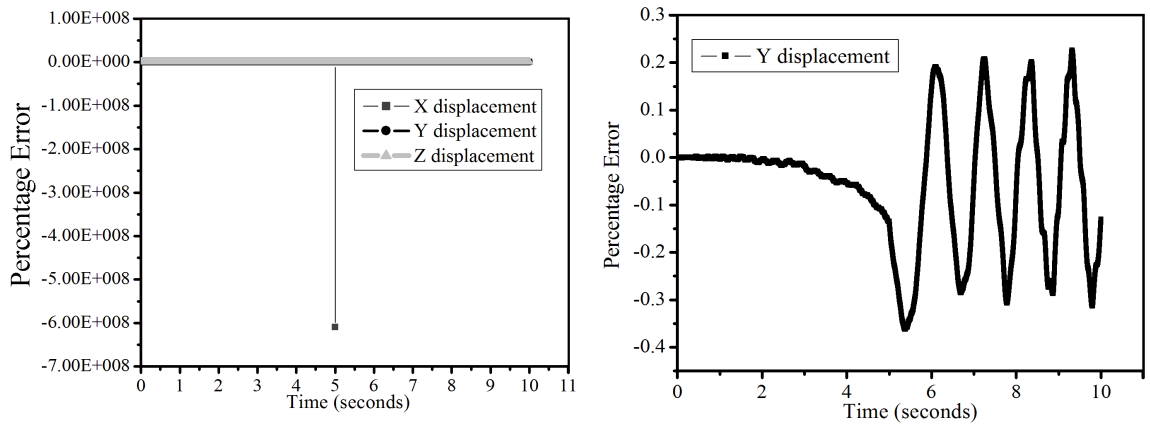

Fig. 6.11 (a) Percentage error in *x*, *y* and *z* displacements and (b) percentage error in *y* displacement

It is observed very clearly from these results that simulator tracks the command displacement in *x*-direction exactly with minimum error of -6×10^{8} % which is approximately zero and hence can be neglected. For displacement in *y*-direction, the response tracks the command exactly initially and then with maximum error of 0.22 % which is very minimal. Similarly, the response matches the command in *z* direction with zero error for 0 to 5 s and with 0.00025 m error for 5 to 10 s. Therefore, it is seen that the simulator tracks the desired trajectory in all directions with minimal error which can be neglected easily. The forward model follows the command of inverse model for controller gain of 100000. If the controller gain is further increased, the error can totally be reduced to nil but simulation becomes very slow.

Hence, it is concluded from this study that the thumb in human hand can be taken as an example of a three dimensional hybrid manipulator for which trajectory tracking was done for different phalangeal joints. Within the acceptable range, the command given to

the controllers is followed by the response of the plants. If the gain of the overwhelming controller is further increased, the error limit can be decreased but the time taken by simulation is very large in that case.

6.4 Impedance Control of 3D Hybrid Manipulator

The forces which are developed when the manipulator interacts safely in company of environment or any object are known as forces at contact. These forces need to be controlled in such a way that the force provided by the manipulator must be less than the secure weight limits of the object with which interaction of manipulator takes place. This force control is also essential in trajectory tracking because the object or the manipulator can be damaged unexpectedly by any type of discrepancy. There are two kinds of approaches used to control force in manipulators. These are direct and indirect approaches used for force control [DeSchutter *et al*., 1997; Siciliano & Villani, 2000]. Force measurement is not needed in indirect scheme. Mass at the point of contact and either stiffness or damping can be controlled in this scheme. The accurate representation of the thing of the environment must be recognized fully whereas it is not necessary in direct force control scheme. The fault between the required force and calculated force is needed in direct scheme.

The control of impedance at the point where the robotic arm comes in contact with the object is main trustworthy approach [Raibert & Craig, 1981; Anderson & Spong, 1988; Assuncao & Schumacher, 2003] for direct force control scheme. The direct scheme can also be called as hybrid position force control scheme [Takaiwa & Noritsugu, 2003; Kosuge *et al*., 1996] for which a virtual foundation is combined with an overwhelming controller to apply the impedance control [Chiaverini & Sciavicco, 1993]. This approach has been followed in this chapter for impedance control of a three dimensional hybrid manipulator. A compensation gain is used to adjust the impedance at the boundary of robotic arm and environment. The response has some trajectory tracking error from command during the interaction period. This error is known as amnesia and is removed when the manipulator and object are not interacting. One more loop of compensation is added in the controller for this. Finally, the impedance control scheme developed is

applied to an application of inverted mirror L-shaped path which proves that this manipulator can be used to do impedance control for a machining operation.

6.4.1 Impedance Control Technique

The block diagram of the impedance controller, which will be developed in the following sections, is shown in Fig. 6.12. The reference velocity given to the impedance controller is denoted by V_r. F_{en} is the force of interaction between the manipulator and the environment or object. This force of interaction must be less than the restrictive value of force denoted by F_{lim} to have a safe interaction between the manipulator and the environment. The error between the interaction force and the limiting force is fed to the impedance controller so that reference velocity is revised as V_{re} and this reference velocity is given to the inverse system containing overwhelming controller. The overwhelming controller for the planar hybrid manipulator has been already developed in Chapter 3.

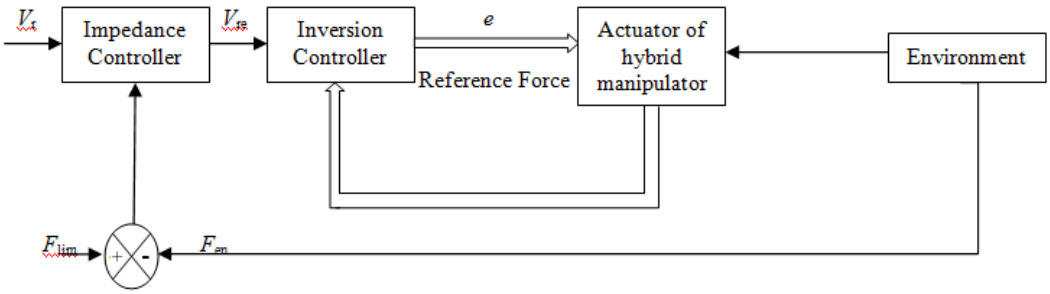

Fig. 6.12 Schema of the integrated impedance controller system

Along with the overwhelming controller, the proportional controller can also be used in manipulators to do force control and trajectory tracking. Fig. 6.13 (a) displays the easiest impedance controller with proportional controller in a bond graph arrangement for one degree-of-freedom robot using overwhelming controller. A force sensor (De) measures the force of interaction between the tip of robot and the environment. A flow detector (Df) measures the velocity of the robot tip. If we are able to compensate the flow at driving point, the stiffness at driving point can also be modulated. The signal of flow that is directly proportional to the difference of the exact contact forces F_{en}, found with sensor detecting force and the restricted force value specified by F_{lim}, is written as

$$f = -\dot{\delta}_{\mathrm{p}} = -\zeta (F_{\mathrm{en}} - F_{\mathrm{lim}}) \quad \forall F_{\mathrm{en}} > F_{\mathrm{lim}} \tag{6.35}$$

where ζ is the term of gain of proportionality. The indicator of flow specified by above equation is given to the inverse system after matching with the velocity of reference as shown in Fig. 6.13 (a). The signal flow graph drawn from this bond graph model is shown in Fig. 6.13 (b) where e denotes effort variable, f denotes flow variable and subscripts represent the bond numbers. $E(s)$ is the transfer function of environmental interaction.

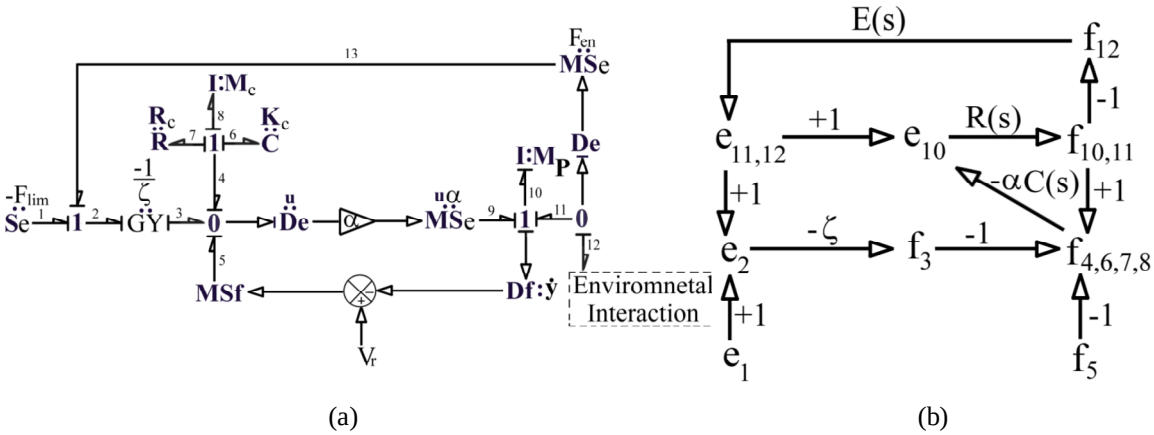

(a) (b)

Fig. 6.13 (a) Bond graph model for the robot having control of force and (b) its signal flow graph

The transfer function between the flow of end-effector of robotic manipulator $f_{10}(s)$ and the reference velocity $f_5(s)$ can be found with application of Mason's gain rule. Henceforth, the transfer function obtained for this system is

$$\frac{f_{10}(s)}{f_5(s)} = \frac{\alpha\, C(s) R(s)}{1 + \alpha\, C(s) R(s) + E(s) R(s) - \zeta\alpha\, C(s) R(s) E(s)} \tag{6.36}$$

where α is the gain of overwhelming controller. The robot admittance $Y_{\mathrm{r}}(s)$ at the point of interaction is given by

$$Y_r(s) = \frac{1}{Z_r(s)} = \frac{f_{10}(s)}{e_{12}(s)} = \frac{R(s)}{1 + \alpha\, C(s) R(s) + E(s)\, R(s) - \zeta\alpha\, C(s) R(s) E(s)} \tag{6.37}$$

This admittance is the inverse of impedance of the robot Z_r (s) at the same point of interaction. It can be easily seen from the Eqs. (6.36–6.37) that if overwhelming controller gain ($\alpha >> 1$) and $\zeta \to 0$, $f_{10}(s)/f_5(s) = 1$. Also, the impedance value at the point of interaction becomes very high. Therefore, the robustness of trajectory is guaranteed by controller and there will be negligible environmental forces. Moreover, if overwhelming controller's feed forward gain is not very large and the proportional gain (ζ) also rises from zero value, then the value of impedance can be made lesser to adjust the forces of interaction. This effortless impedance control strategy has lesser control loops and feedback gains.

6.4.2 Amnesia Removal Technique

During the interaction of manipulator with the object, trajectory tracking errors are caused by invasion of the trajectory control path into the path corresponding to force control limits. This error developed is because of the decrease in the gain of overwhelming controller (α) for the duration of interaction period such that force control is attained at the expense of correctness of trajectory tracking. This position error built up at the end of a step of force control is known as amnesia. This amnesia error must be eliminated before the next interaction so that it follows the reference trajectory during the period when it is not interacting.

The impedance controller with removal of amnesia is represented in the form of a block diagram as shown in Fig. 6.13. The force controller builds up the loss in positional information (δ_p) during the period of interaction. This information of position is calculated by integration of signal of flow ($\dot{\delta}_p$) that is proportional to the error of force *i.e.* the flow in bond number 3 in the bond graph arrangement shown in Fig. 6.13 (a). Another flow variable (δ_{re}) is given in the inverse system with velocity of reference (V_r) for the duration of period when it is not interacting. This flow variable is proportional to the amnesia error. Henceforth, when $\dot{\delta}_p \neq 0, \dot{\delta}_f = 0$. This amnesia removal rate $(\dot{\delta}_f)$ is a term derived from trial and error [Kumar & Mukherjee, 1989; Kumar, 1994; Pathak *et al.*, 2005] and is given as

$$\dot{\delta}_{\mathrm{f}} = G \,\mathrm{x}\, e^{(t-t_0)} \int \varsigma \left(F_{\mathrm{en}} - F_{\mathrm{lim}} \right) \mathrm{dt} \tag{6.38}$$

where G is a gain and t_0 is the initial instant, *i.e.* the point at the end of a step of force control.

Therefore, in addition to the velocity of reference, this signal of flow $\left(\dot{\delta}_{\mathrm{f}}\right)$ is also given to the inverse controller. The quantity of accommodated position recovered is also noted down simultaneously such that $\delta_{\mathrm{p}} = \int \left(\dot{\delta}_{\mathrm{p}} - \dot{\delta}_{\mathrm{f}} \right) \mathrm{dt}$. The function $\phi_{\mathrm{f}}(.)$in Fig. 6.14 models the Eq. (6.38).

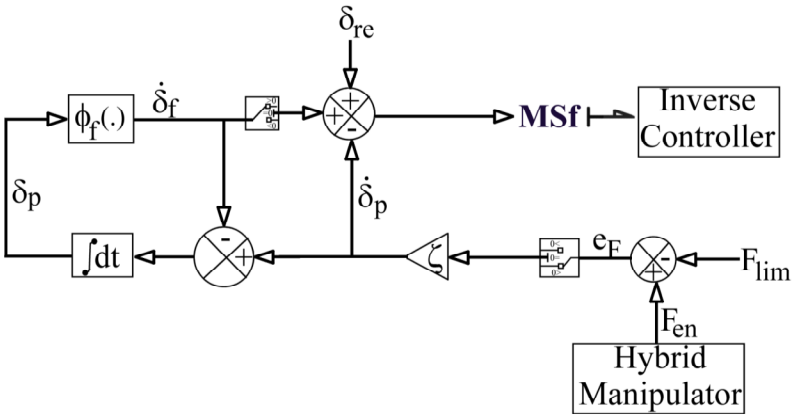

Fig. 6.14 Impedance controller with amnesia removal

6.4.3 Parameters of System and Initial Positions

The various parameter values applied for the simulation are shown in Table 6.5. The values of parameters for plant, pad and inverse controller for the hybrid manipulator have been chosen suitably according to the application. The gain 'α' of overwhelming controller is intentionally taken as 100 (*i.e.* α >>>1) here and the value of proportional controller gain 'ζ' is taken near to zero because a high value of gain implies impedance control strategy in a better way and there is minimum error in trajectory tracking, as already explained in above section. The interaction with the environment is assumed here to be fully acquiescent with stiffness 'K_{en}' and without any damping $\left(R_{\mathrm{en}_x} = R_{\mathrm{en}_y} = R_{\mathrm{en}_z} = 0\right)$. Subscripts *x*, *y* and *z* for stiffness 'K_{en}' in Table 6.5 show the

respective directions. The gains used for compensation, restrictive forces and gain used to remove amnesia in *x*, *y* and *z* paths are denoted by parameters ζ, $F_{\lim}$ and *G* with *x*, *y* and *z* in subscripts showing the respective directions. The platform moves in three directions of *x*, *y* and *z*, whereas it does not rotate about any of those axes. All the parameters are displayed in the Table 6.5.

Table 6.5 Parameter values applied for the simulations

Sub systems	Parameter values			
Actuator	$k_{\mathrm{p}} = 10^7$ N/m	$r_{\mathrm{p}} = 500\,\mathrm{Ns/m}$		
Platform	$M_{\mathrm{P}} = 100\,\mathrm{kg}$	$J_{\mathrm{P}} = 5\,\mathrm{kg\,m^2}$	$M_{\mathrm{P}}^{*} = 1\,\mathrm{kg}$	$J_{\mathrm{P}}^{*} = 0.1\,\mathrm{kg\text{-}m^2}$
Controller in Inverse system	$K_{\mathrm{c}} = 10^7$ N/m	$R_{\mathrm{c}} = 500\,\mathrm{Ns/m}$	$M_{\mathrm{c}} = 300\,\mathrm{kg}$	$J_{\mathrm{c}} = 10\,\mathrm{kg\text{-}m^2}$
	$\alpha = 100$			
	$K_{\mathrm{en}_x} = 120\,\mathrm{N/m}$	$K_{\mathrm{en}_y} = 1000\,\mathrm{N/m}$	$K_{\mathrm{en}_z} = 0$	$R_{\mathrm{en}_x} = 0\,\mathrm{Ns/m}$
Force Controller	$\zeta_x = 0.01$	$\zeta_y = 0.1$	$\zeta_z = 0$	$R_{\mathrm{en}_y} = 0\,\mathrm{Ns/m}$
	$F_{\lim_x} = 10$ N	$F_{\lim_y} = 10\,\mathrm{N}$	$F_{\lim_z} = 0\,\mathrm{N}$	$R_{\mathrm{en}_z} = 0\,\mathrm{Ns/m}$
	$G_x = -5$	$G_y = -10$	$G_z = 0$	

The initial conditions taken here for the three dimensional hybrid manipulator are shown in Table 6.6. All the values in *z* direction are taken zero here because the path which we will consider later to be followed by the manipulator is a two-dimensional L-shaped path in *x*-*y* plane and force control will also be done for this trajectory.

Table 6.6 Initial conditions for the 3D hybrid manipulator

	Points	*x* (m)	*y* (m)	*z* (m)		Points	*x* (m)	*y* (m)	*z* (m)
Lower Manipulator	A	0.5	2.55	0	Upper Manipulator	A	1.5	5.1	0
	G	1.5	2.55	0		G	2	5.1	0
	B	2.5	2.55	0		B	2.5	5.1	0
	C	0	0	0		C	0.5	2.55	0
	D	2	0	0		D	1.5	2.55	0
	E	3	0	0		E	2.5	2.55	0

6.4.4 Interaction Force Control

The path to be followed by the hybrid manipulator is shown in Fig. 6.15 where point G of the upper movable platform will trace the path from A to C. The force or torque interaction between the tool attached on the platform and the environment is measured by the sensor measuring force or torque that is fixed on the upper movable platform of the hybrid manipulator. This force of interaction is compared with the restricted force value given in Table 6.5 for force controller and then the compensation gain ζ is used to adjust the impedance at the point of interaction.

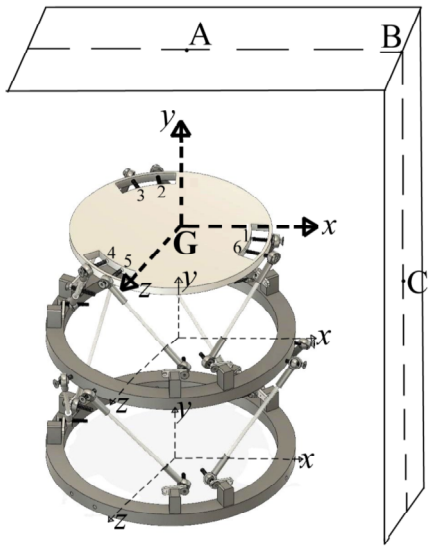

Fig. 6.15 L-shaped path to be followed by the moving platform

The simulation is done for 4 s. For time 0–0.1 s, the platform will move 0.2 m upwards in *y*-direction only. Then force control along *y*-direction is done for time 0.1–1.2 s. Afterwards, it will come 0.2 m down in time 1.2–1.3 s. From 1.3–2 s, amnesia removal in inertial *y*-direction is done so that trajectory is fully tracked during time 2–3.3 s. The velocity in *y*-direction is zero for final time duration of 3.3–4 s in inertial *y*-direction. Similarly, for initial time of 0–1.3 s, trajectory is fully tracked in inertial *x*-direction and the velocity along *x*-direction is zero for next 1.3–2 s. It moves 0.2 m in positive *x*-direction for time 2–2.1 s and force control along *x*-direction is done for time 2.1–3.2 s. During next 0.1 s, *i.e.* from 3.2–3.3 s, the platforms returns to the starting point by

moving 0.2 m backwards and finally amnesia removal is done from 3.3–4 s. The command velocities given to the inverse controller in x and y directions for doing trajectory tracking, amnesia removal and force control are shown in Eqs. (6.39) and (6.40).

$$\left.\begin{aligned}\dot{x} &= 0.1 \;\forall\; 0 \le t \le 1.3\\ &= 0 \;\; \forall 1.3 \le t \le 2\\ &= 0.2 \;\forall\; 2 \le t \le 2.1\\ &= 0 \;\forall\; 2.1 \le t \le 3.2\\ &= -0.2 \;\forall\; 3.2 \le t \le 3.3\\ &= 0 \;\forall\; 3.3 \le t \le 4\end{aligned}\right\} \tag{6.39}$$

$$\left.\begin{aligned}\dot{y} &= 0.2 \;\forall\; 0 \le t \le 0.1\\ &= 0 \;\; \forall 0.1 \le t \le 1.2\\ &= -0.2 \;\forall\; 1.2 \le t \le 1.3\\ &= 0 \;\forall\; 1.3 \le t \le 2\\ &= -0.1 \;\forall\; 2 \le t \le 3.3\\ &= 0 \;\forall\; 3.3 \le t \le 4\end{aligned}\right\} \tag{6.40}$$

The graphs of command and response of locations in x and y paths *vs.* time at the time of controlling force without removal of amnesia are displayed in Fig. 6.16 (a) and Fig. 6.16 (b), respectively. The force control and amnesia error is displayed in these figures. In both these cases, the tool is not able to come at the starting point after finishing one cycle.

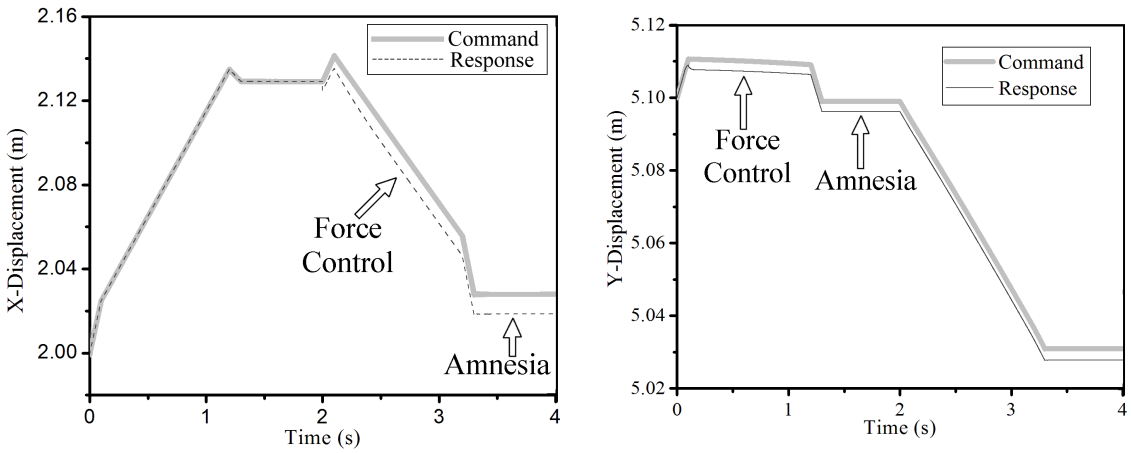

(a) (b)

Fig. 6.16(a) Reference and actual displacement in *x* direction and (b) Given input and measured output location in *y* direction for controlling force without removal of amnesia

It is clearly seen from Fig. 6.16 that initially, the reference trajectory given to the manipulator is exactly tracked in *x*-direction as shown in Fig. 6.16 (a), *i.e.* the point G of the platform moves from point A to B as shown in Fig. 6.15. During this time, force control is done in *y*-direction. Also, there is some difference in the command and response of *y*-displacement for this time duration, which is called amnesia error as shown in Fig. 6.16 (b). Then the platform moves from point B to point C as shown in Fig. 6.15, *i.e.* in inertial *Y*-direction so that trajectory tracking is done fully in direction of *y*-axis as displayed in Fig. 6.16(b). The force control is done in *x*-direction for this time after which there comes some difference in command and response of *x*-displacement, known as amnesia error as shown in Fig. 6.16 (a). It is observed during the whole time, there comes some difference in reference displacements given and actual displacement measured both in *x* and *y* directions. This is able to be removed by removal of amnesia.

The graphs of reference and actual positions in *x* and *y* paths *vs.* time at the time of controlling force with removal of amnesia are displayed in Fig. 6.17 (a) and Fig. 6.17 (b), respectively. The force control and removal of amnesia is illustrated in these figures.

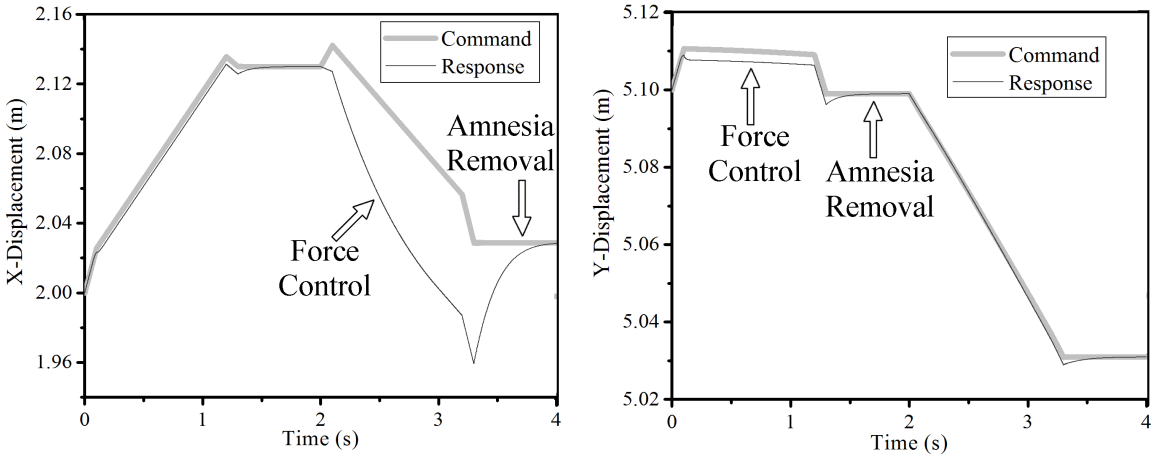

(a) (b)

Fig. 6.17(a) Input *x* position and output *x* position and (b) Input *y* position and output *y* position for controlling force with removal of amnesia

It is noticed from Fig. 6.17 (b) that force control has been done in the inertial path of *y*-axis at the time of communication during the movement of centre of gravity of the upper moving platform in *x*-direction from A point to B point and afterwards amnesia removal technique is implemented to remove amnesia during non-interaction period so that command is followed by response. Similarly, it is noticed from Fig. 6.17 (a) that force control has been done in the inertial path of *x*-axis at the time of communication during the movement of centre of gravity of the upper moving platform in *y*-direction from B point to C point and afterwards amnesia removal technique is implemented to remove amnesia during non-interaction period so that command is followed by response. It is observed clearly from both the figures that the tool reaches the beginning point after finishing one cycle.

The forces of interaction encountered during this time along directions of *x* and *y*-axis are plotted against time and are displayed in Fig. 6.18 (a) and Fig. 6.18 (b), respectively. It is clearly noticed that the force developed is larger than the restricted force value (10 N) in both directions of inertial *x* and *y*-axis during the time of force control in both directions. This increase is because of the moving platform's inertia. The force developed is larger than the limiting value of force even though the tool touches the environment initially. Afterwards, force control is done near to the restricted force value at the time of interaction in both inertial *x* and *y*-directions. In Fig 6.18, force control in *x* direction is

available for time from 2.1 s to 3.2 s. Force control in *y* direction is available for time from 0.1 s to 1.2 s. This can be seen from Eq. 6.39 and Eq. 6.40. Also Fig. 6.16 and Fig. 6.17 clearly depict the same duration of this force control along *x* and *y* directions. Hence, force control in both directions is available for same duration of 1.1 s in Fig. 6.18.

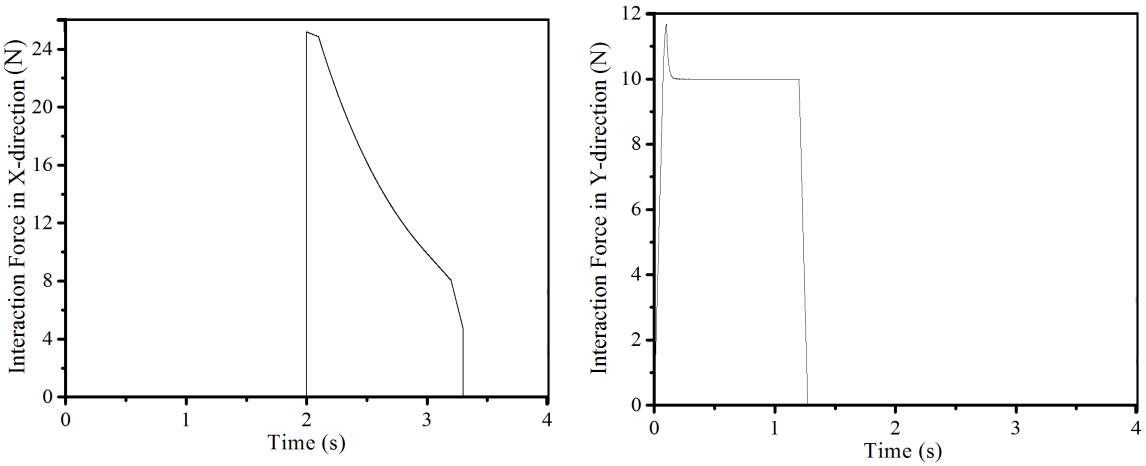

(a) (b)

Fig. 6.18 Forces of interaction along (a) *x*-direction and (b) *y*-direction

6.5 Conclusions

The planar hybrid manipulator developed earlier in Chapter 3 was made a three dimensional hybrid manipulator in this chapter. The forward dynamics model was built for this and then inverse model was built using the overwhelming control strategy to give it stability against disturbances and uncertainties of some parameters. The thumb in right hand of a human is taken as an example of a three dimensional hybrid manipulator and trajectory tracking was done for various phalangeal joints. The response follows the command exactly with a very negligible error. This error can further be reduced if controller gain is increased further but simulation time will be very large in that case.

An impedance control strategy for a three dimensional hybrid manipulator was considered in this chapter. The inverse model developed for trajectory tracking without consideration of the inertia of the actuators is used for implementing force control

strategy. At the interface of the manipulator and the environment, the environmental forces are restricted by adjusting the force controller and modulating the impedance. The amnesia error coming because of force control is removed at the time when there is no interaction in such a way that the command is followed by the response before the next interaction of tool and the environment. An application of an inverted mirror L-shaped path was considered in the chapter by controlling the forces in different directions. The forces of interaction are larger than threshold limits initially because of the moving platform's inertia of the hybrid manipulator. The information taken for location has some error which was eliminated fully with the help of a trial and error based approach to remove amnesia.

The development of a three dimensional hybrid manipulator and its application for drawing an arc along with its force control application for an inverted mirror L-shaped path was the major objective covered in this thesis. Also, the development of a planar hybrid manipulator with its two applications for bending of a human vertebrae and human hand grasping an object was the another major applications considered in this thesis.

Chapter 7

Conclusions

This dissertation shared bond graph model-based trajectory-tracking, model reduction, work-space analysis and impedance control of hybrid manipulators. The control approaches are detailed to increase the dynamic implementation of hybrid manipulators and for controlling force at the boundary of the robot with the environment.

Three degrees-of-freedom planar hybrid manipulator containing six actuators, a fixed base and two platforms was proposed in Chapter 3 with each actuator being a hydraulically driven piston-cylinder link. Its dynamic model for forward dynamics was constructed by bond graph approach using all kinematic constraints. An overwhelming control strategy was illustrated with a pedagogical example to prove its efficiency in building a computationally efficient yet simple inverse dynamic system neglecting some dynamics of forward model without considering the inertia of the actuators. The efficiency of the inverse system, *i.e.* the ability to detect correct position and the simulation time needed, was tested with application on human vertebrae and thumb of a human hand. Then it was successfully implemented for translational motion and lateral bending of human vertebrae and also for object grasping by thumb and index finger. The simulation results prove that the inertias of the actuators add major quantity of forces required by the actuators.

Further, the model reduction for forward and inverse models of planar parallel and hybrid manipulator was done in Chapter 4 using Eigen value sensitivity method. The model is reduced in such a way that the dynamics of the reduced model remains same as the original system. Firstly, a detailed approach of Eigen value sensitivity method was illustrated and implemented on a pedagogical example of a mass spring damper system to illustrate the application of model reduction method which shows the formation of two effect matrices for energy storing and energy dissipating elements of a system. The elements of the effect matrices are the measure of sensitivity of Eigen value to an

element. Finally, a reduced system is obtained after neglecting rows and columns containing Eigen values with no or very little importance. The reduced system is modelled with the help of bond graph. The results are compared between the full system and reduced system. The performance for trajectory tracking of a circular path was compared between full model and reduced model and same results were obtained for both planar parallel and hybrid manipulator. The reduced model and full model represent same dynamics of the system but the simulation time and the amount of calculations are reduced with the reduced order model.

Then the planar hybrid manipulator proposed in Chapter 3 was implemented with ball screw feed drive mechanisms for its actuators in Chapter 5. The forward and inverse dynamics of ball screw feed drive mechanism was illustrated with a bond graph arrangement. Then, the planar hybrid manipulator with ball screw feed drives used as its actuators are modelled for forward and inverse dynamics. The same earlier approach of overwhelming controller was used to build an inverse model. Afterwards, its performance is checked for trajectory tracking of a double semi-circular path. A proportional controller was used to construct a model for reaching the target given to planar hybrid manipulator in a suitable time. The same model was also used for performing workspace analysis of planar hybrid manipulator for the same trajectory earlier tracked by it with the calculation of the workspace area also shown. The shape of the workspace along with its minimum area is determined in which the trajectory should be clean and free from the disturbance of any foreign object to avoid collision.

Finally, in the last chapter of thesis, the planar hybrid manipulator developed earlier in Chapter 3 was made a three dimensional hybrid manipulator and its impedance control was also considered in this chapter. Firstly, the forward dynamics bond graph model was constructed which includes modelling of the Newton-Euler equations, coordinate transformations and Euler angle computations with actuator model in it. The inverse model of the system was developed by neglecting the inertia of the actuators through implementation of an overwhelming controller approach. The thumb in right hand of a human is taken as an example of a three dimensional hybrid manipulator and trajectory tracking was done for various phalangeal joints while drawing an arc on a white board.

Further, the bond graph arrangement was implemented for overwhelming controller along with force controller for a six degrees-of-freedom three dimensional hybrid manipulator. At the interface of the manipulator and the environment, the environmental forces are restricted by adjusting the force controller and modulating the impedance. The impedance is modified with a feedback strategy at the time of interaction that changes the command of trajectory given to the manipulator in such a way that it moves on some other path rather than the path given with approximately steady force of interaction. The amnesia coming because of force control, *i.e*. the error in paths gathered at the time of controlling force, is removed at the time when there is no interaction in such a way that the command follows the response before the next interaction of tool and the environment. An application of an inverted mirror L-shaped path was considered in the chapter by controlling the forces in different directions. The forces of interaction are larger than threshold limits initially because of the moving platform's inertia of the hybrid manipulator. The information taken for location has some error which was eliminated fully with the help of a trial and error based approach to remove amnesia.

Few areas have been suggested to explore further based on the dissertation work. These areas are as follows:

1. This control scheme can be used for the condition when the base of the hybrid manipulator is not fixed to the ground. So, it can be extended for performing heave and bending of the platform.
2. The revolute joints which connect the actuators with the base and the platform can be modelled.
3. During workspace analysis, it was assumed that platform has constant orientation. This orientation can be made variable and then workspace analysis may be performed.
4. A real hybrid manipulator may be manufactured to test it experimentally for trajectory tracking and the machining operation by controlling force.

REFERENCES

Anderson RJ and Spong MW. Hybrid impedance control of robotic manipulators. *IEEE Journal of Robotics and Automation*, 1988; 4 (5): 549–556.

Arabshahi ZH and Novinzadeh BA. Impedance control of the 3 RPS parallel manipulator. In: *Proceedings of the 2nd RSI/ISM International Conference on Robotics and Mechatronics*, Tehran, Iran, 2014, pp. 486–492.

Ardayfio D. David. *Fundamentals of Robotics*. 1987 (USA), pp. 28.

Assuncao V and Schumacher W. Hybrid force control for parallel manipulators. In: *11th Mediterranean conference on control and automation*, Rhodes, Greece, 2003, pp. T2–010.

Banton RA. Biomechanics of the spine. *Journal of the Spinal Research Foundation*, 2012; 7 (2): 12–20.

Bera TK, Samantaray AK and Karmakar R. Robust overwhelming control of a hydraulically driven three degrees of freedom parallel manipulator through a simplified fast inverse model. *Proceedings of the Institution of Mechanical Engineers, Part I: Journal of Systems and Control Engineering*, 2010; 224 (2): 169–184.

Bera TK and Samantaray AK. Bond graph model-based inversion of planar parallel manipulator systems. *International Journal of Modelling and Simulation*, 2011; 31 (4): 331–342.

Bera TK and Samantaray AK. Consistent bond graph modeling of planar multi body systems. *World Journal of Modelling and Simulation*, 2011; 7 (3): 173–188.

Bera TK, Bhattacharya K and Samantaray AK. Evaluation of antilock braking system with an integrated model of full system dynamics. *Simulation Modelling Practice and Theory*, 2011; 19: 2131–2150.

Bera TK, Samantaray AK and Karmakar R. Bond graph modelling of planar prismatic joints, *Mechanism and Machine Theory*, 2012a; 49: 2–20.

Bera TK, Merzouki R, Ould Bouamama B and Samantaray AK. Force control in a parallel manipulator through virtual foundations. *Proceedings of IMechE Part I: Journal of Systems and Control Engineering*, 2012b; 226 (8): 1088–1106.

Bergero F, Kofman E and Cellier F. A novel parallelization technique for DEVS simulation of continuous and hybrid systems. *Simulation: Transactions of the Society for Modeling and Simulation International*, 2012; 89 (6): 663–683.

Bhattacharyya R, Sarangi S and Samantaray AK. Effect of stress-softening on the ballooning motion of hyperelastic strings. *International Journal of Engineering Science*, 2015; 96: 19–33.

Bidard C. Kinematic structure of mechanisms: a bond graph approach. *Journal of the Franklin Institute*, 1991; 328 (5–6): 901–915.

Borutzky W. *Bond graphs: a methodology for modelling multidisciplinary dynamic systems*. 2004 (SCS Publishing House, Erlangen, San Diego).

Borutzky W. Bond graph modelling and simulation of multidisciplinary systems – An introduction. *Simulation Modelling Practice and Theory*, 2009; 17: 3–21.

Bos AM. Modelling Multibody Systems in terms of Multibond Graphs, with application to a motorcycle, Ph.D. Thesis, Twente University, 1986.

Boughdiri R, Nasser H, Bezine H, Sirdi KMN, Alimi MA and Naamane A. Dynamic Modeling and Control of a Multi-Fingered Robot Hand for Grasping Task. In: *International Symposium on Robotics and Intelligent Sensors*, 2012, pp. 923–931.

Breedveld PC. *Physical Systems Theory in terms of Bond Graphs*, Ph.D. Thesis, Twente University, Enschede, 1984.

Brown FT. *Engineering System Dynamics: A Unified Graph-Centered Approach*, 2007 (Taylor & Francis Group, FL).

Buchli J. Force, compliance, impedance and interaction control. In: *Summer school dynamic walking and running with robots*, Zurich, 2011, pp. 212–243.

Carbone G, Ceccarelli M and Teolis M. A numerical evaluation of the stiffness of CaHyMan (Cassino Hybrid Manipulator). In: *2nd Workshop on Computational Kinematics*, Seoul, 2001, pp. 145–154.

Carbone G and Ceccarelli M. A Stiffness analysis for a hybrid parallel-serial manipulator. *Journal of Robotica*, 2004; 22 (5): 567–576.

Ceccarelli M, Ottawiano E and Carbone G. A study of feasibility for a novel parallel-serial manipulator. *Journal of Robotics and Mechatronics*, 2002; 14: 304–312.

Cellier FE. Bond Graphs: The right choice for educating students in modelling continuous-time physical systems. *Simulation*, 1995; 64 (3): 154–159.

Cellier FE and Nebot À. The modelica bond graph library. In: *Proceedings of the 4th International Modelica Conference*, Hamburg, 2005, pp. 57–65.

Chablat D, Wenger P and Angeles J. The kinematic design of a 3-DOF hybrid manipulator. *Integrated Design and Manufacturing in Mechanical Engineering* (Chapter 4). Springer Netherlands, 1998, 225–232.

Chan SP, Yao B, Gao WB and Cheng M. Robust impedance control of robot manipulators. *International Journal of Robotics and Automation*, 1991; 6 (4): 220–227.

Chatti N, Gehin A-L, Ould Bouamama B and Merzouki R. Functional behaviour models for the supervision of an intelligent and autonomous system. *IEEE Transactions on Automation Science and Engineering*, 2013; 10 (2): 431–445.

Chaudhari SP, Patil SL, Pandey SK and Sinha S, Performance Analysis of BLDC Motor on Sinusoidal and Square Wave Supply, In: *IEEE International Conference on Power Electronics, Drives and Energy Systems* (PEDES), Trivandrum, India, 2016.

Cheah CC and Wang D. Learning impedance control for robotic manipulators. *IEEE Transactions on Robotics and Automation*, 1998; 14 (3): 452–465.

Cheng HH. Real-time manipulation of a hybrid serial and parallel driven redundant industrial manipulator. *ASME Journal of Dynamic Systems, Measurement and Control*, 1994; 116: 687–701.

Chiaverini S and Sciavicco L. The parallel approach to force/position control of robotic manipulators. *IEEE Transactions on Robotics and Automation*, 1993; 9 (4): 361–373.

Cho W. A bond graph approach to the modelling of general multibody dynamic systems. *KSME International Journal*, 1998; 12 (5): 888–898.

Choi BO, Lee MK and Park KW. Kinematic and Dynamic Models of Hybrid Robot Manipulator for Propeller Grinding. *Journal of Robotic Systems*, 1999; 16 (3): 137–150.

Cincinnati M. *Industrial Robot: An International Journal*, 1980; 7 (3): 160–162.

Connoly TJ and Longoria RG. An approach for actuation specification and synthesis of dynamic systems. *Journal of Dynamic Systems, Measurement and Control*, 2009; 131 (3): 1–15.

DasGupta A. A dynamic singularity based design of a free-flying planar manipulator. *Proceedings of the Institution of Mechanical Engineers, Part C*: *Journal of Mechanical Engineering Science*, 2007; 221 (6): 563–659.

Dasgupta K, Ghoshal SK and Kumar N. Modelling and simulation of a hydrostatic transmission system using two motor summation drive. *Journal of Modeling, Simulation, Identification and Control*, 2013; 1 (3): 89–104.

Dauphin-Tanguy G, Rahmani A and Sueur C. Bond graph aided design of controlled systems. *Simulation Practice and Theory*, 1999; 7 (5–6): 493–513.

Dauphin-Tanguy G. *Les Bond Graphs*, 2000 (Hermes Science Europe Ltd., Paris).

Davidson AM and Walters IR. Linear system reduction using approximate moment matching. In: *IEE Proceedings on Control Theory and Applications*, 1988; 135 (2): 73–78.

DeSchutter J, Bruynincks H and Spong MW. Force control: a bird's eye view. In: *Siciliano B. (ed.) IEEE CSS/ RAS international workshop on control problems in robotics and automation: future directions*, San Diego, CA, 1997, pp.1–17. Springer Verlag.

Drozde W, and Pacejka HB. Development and Validation of a Bond Graph Handling Model of an Automobile. *Journal of the Franklin Institute*, 1991; 328 (5/6): 941–957.

Frey S, Dadalau A and Verl A. Expedient modeling of ball screw feed drives. *Production Engineering Research and Development*, 2012; 6 (2): 205–211.

Gawthrop PJ. Bond graphs: A representation for mechatronic systems. *Mechatronics*, 1991, 1 (2), 127–156.

Gawthrop PJ. Physical model-based control: a bond graph approach. *Journal of the Franklin Institute*, 1995; 332 (3): 285–305.

Gawthrop PJ and Smith L. *Metamodelling: Bond Graphs and Dynamic Systems*, 1996 (Prentice Hall International (UK) Limited, Hemel Hempstead).

Gawthrop PJ. Physical interpretation of inverse dynamics using bicausal bond graphs, *Journal of the Franklin Institute*, 2000; 337 (6): 743–769.

Gawthrop PJ and Bevan GP. Bond-graph modeling. *IEEE Control Systems Magazine*, 2007; 27 (2): 24–45.

Ghosh AK, Mukherjee A and Faruqi MA. Computation of driving efforts for mechanisms and robots using bond graphs. *Journal of Dynamic Systems, Measurement and Control*, 1991; 113 (4): 744–748.

Ghoshal SK and Samanta S. Robust fault diagnosis and prognostics of a hoisting mechanism: a simulation study. *International Journal of Engineering Science and Technology*, 2011; 3 (2): 962–980.

Granda JJ. The role of bond graph modeling and simulation in mechatronics systems: An integrated software tool: Camp-G, Matlab–Simulink. *Mechatronics*, 2002; 12 (9–10): 1271–1295.

Goldenberg AA. Implementation of force and impedance control in robot manipulators. In: *IEEE International Conference on Robotics and Automation*, Philadelphia, PA, USA, 1988; 1626–1632.

Gosselin C and Angeles J. The optimum kinematic design of a planar three degree of freedom parallel manipulator. *Journal of Mechanisms, Transmission and Automation in Design*, 1988; 110 (1): 35–41.

Gosselin C and Jean M. Determination of the workspace of planar parallel manipulators with joint limits. *Robotics and Autonomous Systems*, 1996; 17: 129–138.

Gough VE and Whitehall SG. Universal tire test machine. In: *Proceeding of Ninth International Automobile Technical Congress FISITA, IMechE*, London, 1962, pp. 117–137.

Heginbotham WB, Sengupta AK and Appleton E. An ASEA Robot as an open die forging manipulator. *IFAC Proceedings Volumes*, 1979; 12 (10): 183–193.

Hogan N. Impedance Control: An Approach to Manipulation. In: *American Control Conference*, San Diego, CA, USA, 1984, pp.6–8.

Hogan N. Impedance Control: An Approach to Manipulation: Part I– Theory. *Journal of Dynamic Systems, Measurement and Control, Transactions of ASME*, 1985; 107 (1): 1–7.

Hogan N. Stable execution of contact tasks using impedance control. In: *IEEE International Conference on Robotics and Automation*, Raleigh, NC, USA, 1987, pp. 1047–1054.

Hosseinzadeh M, Aghabalaie P, Talebi HA and Shafie M. Adaptive hybrid impedance control of robotic manipulators. In: *36th Annual Conference on IEEE Industrial Electronics Society, IECON*, Glendale, AZ, USA, 2010, pp. 1442–1446.

Huang MZ, Ling SH and Sheng H. A study of velocity kinematics for hybrid manipulators with parallel-series configurations. In: *IEEE International Conference on Robotics and Automation*, Atlanta, GA, 1993, 1, pp.456–461.

Huang MZ and Ling SH. Kinematics of a class of hybrid robot mechanisms with parallel and series modules. In: *IEEE International Conference on Robotics and Automation*, San Diego, CA, 1994, 3, pp.2180–2185.

Jiang ZH. Impedance control of flexible robot manipulators. 2008. www.intechopen.com

Junco S, Diéguez G and Ramírez F. On commutation modeling in bond graphs. In: *8th International Conference on Bond Graph Modeling and Simulation*, San Diego, California, USA, 2007.

Junco S and Donaire A, Bond graph modeling and simulation of electrical machines, Chapter in: *Bond Graph Modeling of Engineering Systems*, 2011 (Springer).

Karnopp DC and Margolis DL. Analysis and simulation of planar mechanism systems using bond graphs. *Journal of Mechanical Design*, 1993; 101 (2): 187–191.

Karnopp DC, Margolis DL and Rosenberg RC. *System Dynamics, Modeling and Simulation of Mechatronic Systems*, 2000 (John Wiley & Sons, NY).

Kelly R, Carelli R, Amestegui M and Ortega R. On adaptive impedance control of robot manipulators. In: *IEEE International Conference on Robotics and Automation*, Scottsdale, AZ, USA, 1989, pp. 572–577.

Khadabadi UB and Pilli SC. Analysis of mechanisms using bond graphs. In: *National Conference on Machines and Mechanisms*, 2005, pp. 31–37.

Khatib O, Roth B and Waldron KJ. The Design of a High-Performance Force Controlled Manipulator. In: *8th World Congress on the Theory of Machines and Mechanisms*, Prague, 1991; 2: 475–478.

Kochan A. Parallel Robots perfect propellers. *Industrial Robot: An International Journal*, 1996; 23 (4): 27–30.

Kosuge K, Takeo K, Taguchi D, Fukuda T and Murakami H. Task-oriented force control of parallel link robot for the assembly of segments of a shield tunnel excavation system. *IEEE/ASME Transactions on Mechatronics*, 1996; 1 (3): 250–258.

Krishnaswamy K and Li PY. Bond graph based approach to passive teleoperation of a hydraulic backhoe. *Journal of Dynamic Systems, Measurement and Control*, 2006; 128 (1): 176–185.

Kumar CS and Mukherjee A. Robust control of a robot manipulator on a flexible foundation. In: *Proceedings of Fourth International Conference on CAD/CAM, Robotics & Factories of Future*, 1989, pp. 727–742.

Kumar CS. Shaping the interaction behaviour of manipulators through additional passive degree of freedom: A new approach to the impedance control, Ph.D. Thesis, IIT Kharagpur, 1994.

Lalonde RJ, Hartley TT and De Abreu-Garcia JA. Least squares model reduction. *Journal of the Franklin Institute*, 1992; 329 (2): 215–240.

Lawrence DA. Impedance control stability properties in common implementations. In: *IEEE International Conference on Robotics and Automation*, Philadelphia, PA, USA, 1988, pp. 1185–1190.

Lee MK, Park KW and Choi BO. Kinematic and dynamic models of hybrid robot manipulator for propeller grinding. *Journal of Robotic Systems*, 1999; 16 (3): 137–150.

LeSage JR and Longoria RG. Mission feasibility assessment for mobile robotic systems operating in stochastic environments. *Journal of Dynamic Systems, Measurement and* Control, 2014; 137 (3): 031009-1–031009-11.

Lippiello V, Siciliano B and Villani L. A position-based visual impedance control for robot manipulators. In: *IEEE International Conference on Robotics and Automation*, Roma, Italy, 2007, pp. 2068–2073.

Lopes AM and Almeida FG. Acceleration based force impedance control of a six dof parallel manipulator. *Industrial Robot: An International Journal*, 2007; 34 (5): 386–399.

Louca LS, Stein JL, Hulbert GM and Sprague J. Proper model generation: An energy based methodology. *Simulation Series*, 1997; 29: 44–49.

Lowrance EW and Latimer HB. Weights and variability of components of the human vertebral column. *The Anatomical Record*, 1967; 159 (1): 83–88.

Luo RC, Huang HB, Yi CY and Perng YW. Adaptive impedance control for safe robot manipulator. In: *Proceedings of the 8th World Congress on Intelligent Control and Automation*, Taipei, Taiwan, 2011, pp. 1146–1151.

Margolis D and Shim T. A bond graph model incorporating sensors, actuators, and vehicle dynamics for developing controllers for vehicle safety. *Journal of the Franklin Institute*, 2001; 338 (1): 21–34.

McCain H. A hierarchically controlled, sensory interactive robot in the automated manufacturing research facility. In: *IEEE International Conference on Robotics and Automation*, St. Louis, MO, USA, 1985

Medjaher K, Samantaray AK, Ould Bouamama B and Staroswiecki M. Supervision of an industrial steam generator. Part II: Online implementation, *Control Engineering Practice*, 2006; 14 (1): 85–96.

Medjaher K, Samantaray AK and Ould Bouamama B. Bond graph model of a vertical U-tube steam condenser coupled with a heat exchanger. *International Journal of Simulation Modelling Practices and Theory*, 2009; 17 (1): 228–239.

Merlet JP. *Parallel Robots*, 2012, pp. 50.

Mishra AK, Raina R, Yadav SB, Verma A, Sarangi S and Saha A. Modeling and simulation of levitating ball by electromagnet using bond graph. In: *Proceedings of the 1st International and 16th National Conference on Machines and Mechanisms (iNaCoMM2013)*, Roorkee, India, 2013, pp. 42–48.

Mitra AK and Das S. Solution of inverse problems by using the boundary element method. *Boundary Element Technology VII*, 1992; 721–731.

Moore BC. Principal component analysis in linear systems: controllability, observability and model reduction. *IEEE Transactions on Automation and Control*, 1981; 26 (1): 17–32.

Mukherjee A, Karmakar R and Samantaray, AK. *Bond Graph in Modeling, Simulation and fault Identification*, 2006 (CRC Press, FL).

Nagar SK and Singh SK. An algorithmic approach for system decomposition and balanced realized model reduction. *Journal of the Franklin Institute*, 2004; 341: 615–630.

Ngwompo RF, Scavarda S and Thomasset D. Inversion of linear time-invariant SISO systems modelled by bond graph. *Journal of the Franklin Institute*, 1996; 333 (2): 157–174.

Ngwompo RF and Gawthrop PJ. Bond graph-based simulation of non-linear inverse systems using physical performance specifications. *Journal of the Franklin Institute*, 1999; 336 (8): 1225–1247.

Ngwompo RF, Scavarda S and Thomasset D. Physical model-based inversion in control systems design using bond graph representation Part 1: theory. *Journal of Systems and Control Engineering, IMechE,* 2001a; 215 (2): 95–104.

Ngwompo RF, Scavarda S and Thomasset D. Physical model-based inversion in control systems design using bond graph representation Part 2: applications. *Journal of Systems and Control Engineering, IMechE,* 2001b; 215 (2): 105–112.

Orbak AY, Türkay OS, Eskinat E and Youcef-Toumi K. Model reduction in the physical domain. *Journal of Systems and Control Engineering, Proceedings of the Institution of Mechanical Engineers* 2003; 217 (6): 481–496.

Orbak AY, Eskinat E and Turkay OS. Physical parameter sensitivity of system eigen values and physical model reduction. *Journal of the Franklin Institute*, 2004; 341 (7): 631–655.

Orbak AY. *Physical model reduction-A Bond graph approach for engineering systems*. 2010 (LAP LAMBERT Academic Publishing AG & Co. KG, Germany).

Otter M, Elmqvist H and Cellier FE. Modeling of Multibody Systems with the Object-Oriented Modeling Language Dymola. *Nonlinear Dynamics*, 1996; 9 (1–2): 91–112.

Ould Bouamama B, Dauphin-Tanguy G, Staroswiecki M and Bravo AD. Bond graph analysis of structural FDI properties in mechatronics system, In: *IFAC Conference on Mechatronic Systems*, Darmstadt, Germany, 2000, 33 (26): 989–994.

Ould Bouamama B, Staroswiecki M and Dauphin-Tanguy G. Actuator fault detection using a bond graph approach, In: *European Control Conference (ECC)*, Portugal, 2001, 2, pp. 735–740.

Ould Bouamama B, Medjaher K, Bayart M, Samantaray AK and Conrard B, Fault detection and isolation of smart actuators using bond graphs and external models, *Control Engineering Practice*, 2005; 13 (2): 159–175.

Ould Bouamama B, Medjaher K, Samantaray AK and Staroswiecki M, Supervision of an industrial steam generator. Part I: Bond graph modelling, *Control Engineering Practice*, 2006; 14 (1): 71–83.

Ould Bouamama B, Harabi ER, Abdelkrim MN and Gayed BMK, Bond graphs for the diagnosis of chemical processes, *Computers and Chemical Engineering*, 2012; 36: 301–324.

Pathak PM, Mukherjee A and Dasgupta A. Impedance control of space robots using passive degrees of freedom in controller domain. *Journal of Dynamic Systems, Measurement and Control, Transactions of ASME*, 2005; 127 (4): 564–578.

Pathak PM, Mukherjee A and Dasgupta A. Impedance control of space robot. *International Journal of Modelling and Simulation*, 2006a; 26 (4): 316–322.

Pathak PM, Mukherjee A and Dasgupta A. Attitude control of a free-flying space robot using a novel torque generation device. *Simulation*, 2006b; 82 (10): 661–677.

Pathak PM, Kumar RP, Mukherjee A and Dasgupta A. A scheme for robust trajectory control of space robots. *Simulation Modelling Practice and Theory*, 2008; 16 (9): 1337–1349.

Paynter HM. *Analysis and Design of Engineering Systems*, 1961 (M.I.T. Press, Cambridge).

Peng Y, Yu H and Du ZJ. Design and Kinematic Analysis of a hybrid manipulator for spine surgery. In: *IEEE International Conference on Mechatronics and Automation*, Harbin, China, 2016.

Raibert MH and Craig JJ. Hybrid position force control of manipulators. *Journal of Dynamic Systems, Measurement and Control*, 1981; 103 (2): 126–133.

Ramadan AA, Takubo T, Mae Y, Oohara K and Arai T. Developmental process of a chopstick like hybrid Structure two fingered micromanipulator hand for 3-D manipulation of microscopic objects. *IEEE Transactions on Industrial Electronics*, 2009; 56 (4): 1121–1135.

Ricard R and Gosselin C. On the development of hybrid planar manipulators. In: *Proceedings of the 36th Midwest Symposium on Circuits and Systems*, Detroit, MI, 1993, 1: pp. 398–401.

Rosenberg R. State-space formulation for bond graph models of multi-port systems. *Journal of Dynamic Systems, Measurement and Control, Transactions of ASME*, 1971; 93 (1): 35–40.

Safonov MG and Chiang RY. A Schur method for balanced-truncation model reduction. *IEEE Transactions on Automation and Control*, 1989; 34: 729–733.

Saha SK. Dynamics of serial multibody systems using the decoupled natural orthogonal complement matrices, *ASME Journal of Applied Mechanics*, 1999; 66: 986–996.

Saha SK and Schiehlen WO. Recursive kinematics and dynamics for parallel structured closed loop multibody systems. *Mechanics of Structures and Machines*, 2001; 29 (2): 143–175.

Samantaray AK and Ould Bouamama B. *Model-based Process Supervision*, 2008 (Springer Verlag, London).

Sarangi S, Bhattacharyya R and Beatty MF. Effect of stress softening on the dynamics of a load supported by a rubber string. *Journal of Elasticity*, 2008; 92 (2): 115–149.

Sarkhel P, Banerjee N and Hui NB. Analysis and control of a six link serial manipulator with flexible joints. In: *Ist International and 16th National Conference on Machines and Mechanisms*, Roorkee, India, 2013, pp. 992–998.

Schilders W. Introduction to model order reduction. In: *Model order reduction: Theory and applications*. Springer, 2008.

Sharon A, Hogan N and Hardt DE. Controller design in the physical domain. *Journal of the Franklin Institute*, 1991; 328 (5–6): 697–721.

Siciliano B and Villani L. Robot force control. Dordrecht: Kluwer, 2000.

Singh A, Singla E, Soni S and Singla A. Kinematic modeling of a 7-DOF spatial hybrid manipulator for medical surgery. *Proceedings of the Institution of Mechanical Engineers, Part H: Journal of Engineering in Medicine*, 2017; 232 (1): 12–23.

Singh M. Model reduction in vehicle dynamic systems. M.E. Thesis, Mechanical Engineering Department, Thapar Institute of Engineering and Technology (Deemed University), Patiala, India, 2015.

Sirouspour MR and Salcudean SE. Nonlinear Control of Hydraulic Robots. *Robotics and Automation*, 2001; 17 (2): 173–182.

Skelton RE. and Yousuff A. Component cost analysis of large scale systems. *International Journal of Control*, 1983; 37 (2): 285–304.

Slone RD, Lee FAJ and Lee R. A comparison of some model order reduction techniques. *Electromagnetics*, 2002; 22: 275–289.

Stewart D. A platform with six degrees of freedom. *Proceedings of Institution of Mechanical Engineers*, 1965–1966; 180 (15): 371–386.

Stoenescu ED and Marghitu DB. Effect of prismatic joint inertia on dynamics of kinematic chains. *Mechanism and Machine Theory*, 2004; 39 (4): 431–443.

Sueur C and Dauphin-Tanguy G. Bond graph approach for multi-time scale system analysis. *Journal of the Franklin Institute*, 1991; 328 (5): 1005–1026.

Tachi S, Sakaki T, Arai H, Nishizawa S and Pelaez-Polo JF. Impedance control of a direct-drive manipulator without using force sensors. *Advanced Robotics*, 1991; 5 (2): 183–205.

Takaiwa M and Noritsugu T. Development of force displaying device using pneumatic parallel manipulator and application to palpation motion. In: *IEEE International Conference on Robotics and Automation*, Taipei, Taiwan, 2003, pp. 4098–4103.

Thoma J and Ould Bouamama B. *Modelling and Simulation in Thermal and Chemical Engineering*, 2000 (Springer-Verlag, New York).

Tsai LW. Solving the Inverse Dynamics of a Stewart-Gough Manipulator by the Principle of Virtual Work. *Journal of Mechanical Design*, 2000; 122 (1): 3–9.

Tonchoff HK, Gunther G and Grendel H. Vergleichende Betrachtung paralleler and hybrider Strukturen. In: *Proceedings of Conference on New Machine Concepts for Handling and Manufacturing Devices on the basis of Parallel Structures*, VDI N. 1427, Braunschweig, pp. 249–270.

Van-Dijk J, and Breedveld PC. Simulation of system models containing zero-order causal paths-I. Classification of zero-order causal paths. *Journal of the Franklin Institute*, 1991; 328 (5–6): 959–979.

Vinoth V, Singh Y and Santhakumar M. Indirect disturbance compensation control of a planar parallel (2-PRP and 1-PPR) robotic manipulator. *Robotics and Computer-Integrated Manufacturing*, 2014; 30: 556–564.

Waldron KJ, Raghavan M and Roth B. Kinematics of a Hybrid Series-Parallel Manipulation System. *ASME Journal of Dynamic Systems, Measurement and Control*, 1989; 111 (2): 211–221.

Wang X and Chen W. Command assignment method of a serial-parallel hybrid flight simulator. In: *Control and Decision Conference (CCDC)*, Qingdao, China, 2015a.

Wang X and Chen W. Kinematics analysis of a high dynamic serial-parallel hybrid flight simulator. In: *Control and Decision Conference (CCDC)*, Hangzhou, China, 2015b.

Xiheng H. FF-Pade method of model reduction in frequency domain. *IEEE Transactions of Automation and Control*, 1987; 32 (3): 243–246.

Yan L, Chen MI, Yeo S-h, Chen Y and Yang G. A high dexterity low degree-of-freedom hybrid manipulator structure for robotic lion dance. *Journal of Zhejiang University-Science A(Applied Physics & Engineering)*, 2010; 11 (4): 240–249.

Yang G, Chen I, Yeo SH and Lin W. Design and Analysis of a Modular Hybrid Parallel-Serial Manipulator for Robotised Deburring Applications. In: *Smart Devices and Machines for Advanced Manufacturing*. 2008 (Springer-London), pp. 167–188.

Ye Y and Youcef-Toumi K. Subsystem's Influence on a System Eigen Value. In: *Proceedings of the IEEE Southeastcon*, Cambridge, MA, 2000, pp. 261–267.

Yildiz İ, Ömurlü VE and Sağirli A. Dynamic modeling of a generalized Stewart platform by bond graph method utilizing a novel spatial visualization technique. In: *International Review of Mechanical Engineering (IREME)*, 2007; 2 (1): pp. 702–713.

Yildiz İ, Ömurlü VE and Sağirli A. A novel visualization technique in bond-graph method for modeling of a generalized Stewart platform. In: *Proceedings of the 2008 IEEE International Conference on Robotics and Biomimetics*, Bangkok, Thailand, 2009, pp.780–785.

Youcef-Toumi K and Gutz DA. Impact and Force Control: Modeling and Experiments. *Journal of Dynamic Systems, Measurement and Control, Transactions of ASME*, 1994; 116: 89–98.

Yuh J, Young T and Baek YS. Modeling of a flexible link having a prismatic joint in robot mechanism–experimental verification. *Robotics and Automation*, 1989; 2: 722–727.

Zakerzadeh MR, Tavakoli M, Vossoughi GR and Bagheri S. Inverse Kinematic/Dynamic Analysis of a new 4-DOF Hybrid (Serial-Parallel) Pole Climbing Robot Manipulator. *Climbing and Walking Robots*, pp. 919–934 (Springer).

Zanganeh KE. Kinematics of manipulators with parallelism, modularity and redundancy: analysis and design. PhD Thesis, McGill University, Montreal, Quebec, Canada, 1995.

Zeid AA and Overholt JL. Singularly perturbed formulation: Explicit modeling of multibody systems. *Journal of the Franklin Institute*, 1995; 332 (1): 21–45.

Zhang DC and Song MS. Forward kinematics of walking machines with pantograph legs based on selections of independent joints. *Journal of Field Robotics*, 1992; 9 (7): 955–971.

Zhang L, Wang J and Wang L. Analysis and Simplification of the Rigid Body Dynamic Model for a 6-UPS Parallel Kinematic Machine under the Uniform Motion Condition. In: *Proceedings of the 2003 IEEE International Conference on Robotics, Intelligent Systems and Signal Processing*, Changsha, Hunan, China, 2003.

Zhou K, Doyle JC and Glover K. Robust and Optimal Control. Prentice Hall, Inc, Engelwood Cliffs, New Jersey, 1996.

Zhu Y and Barth EJ. Passivity-based impact and force control of a pneumatic actuator. *Journal of Dynamic Systems, Measurement and Control, Transactions of ASME*, 2008; 130 (2): 024501-1–024501-7.

Curriculum Vitae

Rashmi Arora did his graduation (Bachelor of Technology) in Mechanical Engineering from Giani Zail Singh Campus College of Engineering and Technology (formerly Giani Zail Singh College of Engineering and Technology (G.Z.S.C.E.T.), Bathinda, Punjab, India in the year 2005. After that she has worked for one year as Lecturer at Desh Bhagat University (formerly Desh Bhagat Engineering College), Mandi Gobindgarh, Fatehgarh Sahib, Punjab. She obtained her Master of Engineering (M.E.) degree in CAD/CAM & Robotics from Thapar Institute of Engineering & Technology (Deemed to be University) (formerly Thapar University), Patiala, Punjab in the year 2008. Then she worked as Trainee Engineer at Ideas Design Solution Pvt. Ltd, Gurgaon (2010) and as a Faculty at different colleges in India (2008–2010, 2012–2013). In the year 2013, she joined in the Ph.D. Program at Thapar Institute of Engineering & Technology (Deemed to be University), Patiala, Punjab as a Research Scholar to pursue her research work in the area of bond graph modelling and control of hybrid manipulators. She is presently working in Chandigarh University, Mohali as Assistant Professor in Mechanical Engineering Department since 2016. She has 5 journal papers and 7 conference papers.